Spring 5-15-2015

Photocatalytic Mineralization of Phenol on Fluidized Titanium Oxide-Coated Silica Gel

Guillermo J. Rincon
University of New Orleans, grincon@outlook.com

Photocatalytic Mineralization of Phenol on Fluidized Titanium Oxide-Coated Silica Gel

A Dissertation

Submitted to the Graduate Faculty of the
University of New Orleans
in partial fulfillment of the
requirements for the degree of

Doctor of Philosophy
in
Engineering and Applied Science
Environmental Engineering

by

Guillermo J. Rincón

M.S., University of New Orleans, 2011
B.S., Universidad del Zulia, 2000

May, 2015

Acknowledgement

I would like to thank my advisor Professor Enrique La Motta for his guidance, support and encouragement during my time as a graduate student at the University of New Orleans. I would also like to thank the Graduate School for its financial support through the Ernest G. Chachere doctoral fellowship.

And to my beloved friend, who always believed in me, infinite thanks.

Guillermo J. Rincón

Table of Content

List of Figures

List of Tables

List of Symbols and Abbreviations

A_m: External silica surface area per gram

A_R: Irradiated surface area

C: Substrate concentration

C_0: Initial COD

C_L: Minimum COD

CB: Conduction band energetic level

COD: Chemical oxygen demand

CVD: Chemical vapor deposition

d: Silica gel particle's mean geometric diameter

DC: Direct current

DO: Dissolved oxygen

E_C: Energy of the CB edge

E_F: Fermi energy level

E_g: Bandgap between CB and VB

E_R: Irradiance at irradiated surface

E_V: Energy of the VB edge

EPD: Electrophoretic deposition

EPR: Electron paramagnetic resonance

ESR: Electron spin resonance

h: Planck's constant (6.63×10^{-34} J s)

h^+: Photohole

$h\nu$: Photon energy

K: Langmuir-Hinshelwood adsorption equilibrium constant

k: Photocatalytic pseudo-constant

K_{app}: Apparent rate constant

k_B: Boltzmann constant (1.38×10^{-23} J K^{-1})

k_{LH}: Langmuir-Hinshelwood rate constant

k_ω: Correlation coefficient in power fit equation

L_D: Debye length

L-H: Langmuir-Hinshelwood

L_R: Irradiated reactor's length

M_{ads}: Adsorbed electron acceptor

N_C : Effective density of states in the CB (~10^{19} cm^{-3})

N_D : Effective density of states in the VB (~10^{17} cm^{-3})

PEC: Photoelectrochemical

pH_{zpc}: Zero charge potential pH

pK_a: Acid dissociation constant

q : Elementary charge

Q_{UV}: Accumulated energy

$Q_{0.5}$: Accumulated energy for mineralization of 50% of initial COD

r: Reaction rate

R_{ads}: Adsorbed electron donor

SHE: Standard hydrogen electrode

t: Time

T: Temperature

TiO_2: Titanium oxide

TOC: Total organic carbon

UV: Ultraviolet

v : Frequency of light wave

VB: Valence band energetic level

V_R: Irradiated volume

V_T: Total liquid volume in reactor

W: Width of the space charge layer

α: Semiconductor's reciprocal absorption length

ε: Particle porosity

$\Delta\phi_{SC}$: Potential drop within space charge layer

φ: Particle sphericity fator

Φ_R: Radiant flux

λ_g : Semiconductor's absorption edge

ψ : Incident light intensity

θ : Surface coverage

Abstract

A bench-scale tubular reactor with recirculation was built in order to study the efficiency of the photocatalytic oxidation of phenol on fluidized titanium oxide-coated silica gel beads. A UV-C lamp placed along the central vertical axes of the reactor was used as source of photons. A bed of silica gel beads was fluidized by means of fluid recirculation and forced to follow upward helical flow around the lamp. Anatase was successfully synthetized on silica gel particles of average diameters 224, 357 and 461 µm, as confirmed by scanning electron micrographs, through a sol-gel technique using a titanium (iv)isopropoxide / hydrochloric acid / ethanol precursor.

Data was obtained from multiple 8-hours photocatalytic experiments using a determined mass of beads fluidized in an aqueous solution of known initial phenol concentration. Contaminant degradation with irradiation time was measured as COD. Beads that had been subjected to three consecutive coating procedures produced an 8-h removal efficiency 10% higher than beads with a single coat. 20 g L^{-1} of silica beads was found to be the optimum load for the experimental reactor configuration regardless of beads size, although efficiency increased with decreasing size of the latter.

Experimental results confirmed that the efficiency of phenol photocatalytic degradation decreases with increasing pollutant concentration. Also, the highest removal was achieved with initial pH 3, and it decreased with increasing pH. When NaCl was added to the solution, COD removal increased with increasing salinity. Additionally, it was found that dissolved oxygen is indispensable for photocatalysis to proceed, and that saturation of the treated mixture with oxygen was effectively achieved by keeping the liquid surface in contact with pure oxygen at 1 atm.

Finally, statistical analysis of the data showed that photocatalytic mineralization of phenol-derived COD under the experimental conditions follows exponential decay. Based on this finding, a correlation model was proposed for the accurate prediction (minimum $R^2 = 0.9840$) of the COD removal efficiency of the reactor for any given initial COD.

Key words: Titanium oxide, photocatalysis, advanced oxidation process, semiconductor, photo-reactor, anatase, phenol oxidation, sol-gel method, catalyst synthesis, silica gel beads, bed fluidization, UV-C irradiation, chemical oxygen demand, photon, absorption, exponential decay model, statistical analysis.

1

Introduction

TiO$_2$ photocatalysis represents a promising class of oxidation techniques that are intended to be both supplementary and complementary to the conventional approaches for the destruction or removal of refractory and trace organic contaminants in water and air (Ding et al., 1999; Alfano et al., 2000). Light-induced redox reactions take place on the surface of a catalyst and unselectively oxidize the contaminants into non-toxic products such as water, CO$_2$ and simple mineral acids (Hoffmann et al., 1995; Zhang el al., 1996; Crittenden et al., 1997; Malato et al., 2002). These processes operate at ambient temperature and pressure and they do not require the addition of expensive oxidants. To date, TiO$_2$ photocatalysis has been successfully demonstrated in the destruction of a variety of organic and inorganic contaminants such as aromatics, haloaromatics, alkanes, alkenes, haloalkenes, insecticides, pesticides, detergents, textile dyes, humic substances and transition metals (Linsebigler et al., 1995; Hoffmann et al., 1995; Mills and Le Hunte, 1997; Fujishima et al., 2000).

The photocatalytic reaction is a surface-mediated process; therefore, a high surface area is essential to achieve efficient degradation of contaminants. Powdered TiO$_2$ dispersion systems employed in most studies require an additional separation step to recover the catalyst from the effluent water. This represents a major drawback for large scale application of such systems, as the separation step is generally energy intensive and overall capital investment and running cost of the process would be increased by the need for additional equipment and energy consumption

(Byrne et al., 1998, 2002). Pozzo et al. (1997) estimated that the cost requirement for post-treatment recovery of small catalyst particles may even invalidate altogether the amount of energy savings claimed for a solar induced decontamination process. For easy handling, TiO_2 photocatalyst may be immobilized onto supports made of materials such as quartz, glass, zeolite or silica gels, eliminating or minimizing the need for post-treatment removal (Zhang et al., 1994; Nogueira and Jardim, 1996; Byrne et al., 2002). In recent years, immobilized TiO_2 photocatalyst systems have received increasing attention because they also have found application as self-cleansing surface, on top of the conventional use in water and gaseous remediation.

While the immobilized-catalyst system does provide a solution to the solid-liquid separation problem, such a system still exhibits several shortcomings that need to be addressed. Firstly, immobilization of TiO_2 may translate into low surface area to volume ratios, which results in restricted processing capacities due to possible mass transfer limitations (Turchi and Ollis, 1988; Matthews, 1991). There also exists the possibility of inherent inefficiencies introduced by light absorption and light scattering in the particle suspension medium, as well as the generation of significant pressure drop in the system, catalyst fouling or catalyst wash out, and the introduction of new technical challenges such as the need for in situ catalyst regeneration (Parent et al., 1996).

This document presents the results of research conducted by the author to develop and study a novel photocatalytic system, based on UV-C irradiation of fluidized TiO_2-coated silica gel particles in a tubular reactor. The motivation for this configuration is that fixation of the catalyst onto a large enough support facilitates the retention and recovery of the catalyst, while fluidization of such support in the medium maximizes exposure of the TiO_2 film to light, thus improving mass transfer on the catalyst surface and enhancing its surface area-to-volume ratio.

Chapter 2 presents an overview on semiconductor photocatalysis theory, its fundamentals and technological present status, including photocatalysis kinetic modeling and catalyst synthesis and deposition techniques. Chapter 3 explains the experimental work performed in the laboratory, showing details on reactor configuration and analytical procedures. Chapter 4 presents the results and discussion of the experimental data. Finally, in chapter 5, research findings are summarized and conclusions and recommendations are presented.

1.1. Background

In the modern oil industry, there are two major generators of oily wastewater that may impact the quality of seawater: Oil spills and discharges of both untreated and partially treated produced water. The preferred approach for cleaning up an oil spill in U.S. territorial waters is to contain and thicken the oil slick with booms, and then place skimmers to remove the floating oil (Argonne National Laboratory, 2009). Unfortunately, the recovered material is a mixture of a water-in-oil emulsion and free water. Since the recovered water substantially reduces the storage space available at the site of skimming operations, chemical demulsifiers are usually added to promote oil-water separation, and thus be able to separate the oil from the water. Once this separation is achieved by gravity, the water is usually stored or transferred to barges. The decanted water cannot be discharged back to the ocean because it contains large concentrations of oil and grease, dispersants, demulsifiers, and dissolved hydrocarbons. The usual practice is to carry this oily wastewater to shore for further processing at treatment plants or for deep-well injection. According to the MC252 Weekly Waste Tracking Cumulative Report by Disposal Facility (OSPAR, 2006), $3.1x10^4$ m^3 of oily liquid waste was the cumulative amount manifested as of 08/01/10 after the Gulf of Mexico oil spill. This wastewater was transported to disposal facilities

located throughout the Gulf of Mexico states. Brown et al. (2009) claim that 1.1×10^5 m^3 of oily water mixture had been collected at the oil spill site through June 2010, some of which made its way to Texas for permanent disposal in underground salt domes and injection wells. Thus, large volumes of oily wastewater were transported from the original collection point at the Gulf of Mexico to final disposal sites located as far as Texas and Florida.

This amount of oily wastewater generated at the Gulf oil spill pales in comparison to the volume of produced water generated in the US: 9.2 million m^3 per day (Vik, 2007). For every cubic meter of oil extracted in the US, 12 cubic meters of produced water are generated, of which less than 3% corresponds to federal offshore activities. A much larger figure is presented by Brown et al. (2009), who point out that there are currently 118 oil and gas exploration and production facilities operating in the territorial seas of Louisiana, and that it is anticipated that 150 new wells will be constructed in upcoming years. These authors indicate that approximately 5.5×10^5 m^3 of produced water are discharged into the Gulf of Mexico each day by offshore oil and gas facilities located in Louisiana. The same authors (Brown et al., 2009) describe that there are over fifty individual constituents currently found in produced waters discharged into the Gulf of Mexico, including monocyclic and polycyclic aromatic hydrocarbons, aliphatic hydrocarbons, and phenols, about twenty different metals, and radium-226 and radium-228.

NPDES general permits issued by the U.S. EPA regional offices currently authorize offshore produced water discharges into the Gulf. All of the permits contain a monthly average limit of 29 mg/L and a 42-mg/L daily maximum limit for oil and grease (OSPAR, 2006). Effective January 1, 2007, the Oslo Paris Convention (OSPAR) has agreed that no individual offshore installation should exceed a performance standard for dispersed oil of 30 mg/l for produced water discharged into the sea (OSPAR, 2006). In Norway, the oil operators have agreed to implement a

policy of zero environmental harmful discharges (ZHD) after 2005 (Vik, 2007).

In 2009, the Colorado School of Mines (CSM, 2009) generated a comprehensive report on existing and emerging technologies to treat produced water. These technologies include stand-alone treatment processes such as basic separation through biological filters, hydrocyclones, flotation, membrane separation, thermal technologies, adsorption, UV disinfection and chemical oxidation, as well as combined processes that integrate different basic technologies for an enhanced treatment output. Since the volume of produced water generated in off-shore operations represents only a small fraction of the total, most of these processes are designed for on-shore operations and to meet required standards for water reuse (re-injection into reservoir) or disposal.

Previous research conducted by the author (Rincón et al., 2012) demonstrated that oily emulsions can be effectively treated using a combination of electrocoagulation/electroflotation processes (EC/EF) to meet or exceed the NPDES discharge limits for oil and grease into natural waters. Nevertheless, EC/EF is still not capable of producing a ZHD effluent, since it only removes colloidal contaminants, leaving all the dissolved organic pollutants behind. These dissolved or soluble components, responsible for the high chemical oxygen demand (COD) of this water, are difficult to remove.

An ideal wastewater treatment process should be cost effective and, most importantly, it must not produce any hazardous by-products. In the past two decades, photocatalytic degradation of recalcitrant organics has been widely investigated and found to be a viable technology for removing dissolved contaminants from wastewater. It is effective for the removal of organic pollutants and microorganisms (Saquib et al., 2007; Josef et al., 2006).

As explained in Section 2.5, heterogeneous photocatalysis technology takes advantage of the capacity of semiconductor materials (i.e. TiO_2) to undergo redox reactions when irradiated with UV light while suspended in water, leading to the generation of hydroxyl radicals ($OH^\bullet$) and the destruction of organic contaminants. In absence of a catalytic active substance, the oxidation of the most hydrocarbons proceeds rather slowly. The reaction rate can be substantially increased using a heterogeneous photocatalytic system, which consists of a semiconductor surface (photo catalyst) in close contact with the liquid stream. Exposing the catalyst to UV light generates excited states, which are able to initiate subsequent processes like redox reactions and molecular transformations (Jacquot et al., 1996). In semiconductors, like TiO_2, a portion of the photo-excited electron-hole pairs diffuse to the surface of the catalytic particles and take part in the chemical reaction with the adsorbed donor or acceptor molecules. The holes can oxidize donor molecules whereas the conduction band electrons can reduce appropriate electron acceptor molecules. The following equations summarize the set of complex reactions presented in Section 2.5, and describe the oxidation and reduction mechanism (Zou et al., 2007):

$$TiO_2 \xrightarrow{h\upsilon} TiO_2\left(e_{CB}^- + hole_{CB}^+\right) \tag{3.1}$$

$$TiO_2\left(e_{CB}^- + hole_{CB}^+\right) \xrightarrow{recombination} TiO_2 + heat \tag{3.2}$$

$$H_2O \rightarrow OH^- + H^+ \tag{3.3}$$

$$hole_{VB}^+ + OH_{ads}^- \rightarrow OH^\bullet \tag{3.4}$$

The heterogeneous photo catalytic oxidation with TiO_2 meets the following requirements that could make it competitive with respect to other processes oxidizing contaminants (Jacquot et

al., 1996): (a) it is a low-cost material, easy to use, and easily available. (b) The reaction is quite fast at mild operating conditions (room temperature, atmospheric pressure). (c) A wide spectrum of organic contaminants can be converted to water and CO_2. (d) No chemical reagents are added and no side reactions are produced.

Titanium dioxide has been extensively used as a photo catalyst (Akpan and Hameed, 2009; Tada et al., 2009; Taga, 2009; Gaya and Abdullah, 2008; Aprile et al., 2008; Pichat, 2007; D'Auria et al., 2009; Yue et al., 2008; Berry and Mueller, 1994) but applications to oil spills have not been extensively studied. Several reports have discussed the use of TiO_2 for oil degradation (Zou et al., 2007; An et al., 2004) but due to the limited number of studies, the limited number of source oils, and the lack of mechanistic and product data, much remains poorly understood in these systems. Nevertheless, because of its low cost, low toxicity, and wide availability, this material is a good candidate for photo catalytic decomposition of petroleum.

Using titanium dioxide as photocatalyst and UV light as the energy source, this process has successfully reduced organic pollutants and microorganisms concentration in wastewater (Chen et al., 2007; Chong et al., 2010).

Two photocatalyst configurations have been used: in slurry form and immobilized on a support. In a slurry reactor, the photocatalyst particles will be freely dispersed in the bulk throughout the reactor volume. In immobilized-photocatalyst reactors, the catalyst will be anchored to a support such as fiberglass, activated carbon, fiber optic cables, glass, glass beads, glass wool, membranes, quart sand, zeolites, silica gel, stainless steel or Teflon (De Lasa et al., 2005). Photocathalytic activity is superior in TiO_2 slurry reactors, mainly because of improved liquid to solid mass transfer and a high total surface area of photocatalyst per unit volume, both of which is limited in immobilized TiO_2 reactors. However, slurry type operations have the

disadvantage of requiring post-treatment separation of the catalyst, increasing complexity and operational cost. Table 3.1 shows a comparison between both types of reactors.

Table 1.1. Suspended vs. immobilized photocatalytic systems (De Lasa et al., 2005)

Slurry reactors	Immobilized reactors
Advantages: ▪ Fairly uniform catalyst distribution ▪ High photocatalytic surface area to reactor volume ratio ▪ Limited mass transfer ▪ Minimum catalyst fouling effects due to the possible continuous removal and catalyst replacement ▪ Well mixed particle suspension ▪ Low pressure drop to the reactor	Advantages: ▪ Continuous operation ▪ Improved removal of organic material from water phase while using a support with adsorption properties ▪ No need for an additional catalyst separation operation
Disadvantages ▪ Requires post-process filtration ▪ Important light scattering and adsorption in the particle suspended medium	Disadvantages ▪ Low light utilization efficiencies due to light scattering by immobilized photocatalyst ▪ Restricted processing capacities due to possible mass transfer limitations ▪ Possible catalyst deactivation and catalyst wash out

Until recently, the slurry photocatalytic reactor was still the preferred configuration owing to its high total surface area of photocatalyst per unit volume and ease of photocatalyst reactivation. The photocatalyst particles can be separated by settling tanks or external cross-flow filtration systems to enable continuous operation of the slurry reactor. On the other hand, immobilization and the support material in immobilized reactors influence the photocatalyst activity. The surface area of the catalyst is minimized since the coating layer has a lower porosity (Balasubramaniam et

al., 2004). It was also reported that the type of support material influences the adsorption characteristics and consequently the decomposition rate of pollutants (Sakthievel et al., 2002). Furthermore, immobilized catalyst showed flow rate dependence of the reaction (Bideau et al., 1995; Kobayakawa et al., 1998). Thus, the support should have the following characteristics (Pozzo et al., 1997): (i) transparent to irradiation; (ii) strong surface bonding with the TiO_2 catalyst without negatively affecting the reactivity; (iii) high specific surface area; (iv) good adsorption capability for organic compounds; (v) separability; (vi) facilitating mass transfer processes and (vii) chemically inert.

For this technology to be applicable, the reactor has to be designed in a way so that optimal irradiation of the immobilized catalyst is guaranteed, and that it is operated continuously. Pareek at al. (2008) addressed that the most important factors in configuring a photocatalytic reactor are the total irradiated surface area of catalyst per unit volume and light distribution within the reactor. It has been also concluded that the photocatalytic action is local, requiring the triple encounter of the surface, the reactant(s) and the photons (Bideau et al., 1995).

A technically feasible solution for solving the downstream separation of photocatalyst nanoparticles after treatment is via the application of a hybrid process in which the photocatalyst is synthesized and fixed on a substrate that can be retained in the reactor post-treatment. Using a tubular continuous-flow reactor packed with TiO_2 photocatalyst immobilized on 2 mm diameter silica gel beads, Kobayakawa et al. (1998) were able to efficiently decompose water contaminants at high flow rate. Hanel et al. (2010) used a cylindrical quartz tube packed with immobilized TiO_2 on glass beads to eliminate phenol in water. However, packed bed reactors require the assistance of various parabolic light deflectors to transfer the photons to the catalyst surface. To achieve uniformity in photon flux distribution within the reactor, a correct position of light source is

essential. The use of this type of reactors has become unfavorable nowadays due to the need of special configuration and high operating costs (Chong et al., 2010).

However, an alternative to packed bed reactors is bed fluidization, given that the particulate support onto which the catalysts has been fixed can be entirely fluidized throughout the reactor volume. Abhang et al. (2011) were able to degrade phenol in water using a fluidized bed rectangular reactor. TiO_2 nano-powder was anchored onto 2 mm diameter silica gel particles, placed in a rectangular chamber illuminated with UV light and fluidized by means of air bubbling. The authors showed that successful implementation of photocatalytic reactors requires increasing the number of photons absorbed onto the catalyst surface per unit time and per unit volume.

In the quest to identifying the effectiveness of photocatalytic degradation treatment using suspended TiO_2 particles, many extrinsic and intrinsic parameters have been investigated; among them irradiation time, solution pH, temperature, initial concentration of substrate, catalyst concentration, photo-reactor design and light intensity (Huang et al., 2007; Fotiadis et al., 2007; Chen et al., 2007; Singh et al., 2007; Tang et al., 2004). For example, the degradation efficiency of the substrate decreases with increasing substrate concentration (Singh et al., 2007). It was also found that the initial reaction rate is directly proportional to the catalyst concentration (Huang et al., 2007). Also, the degradation efficiency improved with increasing incident light intensity (Huang et al., 2007).

1.2. Objective and Scope of the Research

Making use of a bench-scale physical model, the main objective of the present research is to investigate the feasibility of the photocatalytic oxidation of phenol, measured as chemical oxygen demand (COD), on fluidized TiO_2-coated silica gel micro-beads and effect of selected

intrinsic and extrinsic parameters on the process efficiency. The research conducted on this variation of the traditional TiO_2 slurry-type reactor and packed-bed reactors for photocatalytic oxidation, required the completion of a development and experimental phase that included:

- Design and construction of a bench scale photocatalytic reactor.
- Selection of type of particulate support for photocatalyst.
- Selection of method for photocatalyst deposition.
- Experiment design, including single experiment duration, definition of study variables and parameters, and analytical methods selection.

The developed system was evaluated by measuring COD disappearance with irradiation time in a number of experiments in which different parameters, such as the mass and size of silica gel, phenol concentration, pH, salinity, dissolved oxygen concentration and number of TiO_2 coatings, were varied in order to stablish their influence on the process efficiency.

The presence of the synthetized TiO_2 layer on the silica support was confirmed through scanning electron microscopy, and the amount of catalyst deposited after each coating procedure was also measured, showing that anatase was effectively formed through the selected sol-gel procedure and that silica's surface coverage increased with repeated applications.

The final phase of data analysis shows that photocatalysis on TiO_2-coated silica beads can be a viable alternative to photocatalysis on anatase nano-powder. This finding is accompanied by a comparative study of the effect of the evaluated variables on contaminant degradation and a statistical model for predicting the efficiency of the system based on initial phenol load.

2

Overview of Fundamentals

2.1. Background

Research on TiO_2 started when Fujishima and Honda (1972) began investigating the properties of TiO_2 in water photoelectrolysis using a photoelectrochemical cell. Utilizing the strong photo-reduced oxidation power of TiO_2, oxygen evolution occurs at the TiO_2 electrode, while hydrogen evolves from the Pt counter electrode. These findings attracted the attention of the scientific community, as there was an increasing interest in developing synthetic systems capable of harvesting solar energy and convert it into chemical or electrical energy. Although notable progress has since been made, the quantum efficiency of such system has been reported to be low (Hashimoto et al., 2005). Another approach to utilize solar energy involves the dye sensitization of TiO_2 in a regenerative photoelectrochemical cell. A single redox couple exists in the cell, the reduced form is oxidized at the TiO_2 photoanode and the oxidized form is reduced at the counter electrode (Hagfeldt and Gratzel, 1995). Gratzel et al. achieved conversion efficiencies of 10 to 11% in the 1990s by using ruthenium complexes as sensitizers (Nazeeruddin et al., 1993, 1997).

Meanwhile, TiO_2 photocatalysis has become one of the most investigated technologies for elimination of environmental contaminants since the success of Frank and Bard (1977) in demonstrating the decomposition of cyanide in the presence of powdered TiO_2. Ever since,

laboratory and field studies have continually confirmed the application of TiO_2 photocatalysis in the destruction of a large variety of contaminants (Mills and Le Hunte, 1997; Fujishima et al., 2000; Herrmann, 2005). The fact that the studies were generally conducted using a TiO_2 powdered dispersion renders its application on a large scale energy intensive since post-treatment separation of the nanopowder would be required or, at least, desirable. For the purpose of easy handling, research has shifted to the development and application of immobilized systems. TiO_2 photocatalysis has also been used to eliminate taste and odor generating contaminants, gaseous organic matter (Cai et al., 1991; Heller, 1995; Heneghan et al., 2004), as well as for the reductive deposition of heavy metals such a s platinum, palladium, gold, rhodium and silver from aqueous solution onto surfaces (Ollis et al., 1991; Albert et al., 1992; Inel and Ertek, 1993; Herrmann, 2005). The concept of light-cleaning materials coated with a TiO_2 photocatalyst film has also attracted significant attention. In addition to the photo-induced redox reactions on adsorbed substances, the photo-induced hydrophilic conversion of TiO_2 itself assists in the surface cleaning process. Adsorbed substances can easily be washed away by water when there is insufficient photon energy to completely oxidize them (Mills and Le Hunte, 1997; Pilkington Group Limited: 08/06/2008: How self-cleaning glass works).

Compared to other materials for photocatalysis, TiO_2 has proven to be the most suitable for widespread environmental application. TiO_2 is highly active, stable under photo and chemical corrosive environments, inexpensive, and safe to humans and the environment (Hashimoto et al., 2005). In this chapter, topics of particular interest are (2.2) the general electronic properties of semiconductors; (2.3) the operating principles of a photochemical reactor ; (2.4) photo-effects at TiO_2 bulk and nanocrystalline catalyst-substrate interface; (2.5) insights into light induced oxidative pathways of organics; (2.6) kinetic scheme to describe photocatalytic processes; (2.7)

factors that affect reaction rates in a typical photo catalytic process; (2.8) application of photocatalysis and commercially available photocatalytic products; and (2.9) research efforts in the synthesis of TiO_2 films.

2.2. Optical Absorption and Bandgap Photo-Excitation

The electronic energy level in a solid is described by the band model. Large numbers of electronic levels are formed as the atomic orbitals interact with one another. These resultant electronic levels are closely positioned and form a continuum of energy levels (Eyring, 1970). The levels in which electrons are free to flow and conduct electricity constitute the conduction band (CB), and the levels completely occupied by the electrons represent the valence band (VB). The energy difference between these bands is known as the bandgap, E_g. A schematic diagram of the electronic structure of an insulator, a semiconductor, and a conductor is given in Figure 2.1.
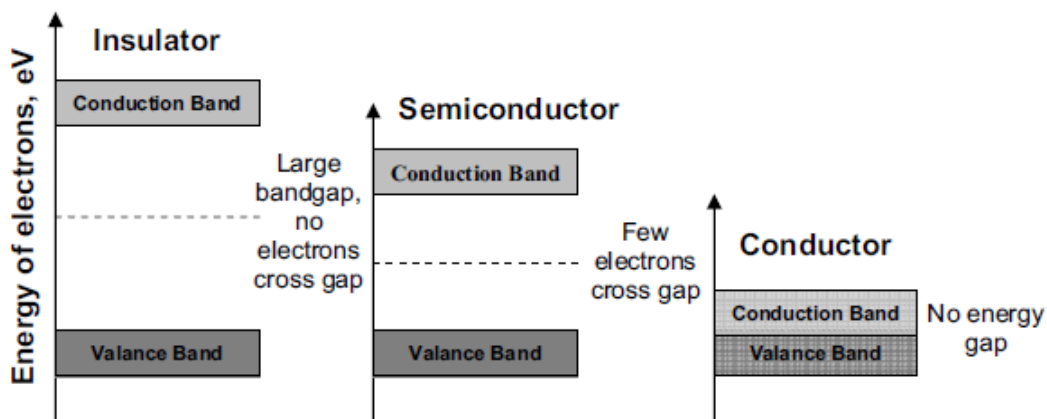
Figure 2.1. Energy bands in insulator, semiconductor and conductor (Singleton, 2001)

In conductors such as metals, there is a continuum of electronic states. Valence electrons move freely to conduct electricity. A bandgap exists between the VB and the CB in semiconductors and insulators. The large bandgap in insulators does not allow electrons injection into the CB. Electrons in a completely filled band do not conduct electricity. Semiconductors, however, absorb light below the fundamental absorption edge, λ_g, to inject electrons into the CB and generate holes (electron deficiencies) in the VB. These charge carriers can recombine or be present at the semiconductor surface to carry out redox reactions. The de-excitation of these charge carriers favors the path which minimizes the lifetime of the excited state (Linsebigler et al., 1995). λ_g is related to the bandgap energy via the following equation (Gratzel, 1988):

$$\lambda_g \left(\text{nm}\right) = \frac{1240}{E_g \left(\text{eV}\right)} \tag{2.1}$$

The E_g of a semiconductor can be determined by means of optical absorption. Near λ_g the absorption behaviors of a semiconductor are depicted by the following function (Hagfeldt and Gratzel, 1995):

$$\alpha h v = \text{const}\left(h v - E_g\right)^n \tag{2.2}$$

where α is the reciprocal absorption length, h is the Planck's constant, v is the frequency of the light wave, and E_g is the bandgap energy, $n = 0.5$ for a direct transition and $n = 2$ for an indirect transition. Electron distribution in a semiconductor is described by the Fermi level, E_F. Electron occupancy is approximately half when the energy level is at the E_F (Morrison, 1980). E_F also locates the energy of both charge carriers at the semiconductor-electrolyte interface (Litter, 1999), and it is indicative of the thermodynamic limitations for the photoreactions that can take place

(Hagfeldt and Gratzel, 1995). For a perfect semiconductor, the E_F is located in the middle of the E_g at zero Kelvin (Morrison, 1980).

The presence of impurities or defects caused by vacancies, interstitials, dislocations, and grain boundaries in the semiconductors perturbs their electronic structures by donating electrons to the CB (Morrison, 1980). These perturbations give rise to new energy levels to produce n-type and p-type semiconductors. In an n-type semiconductor, electrons are the majority carrier, while in a p-type semiconductor, holes are the majority carrier. TiO_2, ZnO, WO_3 and Fe_2O_3 are naturally n-type semiconductors, while Cu_2O, NiO, and Cr_2O_3 are p-type semiconductors. Semiconductors such as Si, GaAs, and InP can be made to exhibit n or p-type behavior by introducing different impurities (Lindgren, 2004). For an n-type semiconductor, the E_F lies close to the CB, and can be approximated by the following equation (Morrison, 1980):

$$E_F = E_C - k_B T \ln \frac{N_C}{N_D}$$
(2.3)

where N_C (~10^{19} cm^{-3}) is the effective density of states in the CB, N_D (~10^{17} cm^{-3}) is the donor density, k_B is the Boltzmann constant, T is the temperature, and E_C is the CB edge energy.

Figure 2.2 depicts the band positions of various semiconductors that are in contact with aqueous media at pH 0 together with the redox potentials of water. Thermodynamically, the potential of the conduction band edge (E_C) must be more negative than the reduction potential of a chemical species in order to photo-reduce the particular chemical species, whereas the potential of the valence band edge (E_V) must be more positive than the oxidative potential of a chemical species in order to photo-oxidize the chemical species (Litter, 1999). Energy levels in between the VB and CB are often referred to as traps or recombination centers, depending on the electron

life time in the state (Bahnemann et al., 1997). These sub-bandgap energy states are originated

from defects in the crystal structure of the semiconductor. By using time-resolved laser flash

photolysis on TiO_2, Bahnemann et al. (1997) classified the traps into shallow and deep traps, based

on the energy distance from CB. It was reported that the charge carrier recombination was fast in

shallow traps, and shallowly trapped holes exhibited high oxidation potential. In contrast, charge

carriers were long lived (~200 nanoseconds) in deep traps, and deeply trapped holes were

unreactive towards hole scavengers (Bahnemann et al., 1997). The redox potentials of the trapped

electrons or holes are inherently lowered compared to the CB or VB potentials. The trapping and

de-trapping of electrons in these sub-bandgap energy states play an important role in the charge

transport and recombination dynamics in polycrystalline and nanostructured semiconductors

(Hagfeldt and Gratzel, 1995).
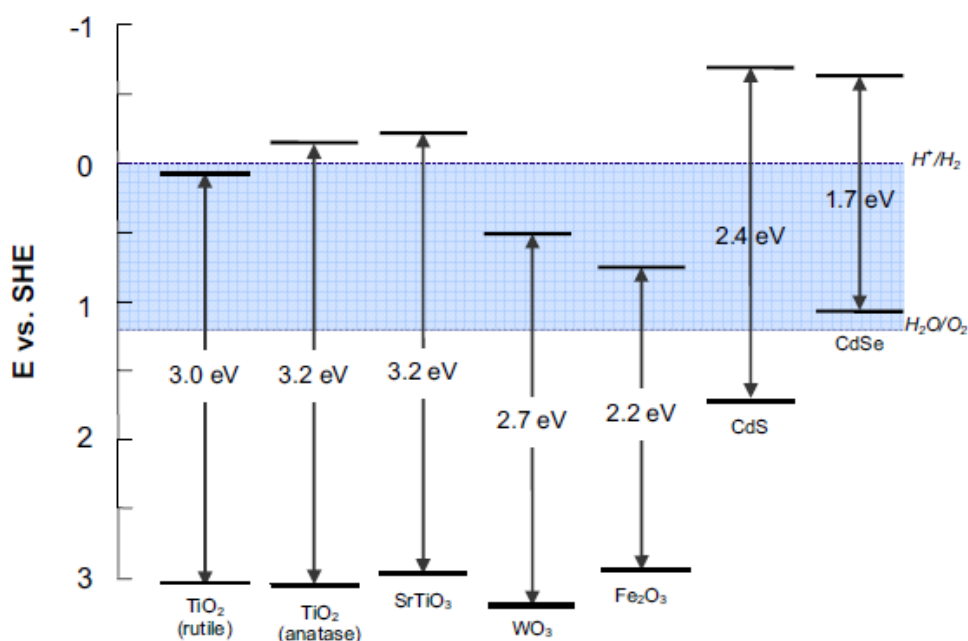
Figure 2.2. Band edge position for various semiconductors in contact with aqueous electrolyte at pH 0 (Serpone and Pelizzeti, 1989). The bandgap of TiO_2 in anatase allotropic form is approximately 0.2 eV higher than that of rutile.

Owing to the high E_v position (3.1 V vs. SHE), TiO$_2$ has a strong oxidation power and high photocatalytic reactivity toward different organics. This semiconductor is stable and does not suffer from chemical corrosion or photo-corrosion. Unfortunately, TiO$_2$ exhibits low absorption properties in the visible spectrum, as the large E_g requires wavelengths shorter than 400 nm for excitation. A great deal of research has focused on lowering the threshold energy for excitation of TiO$_2$ in order to harvest visible light for photochemical energy conversion (Asahi et al., 2001; Khan et al., 2002; Piera et al., 2003; Diwald et al., 2004). ZnO is another semiconductor that has large E_g. It is unstable in illuminated aqueous solution as it is preferentially oxidized by the photo-generated holes and releases Zn^{2+} ions (Bahnemann et al., 1987; Carraway et al., 1994; Sun et al., 2007). Zn(OH)$_2$ is formed on the particle surface and results in catalyst inactivation over time. Small bandgap semiconductors such as CdS, CdSe and Fe$_2$O$_3$ are excellent in utilizing solar energy. However, these materials lack the stability for catalysis in aqueous medium as they readily undergo photoanodic corrosion (Howe. 1998; Fisher et al., 1989; Kaesche, 2003). WO$_3$ has also been investigated as a potential photocatalyst but it exhibited lower photocatalytic activity than TiO$_2$ (Angelidis et al., 1998). Clearly, there is no semiconductor that fits the list of ideals. Despite its substantial limitation, TiO$_2$ appeared to be the most promising for photocatalytic oxidation of organic pollutants as it provided the best compromise between catalytic performance and stability in aqueous media.

2.3. The Photoelectrochemical Cell

A typical photoelectrochemical (PEC) cell consists of a cathode and a semiconductor photoanode fixed in an electrolyte solution as illustrated in Figure 2.3. Electron-hole pairs are

formed by irradiating the semiconductor, and electron transfer processes occur over the electrode/electrolyte interfaces. This disturbs the chemical equilibrium in the cell and creates a photo-voltage. The resulting current of electrons flows from the anode to the cathode via an outer circuit to complete the circuit. In a regenerative PEC cell such as Ru-bipyridyl complexes sensitized solar cell, a single active redox couple is present in the electrolyte, and no chemical reaction takes place in the system (Hagfeldt and Gratzel, 2000; Lindgren, 2004). On the contrary, different redox couples are active at the anode compared to the cathode in a non-regenerative PEC cell. The different redox couples give rise to a net chemical process in the electrolyte when the cell is illuminated with light of sufficient energy (Lindgren, 2004). The PEC cell for water splitting that was reported by Fujishima and Honda in 1972 is one of the examples of non-regenerative PEC cells. At the anode, oxidation of water occurs:

$$2H_2O + 4h_{VB}^+ \rightarrow 4H^+ + O_2 \tag{2.4}$$

At the cathode, electrons reduce protons $\left(H^+\right)$ to hydrogen $\left(H_2\right)$:

$$2H^+ + 2e_{CB}^- \rightarrow H_2 \tag{2.5}$$

The overall reaction is:

$$4hv + 2H_2O \rightarrow O_2 + H_2 \tag{2.6}$$

The operating principles of a photoelectrocatalytic process are similar to water splitting reactions in a PEC cell. Oxidation of organic compounds occurs at the photoanode, while the electrons reduce any electronegative species at the cathode. In both, the powder dispersion and immobilized system, the degree of charge recombination is high as their working potential is given by the open circuit condition. For the photoelectrocatalytic process, semiconductor films

supported on conducting substrates allow for biasing, thus avoiding charge recombination as encountered in unbiased systems.
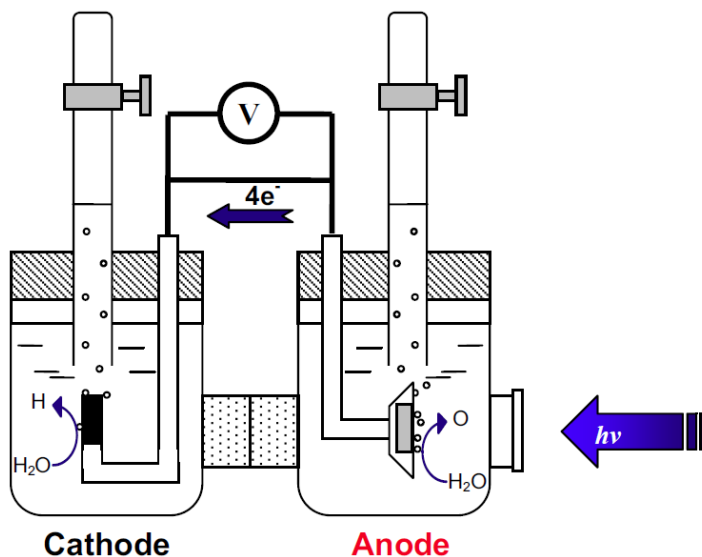
Figure 2.3. Schematic of photoelectrochemical cell for direct water oxidation. O_2 is formed at the anode (TiO_2) by oxidation of water, and H_2 is evolved at the cathode (Pt) by reduction of water (Hashimoto et al., 2005).

2.4. Space Charge Layers and Band Bending

When a bulk semiconductor, such as an ideal crystal, is immersed into an aqueous solution, interfacial charge transfer and formation of a double layer take place in the presence of an electroactive species. If the E_F of the semiconductor lies above that in solution, electrons flow from the inside to the surface to adjust the E_F of the semiconductor (Bard et al., 1991). At the thermodynamic equilibrium, the E_F of the semiconductor is shifted to the position of the redox potential in the solution. A space charger layer (depletion layer) is formed near the surface of the bulk semiconductor. As the semiconductor band edges are fixed, there is difference in potential

20

between the surface and the inside of the semiconductor. This phenomenon is known as band bending. Upon illumination, electrons would drift towards the bulk semiconductor in the direction consistent with the existing electric field, while the holes move in opposite direction to the semiconductor-electrolyte interface (Bard et al., 1991). Only holes are available for reaction at the semiconductor surface. The thickness of the space charge layer is in the order of 1×10^3 nm (Hashimoto et al., 2005). In the electrolyte, corresponding compensating charged layers are formed. The layer closest to the semiconductor surface is called the Helmholtz layer. It contains solvent molecules and ions or molecules that are specifically absorbed (Bard and Faulkner, 2000). Outside the Helmholtz layer is the Gouy-Chapman layer. This layer is made up of non-specifically adsorbed solvated ions (Bard and Faulkner, 2000). Figure 2.4 illustrates the three different situations for an n-type semiconductor in contact with an aqueous solution. Albery and Barlett (1984) derived the potential distribution in a spherical semiconductor particle using a linearized Poisson-Boltzmann equation. The potential difference between the centre of a semiconductor particle ($r = 0$) and a distance r is given by:

$$\Delta\phi_{SC} = \frac{k_B T}{6q}\left(\frac{r-(r_0-W)}{L_D}\right)^2\left(1+\frac{2(r_0-W)}{r}\right)$$ (2.7)

where $\Delta\phi_{SC}$ is the potential drop within the layer, W is the width of the space charge layer, q is the elementary charge, k_B is the Boltzmann constant, T is the temperature and L_D is the Debye length. For large semiconductor particles or planar electrodes, the potential drop over the space charge layer is given by (Bard et al., 1991):

$$\Delta\phi_{SC} = \frac{k_B T}{2q}\left(\frac{W}{L_D}\right)^2$$ (2.8)

Studies in single crystal TiO$_2$ electrodes were most active in the 1970s and early 1980s, when the research interest focused on the photoelectrolysis of water. Among the different facets, rutile (110) surface was extensively investigated as this surface was found to be the most stable thermodynamically (Charlton et al., 1997; Swamy et al., 2002; Lindsay et al., 2005). Other facets will reconstruct upon heating to high temperatures to produce (110) facets (Poirier et al., 1993; Carroll et al., 1994; Thomson and Yates, 2006). Generally, single crystal surfaces are expensive and not suitable for a wide range of applications because of the difficulty in fabricating them. However, it has been regarded that single-crystal semiconductor electrode materials are most likely to represent the ideal situation of the interfacial electron transfer processes (Hagfeldt and Gratzel, 1995; 2000). Early work employing a planar semiconductor for a dye-sensitized cell found that this type of electrode had poor light harvesting efficiency as only the first monolayer of adsorbed dye resulted in an efficient electron injection into the semiconductor (Hagfeldt and Gratzel, 1995).
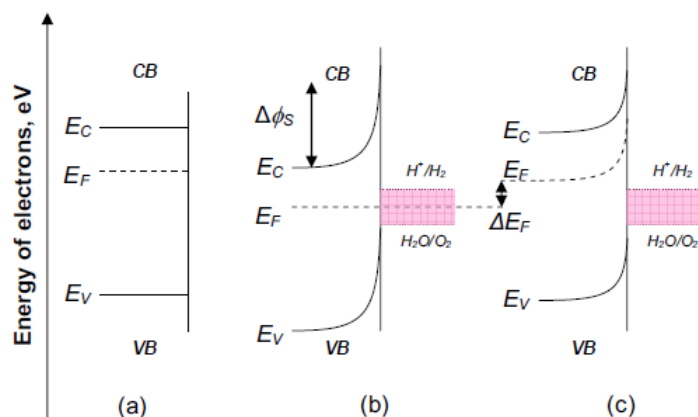
Figure 2.4. Space charge layer formation at an n-type semiconductor-aqueous solution interface (a) at flat band situation; (b) under dark, and (c) when expose to photons of energy higher than the E_g of TiO$_2$ (Lindgren, 2004).

There has been a rapid expansion of research in semiconductors with colloidal dimensions since Gratzel and co-workers published the first report on the light driven redox reactions with a nanocrystalline system in the early 1980s (Gratzel, 1981; Duonghong et al., 1981; Kiwi, 1981). The electronic property of nano-sized particulate semiconductor deviates from the bulk structure. The potential drop within each particle is described by the following equation (Hagfeldt and Gratzel, 1995):

$$\Delta\phi_{SC} = \frac{k_B T}{6q} \left(\frac{r_0}{L_D} \right)^2 \tag{2.9}$$

As the radius of the particle is extremely small, there is no substantial potential drop within the particle. The formation of electric field within the particle is dubious. High dopant levels are required to produce a significant potential difference between the surface and the center of the particle (Hagfeldt and Gratzel, 1995). Charge separation occurs within the particle via diffusion. Upon illumination, electron-hole pairs are oriented in a spatially random fashion along the optical path. These charge carriers would recombine or diffuse to the particle surface for chemical reactions. High efficiencies can be achieved if the diffusion of charge carriers to the particle surface can occur more rapidly than their recombination, followed by the fast removal of at least one type of charge carrier, i.e., either electrons or holes, upon their arrival at the interface (Hagfeldt and Gratzel, 1995, 2000). As both species of charge carriers are present on the surface, a careful consideration of both the oxidative and the reductive paths is required (Hoffman et al., 1995).

A nanocrystalline film is a porous structure built up from interconnecting semiconductor nanoparticles. These films are characterized by high porosity and a large internal surface area. When used as electrodes, the nanosized particles which constituted the films are in electronic contact, allowing for electric charge percolation through such films. This charge transport is

highly efficient, with the quantum yield being practically unity (Nazeeruddin et al., 1993; Hagfeldt et al., 1992). Band bending model from the bulk semiconductor breaks down as the aqueous solution penetrates the entire colloidal film up to the surface of the back contact and a semiconductor/aqueous solution junction exists at each nanoparticle (Soedergren et al., 1994; Franco et al., 1999; Hagfeldt and Gratzel, 2000). The charge separation and transport in a nanocrystalline semiconductor is far from fully understood. A qualitative model was proposed to describe the charge separation in nanocrystalline electrodes based on the results on charge separation measurements in TiO_2, CdS and CdSe films (Hodes et al., 1992; Hagfeldt et al., 1992). Upon illumination, the reaction that consumes holes (for TiO_2) at the interface is much faster than the reaction that consumes electrons and the recombination process. The electrons create a gradient in the electrochemical potential between the particle and the back contact. The driving force for the electron transport to the back contact is the concentration gradient of electrons over the nanocrystalline film. The most efficient charge separation takes place close to the back contact (Hagfeldt et al., 1992). The probability for the electron to recombine depends on the distance between the photo-excited particle and the back contact (Hagfeldt et al., 1992). In recent years, considerable interest has been shown in developing nanocrystalline films from colloidal semiconductors for dye-sensitized solar cells, photoconductors, electrochromic devices and photocatalytic degradation of organic contaminants (Hagfeldt and Gratzel, 1995).

2.5. Light-Induced Electron Transfer Processes

The initial process for TiO_2 photocatalytic oxidation of organic compounds is the generation of electron-hole pairs in the semiconductor particles. These charge carries may be trapped either in shallow or deep traps, and subsequently react with the electron donors or

acceptors adsorbed on the semiconductor surface, or within the surrounding double layer of the charged particle (Linsebigler et al., 1995; Hoffmann et al., 1995). By a combination of electron paramagnetic resonance (EPR) and infrared spectroscopy measurements, Berger et al. (2005) reported that photo-generated electrons are either trapped at localized states with the bandgap (Ti^{3+} centers) or promoted to CB, while photo-excited hole species was detected as O^-. Approximately 90% of photo-excited electrons were found to reside in the CB in TiO_2 (Berger et al., 2005). It has previously been shown that the photo-redox chemistry that occurs at the semiconductor surface is emanated from trapped electrons and trapped holes rather than from free valence band holes and conduction band electrons (Serpone et al., 1996). In the absence of suitable electron and hole scavengers, these charge carriers recombine directly through band-to-band recombination or indirectly via bulk or surface defects with the release of heat (Pichat, 2007). The recombination rate is affected by factors such as charge trapping, the chemisorptions or physisorption of target molecules and the incident light intensity (Thompson and Yates, 2006).

At the semiconductor-liquid interface, the oxidative pathways of organic compounds remain ambiguous and controversial. Photocatalytic oxidation of organics has been proposed to proceed directly via surface oxidation of adsorbate molecules by trapped holes or indirectly by the reactive oxygen species such as $OH^•$, $O_2^{•-}$, $OH_2^•$, H_2O_2, and HO_2^- (Caraway et al., 1994; Herrmann, 2001; Villarreal et al., 2004). Among the reactive species, $OH^•$ appears to be the predominant oxidant as it has the highest thermodynamic oxidation potential (+2.85 eV vs. SHE) (Oppelt, 1998). The $OH^•$ species are formed through the reaction of trapped holes with adsorbed H_2O/OH^- or the reaction of electrons with adsorbed oxygen molecules (Serpone, 1995; Bhatkhande et al., 2002). The existence of $OH^•$ was verified by electron spin resonance (ESR) detection (Riegel and

Bolton, 1995; Hirakawa and Nosaka, 2002; Ueda et al., 2003). Chemical identification of the hydroxylated oxidation intermediates in the system that consists of aromatic compounds, such as benzoic acid (Matthew, 1984), phenol (Trillas et al., 1992; Okamoto et al., 1985), 4-chlorophenol (Bahnemann et al., 1997; Mills et al., 1993) and herbicides (Parra et al., 2002) appears to support the hydroxyl radical mechanism. It was proposed that $OH^{\bullet}$ was responsible for the oxidative attack on the aromatic ring and $OH^{\bullet}$ can diffuse into the solution and subsequently oxidize weakly adsorbed organics (Gonzalez-Elipe et al., 1979; Turchi and Ollis, 1990; Parra et al., 2002).

In the meantime, the adsorption of organic compounds on TiO_2 surface is reported to be critical for direct hole oxidation mechanism. It was found that the degradation of carboxylic acids such as chlorobenzoic acid (Tahiri et al., 1998), oxalic acid, and trichloroacetic acid (Mao et al., 1991) were initiated by direct hole attack via a photo-Kolbe reaction. Carraway et al. (1994) also provided experimental evidence for the direct hole oxidation of tightly bound electron donors such as formate, acetate, and glyoxylate at the semiconductor surface. Ishibashi et al. (2000) estimated the quantum yield of $OH^{\bullet}$ production and hole generation to be $7x10^{-5}$ and $6x10^{-2}$, respectively. As the quantum yield of ordinary photocatalytic reactions are reported to be $\sim10^{-2}$, it was suggested that oxidative reactions on TiO_2 photocatalyst occur mainly via photo-generated holes but not via $OH^{\bullet}$ (Ishibashi et al., 2000). Despite the intense investigation, the findings did not permit the unambiguous delineation of the $OH^{\bullet}$ driven mechanism versus the direct hole oxidation mechanism. In many cases, similar reaction intermediates are expected from these two schemes in an aqueous system under an oxygen rich condition (Bahnemann et al., 1997). Besides, the mechanism of photocatalytic degradation of organic compounds could result from the integration of direct oxidation by holes with oxidation by radical groups, either on the surface or in the solution (Chen et al., 1999a; 1999b). Sun and Pignatello (1995) found that the initial step of photocatalytic

transformation of 2,4-dichlorophenoxyacetic acid was direct hole oxidation at pH 3. At other pH conditions, the reaction shifted to hydroxyl-radical-mediated mechanism. The direct and indirect deactivation paths of photo-generated electron-hole pairs are illustrated in Figure 2.5.
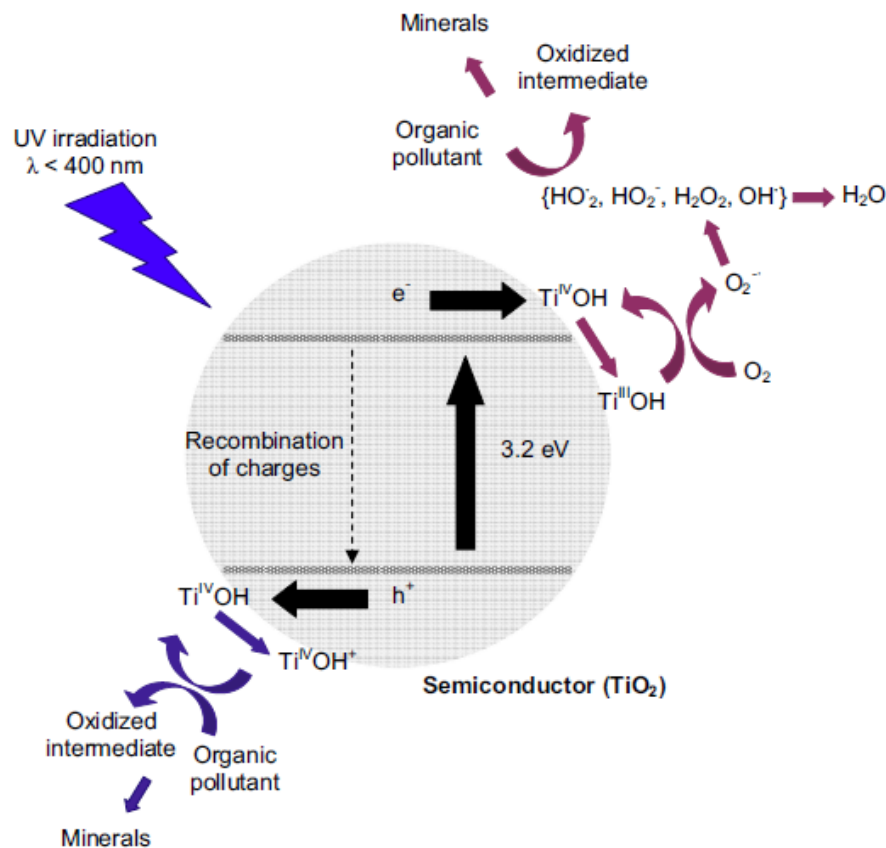
Figure 2.5. Direct and indirect oxidative pathways of organics on TiO_2 photocatalyst (Mills and Le Hunte, 1997).

The different interfacial transfer processes involving electrons and holes and their deactivation by recombination can also be summarized as a series of complex reactions (Equations 2.10-2.25) as follows (Serpone, 1995; Bhatkhande et al., 2002; Hufschmidt et al., 2004):

The excitation by photon (hv) with energy larger than E_g :

$$TiO_2 + hv \rightarrow e_{CB}^- + h_{VB}^+ \qquad (2.10)$$

Charge carriers trapping:

$$\{Ti^{IV}-O^{2-}-Ti^{IV}\}_{bulk}+h^{+}_{VB}\rightarrow\{Ti^{IV}-O^{\bullet-}-Ti^{IV}\}_{bulk} \qquad (2.11)$$

$$\{Ti^{IV}\}+e^{-}_{CB}\rightarrow\{Ti^{III}\} \qquad (2.12)$$
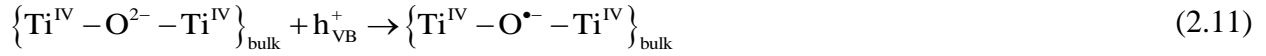
Interfacial electron transfer from adsorbed donor (R) and to adsorbed acceptor (M):

$$R_{ads}+h^{+}_{VB}\rightarrow R^{+}_{ads} \qquad (2.13)$$

$$M_{ads}+e^{-}_{CB}\rightarrow M^{-}_{ads} \qquad (2.14)$$

Charge carriers recombination:

$$e^{-}_{CB}+h^{+}_{VB}\rightarrow heat \qquad (2.15)$$

Formation of hydroxyl radicals:

$$\{Ti^{IV}-O^{2-}-Ti^{IV}\}-OH^{\bullet}_{abs}+h^{+}_{VB}\rightarrow\{Ti^{IV}-O^{2-}-Ti^{IV}\}-O^{\bullet}H_{abs} \qquad (2.16)$$

$$\{Ti^{IV}-O^{2-}-Ti^{IV}\}-OH_{2abs}+h^{+}_{VB}\rightarrow\{Ti^{IV}-O^{2-}-Ti^{IV}\}-O^{\bullet}H_{abs}+H^{+} \qquad (2.17)$$

$$H_2O+h^{+}_{VB}\rightarrow HO^{\bullet}+H^{+} \qquad (2.18)$$

$$HO^{\bullet}+R\rightarrow HO^{-}+R^{+} \qquad (2.19)$$
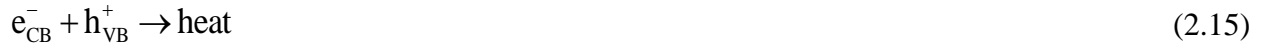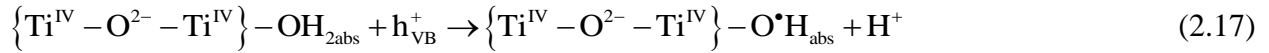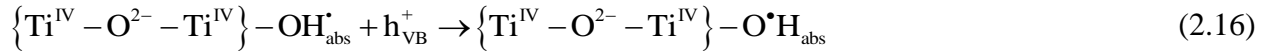
Formation of other peroxy species:

$$O_2+e^{-}_{CB}\rightarrow O^{\bullet-}_{2} \qquad (2.20)$$

$$O^{\bullet-}_{2}+H^{+}\rightarrow HO^{\bullet}_{2} \qquad (2.21)$$

$$O^{\bullet-}_{2}+HO^{\bullet}_{2}\rightarrow O_2+HO^{\bullet}_{2}\rightarrow H_2O_2 \qquad (2.22)$$

$$2HO^{\bullet}_{2}\rightarrow O_2+H_2O_2 \qquad (2.23)$$

$$H_2O_2+e^{-}_{CB}\rightarrow OH^{-}+OH^{\bullet} \qquad (2.24)$$

$$H_2O_2 + O_2^{\bullet -} \rightarrow OH^- + OH^{\bullet} \tag{2.25}$$
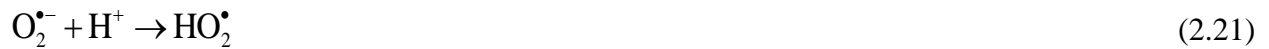
Extensive investigation have been carried out by several research groups (Choi et al., 1994; Serpone et al., 1995; Colombo and Bowman, 1995; Bahnemann et al., 1997; Berger et al., 2005) in order to identify the factors that govern the dynamics of interfacial electron and holes transfer reactions. According to Choi et al. (1994), the process of charge generation is very rapid and is in the order of femtoseconds (fs). By using UV/Vis absorption spectroscopy techniques, Colombo and Bowman (1995; 1996) found that the process of photo-generated electron trapping is in the order of 10^{-10} s. About 90% of the excited pairs may actually recombine within 10^{-9} s upon illumination (Colombo and Bowman, 1995; 1996). Choi et al. (1994) also found that shallow trappings of both holes and electrons took place in the order of 10^{-10} s while deep trappings of electrons required 10^{-8} s. Interfacial charge transfer was estimated to occur between 10^{-7} and up to 10^{-3} s (Choi et al. 1994). Such results highlight that the overall efficiency for interfacial charge transfer is determined by the competition between the recombination and the trapping of charge carriers, as well as by the completion between the recombination of trapped charge carriers and the interfacial charge transfer (Hoffmann et al., 1995; Henderson et al., 2003).

2.6. Reaction Kinetics

When investigating the kinetics of a photocatalytic reaction, there are series of elementary aspects that need to be considered. Among the aspects are mass transport onto catalyst surface, adsorption, electron-pair generation, charge transfer and desorption processes (Ilisz et al., 1999; Herrmann, 2005). The proposed reaction mechanism in a well-mixed powdered-dispersion photo-reactor is usually based on a reaction controlled by adsorption kinetics as mass transfer limitations

have been found to be negligible (Matthews, 1990; Bacsa and Kiwi, 1998). In general, the kinetics of photo-mineralization of organic substrates on steady state illumination fit a Langmuir-Hinshelwood (L-H) kinetic scheme (Ollis, 2005). As the L-H model is surface-area dependent, the reaction rate is expected to increase with irradiation time since less organic substrate will remain after increased irradiation time with higher surface availability. A zero rate of degradation is associated with total mineralization of the target contaminant. Numerous assumptions for the L-H saturation kinetics have been made, and in applying this approach for the determination of rate of photo-mineralization, any of this four possible scenarios is valid: (i) reactions take place between two adsorbed components of radicals and organics; (ii) the reactions are between the radicals in water and adsorbed organics; (iii) reactions take place between the radical on the surface and organics in water; (iv) reaction occurs with both radical and organics in water (Chong et al., 2009).

The L-H model was initially developed to quantitatively describe gaseous-solid reactions (Satterfield, 1970). It was later used by Ollis (1985) to describe solid-liquid reactions. This approach assumes that reactions take place at the surface of the catalyst particle. According to this model, the rate of reaction (r) is proportional to the fraction of surface covered by the substrate (θ):

$$r = -\frac{dC}{dt} = k_{LH}\theta \tag{2.26}$$

Langmuir's equation, which relates the surface coverage θ to the initial concentration of the substrate C, can be expressed as a function of the adsorption equilibrium constant K,

$$\theta = \frac{KC}{1+KC} \tag{2.27}$$

and replacing in Eq. 2.26, gives:

$$r = -\frac{dC}{dt} = k_{LH}\theta = \frac{k_{LH}KC}{1+KC}$$

(2.28)

k_{LH} is the true rate constant, which takes into account several parameters (Fernandez et al., 1995), such as the catalyst mass, photon flow efficiency, O_2 layer adsorbed on TiO_2. The value of k_{LH} is also found to exhibit a dependence on the flow rate, indicating mass transfer dependence (Turchi and Ollis, 1988). K is the L-H adsorption equilibrium constant, or the Langmuir constant. In photocatalytic studies the value of K is obtained empirically through a kinetic study in the presence of light, or it can be obtained using a linearized form of Eq. 2.28, where $1/r$ is plotted against 1/C:

$$\frac{1}{r} = \frac{1}{k_{LH}} + \frac{1}{k_{LH}KC}$$

(2.29)

C is the concentration of organic pollutant or substrate at time t. Applicability of Eq. 2.28 depends on several assumptions, which include: (i) the reaction system is in dynamic equilibrium; (ii) the reaction is surface mediated; (iii) the competition for TiO_2 active sites by the intermediates and other reactive oxygen species is not limiting (Chong et al., 2009).

Eq. 2.28 can be integrated to yield:

$$\ln\left(\frac{C_0}{C}\right) + K\left(C_0 - C\right) = k_{LH}Kt$$

(2.30)

where C_0 is the initial concentration of organic substrate and t is the irradiation time.

Eq. 2.28 will become zero order when the concentration C (mol L^{-1}) is relatively high, that is, larger than 5×10^{-3} (Herrmann, 1999), since KC > 1, in which case the reaction rate will be maximal. In the case of diluted solutions, C (mol L^{-1}) $< 10^{-3}$, KC becomes $\square$ 1, and the denominator of Eq. 2.28 can be neglected, thus turning it into an apparent first order reaction:

$$r = -\frac{dC}{dt} = k_{LH}KC = k_{app}C \qquad (2.31)$$

where k_{app} is the apparent rate constant of a pseudo first order reaction. Therefore, Eq. 2.30 can be simplified to a first order reaction when C_0 is small, in which case the resulting equation is:

$$\ln\left(\frac{C_0}{C}\right) = k_{app}t \qquad (2.32)$$

The apparent rate constant, however, is only served as a comparison and description for the photocatalytic reaction rate in the reactor system.

A lump-sum L-H saturation kinetics profile has also been used to simplify the approximation for a specific photocatalytic reactor system (Minero et al., 1996). In such an empirical lump-sum L-H approach, the degree of organics mineralization is actually expressed in terms of TOC (Eq. 2.33):

$$r_{TOC,0} = \frac{\beta_1[\text{TOC}]}{\beta_2 + \beta_3[\text{TOC}]} \qquad (2.33)$$

Eq. 2.33 allows the prediction of TOC degradation as a function of irradiation time. Similar reciprocal plots of $1/r$ against $1/[\text{TOC}]$ can be used to determine the empirical parameters β_1, β_2 and β_3 as in Eq. 2.29. The irradiation time taken to achieve the fractional degradation of TOC can

also be estimated when Eq. 2.33 is expressed as in Eq. 2.30. This empirical lump-sum approach is a useful tool for approximation of mineralization kinetics in a photo-reactor, provided that sufficient data is collected for the determination of rate parameters (Chong et al., 2010).

2.7. Parameters Influencing the Photocatalytic Process

There are many factors that can affect the reaction rate in a typical photocatalytic process. They can be classified generally into extrinsic and intrinsic parameters. The extrinsic parameters include the pH of the solution, the initial concentration of organics, the light intensity, the catalyst dosage, the temperature, the circulating flow rate, the oxygen flow rate and the presence of ions in solution (Litter, 1999; Basca and Kiwi, 1998; Surender et al., 1998; Xu et al., 1999; Hermann, 2005). The intrinsic properties of the photocatalyst such as the surface area (active site), the crystalline phase, and the porosity can also influence the photocatalytic performance considerably.

2.7.1. Extrinsic Parameters

The incident light intensity (ψ) determines the rate of electron-hole pairs generation, which consequently influences the electron-hole pair concentration on an illuminated semiconductor. For a powdered dispersion system, degradation rates have been found to be proportional to ψ^1 at low intensity, and to $\psi^{0.5}$ at high intensity (Al-Sayyed et al., 1991; Chen and Ray, 1999). The square root dependence of the reaction rate at high intensity is attributed to the enhanced electron-hole recombination.

The pH of the solution has been found to have a number of significant effects on the photocatalytic degradation of organics. Due to the amphoteric nature of TiO_2, hydroxyl groups on

the semiconductor surface can undergo protonation or de-protonation depending on the pH, as follows (Kormann et al., 1991):

$$\square\text{-TiOH}_2^+ \leftrightarrow \square\text{-TiOH} + \text{H}^+ \left(\text{p}K_{a1}^s\right) \tag{2.34}$$

$$\square\text{-TiOH} \leftrightarrow \square\text{-TiO}^- + \text{H}^+ \left(\text{p}K_{a2}^s\right) \tag{2.35}$$

where $\square$-TiO$_2$ represents the "titanol" surface group and $\text{p}K_{a1}^s$ and $\text{p}K_{a2}^s$ are the acid dissociate constants. From a previous study, $\text{p}K_{a1}^s$ and $\text{p}K_{a2}^s$ were reported to be 4.5 and 8.0, respectively, to yield a zero charge potential pH, $\text{pH}_{zpc} \left(\text{pH}_{zpc} = \left(\text{p}K_{a1}^s = \text{p}K_{a2}^s\right)/2\right)$ value of 6.25 (Kormann et al., 1991). The pH_{zpc} value would vary for different samples of TiO$_2$. Below pH_{zpc}, a net positive charge accumulates on the TiO$_2$ surface due to the increasing fraction of the total surface species that are present as $\square$-TiOH$_2^+$, while at a high pH the surface has a net negative charge due to a significant fraction of the total surface sites being present as $\square$-TiO$^-$ (Kormann et al., 1991). The effect of pH on the reaction rate can be interpreted in terms of electrostatic interactions between the charged TiO$_2$ surfaces and the organics. For organics that undergo de-protonation/protonation reactions, the change in pH will influence their adsorption quantity as well as the surface complexation modes. In addition, the pH also changes the band edge energy or flat band potential, E_F of TiO$_2$ in solution. The E_F follows Nernstian pH dependence and decreases by 59 mV per pH unit (Ward et al., 1983). This changes the redox potentials of the photo-generated electrons and holes in the conduction and valence bands. In a slurry type reactor, there has been evidence that the pH has an influence on the dispersion stability, and therefore the observed photo-degradation rates (Dyk and Heyns, 1998). The pH of the solution has also been reported to affect the stability of photocatalyst that is immobilized on a support. It was found that the coated film

showed excellent stability in the range of pH 2-9. Outside this pH range, the coating became unstable and was stripped off the glass support (Haarstrick et al., 1996).

Dissolved oxygen plays an imperative role in the overall photocatalytic reaction. In the absence of any highly electronegative species, adsorbed O_2 molecules scavenge electrons from TiO$_2$ surface to form O_2^- (Szczepankiewicz et al., 2000; Xiao-e et al., 2000; Berger et al., 2005). Gerischer et al. (1992; 1993) analyzed the photooxidation kinetics of organic molecules on the powdered TiO$_2$ dispersion and found that the rate of photooxidation is equal to and limited by the reduction rate of the dissolved oxygen in the solution. According to their findings, if O_2 is not reduced at a sufficiently high rate, electrons accumulate on the photocatalyst particles, and the rate of recombination is enhanced until the sum of the electron-hole recombination and the electron transfer to O_2 is equal to the rate of the hole photo-generation (Gerischer, 1993; Gerischer and Heller, 1992). Berger et al. (2005) showed that an additional of ~83% O_2^- was produced as photo-generated electrons were transferred to O_2 during irradiation. Unlike the photocatalysis reaction, the efficiency of photoelectrocatalysis is less dependent on the dissolved oxygen concentration, due to the retarding effect of applied potential on electron-hole recombination. Kim and Anderson (1994) reported that photoelectrocataltytic systems could be used in anaerobic conditions as the electrons reduce any available species on the cathode. The presence of oxygen also enhances the formation of superoxide radical $O_2^{\bullet-}$. As mentioned earlier, this radical is capable of attacking other organic molecules and could function as an alternative source of surface bound hydroxyl radicals upon protonation (Fox and Dulay, 1993).

Dissolved ions in solution can significantly affect the photocatalysis process (Abdullah et al., 1990; Fernandez-Nieves et al, 1999; Chen et al, 1997; Lu et al, 1999; Beydoun et al., 2002;

Lam et al., 2005). As a consequence of competitive adsorption on the photo-activated reaction sites, and for photo-generated holes, the presence of sulphate, chloride and phosphate ions, even at a concentration of 1 mM, can reduce the rate by 20 to 70% (Abdullah et al., 1990). For example, Abdullah et al. (1990) reported that chloride ion interacts with photo-generated holes to generate chlorine radicals which do not initiate any oxidation reactions of the pollutant. Transition metal ions such as Fe^{3+} and Cu^{2+} have also been found to induce significant effect on photocatalytic reactions. Beydoun et al. (2002) reported that the presence of 5 mM Cu^{2+} improved the photocatalytic oxidation of sucrose by 3 times compared to the oxidation by the pure TiO_2 system. The enhancement was attributed to electron trapping by the Cu^{2+} $\left(Cu^{2+} + e^- \rightarrow Cu^+ + e^- \rightarrow Cu \right)$ which subsequently quenched the recombination reaction as well as to homogeneous reactions such as photo-redox cyclic and photo-Fenton type reactions (Beydoun et al., 2002). Lam et al. (2005) found that Fe^{3+} enhanced the photochemical and photocatalytic oxidation of resorcinol. $OH^{\bullet}$ was said to yield from Fe(III) hydroxo-complex and advanced the oxidation of the organic (Lam et al., 2005).

2.7.2. Intrinsic Parameters

TiO_2 can exist in either amorphous or crystalline form. The crystalline TiO_2 has three polymorphs, namely anatase, rutile, and brookite (Gamboa and Pasquevich, 1992; Yang et al., 1997). Upon heating, the metastable forms, brookite and anatase, transform exothermically and irreversibly to the stable rutile form. The photocatalytic activity of anatase has been extensively studied. In general, it is usually assumed that anatase is more photocatalytically active than rutile (Chhabra et al., 1995; Basca and Kiwi, 1998), although there is some evidence that this is not always the case. Domenech (1993) has shown in his study that a rutile sample is a better

photocatalyst than anatase for the oxidation of cyanide. Abe et al. (2001) also claimed that rutile is more active than anatase towards the oxidation of water. In many photoelectrochemical studies of TiO_2, no clear distinction is made between the behavior of anatase and that of rutile. When the inferior role of rutile is observed, it is often related to the lower concentration of surface hydroxyl groups. The surface hydroxyl group is responsible for the adsorption of oxygen in TiO_2. Oosawa and Gratzel (1984; 1988) have previously shown that by removing the surface hydroxyl on TiO_2 through calcinations, the photocatalytic generation of oxygen could be increased significantly compared to the uncalcinated sample. Given that oxygen adsorption is required to trap the photoelectrons during photocatalysis, the low hydroxylation in rutile would result in higher recombination of electron-hole pairs compared to anatase, and therefore, produce lower quantum efficiency.

In applied catalysis, a high surface area is beneficial as it provides higher concentration of active sites per square unit, which generally leads to superior reactivity (Abrahams et al., 1985). In the case of TiO_2, the number of active sites is taken as the product of the surface density of OH groups and the specific surface area (Mills and Le Hunte, 1997). Physical gas adsorption is normally the technique of choice to measure the surface area of TiO_2 powder. However, the actual surface area of the TiO_2 photocatalyst dispersed in solution will also depend on the degree of aggregation. Although all the surface sites occupied by the hydroxyl groups might not be necessarily active, Kobayakawa et al. (1990) had pointed out that the concentration of $OH^\bullet$ is closely related to the density of surface hydroxyl groups.

2.8. Applications and Commercially Available Photocatalytic Processes and Products

Most of the early work on photocatalysis focused on the use of semiconductors in the powdered dispersion form. As a result, extensive work on the synthesis of TiO_2 photocatalyst has been carried out by different groups. Predictably, different samples of TiO_2 exhibit different photocatalytic activities towards the same organic substrate under otherwise identical experimental conditions (Mills and Sawunyama, 1994; Serpone et al., 1996). Variances in morphology, crystal phase, specific surface area, particle aggregate size and surface density of OH groups in the TiO_2 samples are attributed to such differences in activity (Mills and Le Hunte, 1997). By common consent, a standard form of TiO_2 is needed such that general findings of one group can be related to another. Degussa P25 is a commercially available TiO_2 sample. Owing to its high photoactivity towards a wide range of organic substrates, it has been set as the standard for photonic efficiency comparison for various photocatalyst (Serpone et al., 1996; Serpone, 1997; Ohtani, 2008). The material is produced from high temperature (1200 C) flame hydrolysis of $TiCl_4$ in a stream of hydrogen and oxygen. It consists of non-porous crystals of anatase and rutile in a ratio of 80:20 (Mills and Le Hunte, 1997). It is manufactured for use as a thermal stabilizer for heat resistant silicone rubber (Fujishima et al., 1999). Other commercially available photocatalyst include the ST series, produced by Ishihara Sakai Chemical Industries, and Hombikat UV100, supplied by Sachtleben Chemie.

There are several companies that promote semiconductor photocatalysis as a method for water purification and also provide commercial scale photo-reactor systems for such application. For example, Purifics Environmental Technologies Inc. is a Canada-based water purification company which supplies industrial photocatalytic treatment systems to remediating ground water. Their Photo-Cat ® system utilizes TiO_2 in the form of powdered dispersion and operates at pH 3

or lower to avoid iron fouling (Purifics ES Incorporated: 15/06/2008: Photo-Cat). The TiO_2 powder is recovered via a proprietary filtration system. The use of powdered TiO_2 dispersions in commercial photo-reactors is attractive because such dispersions are cheap, very effective, and easy to replace. However, a method of filtration is required to allow for the separation of photocatalyst and the purified effluent. This step is no easy task, and has restricted the widespread application of this technology for water treatment.

In recent years, there is a growing interest in the use of thin, transparent TiO_2 films for the photo-destruction of thin organic films. Such TiO_2 films need to be clear, adherent and photoactive. In order to obtain such TiO_2 films, the particles used must be smaller than the wavelength of visible light, typically less than 30 nm. This largely rules out the use of Degussa P25 particles, which have aggregate particle diameters of approximately 0.1 μm. Numerous research groups have developed several methods for creating such films. It usually involves a sol-gel process in which a titanium alkoxide is hydrolyzed, coated onto a glass substrate, and subsequently calcinated at high temperature (~500 C) for a short period. The thickness of the film is usually in the range of 100 nm. In addition to being photocatalytically active, these films are also capable of photo-induce super-hydrophilicity. Upon ultra-bandgap irradiation, the surface properties of the TiO_2 film are altered and it becomes exceedingly hydrophilic. As a consequence, water droplets cannot form on the film, but spread across its surface. These films have an anti-fogging action.

TOTO is a major ceramics company in Japan that appears to be one of the pioneers in applying super-hydrophilic photocatalyst technology to their products. These products are commercialized under the name of Hydrotech TM. The procedure consists on depositing the TiO_2 photocatalyst onto a thin plastic film before being applied onto mirrors or tiles (TOTO Limited:

20/06/2008: Principle of Hydrotech Technology). Murakami Corporation is another Japanese company that supplies TiO_2 coated mirrors. A layer of TiO_2 is coated onto a porous silica film. The silica layer is highly hydrophilic but tends to lose this property over time as stains are deposited. The function of the TiO_2 underlayer is to photo-degrade any organic material that may deposit onto the surface of the film, thus preserving the overall hydrophilic nature of the coating (Murakami Corporation: 21/06/2008: Hydrophilic Clear Mirror). There are also a few companies that supply TiO_2 coated self-cleaning glass, such as Activ TM, produced by Pilkington Glass, and SuncleanTM, supplied by Pittsburgh Plate Company. Most of above mentioned companies employ a chemical vapor deposition method to prepare their TiO_2 coatings.

In addition to the previously discussed applications, Matthews et al. (1990) described a method which uses TiO_2 photocatalyst to convert organic carbon to CO_2 in order to determine the amount of organic carbon in water. Based on the same concept, Fox and Tien (1988) also reported a flow-through TiO_2/Pt photochemical detector suitable for attachment to a high-pressure liquid chromatograph for the detection of oxidizable functional groups. More recently, photoelectrochemical methods to determine chemical oxygen demand have been developed based on the principles of photocatalysis and photoelectrocatalysis (Kim et al., 2000; Zhao et al., 2004).

2.9. Preparation of TiO_2 Films

Creating TiO_2 films onto the surface of various substrates has been done by many research groups. Often, the immobilization technique and the post immobilization heat treatment determine the crystal structure, crystallinity, particle size and surface hydroxyls of the TiO_2 films produced, which in turn establishes the photocatalytic properties of the catalyst. The different techniques used are summarized in the following section:

2.9.1. Powder Films

Pre-synthesized TiO_2 powders can be deposited on a substrate using "doctor Blading" method. In this method, separately made photocatalyst such as Degussa P25 is ground in a mortar in a mixture of water, acetyl acetone and surfactant to obtain a well-dispersed colloidal sol (Cao et al., 1996). The colloidal sol is then dropped on a substrate and spread with a glass rod to give a thick TiO_2 film. Scotch tape is usually used as spacer to adjust the thickness of the film. The air-dried film is then sintered to improve the adherence and conductance of the particles onto the substrate. This procedure is relatively simple and has been adopted widely to prepare TiO_2 electrodes for dye-sensitized solar cells. However, such films are usually not mechanically robust and be easily removed by rubbing or by applying the 3M Scotch Tape test, and thus highly unsuitable for photocatalytic applications (Mills and Le Hunte, 1997). Besides, the optical opacity of TiO_2 powder films renders them unsuitable for many of the current commercial applications such as transparent photoactive coatings on glass or ceramics.

Pre-synthesized TiO_2 can also be deposited onto a substrate by electrophoretic deposition (EPD). In this technique, charged particles in a suspension of electrolyte, particles, additives and solvent are moved toward an oppositely charged electrode and are deposited onto a substrate under an applied DC electric field (Byrne et al., 1998; Yum et al., 2005). The films obtained from this method are reproducible. This technique is particularly useful when the substrate is susceptible to high temperature thermal treatment. Other advantages of EPD include its low cost, the fact that it is relatively fast and reproducible, and its potential for use in continuous processing.

An alternative method for TiO_2 immobilization presented in the literature refers to the deposition of pre-synthesized TiO_2 on a porous substrate like silica gel or quartz by preparing a

suspension with Degussa P25 and water through sonication for a few minutes, followed by wet deposition on the target substrate. Then, the substrate is dried at high temperature (~500 °C) for an hour, till the TiO_2 has anchored (Bideau et al., 1995, Vinodgopal and Kamat, 1995).

2.9.2. Chemical Vapor Deposition

Chemical vapor deposition (CVD) is a generic name for a group of processes that involve depositing a solid material from a gaseous phase. During the process, a volatile compound of the substance to be deposited is vaporized and the vapor is thermally decomposed or reacted with other gases, vapors or liquids to yield a non-volatile reaction product which deposit onto the supports (Rice, 1987; Jung et al., 2005; Murakami et al., 2004). The supports are normally held at an elevated temperature (800 °C – 1150 °C), and the deposition chamber is maintained at a reducing atmosphere (Jung et al., 2005; Rice, 1987; Murakami et al., 2004). Flow rate, gas composition, deposition temperature, pressure, deposition chamber geometry, are the process parameters by which deposition can be controlled to have the desired characteristics (Shinde and Bhosale, 2008). As CVD is capable of depositing high quality thin films without post-annealing for crystallization, this method is employed commonly in the industry for the deposition of TiO_2 films on glass supports. In addition, this process is able to evenly coat variable shaped surfaces such as screws threads, blind holes or channels or recesses, without build-up on edges (Kempster: 01/07/2008: Recent Development in Chemical Vapor Deposition). CVD is also claimed to be less costly than their wet counterparts due to the expensive precursors (i.e. metal alkoxides) used in the wet chemical precipitation methods (Ying and Sun, 1997). Despite its advantages, CVD often involves dealing with toxic and corrosive gases, and it also has to be carried out at relatively high temperatures, therefore limiting its application only onto supports that can tolerate such conditions.

2.9.3. Oxidation of Ti Metal

Due to the reactive nature of titanium, a natural oxide film normally forms on the metal. The thickness of this oxide layer ranges from 5 to 70 Å, depending on the composition of the metal and the surrounding medium (Aladjem, 1973). The formation mechanism of anodic oxide films starts with the development of an adsorbed layer of oxygen on the metal surface. The formation of the oxide layer is preceded by the electric charging of the double layer at the metal-electrolyte interface (Young, 1961; Yahalom and Zahavi, 1970; Aladjem, 1973). The oxide growth involves field-assisted migration of Ti^{2+} ions through the oxide films. Both Ti^{2+} and O^{2-} contribute simultaneously to the growth at the oxide solution interface (Yahalom and Zahavi, 1970; Ammar and Kamal, 1971a; 1971b). The growth behaviors and properties of the oxide layer are critically influenced by electrochemical parameters (Sul et al., 2001). The increasing thickness of the oxide layer results in the systemic changes of the surface topography, particularly in the surface pore configuration (Jeong, 1993). The role of the electrolyte in this formation mechanism has been studied in detail. It is generally accepted that the nature of the anions influences both the chemical composition (Tabrizi, 1989) as well as the crystal structures of the TiO_2 (Mattsson and Rolander, 1985; Arsov et al., 1991; Fonseca et al., 1995).

2.9.4. Sol-Gel Technique

The sol-gel technique is one of the most common for preparing TiO_2 films. This process generates inorganic oxides via gelation, precipitation or hydrothermal treatment (Ying and Sun, 1997; Niederberger, 2007). The main step in this process involves the hydrolysis of a precursor material, such as a metal alkoxide or an inorganic salt, to form oxides. The reaction between the precursor material and water results in the formation of a M-OH bond:

$$Ti\text{-}(OR)_4 + H_2O \rightarrow (RO)_3\text{-}Ti\text{-}OH + ROH \qquad (2.36)$$

Once the OH groups are created, propagation occurs through a polycondensation process producing condensates (Gopal et al., 1997). The three competitive mechanisms of condensation are summarized as follows:

Olation
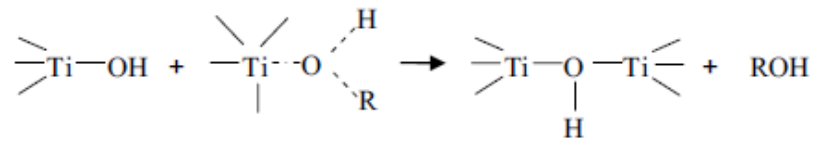
Alcoxolation
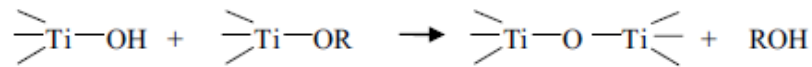
Oxolation

A heat treatment step is usually required to transform the amorphous oxide formed into a crystalline form. By varying certain parameters during the hydrolytic condensation, one can change the kinetics of the reactions that form the molecular structure (Sullivan and Cole, 1959; Yoldas, 1982; Schubert, 2005). This allows for the tailoring of certain desired structural characteristics, such as compositional homogeneity, grain size, particle morphology and porosity (Ying and Sun, 1997). These parameters include the type of metal alkoxide (alkyl groups in the

alkoxide), the amount of water (R value = H_2O/metal alkoxide mole ratio), pH (catalyst), concentration of metal alkoxide (molecular separation by dilution), aging and the reaction temperature (Yoldas, 1984).

The main advantage of the sol-gel technique is that it allows extremely uniform mixtures of different colloidal oxides to form a sol or a gel that is homogeneous on a molecular or nanometer scale. The other motivation for sol-gel processing includes higher purity products, and lower processing temperatures, when compared to CVD. The process also permits to generate nanocrystalline materials with little capital investment (Ying and Sun, 1997; Niederberger, 2007). However, the sol-gel technique requires long processing times, and is prone to shrinkage of products during drying and sintering.

Considerable effort has been extended to understand the reaction mechanisms involved during the different processes used for preparing TiO_2 films, and to identify key experimental parameters which can be manipulated to control these systems.

3

Experimental Phase

This section describes the equipment, materials and methods used during the laboratory experimental phase of the research. In this chapter, the following topics are discussed in detail:

- Description of the photocatalytic treatment system, including characteristics and components of the bench-scale tubular reactor, UV-C source and peristaltic pump.

- TiO_2 photocatalyst deposition on granular silica gel by the selected sol-gel technique.

- Experiment design and methodology for evaluation of the following system characteristics:

  o TiO_2 uniformity and stability

  o Reactor maximum efficiency

  o Effect of intrinsic and extrinsic parameters (mass and size of silica gel, number of photocatalyst coats, aeration, initial contaminant concentration, conductivity and pH) on contaminant photo-degradation.

An introductory section briefly describing the preliminary research leading to the final system design has also been included.

3.1. Preliminary Research

Initial stages of the present research focused on defining the objectives of the project and accordingly selecting the type of treatment process for experimental development. Aiming to investigate the effectiveness and efficiency of an advanced TiO_2-based oxidation technology on

hydrocarbons-contaminated wastewater, photoelectrocatalysis was initially researched owing to its apparent simplicity and superior efficiency in comparison to more conventional methods like photocatalysis and catalytic/chemical oxidation. Several attempts to carry out the proposed project were made during a research phase that extended for approximately 2 years, from the fall of 2011 until mid-2013, including the fabrication of the photoelectrocatalytic bench-scale reactor shown in Figures 3.1 a and b.

The design and construction of a photoelectrocatalytic rectangular batch reactor with recirculation made of UV-resistant acrylic laminate began in September of 2011. Titanium plates 305 mm x 355 mm x 6 mm were used as the cell electrodes, and an electric voltage applied from a regulated DC power supply. The source of photons consisted in three UV-C lamps centrally aligned along the longitudinal axes of the vessel and encased in high-transparency quartz sleeves. 6 liters of bulk liquid would be recirculated horizontally through 4 evenly spaced inlet/outlet ports using a peristaltic pump, as seen in Figures 3.1 a and b.
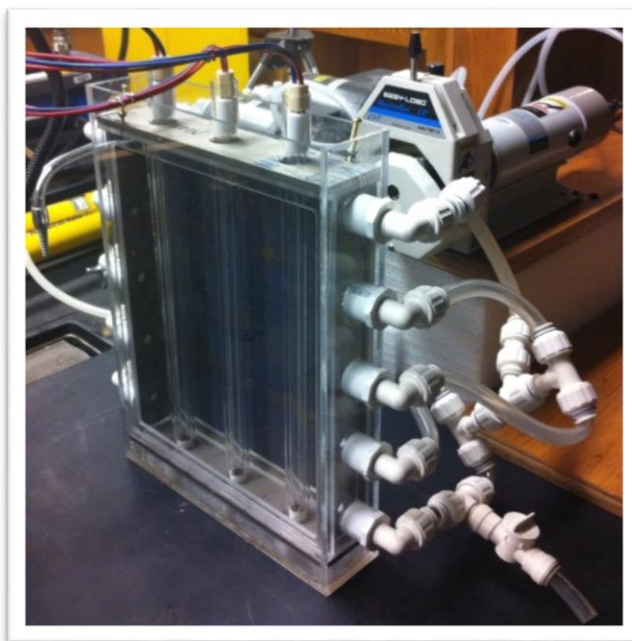
Figure 3.1.a. Photoelectrocatalytic bench-scale reactor
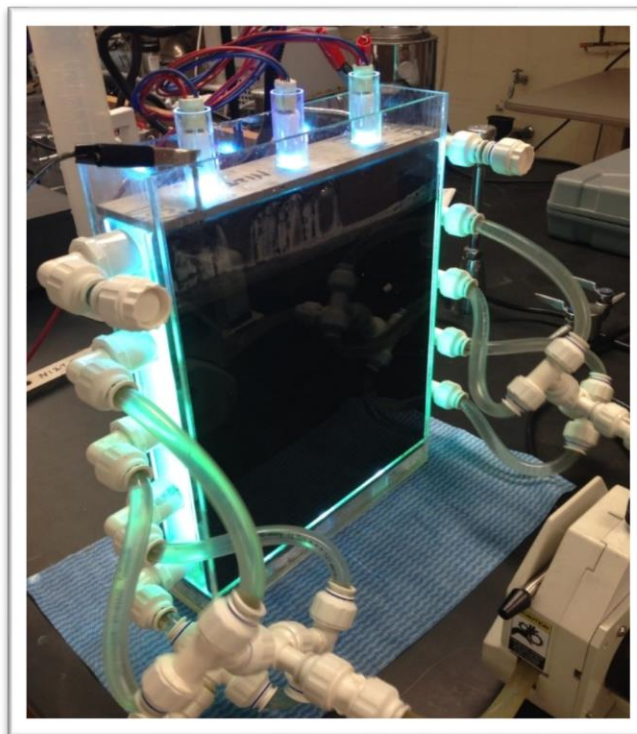
Figure 3.1.b. Photoelectrocatalytic bench-scale reactor

It was thought that by coating the titanium plates with a film of TiO_2, catalyst would be activated by the UV irradiation from the lamps, while the applied electric potential would impede recombination of the photo-generated electron-hole sites. Initially, TiO_2 was deposited sequentially onto the plates by spray pyrolysis using a 15% w/w anatase aqueous dispersion provided by US Research Nanomaterials Inc. The resulting catalyst coat, depicted in Figure 3.2, showed poor adherence to the metal surface during photoelectrocatalytic experiments, falling off after few hours of use. Next, a different method consisting in direct TiO_2 synthesis on the metal surface by a hydrothermal process (Mali et al., 2011) was attempted. According to this method, the metal plates were placed in a Teflon®-coated container, covered with a $TiCl_4$/ethanol/HCl/HNO_3/NaCl precursor solution and heated at 120°C for 3 hours, as shown in Figure 3.3. The procedure could not be completed due to the decomposition of Teflon® at high temperatures and low pH.

Figure 3.2. Titanium plate coated by spray pyrolysis.

Figure 3.3. Teflon® tray containing titanium plate submerged in precursor solution.

Finally, it was decided to leave the metal plates uncoated and add the catalyst in the form of anatase nano-powder directly to the bulk liquid in an attempt to use the reactor as a photocatalytic system. The results obtained from several experiments showed low catalyst efficiency possibly due to insufficient photon supply. This reactor was abandoned in early 2013.

Later that year, the construction of the stainless steel tubular reactor described in Section 3.2 was started. This reactor was initially conceived as a photoelectrocatalytic system, with the original design including a UV bulb encased in a TiO_2-coated electrically conducting quartz sleeve. An electric potential would be applied to the conductive glass by a DC power supply. Attempts were made to apply fluorine-doped-tin-oxide (FTO) conducting coatings onto the quartz support by spray pyrolysis according to the method described by Shinde et al. (2008). A stannic chloride pentahydrate/ammonium fluoride precursor was sprayed onto the clean quartz sleeve through a nozzle using compressed air as carrier gas. Next, using the same application technique, a TiO_2 thin film synthetized from a titanium (iv) isopropoxide/isopropanol mixture would be deposited onto the conductive support, as explained by Ayieko et al. (2012). By following this procedure, it was not possible to reproduce the results reported in the literature. The coated quartz surface never reached the conductivity necessary for the intended application, forcing to reengineer the existing reactor design, which later resulted in the definitive photocatalytic treatment system described in the following sections.

3.2. Photocatalytic Treatment System

The photocatalytic treatment system designed and constructed for the present research consists of a stainless steel tubular batch reactor equipped with a concentric UV-C lamp, shown in Figure 3.4.a and 3.4.b. During operation, a bed of silica gel particles coated with TiO_2 is fluidized

uniformly throughout the bulk liquid in the reactor by means of fluid recirculation. Phenol was selected as the model contaminant, and its degradation rate under different operational conditions was measured using chemical oxygen demand (COD) as indication of pollutant concentration.

The selection and design of the photocatalytic reactor was made considering ease of implementation and light distribution uniformity across the bulk. Stainless steel 316 was used for all parts of the reactor, and it consists of a vertical tube 457 mm long, 50.8 mm inside diameter and 800 ml total capacity. The photon source is a UV-C lamp (LMP-GPH436T5L/HO/4PSE) with a nominal output of 120 μW cm^{-2} at 254 nm. It is placed concentrically inside the reactor and encased in a high clarity quartz sleeve of 25.4 mm external diameter. The resulting annular area of the reactor is 1.6×10^{-3} m^2.

The irradiated length, which corresponds to the arc section of the lamp submerged in liquid is 375 mm, then yielding an effective or irradiated volume of 600 ml.
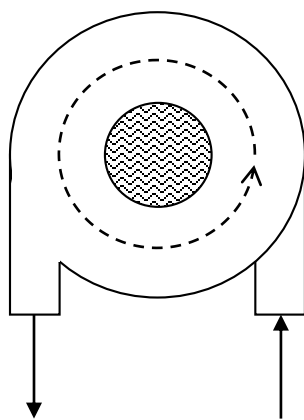
Figure 3.4.a. Plan view of the photocatalytic reactor showing the placement of inlet and outlet ports, and fluid circulation pattern.
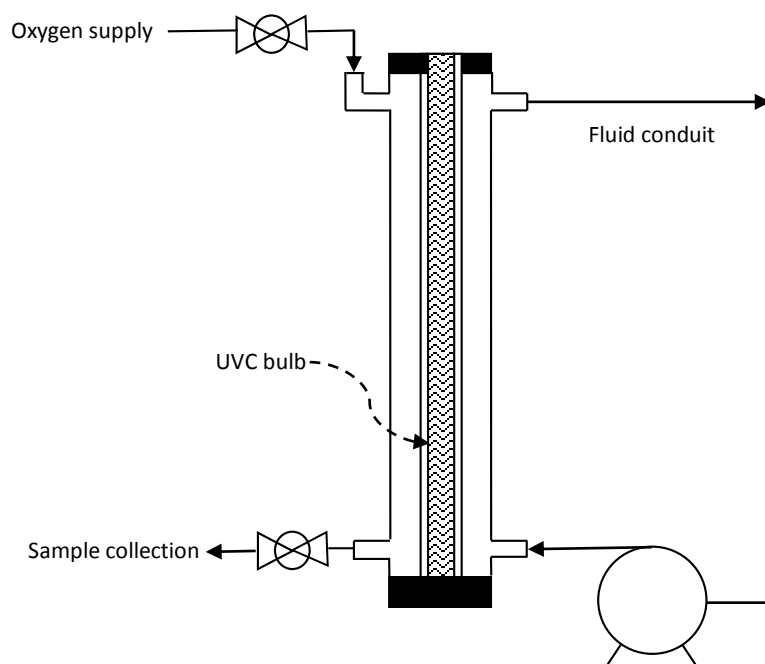
Figure 3.4.b. Elevation view of the photocatalytic treatment system showing the placement of inlet, outlet and oxygen supply ports, and fluid conduits.

Table 3.1 shows a summary of the fixed characteristics and operational parameters of the reactor, such as irradiance and radiant flux, of the photocatalytic treatment system.

Table 3.1. Characteristics and operational parameters of treatment system

Parameter		Parameter	
Reactor inside diameter	50.8 mm	Irradiated length (L_R)	375 mm
Bulb case outside diameter	25.4 mm	Irradiated surface area (A_R)	14962 mm^2
Annular area	1600 mm^2	Irradiated volume (V_R)	600 ml
Annular area width	12.7 mm	Irradiance at A_R (E_R)	25 mW cm^{-2}
Total volume (V_T)	800 ml	Radiant flux at A_R (Φ_R)	3740 mW

The intensity of irradiated UV-C light perpendicular to the surface of the lamp as measured with a UV sensor (Cole Parmer Digital Radiometer UVX-25) is shown in Figure 3.5.
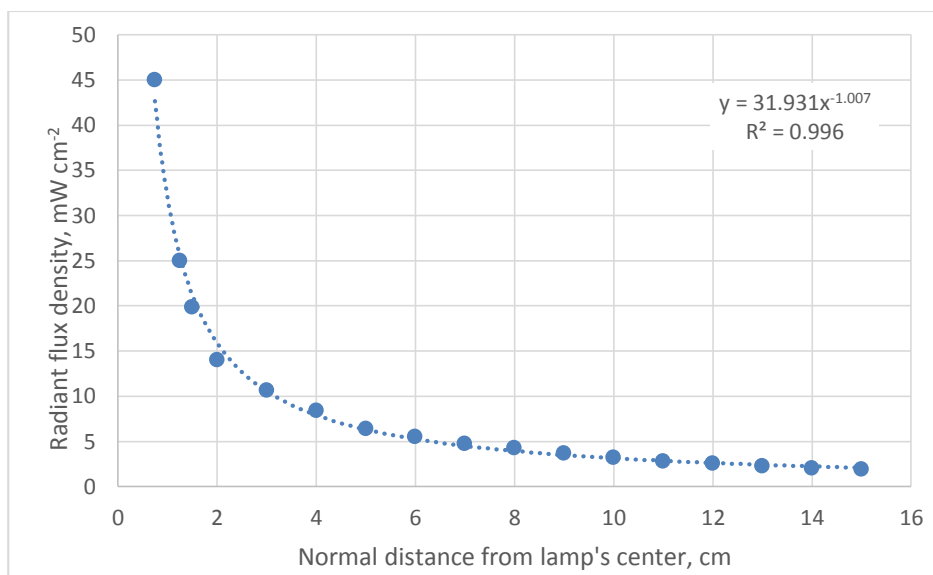
Figure 3.5. Irradiance profile of UV lamp at 254 nm
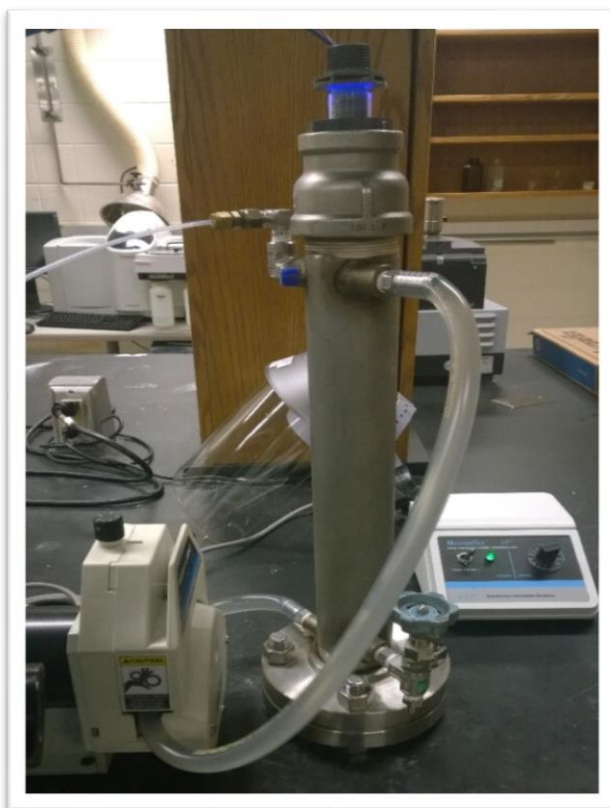
Figure 3.6. Bench-scale photocatalytic treatment system as used in the experimental phase.

At the top of the tube, rubber rings seal the reactor by closing the gap between the quartz casing and the internal metal surface, allowing for the supplied oxygen to remain above and in contact with the liquid surface at about 1×10^3 kPa. Stainless steel fittings that serve as water inlet and outlet ports are perpendicular and tangential to the surface of the tube (Figure 3.4.a), with the inlet placed at the bottom and the outlet port at the top of the reactor length. As result, the fluid flows upward and in a helical pattern inside the reactor. Additional inlets placed at the top and bottom end of the tube allow for water loading and oxygen supply, and sample withdrawing, respectively. Mixing in the batch reactor is achieved through fluid recirculation with a peristaltic pump (Cole Parmer Masterflex I/P modular analog pump with benchtop controller, model 77601-10), and Tygon E-LFL Masterflex tubing of 12.7 mm internal diameter, as shown in Figure 3.4.b and 3.6. The benchtop controller of the pump allows for flow rate variation in the range between 1.4×10^{-5} m^3 s^{-1} and 1.3×10^{-4} m^3 s^{-1} as shown in Figures 3.7.
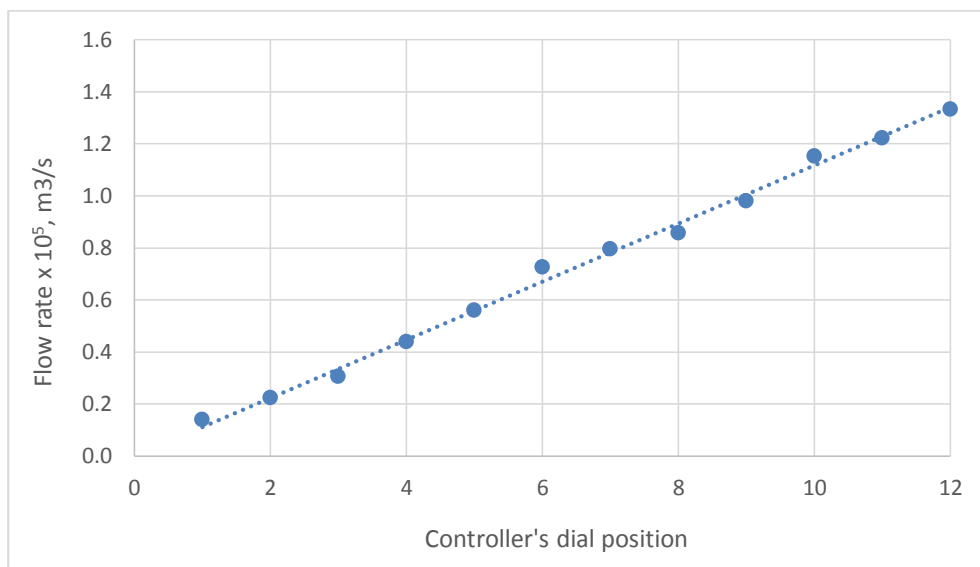
Figure 3.7. Peristaltic pump calibration curve.

3.3. Phenol as Model Pollutant

Most of the documented kinetic or mechanistic studies over the irradiated TiO_2 surface usually involve a single model organic substrate. In the present research, phenol was selected as the target contaminant for all photocatalytic degradation experiments. Phenol is an aromatic organic compound characterized by a hydroxyl (-OH) group attached to a carbon atom that is part of an aromatic ring. It is known to be poorly adsorbed onto TiO_2 surface and it also presents the back reaction in the degradation mechanism (Valencia et al., 2011).

Under UV-Vis irradiation, an aqueous solution of phenol has a characteristic absorption spectrum with clearly identifiable behavior. A shown in Figure 3.8, in a 1 mmol L^{-1} aqueous phenol solution, absorption typically peaks at around 216 and 269 nm. This means that phenol is susceptible to direct mineralization through UV-C photolysis or photocatalysis, and such transformation can be tracked by monitoring the corresponding changes in its absorption profile.
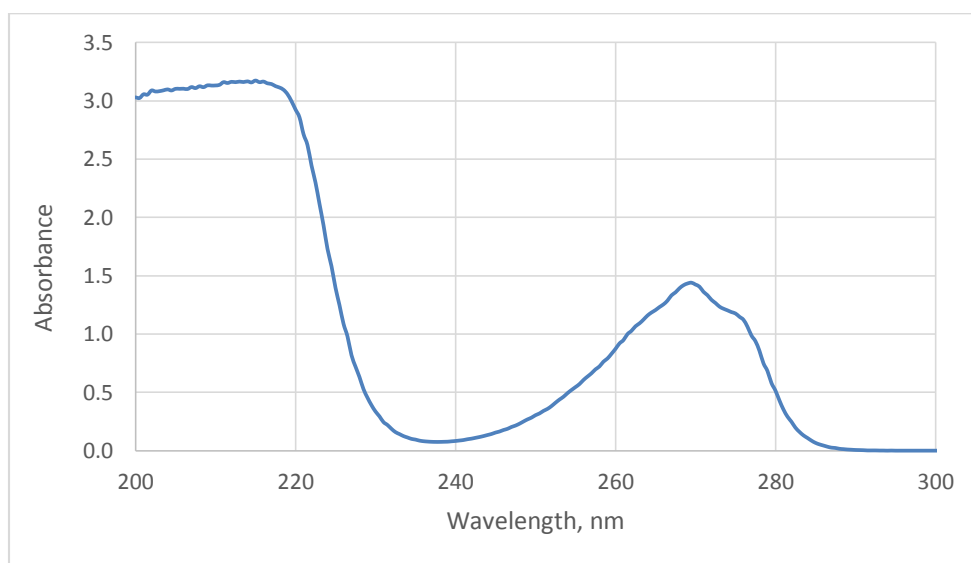
Figure 3.8. UV-Vis absorption spectrum of a 1.0 mmol L^{-1} aqueous phenol solution

Phenols and their degradation products (polyphenols, quinones, etc) are major toxic aquatic pollutants and they can inhibit or even eliminate micro-organisms in biological treatment plants (Laoufi et al., 2008). Also, as they are relatively stable and more soluble in water than alcohols, it is rather difficult to achieve their degradation to safe levels in the range of $0.1 - 1.0$ mg L^{-1}. Even though photocatalysis has been proven to be an effective technique for eliminating phenolic compounds from wastewater, as complete mineralization has been achieved under a variety of conditions (Serpone et al., 1993; D'Oliveira, 1990; Azevedo et al., 2009; Laoufi et al., 2008; Bessa et al., 2001; Al-Rasheed et al., 2003, Tao et al., 2003), literature addressing the photocatalytic degradation of phenols in a fluidized bed reactor is scarce to this day.

The path to complete mineralization of phenol involves the formation of numerous intermediates (Grimes and Ngwang, 2000). Fourteen intermediates have been identified when conducting experiments on phenol degradation. However, out of all the intermediates found, only three were formed in significant amounts: hydroquinone, catechol, and 3-phenyl-2-propenal, in this order (Azevedo et al., 2009). Although hydroquinone and catechol are more toxic than phenol (Arana et al., 2010), acute toxicity tests showed that none of the intermediates, at the concentrations generated in the reaction mixture, exhibited a higher toxicity than the parent compound (Azevedo et al., 2009).

From the engineering standpoint, the indirect mineralization path of phenol, which is characteristic of most aromatic hydrocarbons, combined with the non-selective nature of the $OH^\bullet$ and other oxidative radicals, means that the disappearance rate of the studied compound with irradiation time should not be referred as a reliable standard for reactor design purposes. Instead, the concentration of organics can be expressed collectively as COD or TOC concentration to yield an in-depth, all-inclusive understanding of the photo-mineralization process.

Phenol of molecular biology grade from Sigma Aldrich was used as the substrate in the synthetic wastewater. A known concentration of phenol was dissolved by mixing in deionized water to achieve the desired COD in the final solution. Complete oxidation of phenol to carbon dioxide and water occurs according to the following reaction:

$$C_6H_5OH \ + \ 7O_2 \ \xrightarrow{yields} \ 6CO_2 \ + \ 3H_2O$$
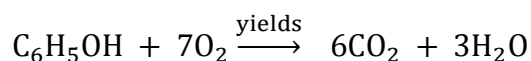
Therefore, for a given concentration of phenol in an aqueous solution, the theoretical COD can be estimated according to the relationship:

$$COD = \frac{mmoles \ of \ Phenol}{L} \ x \ 224 \ \frac{mg}{mmol} \tag{3.1}$$

where COD is the chemical oxygen demand in mg L^{-1} of solution.

Given the multiple intermediate products of phenol mineralization, the above relationship only applies to the initial aqueous phenol solution, in which phenol has not yet undergone any transformation toward the final oxidation products. Once photocatalytic reactions initiate, the COD of the solution will reflect the concentration of the remaining phenol plus that of the reaction intermediates.

3.4. TiO₂ Synthesis and Deposition

The fluidized bed reactor devised for this research is expected to maximize exposure of the surface bounded catalyst to photon radiation, improving quantum efficiency over the limited light penetration achieved in fixed-bed reactors. Also, by having the TiO$_2$ fixed to the bed particles, downstream separation of the catalyst is not necessary.

The selected bed material consists of high-purity grade silica gel particles (SiO$_2$, Davisil Grade 636) size range 250 to 500 μm (35-60 mesh) supplied by Sigma Aldrich. Figure 3.9 shows the particle size distribution analysis performed on 1 kg of silica gel. Experiments were performed using sieve-separated particles retained in the 0.2, 0.3 and 0.425 mm sieves with mean geometric diameters of 0.224, 0.357 and 0.461 mm, respectively. A bed of silica gel of any of the evaluated sizes is fully expanded throughout the annular volume of the reactor in the experimental range of flow rate, while also allowing for rapid particle settling after the operation stops.
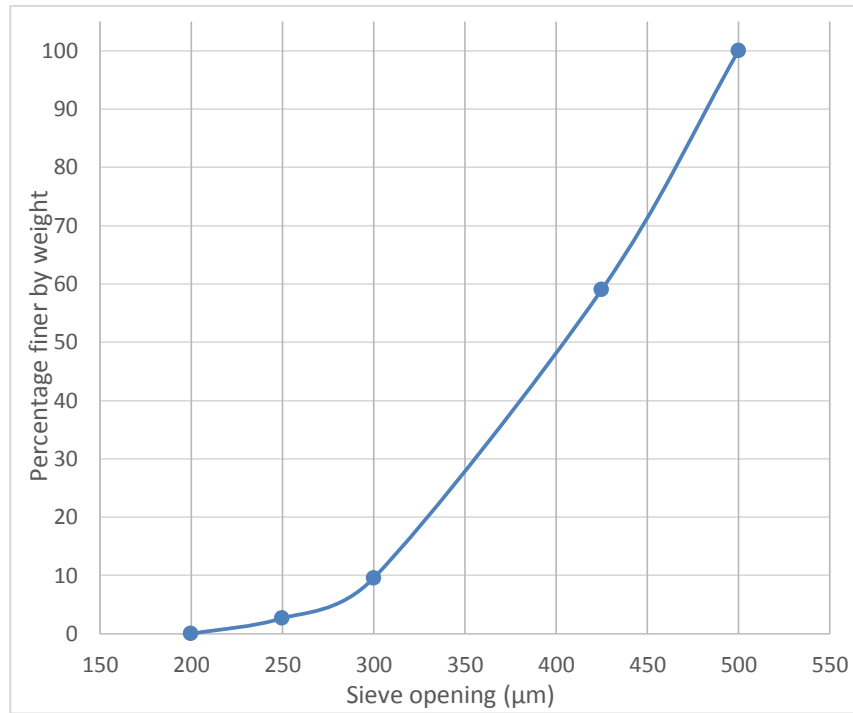
Figure 3.9. Cumulative size-frequency for Davisil silica gel 35-60 mesh.

For a silica sample of any of the selected sizes, bed porosity (ε) in water was calculated to be 0.45, with an approximate pore volume of 0.95 ml g^{-1} of silica gel. A sphericity factor (φ) of 0.78 was chosen for the silica gel beads due to the angular shape of the sample particles observed under the scanning electron microscope. The external silica surface area was then find through the following equation:

$$A_m = \frac{\text{Pore volume}}{\varphi} \frac{6(1-\varepsilon)}{d\varepsilon} \qquad\qquad (3.2)$$

where d represents the mean geometric diameter of the silica beads.

Table 3.2 shows the external surface area per unit mass for the different particle diameters used as catalyst support.

Table 3.2. External surface area per unit mass for different silica gel particle diameters.

Mean geometric diameter (d), m	Hydraulic radius of silica beads (R), m	External silica surface area per gram (A_m), m^2 g^{-1}
2.24E-04	2.38E-05	3.99E-02
3.57E-04	3.80E-05	2.50E-02
4.61E-04	4.90E-05	1.94E-02

TiO_2 was synthetized and deposited on the silica gel particles by dip coating and heating of a TiO_2 precursor solution using a modified procedure of the sol-gel method presented by Kobayakawa et al. (1998). According to this technique, 2.7 ml of concentrated HCl were added into a mixture of 15 ml titanium (IV) isopropoxide (98+% by Acros Organics) and 100 ml absolute ethanol. A 100 ml beaker containing silica gel beads was placed in a 300-ml beaker containing ethanol. This 300-ml beaker was covered with a watch glass and warmed at 80 °C for 1 hour. Silica gel beads were then washed with ethanol, immersed in the precursor solution for 90 min, filtered using suction, and dried at 110°C following drying at room temperature overnight. Silica gel beads were then heated in an electric furnace at 450°C for 3 hours to convert the precursor gel, formed by coated sol gelation with water vapor in air during filtration and drying, to TiO_2 (Kobayakawa et al., 1998). In this last step, the electric furnace automatically increased temperature at 10°C min^{-1} until reaching 450°C, then the resultant sample was allowed to cool

naturally in the furnace. To increase the amount of fixed TiO_2, the above process, starting from ethanol treatment, can be repeated as many times as desired. For the purpose of this research, up to three sol-gel layers were applied onto silica gel beads using the above described coating method, and its weight recorded after each deposition. The quality and uniformity of the photocatalyst layer was also analyzed by direct observation of the deposited material through scanning electron microscopy with a Carl Zeiss LEO 1530VP-FESEM located in the Advanced Materials Research Institute (AMRI) of the Department of Chemistry at UNO.

The mass of fixed catalyst on the silica particles increases with the number of layers, and the latter affects the quality and uniformity of the deposited TiO_2. Consequently, the amount of TiO_2 deposited determines the surface area of catalyst available for irradiation, and therefore, the overall photocatalytic efficiency of the system. Kobayakawa et al. (1998) reported one single layer to be optimum for catalyst uniformity and treatment efficiency.

3.5. Photocatalytic Experiments and Analytical Methods

All the experiments described in this document where performed in the Analytical Chemistry Laboratory of the Department of Civil and Environmental Engineering located in Room 125 in the CERM building, making use of the previously described photocatalytic treatment system. A number of experiments were carried out varying different parameters, except for those summarized in Table 3.1, which were kept constant throughout the course of the experimental phase. In a typical photocatalytic experiment, the reactor was loaded with a known mass of coated silica gel beads and 800 ml of an unbuffered phenol aqueous solution of a given concentration. The resulting mixture was then recirculated at a rate of $8.9x10^{-6}$ m^3 s^{-1} (530 ml min^{-1}) with a peristaltic pump.

60

In order to oversaturate the phenol solution with molecular oxygen, a pocket of gas was maintained on top of the bulk liquid at about 101 kPa by feeding compressed oxygen from a cylinder through the top of the sealed reactor at a constant flow rate. Temperature of the mixture in the reactor varied during the course of experiments due to the lack of a temperature control mechanism.

During the first hour of the experiment the mixture was recirculated in the dark (no UV-C lamp) in order to allow for the substrate and coated silica gel to reach adsorption equilibrium. Then, at time zero (0), the first sample was taken and UV-C irradiation was initiated by placing the lamp inside the quartz casing. Subsequent samples were taken at predetermined time intervals throughout the experiment (typical experiment ran for 8 hours after initiating irradiation of the mixture). Each sample consisted in approximately 30 ml of mixture withdrawn from the sampling port of the reactor. Temperature, pH and DO were measured immediately after collection of the sample with Thermo Scientific Orion probes and multimeter. Then, the sample was filtered through a 0.45 μm cellulose nitrate filter (Whatman Ltd.) to remove suspended and colloidal matter (Standard Method 5910 for Determination of UV-C Absorbing Organic Constituents). COD determination was performed with a UV-Vis Spectrophotometer (Hach DR 5000) according to the USEPA Reactor Digestion Method (Method 8000) using Hach TNT Plus 822 and 821 vials for high and low range COD concentrations, respectively, and a Hach DRB200 digital reactor block. Test accuracy is ± 2% for high range and ± 5% for low range COD determination.

Adsorption in the dark (non-UV irradiated mixture), photolysis (UV-irradiated phenol solution) and photocatalysis without added oxygen (UV-irradiated mixture) experiments were carried out as control.

Stability of the surface bound TiO_2 layer was determined by running a series of three consecutive 24-h photocatalytic experiments using the same stock of coated silica gel beads and measuring its COD removal efficiency after each use. At the end of each experiment, the silica gel was recovered, dried in an electric furnace at 120°C for 5 hours, let cool down overnight and reused without further treatment.

The maximum reactor efficiency was stablished as that obtained from a slurry-type reactor. To reproduce such conditions, a set of experiments using a mixture of the phenol solution with initial concentrations varying from 0.25 to 4.0 mmol L^{-1}, and 1.2 g L^{-1} of powdered TiO_2 (anatase nano-powder, < 25 nm particle size, 99.7% trace metals basis by Sigma Aldrich) were performed using the same configuration of the treatment system and analytical methods as in a previously described typical experiment.

In order to determine the optimal concentration of sol-gel-coated silica in the mixture, different mass loads were used (5, 10, 20 and 30 g L^{-1}), while keeping the initial concentration of phenol fixed. Once the optimal amount of coated silica beads in the mixture was found, an additional set of experiments was run to investigate the effect of the size of beads. As mentioned earlier, silica gel of three different average particle sizes were used, 224, 357 and 461 μm. Next, the effect of contaminant load on the system efficiency was determined through experiments where the initial phenol concentration was varied gradually from 0.25 mmol L^{-1} to 4.0 mmol L^{-1} and the mass of coated silica was kept constant. For these experiments, silica gel beads were coated with a single layer of photocatalyst using the technique described in Section 3.3.

The influence of other parameters, like conductivity and pH, on the photocatalytic process was evaluated in a similar fashion. For measuring the effect of pH, experiments with initial pH of

3, 7 and 9.5 were run without controlling any other parameter and letting pH to freely fluctuate over the course of the experiment. Adjustment of initial pH was done with either HCl 0.1 M or NaOH 1 M. The effect of conductivity, as with pH, was determined by modifying the initial conductivity of the phenol solution. NaCl in concentrations of 2 mmol L^{-1} and 20 mmol L^{-1} was used to elevate initial conductivity to 5.50 mS cm^{-1} and 38.6 mS cm^{-1}, respectively.

The effect of the mass of fixed TiO_2 on treatment efficiency was studied by comparing the rate of elimination of COD obtained when using silica coated with one and three layers of photocatalyst for different initial phenol concentrations. These multiple layers were deposited onto silica beads with average size of 357 μm through the same sol-gel coating procedure in Section 3.3.

Comparative analysis of the efficiency of photo-mineralization of phenol under different conditions is usually done by calculating inherent kinetic parameters, usually a global reaction rate constant, or, as suggested by Eq. 2.33, an empirical constant based on the rate of disappearance of a lump-sum parameter (TOC or COD) in accordance with the kinetic mechanisms explained by the Langmuir-Hinshelwood model (Section 2.6). In the case of this research, performing such a kinetic analysis would be incorrect given the operational conditions of the treatment system (uncontrolled temperature) and the nature of COD as a lump parameter involving the pollution strength of several components of the mixture. Ultimately, and since the objective of this research is to evaluate the feasibility of photocatalytically degrade phenol on fluidized TiO_2-coated silica beads rather than developing a kinetic model for such process, and given the above mentioned restrictions, it is both practical and convenient to analyze the experimental results by using parameters that allow for a valid comparison of several individual photocatalytic experiments. Such parameters include the COD removal efficiency or η_{COD}, and the accumulated energy or Q_{UV},

63

in kJ L^{-1} (Kositzi et al., 2004). The latter takes into consideration the radiant flux density, E_R, reaching the surface area of exposed mixture, A_R, as related to the total volume of the reactor, V_T, and is defined as follow:

$$Q_{UV,n} = Q_{UV,n-1} + \Delta t_n E_R \frac{A_R}{V_T} \tag{3.3}$$

where Δt_n is the differential experimental time, and E_R, A_R and V_T as defined in Table 3.1. Since the product of radiant flux density and irradiated surface area yields the radiant flux or Φ_R, Equation 3.3 can be rewritten as:

$$Q_{UV,n} = Q_{UV,n-1} + \Delta t_n \frac{\Phi_R}{V_T} \tag{3.4}$$

UV spectrophotometry was also used for results comparison. The absorbance spectra of the filtrate between 200 nm and 330 nm was recorded by means of a wavelength scan reading using a UV-Vis Spectrophotometer (Hach DR 5000). As suggested by Azevedo et al. (2009), three significant parameters can be obtained from the scanned sample: the disappearance of phenol, which is given by the reduction in the absorption peak at 269 nm; the progress of overall mineralization, indicated by the area under the absorption spectrum curve (it represents a semi-quantitative measure of the concentration of conjugated unsaturated compounds); and the aromatic ring rupture, produced by the absorption of carbonylated and carboxylated compounds, and reflected in the change of absorption between 235 and 240 nm.

4

Experimental Results and Discussion

Results obtained during the experimental phase are presented and discussed in this section. Beginning with results from preliminary experiments, which gave a glimpse on the effects of dissolved oxygen on photo and photocatalytic oxidation efficiency, and on the stability of the surface bound photocatalyst, this section shows the results and analysis of the experimental data obtained as described in Chapter 3, specifically:

- Effects of concentration and size of coated silica beads in the mixture.
- Effects of initial concentration of phenol, dissolved oxygen, pH and conductivity of the solution.
- Variation of photocatalytic phenol oxidation with number of TiO_2 layers.
- Quality and uniformity of deposited TiO_2 film.
- Comparative analysis of phenol oxidation processes efficiency.
- Reactor modeling and system performance prediction.

4.1. Preliminary Results

Exploratory experiments were performed in an early stage of the research in order to stablish the effectiveness of the photocatalytic system when compared to non-catalytic processes such as adsorption and photolysis, and to determine the need for oxygen supply.

The stability or surface-adherence strength of the TiO$_2$ film was investigated by measuring the variation in COD removal efficiency after multiple uses of a single coated silica batch.

4.1.1. Adsorption, Photolysis, Photocatalysis and the Effect of Oxygen on COD Removal.

Figure 4.1 shows the results of 24-hours experiments carried out using a mixture of 3 g L^{-1} of TiO$_2$ nanopowder and a phenol solution with initial COD concentration of 550 mg L^{-1}. Adsorption-, photolysis- and photocatalysis-only experiments were run without external air supply, keeping the system sealed at all times. When feeding air to the mixture, compressed air was supplied through a hose connected to the top of the reactor, as described in Section 3.4. When compressed air was added, photocatalysis removed COD by 98% after 24 hours of treatment, and phenol is completely oxidized into CO$_2$ and water. The final effluent is clear water, with no color or odor.
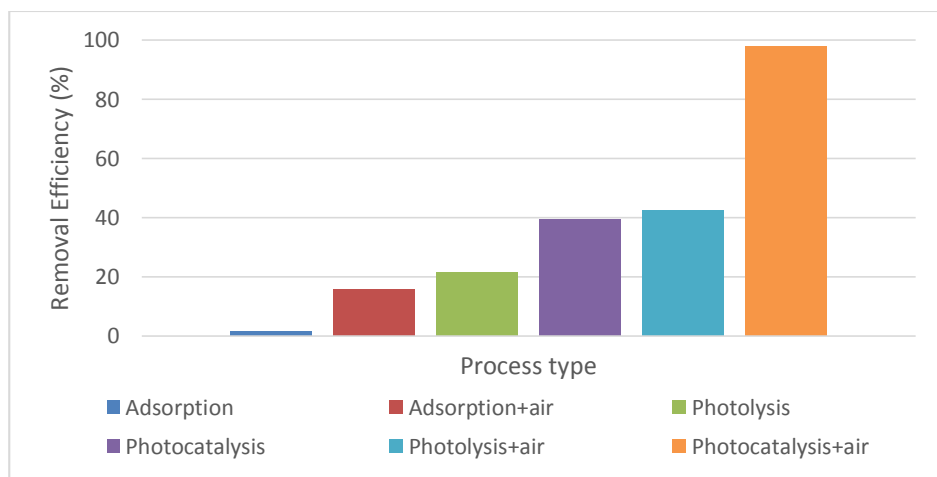
Figure 4.1. Comparison of COD removal efficiency for different processes.

Photolysis with added compressed air and photocatalysis without aeration achieve only partial oxidation of phenols into aromatic intermediates and aliphatic acids (characterized by a brownish color), as seen in Figure 4.2. From these results, the importance of aeration in photocatalytic treatment of the phenolic solution was determined and all subsequent experiments were run under oxygenated conditions.

Figure 4.2. From left to right: Effluent of 24-h photocatalytic treatment (without aeration); effluent of 24-h photocatalytic treatment (with aeration).

4.1.2. Stability of TiO₂ film.

A 35 g batch of silica gel beads were coated three consecutive times with TiO_2 according to the sol-gel procedure described in Section 3.3. Then, in order to determine whether the film was capable of withstanding a full treatment cycle or not, three 24-hours experiments were run using the same silica gel batch, and COD concentration measured in the final filtered and unfiltered effluent. Between experiments, silica beads were dried at 120 °C for 3 hours, then reused in another 24-h run without further treatment. Table 4.1 shows COD removal efficiencies for this set of experiments.

Table 4.1. COD removal efficiency for reused TiO_2-coated silica gel beads.

Sample	24-h COD removal efficiency, %		
	1 cycle	2 cycles	3 cycles
Unfiltered	84.16	79.55	69.65
Filtered	85.87	78.43	74.34

These results show that the TiO_2 film synthesized through the selected sol-gel technique exhibits good adherence to the silica gel and enough catalyst remains attached to its surface so that after three 24-h consecutive photocatalytic experiments COD removal efficiency decreases only by 15%.

Despite of the relatively good stability of the photocatalyst, all subsequent experiments were conducted with unused, freshly coated silica beads, in order to ensure uniformity of the TiO_2 and minimize the number of variables affecting the process outcome.

4.2. Multi-parameter Analysis.

4.2.1. Effect of Size and Concentration of Silica Gel Beads in the Mixture.

Silica gel beads with an average size of 357 μm and a single TiO_2 layer were initially selected to investigate the effect of coated beads concentration in the mixture on the photocatalytic degradation of phenol. For a typical experiment, with an initial phenol concentration of 1.0 mmol L^{-1}, the results of varying the mass of silica in the bulk mixture from 5 g L^{-1} to 30 g L^{-1} are presented in Figure 4.3 (a) and 4.3 (b).
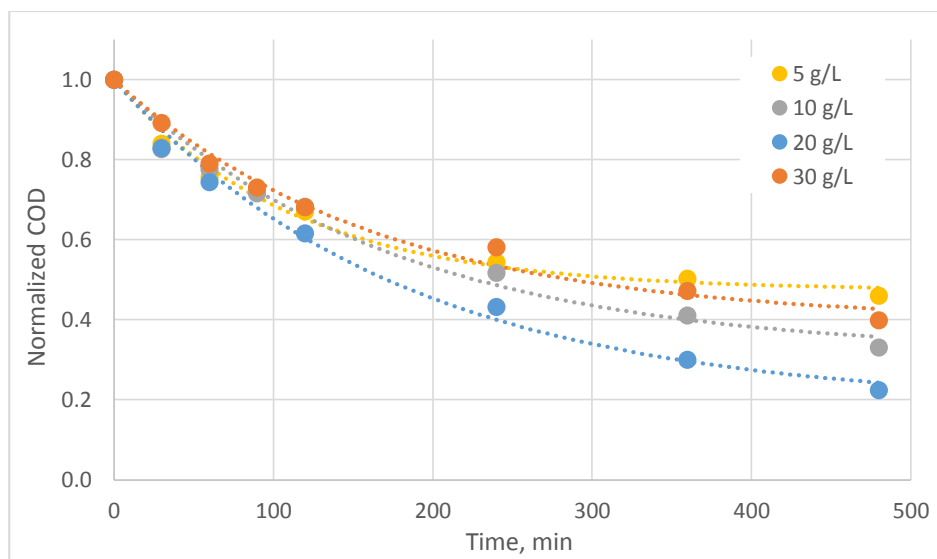
Figure 4.3.a. COD photocatalytic degradation profile in a mixture of 1.0 mmol L^{-1} phenol and different single-layer 357 μm-silica gel beads concentrations.

COD mineralization can also be expressed as a function of accumulated energy, as defined in Equation 3.3, and shown in Figure 4.3(b). In these figures, the ordinate shows the normalized COD, or COD at any time or Q_{UV} divided by the initial COD concentration.
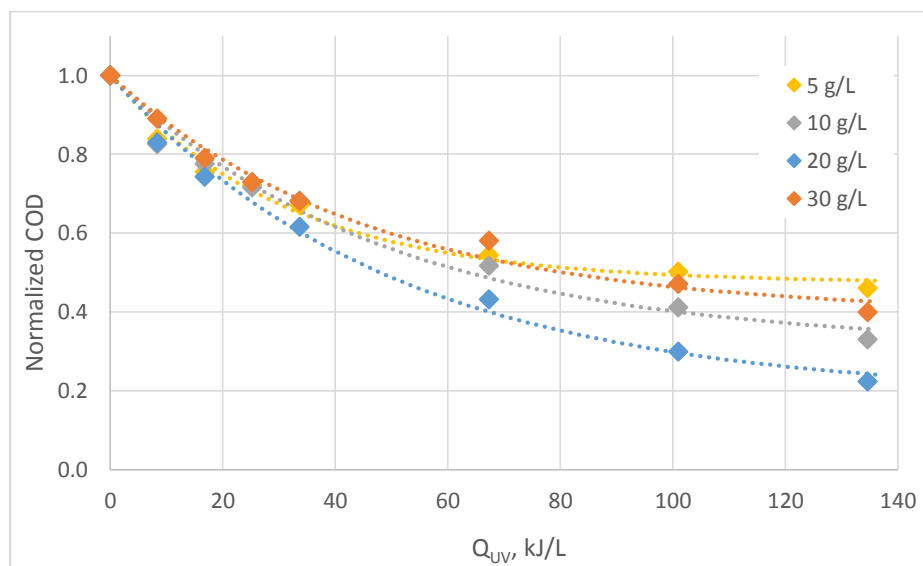
Figure 4.3.b. COD photocatalytic degradation profile in a mixture of 1.0 mmol L^{-1} phenol and different single-layer 357 μm-silica gel beads concentrations.

69

It was earlier explained that mineralization of COD does not follow simple kinetic models, due to the fact that COD is a lump parameter that includes a number of pollutants. Therefore, a single overall reaction rate constant cannot be calculated. In its place, alternative experimentally derived variables such as COD removal efficiency and accumulated energy were obtained as a mean for process comparison. The 8-h COD removal efficiency and the accumulated energy necessary for the mineralization of 50% ($Q_{0.5}$) of the initial dissolved COD values under different operational conditions were generated by fitting of experimental data through non-linear regression using GraphPad Prism 6 ® software. Regression fitting is presented in dotted lines in Figures 4.3.a and b. The variation of 8-h COD removal efficiency and $Q_{0.5}$ with concentration of silica beads is shown in Figure 4.4 and 4.5, respectively.
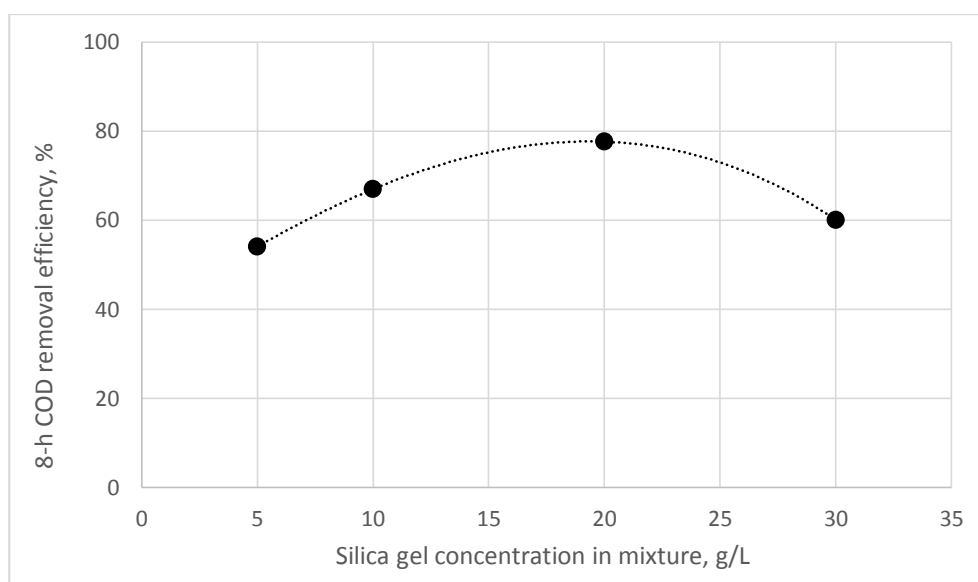
Figure 4.4. Variation of 8-h COD removal efficiency with concentration of single-layer 357 μm-silica gel beads in mixture with 1.0 mmol L^{-1} initial phenol concentration.
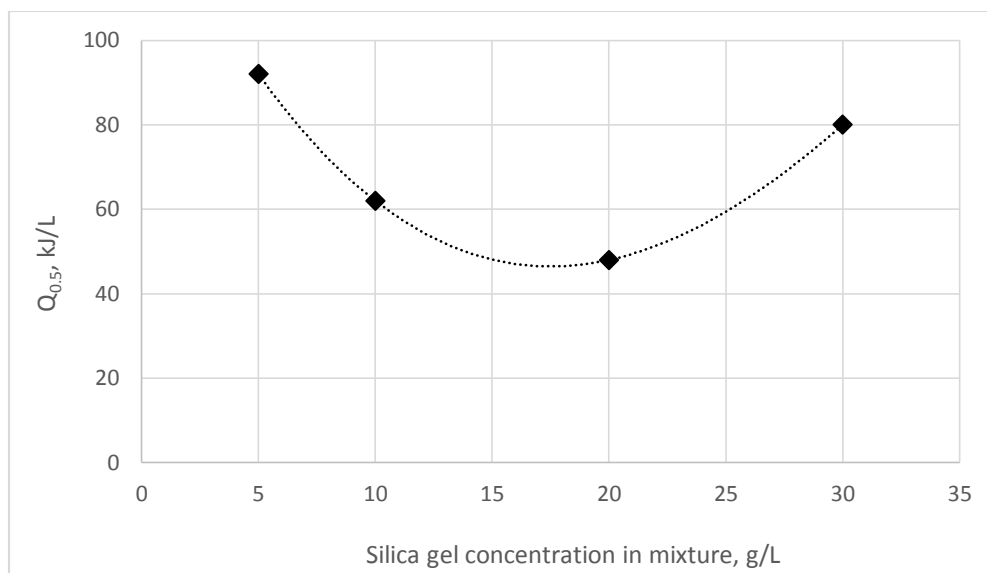
Figure 4.5. Variation of $Q_{0.5}$ with concentration of single-layer 357 µm-silica gel beads in mixture with 1.0 mmol L^{-1} initial phenol concentration.

COD removal reaches a maximum of 78% when the concentration of 357 µm-silica beads is 20 g L^{-1} in the mixture, decreasing to 60% for 30 g L^{-1} and down to 54% for 5 g L^{-1}. Similarly, $Q_{0.5}$ is lowest at 20 g L^{-1} and highest at 5 g L^{-1} of silica gel, going from 48 kJ L^{-1} up to 92 kJ L^{-1}, respectively. The observed behavior indicates that the photocatalytic mineralization of 1.0 mmol L^{-1} of phenol under the current reactor configuration is extremely sensitive to changes in the amount of fluidized silica particles in the bulk liquid.

Since not only concentration but also particle size contribute to the apparent turbidity and light-blocking effect of the liquid mixture, similar experiments were performed using silica beads of 224 and 461 µm diameter. This allowed to measure and compare the combined influence of both parameters in the process efficiency. The results of typical experiments using a mixture of 1.0 mmol L^{-1} initial phenol concentration and varying single-layer 224 µm-silica beads concentration are presented in Figure 4.6.
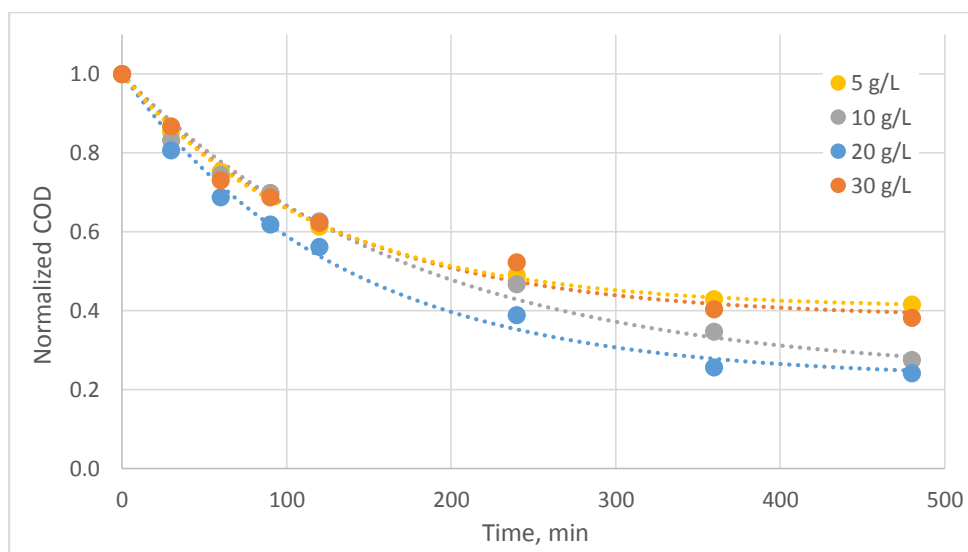
Figure 4.6. COD photocatalytic degradation profile in a mixture of 1.0 mmol L^{-1} phenol and different single-layer 224 μm-silica gel beads concentrations
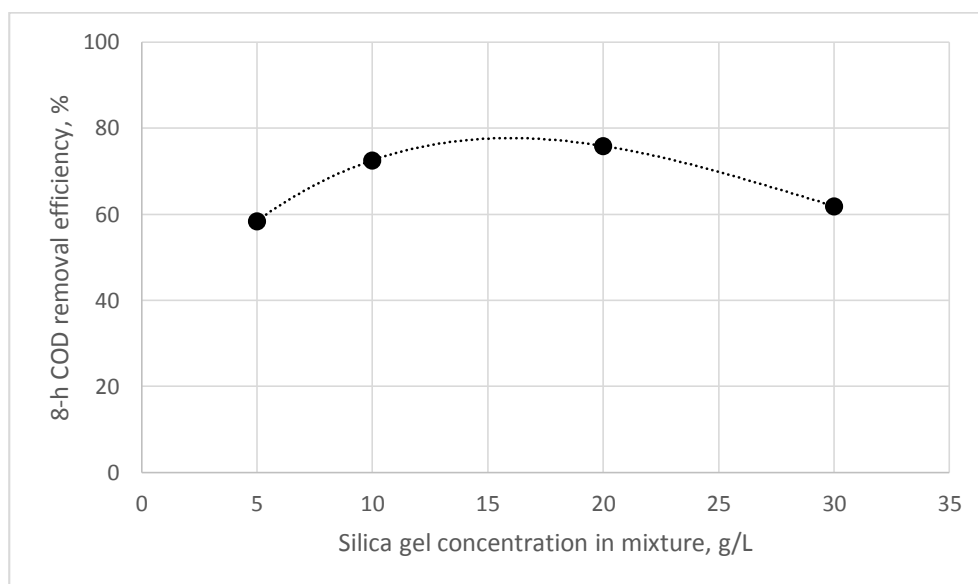
Figure 4.7. Variation of 8-h COD removal efficiency with concentration of single-layer 224 μm-silica gel beads in mixture with 1.0 mmol L^{-1} initial phenol concentration

72

From these results, both the 8-h COD removal efficiency and $Q_{0.5}$ were calculated and plotted as shown in Figures 4.7 and 4.8, respectively.
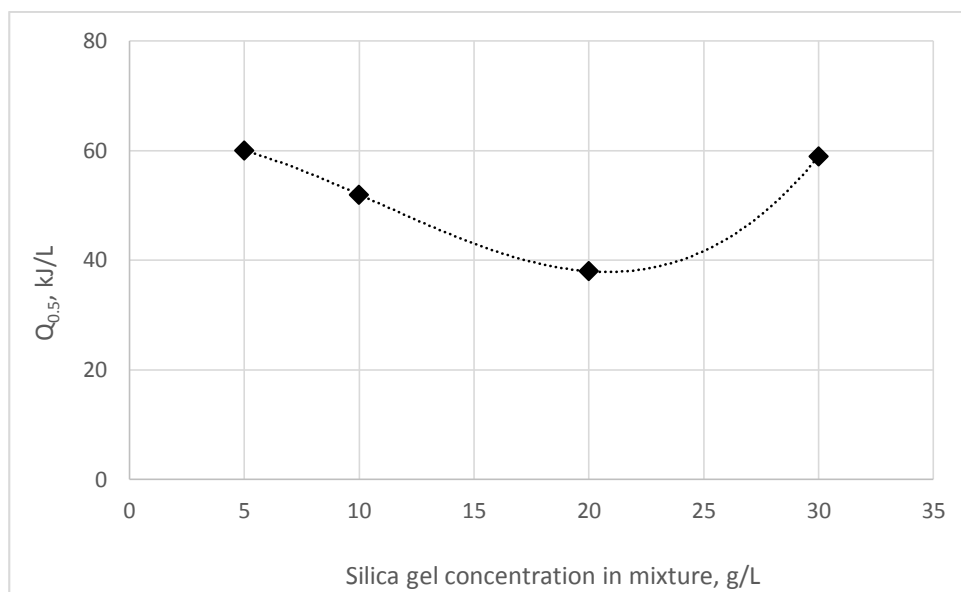
Figure 4.8. Variation of $Q_{0.5}$ with concentration of single-layer 224 µm-silica gel beads in mixture with 1.0 mmol L^{-1} initial phenol concentration
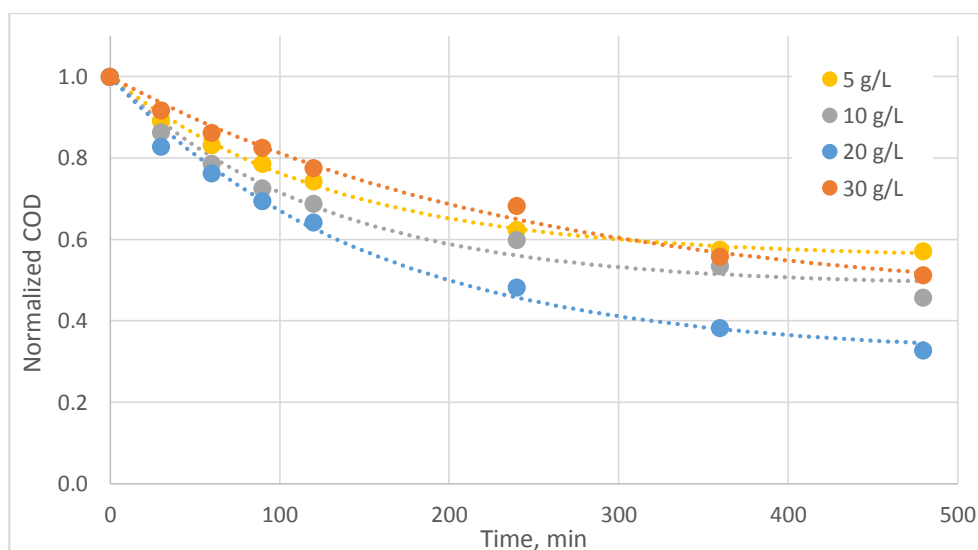
Figure 4.9. COD photocatalytic degradation profile in a mixture of 1.0 mmol L^{-1} phenol and different single-layer 461 µm-silica gel beads concentrations

Finally, when running the photocatalytic experiments for the same mixture of 1.0 mmol L^{-1} initial phenol concentration but with the larger-diameter 461 μm-silica beads, the results presented in Figure 4.9 were obtained.
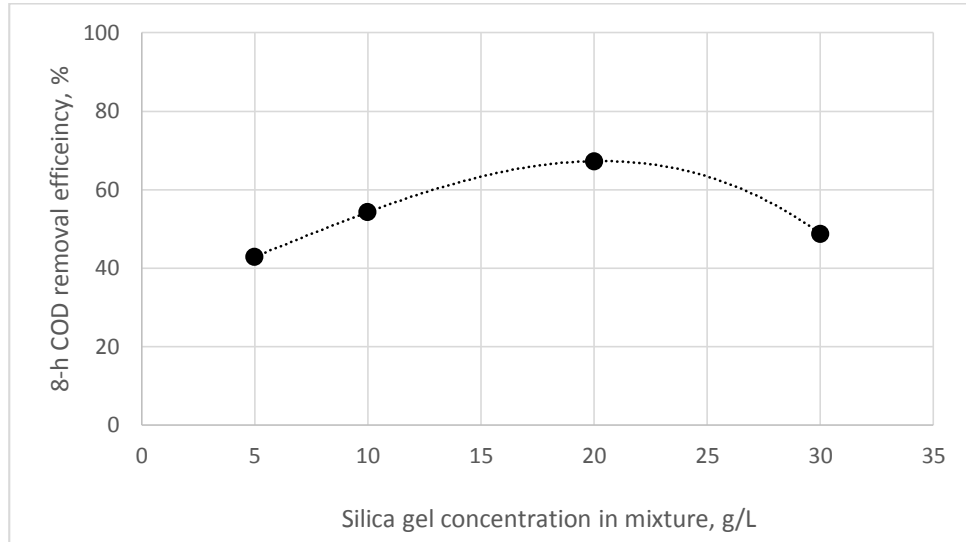
Figure 4.10. Variation of 8-h COD removal efficiency with concentration of single-layer 461 μm-silica gel beads in mixture with 1.0 mmol L^{-1} initial phenol concentration
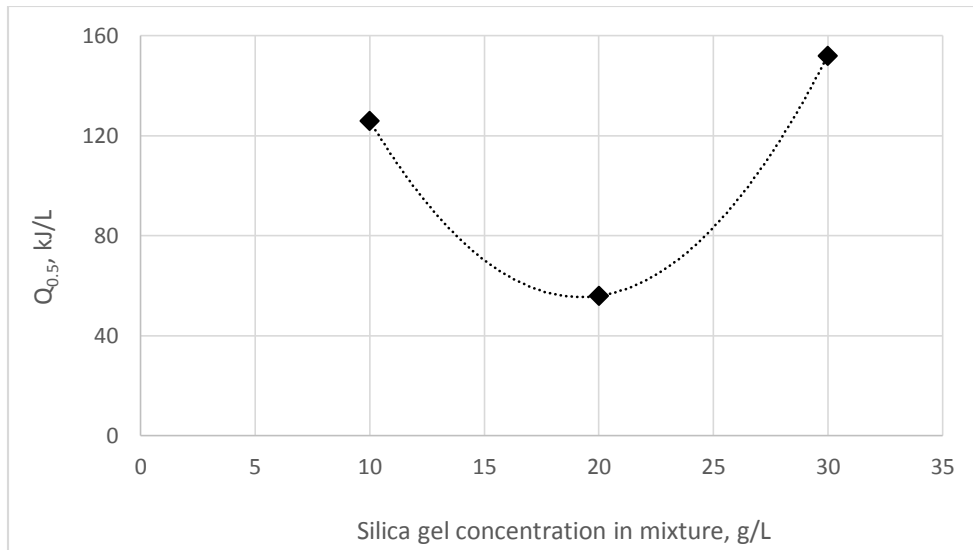
Figure 4.11. Variation of $Q_{0.5}$ with concentration of single-layer 461 μm-silica gel beads in mixture with 1.0 mmol L^{-1} initial phenol concentration

The removal efficiency and $Q_{0.5}$ corresponding to photocatalysis using the largest available silica beads are shown in Figure 4.10 and 4.11.

Figure 4.12 and 4.13 were generated by combining results from removal efficiency and $Q_{0.5}$ variation with silica beads concentration for the three available sizes of silica particles (224, 357 and 461 μm). These figures show the variation of COD removal efficiency and $Q_{0.5}$ with silica beads concentrations for the different beads sizes.

In both instances, process efficiency with silica beads of average size 461 μm result the lowest for the entire experimental concentration range. As observed in Figure 4.12, these reach a maximum COD removal of 67% at 20 g L^{-1}, with a minimum $Q_{0.5}$ of 56 kJ L^{-1} at the same concentration. In contrast, beads of 224 μm are more efficient in removing COD in concentrations from 15 g L^{-1} and lower, and 30 g L^{-1} and above, with beads of 357 μm being slightly more efficient at 20 g L^{-1}, concentration at which they produce a
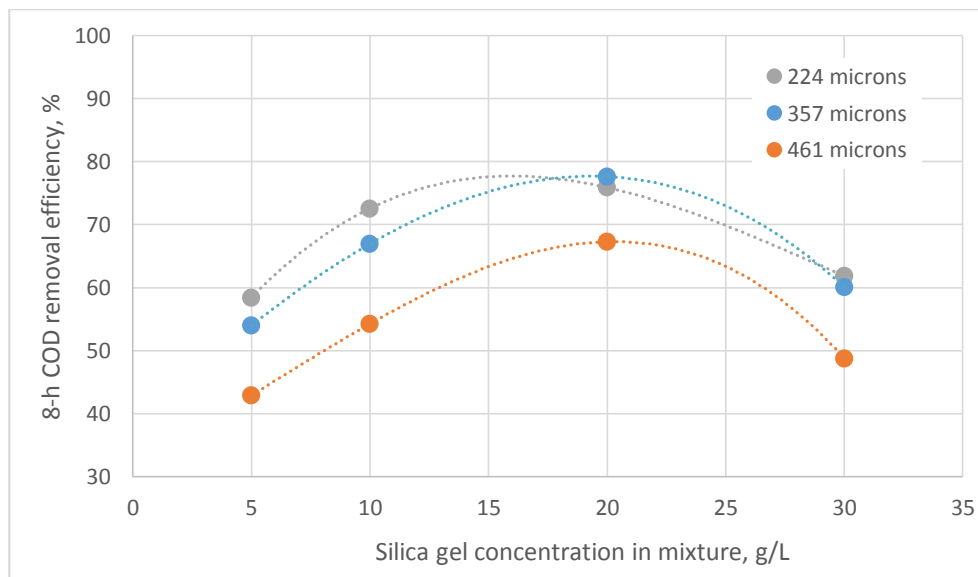
Figure 4.12. 8-h COD removal efficiency variation with concentration of single-layer silica gel beads for different bead sizes and 1.0 mmol L^{-1} initial phenol concentration

maximum COD removal of 78%. Figure 4.13 shows that particles of 224 μm yield the lowest $Q_{0.5}$, with a minimum of 38 kJ L^{-1} at 20 g L^{-1} concentration.
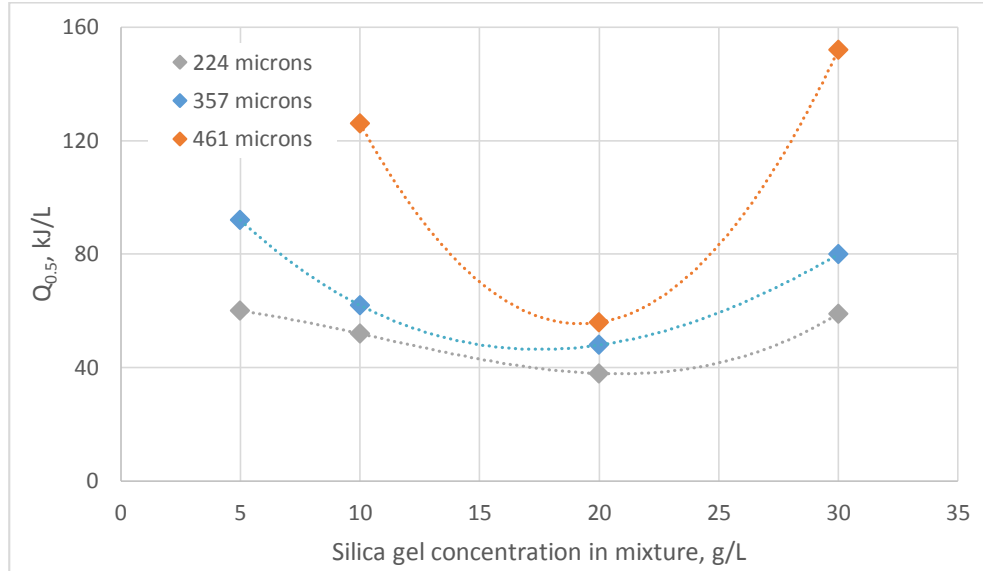
Figure 4.13. $Q_{0.5}$ variation with concentration of single-layer silica gel beads for different bead sizes and 1.0 mmol L^{-1} initial phenol concentration
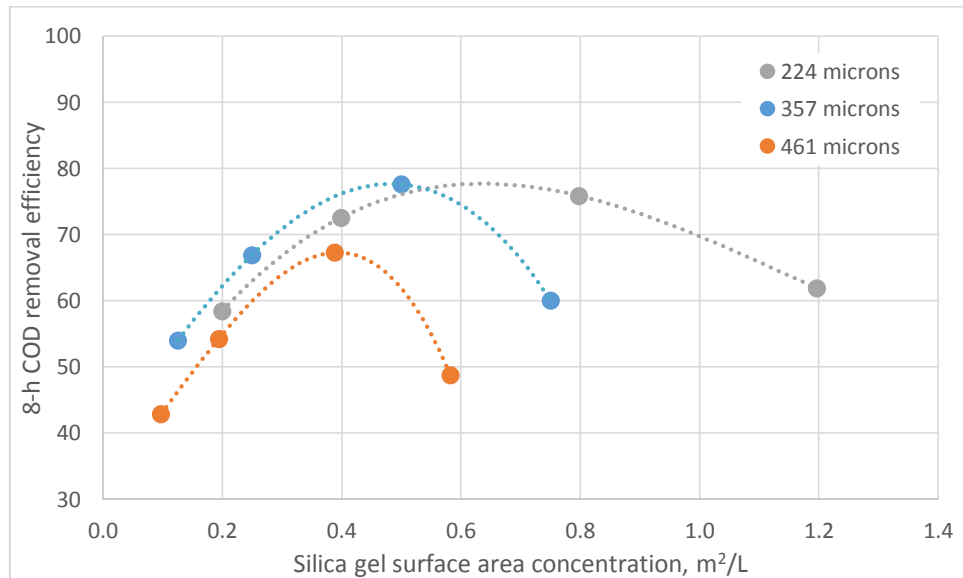
Figure 4.14. 8-h COD removal efficiency variation with single-layer-silica gel beads surface area concentration for different bead sizes and 1.0 mmol L^{-1} initial phenol concentration

Calculating the equivalent surface area, or surface area concentration, for each of the silica gel concentrations tried experimentally allows for better understanding and further analysis of the influence of the mass of catalyst support on the mineralization process in a tubular photo-reactor. Using the data presented in Table 3.2, Figures 4.14 and 4.15 were generated from Figures 4.12 and 4.13, respectively.

Assuming that the applied catalyst layer is uniform across all samples of silica beads, and that the fraction of particle surface covered is the same for all silica sizes, it is evident from these figures that as particle size increases, COD removal efficiency and $Q_{0.5}$ become more sensitive to surface area changes.
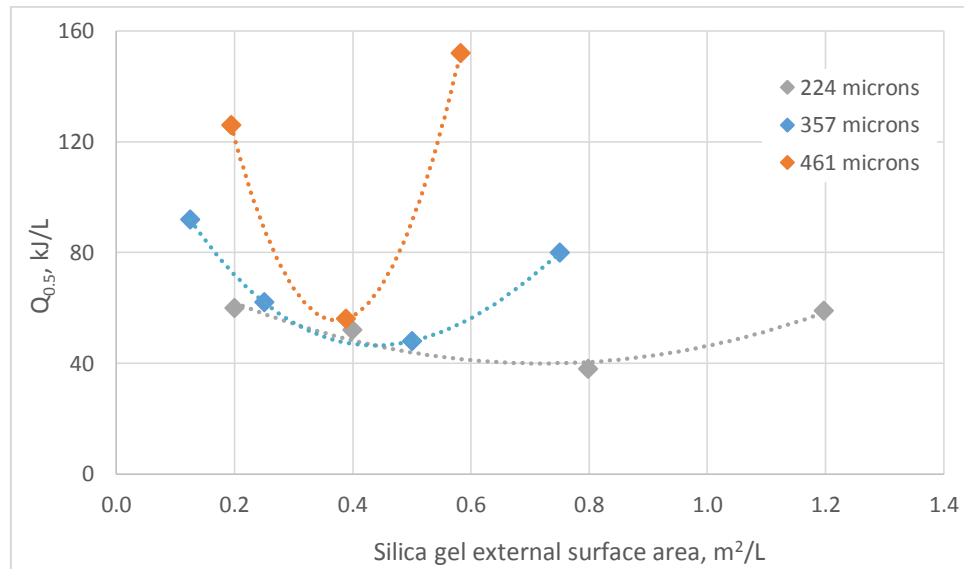
Figure 4.15. $Q_{0.5}$ variation with single-layer-silica gel beads surface area concentration for different bead sizes and 1.0 mmol L^{-1} initial phenol concentration

Figures 4.16 and 4.17 are the result of further data manipulation. They show the change in COD removal and $Q_{0.5}$ with particle size for a constant concentration of silica beads in the bulk liquid.
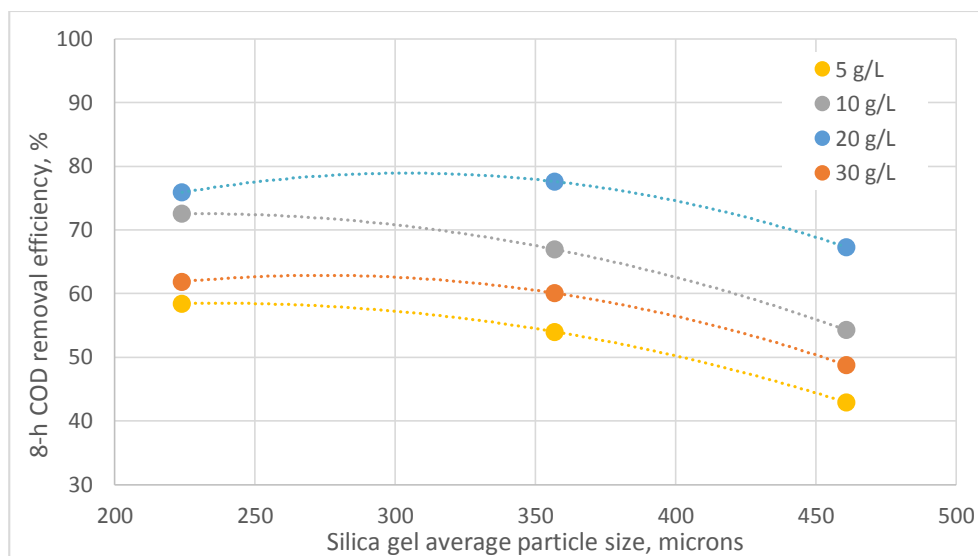
Figure 4.16. 8-h COD removal efficiency variation with silica beads size for different single-layer silica concentrations and 1.0 mmol L^{-1} initial phenol concentration
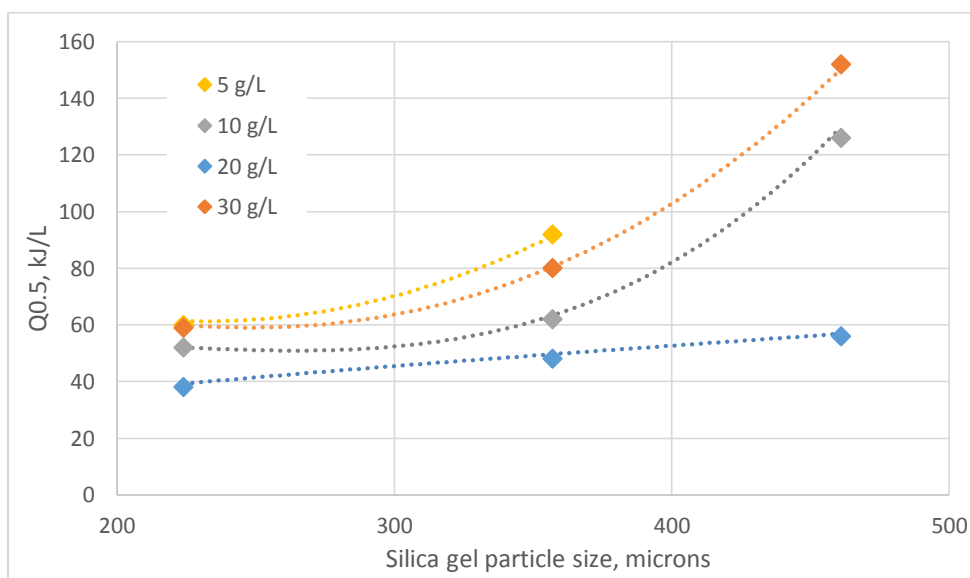
Figure 4.17. $Q_{0.5}$ variation with silica beads size for different single-layer silica concentrations and 1.0 mmol L^{-1} initial phenol concentration

As seen, the photocatalytic degradation of phenol-derived COD in a tubular reactor under the experimental conditions is notably affected by the size and concentration of the

catalyst support. In general, for any mass of fluidized silica gel, the process efficiency

decreases with increasing catalyst-support particle size, as shown in Figures 4.16 and 4.17.

Furthermore, and according to Figures 4.12 and 4.13, for the same mass concentration of

silica gel, the smaller the particle size the higher the COD photo-oxidation rate, which is

an expected outcome, since for a constant mass load of particles, surface area increases

with decreasing particle diameter, as shown in Table 3.2. It has been found that catalysts

with lower surface area provide lower mineralization rates (Arana et al., 2010), and also

that a high [catalyst] surface area is beneficial as it provides higher concentration of active

sites per square unit, which generally leads to superior reactivity (Abrahams et al., 1985).

However, the effect of particle size in the system under study goes beyond that of available

surface area. As seen in Figures 4.14 and 4.15, even for the same surface area

concentration, process efficiency decreased with increasing silica particle diameter, which

indicates that the size of the beads may have a direct influence on photon efficiency by

producing a blocking effect between the light source and the catalyst surface. This is

consistent with results observed in slurry-type reactors, where concentration of TiO_2 in the

system affects the overall reaction rate in a heterogeneous catalytic regime. In this regard,

it has been previously stablished that the amount of TiO_2 is directly proportional to the

overall photocatalytic reaction rate (Gaya and Abdullah, 2008). When the amount of TiO_2

increases above a saturation level (leading to high turbidity), the photon adsorption

coefficient usually decreases radially. The same effect holds true for a fluidized bed reactor,

in which the small catalyst-support particles increase the turbidity in the treated water. An

excess of particles can create a light shielding effect that reduces the surface area of TiO_2

being exposed to illumination. Therefore, there exist an optimal amount of catalyst that

79

yields the maximum degradation efficiency, and its determination constitutes an important design factor for photocatalytic reactors. Figures 4.16 and 4.17 show that for the photocatalytic system under study, 20 g L^{-1} of silica gel beads with an average diameter of 224 μm (equivalent surface area of 0.8 m^2 L^{-1}) and coated with a single layer of TiO$_2$ in a mixture containing an initial phenol concentration of 1.0 mmol L^{-1}, yielded the lowest energy consumption, while particles of 224 and 357 μm (which in both cases is equivalent to a surface area concentration of 0.5 m^2 L^{-1}) in this same concentration produced the highest COD removal in 8-h treatment time. These parameters worsened for lower and higher silica particles concentrations.

The observed influence of catalyst surface area on degradation rate also sheds some light on the photo-oxidation mechanism prevalent for this type of system. It has been reported that for compounds that can react by direct electron transfer, the removal rate decreases with the surface area. The opposite occurred for compounds prone to react through OH$^{\bullet}$ radical-mediated attack (Agrios and Pichat, 2006; Enriquez and Pichat, 2006). Also, the photo-redox chemistry that occurs at the semiconductor surface is emanated from trapped electrons and trapped holes rather than from free valence band holes and conduction band electrons (Serpone et al., 1996), which confirms the surface-bound nature of the interactions between trapped covalent band electrons and valence band holes, and the bulk liquid suggested by the experimental results. Therefore, either by direct substrate oxidation, trapped electron-hole generation of oxidative radicals, or a combination of both mechanisms, the photocatalytic oxidation of phenol is limited by the magnitude of catalyst surface area available for active sites formation, and accessible by the substrate and

photons. In such scenario, mass transfer phenomena would play a secondary, non-limiting role.

4.2.2. Effect of Formation of Intermediates during Phenol Mineralization.

The mechanism through which phenol mineralizes into innocuous compounds involves the transformation of the original aromatic structure into several reaction intermediate sub-products. The attack of hydroxyl radicals activates the phenol aromatic ring through a strong resonance electron-donating effect. It is well known that this effect is felt most strongly at the *ortho* and *para* positions (Alnaizy and Akgerman, 2000). As mentioned in Section 3.2, at least fourteen transient and intermediate compounds have been identified during the course of phenol photocatalytic mineralization with TiO_2. Aromatic intermediates such as hydroquinone, catechol and 3-phenyl-2-propenal have been reported to appear in amounts sufficient to quantify. Although not a subject widely studied, some authors have found the catechol concentration to be as approximately 25 times higher than the hydroquinone concentration at the beginning of the photooxidation reaction, which suggests that the *ortho*-hydroxylation of the aromatic ring is preferred over the *meta* or *para*-substitution (Alnaizy and Akgerman, 2000). Carboxylic acids in the form of benzoic acid, 2-furancarboxylic acid, 2-ethylhexanoic acid, salicylic, maleic, oxalic and formic acids are also produced in the process, causing measurable changes in the pH of the mixture (Azevedo et al., 2009 and Alnaizy and Akgerman, 2000).

A mixture containing 1.0 mmol/L of phenol and 20 g/L of silica gel beads 357 μm in diameter with a single layer of TiO_2 in deionized water was treated in a typical photocatalytic experiment. The UV absorption spectrum between 200 nm and 330 nm of

the filtered effluent was measured at specific time intervals during the experiment. The resulting absorption bands are shown in Figure 4.18. The typical phenol absorption band, recorder before UV irradiation began, shows two distinctive peaks, one at around 217 nm and the other at 269 nm. UV irradiation causes the whole band to shift upwards, which denotes an increased absorbance produced by the presence of highly UV-absorbing intermediate compounds. The appearance of absorption bands at 245-255 nm is typical of the formation of quinonoid structures like hydroquinone (Svetlichnyi et al., 2001). The peaks on the absorption band return to the original levels in less than 240 min of irradiation, which represents between under 50% of the experiment duration. This is compatible with the formation and later degradation of compounds with increased conjugation (Okamoto et al., 1985; Richard and Boule, 1994, Peiro at al., 2001).
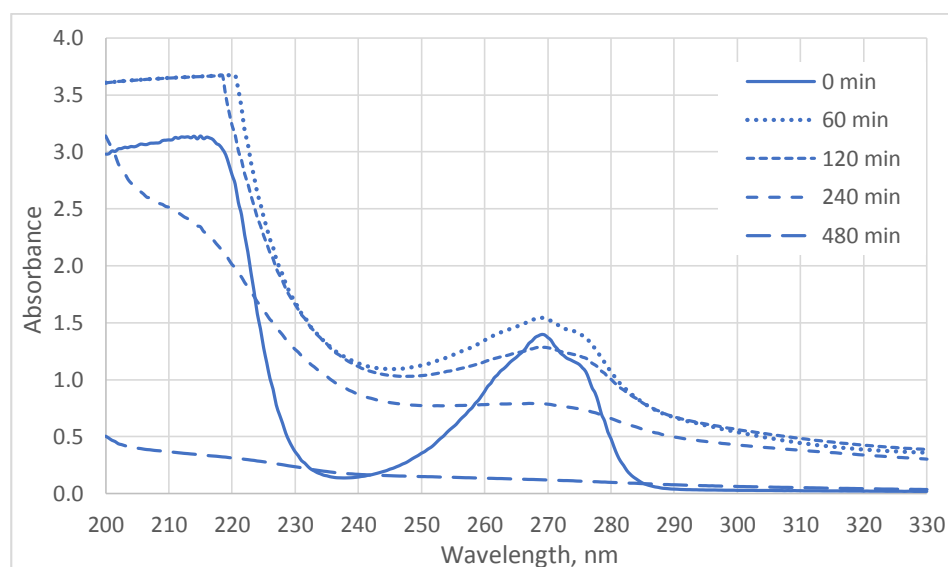
Figure 4.18. Observed UV-absorption bands during photocatalytic mineralization of a mixture with an initial phenol concentration of 1.0 mmol L^{-1}.

Analysis of Figure 4.18 indicates that there is no direct path to phenol mineralization through UV-C photocatalysis, as the transient species formed during irradiation, with their multiple interactions, add even more complexity to the kinetic possibilities. For the oxidation of phenol by electrochemical methods, the following empirical reaction has been proposed (Comninellis and Pulgarin, 1993):

$$[PhOH] \xrightarrow{k_1} \begin{bmatrix} \text{Aromatic} \\ \text{intermediates} \end{bmatrix} \xrightarrow{k_2} \begin{bmatrix} \text{Aliphatic} \\ \text{acids} \end{bmatrix} \xrightarrow{k_3} CO_2 \qquad (4.1)$$
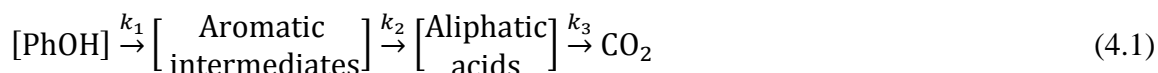
In Equation 4.1, the rate constant k_1 for phenol hydroxylation leading to the formation of intermediates is very high ($k_1 = 10^{10}$ L mol^{-1}s^{-1}) and this reaction can be considered as instantaneous, while rate constants k_2 and k_3 are relatively low at room temperature ($k_2 = 10^8$ L mol^{-1}s^{-1}, $k_3 = 10^5$ L mol^{-1}s^{-1}) but increase considerably with temperature (Comninellis and Pulgarin, 1993).

COD as the control parameter in photocatalytic experiments reflects not only the concentration of phenol but also of the phenolic intermediates and carboxylated acids. Thus, COD elimination rate differs significantly from that of phenol, as shown in Figures 4.19.a and 4.19.b, where the gap between the COD and phenol curves can be attributed to the presence of such photocatalytic subproducts. In an experiment run with an initial phenol concentration of 1.0 mmol L^{-1}, phenol is completely mineralized after 360 min of irradiation, while only 70% of the initial COD is eliminated in the same time frame.

The rate of disappearance of the phenol absorption peak at 269 nm is shown in Figures 4.19.a, while the rate of rupture of the aromatic ring (formation of intermediates) indicated by the absorbance of the effluent at 240 nm is presented in Figure 4.19.b.

As expected, after a sudden increase in absorbance at 269 nm, this peak decreases with irradiation time, which shows that phenol is oxidized at a constant rate until complete elimination. In contrast, the absorption of the effluent at 240 nm increases more than seven fold after starting irradiation, maintaining this same magnitude up to two hours into the experiment, point at which it begins to decline. Such behavior indicates that intermediates start forming immediately in the irradiated mixture at a rate that is proportional to the concentration of the parent phenolic aromatic ring.

The formation of carboxylic acids in a later stage of phenol mineralization is suggested by the decrease in the mixture pH, as shown in Figure 4.20. Here, pH goes from 5.7 to 4.6 in the first 30 min of irradiation. It reaches 3.8 at its lowest point to later increase to around 4.4 at the end of the experiment. It is worth noticing that pH recovery coincides with complete phenol elimination from the mixture, at around 350 min of irradiation.

Although not an objective of this research, detection and identification of phenol mineralization intermediates is an important factor to consider in photocatalytic systems design. As evidenced by its absorption profiles at different wavelength, phenol undergoes a complex path to complete oxidation, leaving behind mineralization subproducts that remain active after its disappearance.
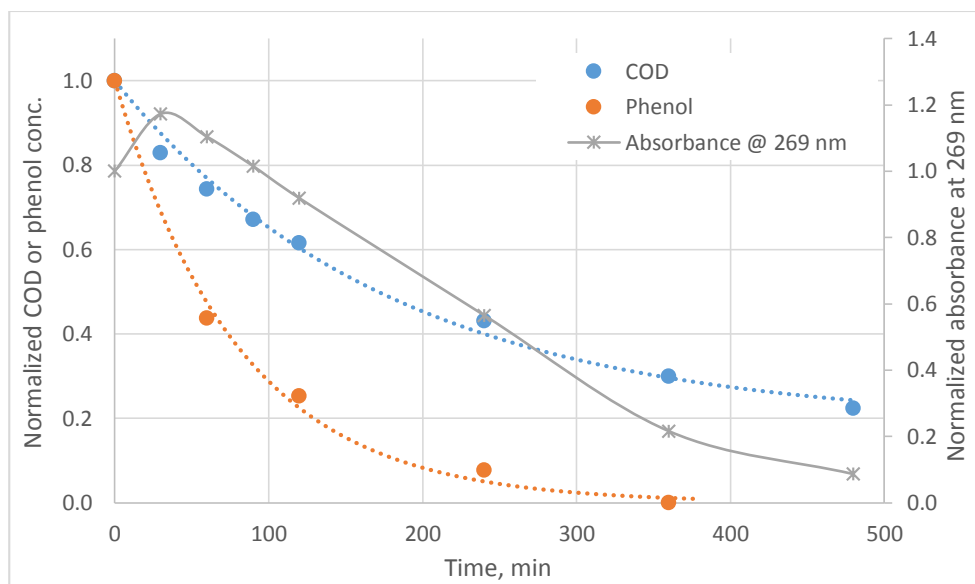
Figure 4.19.a. COD and phenol photocatalytic elimination profile showing absorption at 269 nm in a mixture with 20 g L^{-1} of 357 μm-single layer silica gel beads and 1.0 mmol L^{-1} initial phenol concentration
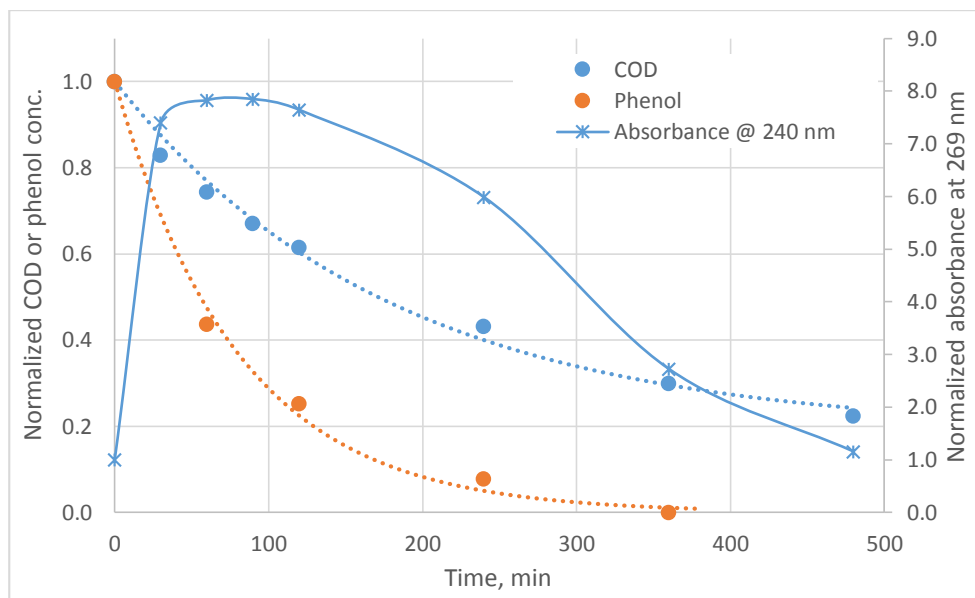
Figure 4.19.b. COD and phenol photocatalytic elimination profile showing absorption at 240 nm in a mixture with 20 g L^{-1} of 357 μm-single layer silica gel beads and 1.0 mmol L^{-1} initial phenol concentration
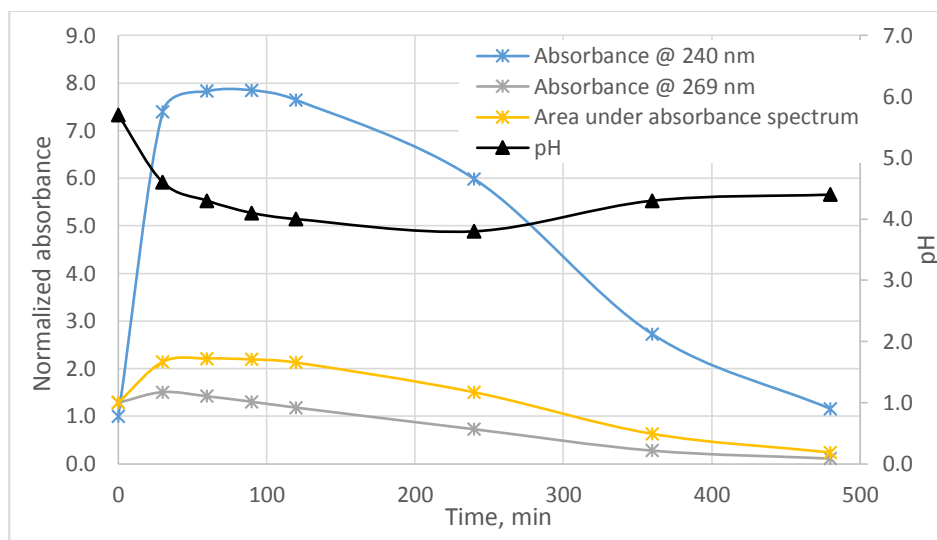
Figure 4.20. Evolution of pH, absorption at 240, 269 nm and area under absorption spectrum of a mixture with 20 g L^{-1} of 357 μm-single layer silica gel beads and 1.0 mmol L^{-1} initial phenol concentration

Intermediates and acids formation and elimination reactions occur simultaneously in the mixture during the course of irradiation. These compounds slow down the photocatalytic oxidation process increasing the time and energy necessary for COD elimination owing to the direct competition over limited unselective reactive sites on the semiconductor surface and to the reduction in photon efficiency caused by the increased absorbance of the mixture. This effect is corroborated by the results observed at higher substrate concentrations and presented in the following section.

4.2.3. Effect of Initial Phenol Concentration.

Pollutant concentration in the irradiated mixture is known to have a significant effect on the photo-degradation rate, especially when the target compounds are not directly

oxidized to carbon dioxide and water, but form intermediate photo-oxidation products in the course to complete mineralization. Such is the case of phenol.

As discussed in Section 4.2.1, the mass concentration of catalyst-support particles, and consequently its active surface area, have also a significant influence on the efficiency of the process under the current reactor configuration. Therefore, the combined effect of both phenol and silica gel beads concentration was studied through a series of photocatalytic experiments where the initial phenol concentration was varied from 0.5 to 2.0 mmol L^{-1} for different mass loads of silica gel beads of 357 μm average diameter and coated with a single layer of TiO_2. The results obtained are presented in Figures 4.21 through 4.23.
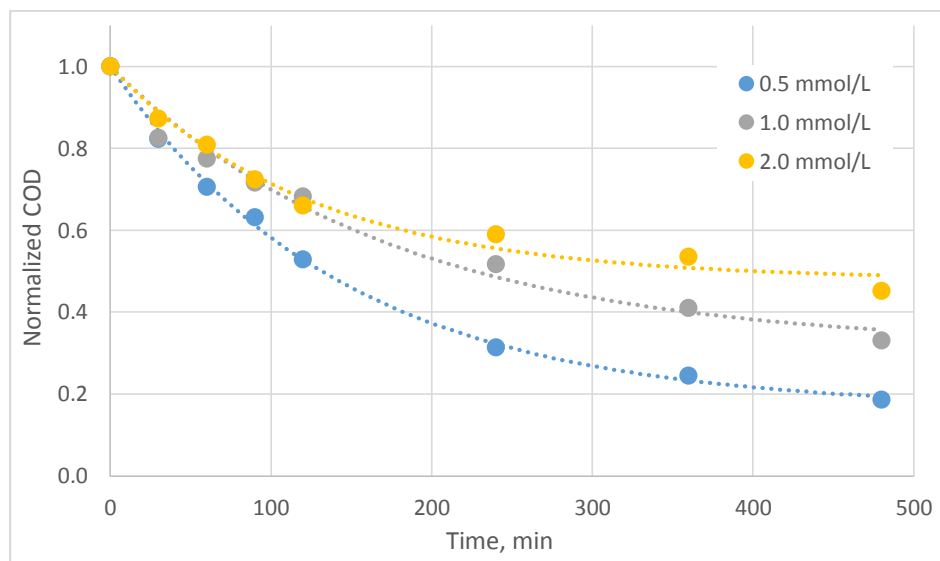
Figure 4.21. COD photocatalytic degradation profile in a mixture of 10 g L^{-1} single-layer 357 μm-silica gel beads and different initial phenol concentrations.
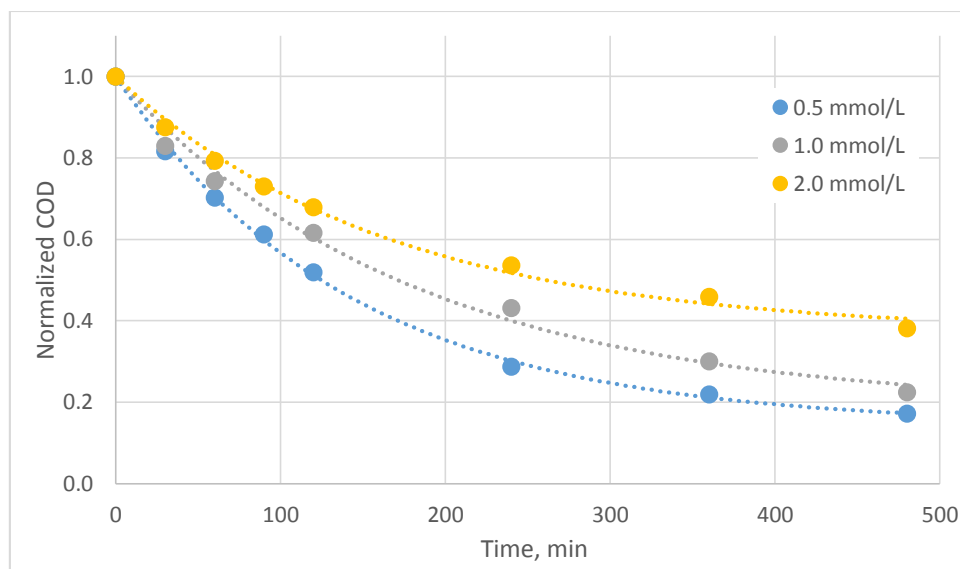
Figure 4.22. COD photocatalytic degradation profile in a mixture of 20 g L^{-1} single-layer 357 μm-silica gel beads and different initial phenol concentrations.
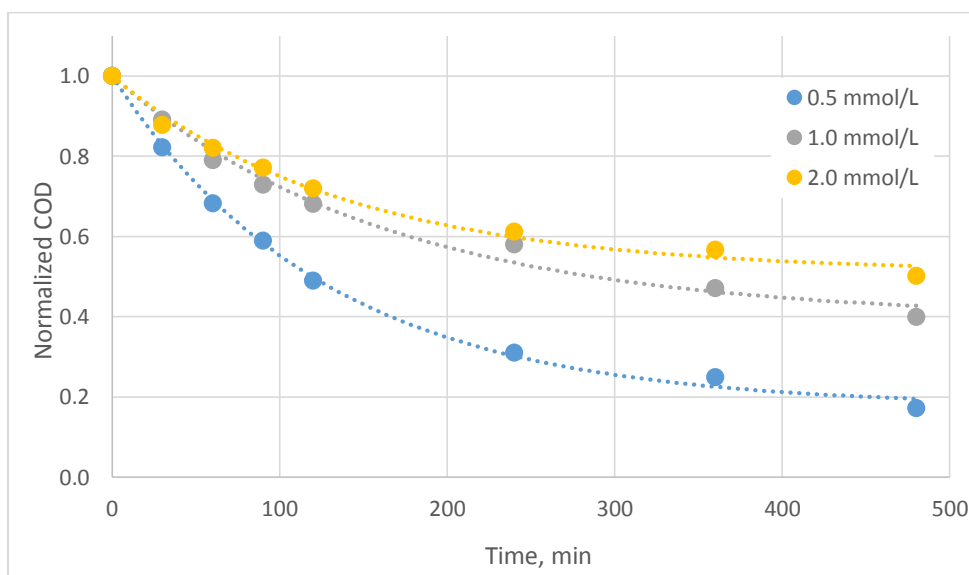
Figure 4.23. COD photocatalytic degradation profile in a mixture of 30 g L^{-1} single-layer 357 μm-silica gel beads and different initial phenol concentrations.

It was found that COD is eliminated from the mixture at all the experimental initial phenol and silica beads loads, although its degradation rate decreases as the substrate

concentration increases. This can be seen in Figure 4.24 and 4.25, which present the 8-h

COD removal efficiency and $Q_{0.5}$ for these group of experiments, respectively.
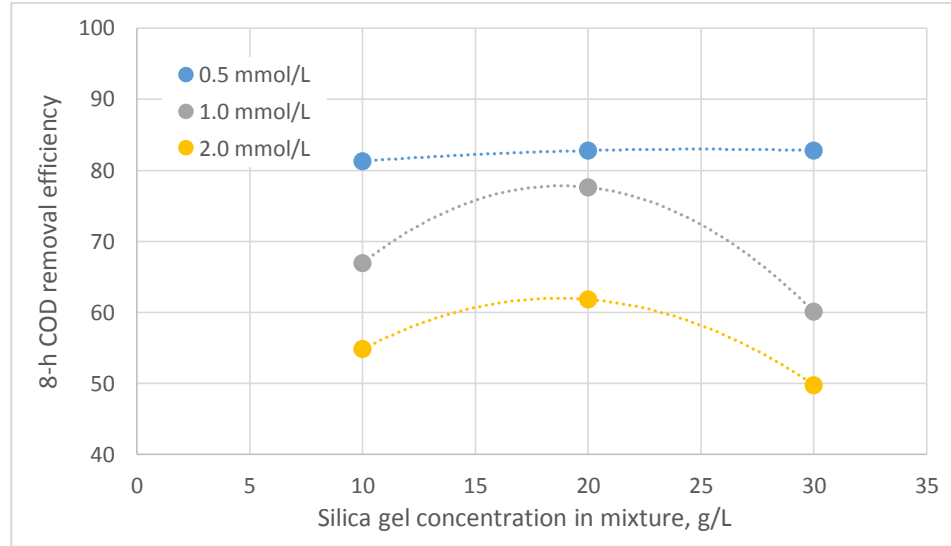
Figure 4.24. 8-h COD removal efficiency variation with single-layer 357 μm-silica gel beads concentration for different initial phenol concentrations
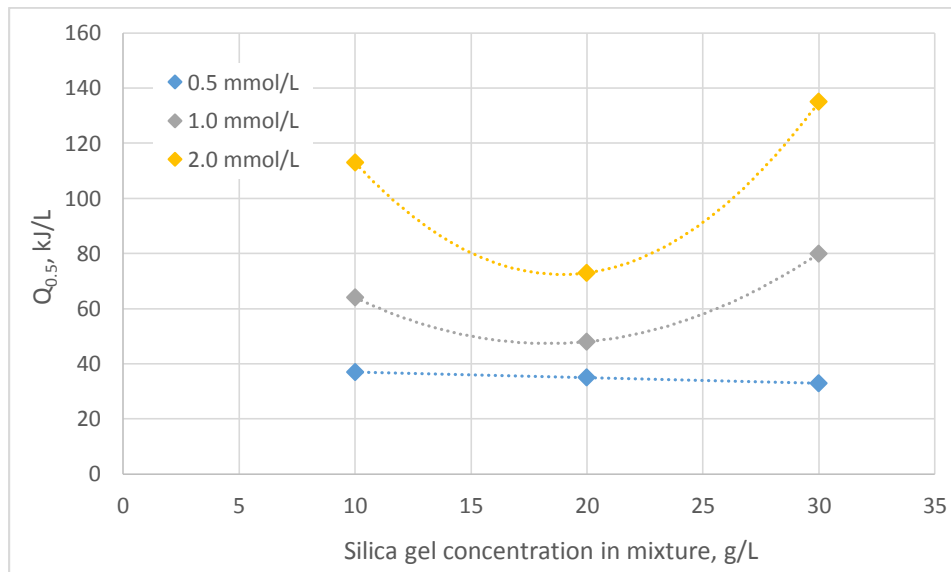
Figure 4.25. $Q_{0.5}$ variation with single-layer 357 μm-silica gel beads concentration for different initial phenol concentrations

As expected, photo-oxidation efficiency decreases as the initial phenol concentration increases. Also, variation of coated silica beads load in the irradiated mixture affects both COD removal rate and the $Q_{0.5}$, which was a previously observed effect in experiments with initial phenol concentration of 1.0 mmol L^{-1}, but as shown in Figures 4.24 and 4.25, this effect becomes negligible at lower substrate concentrations. When these two parameters are plotted against external surface area concentration, the combined influence of phenol and silica beads concentration seems even more substantial. According to Figure 4.26, for the same catalyst surface area available per unit volume, COD removal efficiency is lower for higher substrate loads, with a difference in the fraction of COD removed of up to 30% between 0.5 and 2.0 mmol/L of phenol at the highest equivalent external area concentration. A similar pattern is also observed in Figure 4.27, where the change in the magnitude of $Q_{0.5}$ with exposed surface area exacerbates as the substrate concentration increases.
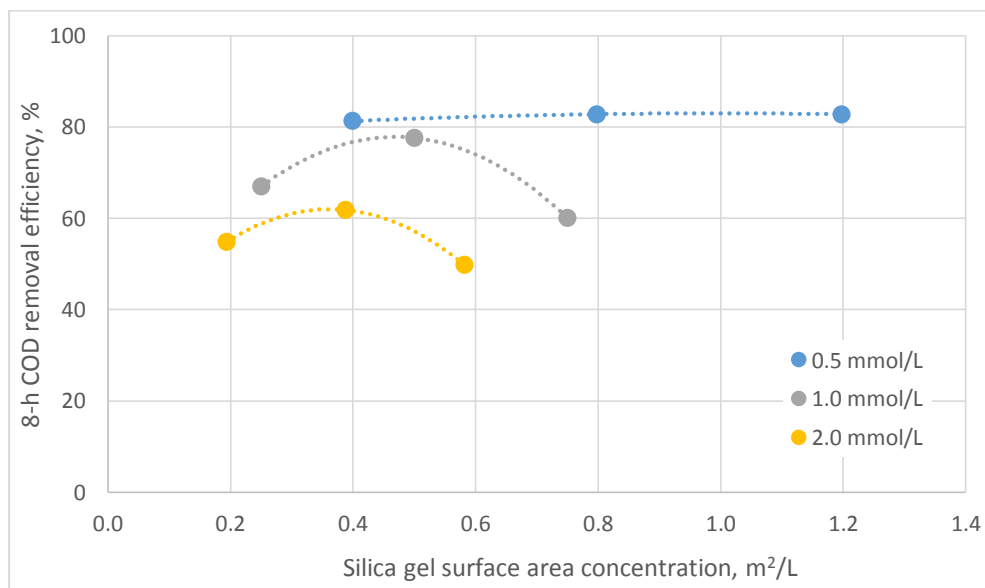
Figure 4.26. 8-h COD removal efficiency variation with single-layer-357 μm-silica gel beads surface area concentration for different initial phenol concentrations
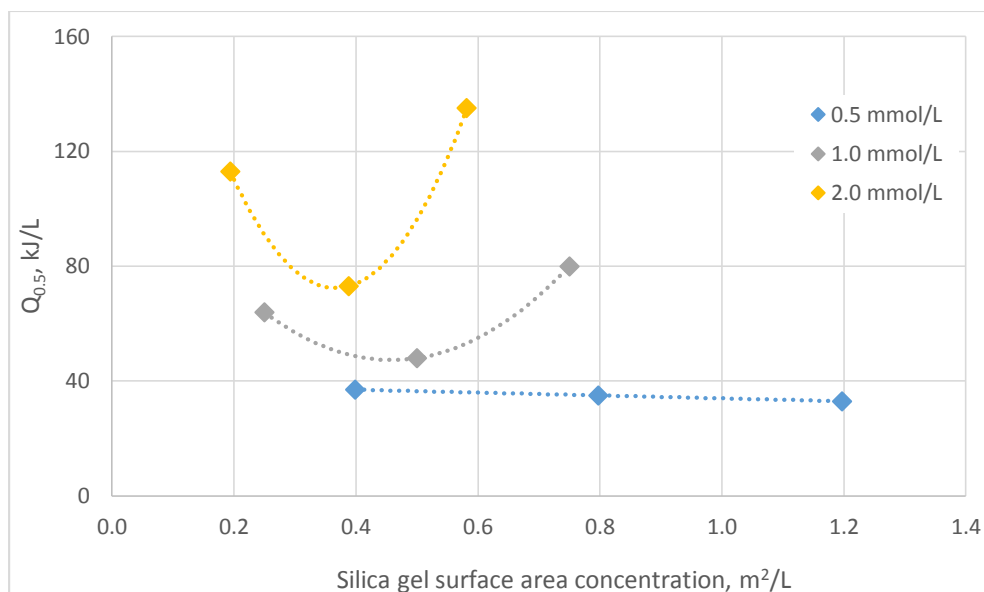
Figure 4.27. $Q_{0.5}$ variation with single-layer-357 μm-silica gel beads surface area concentration for different initial phenol concentrations

As mentioned earlier, the rate of phenol photo-mineralization in a tubular reactor under the experimental arrangement described herein is highly responsive to catalyst load, and the sensitivity of this response is magnified with increasing substrate concentration. However, at low enough concentrations of phenol, COD elimination efficiency is only slightly affected by the mass load of silica, and it sees no significant change over the entire experimental range of silica beads concentrations.

An alternative view of these results is presented in Figures 4.28 and 4.29. Here, the variation in the process efficiency is plotted against initial phenol concentration for different silica mass loads. Besides the expected decrease in efficiency with substrate concentration, these figures clearly show that there exists an optimal mass load of silica particles at which removal is highest and that such load is independent of substrate

concentration. This behavior confirms that the optimum catalyst load is a design parameter determined by the photo-reactor configuration and type of organic substrate.
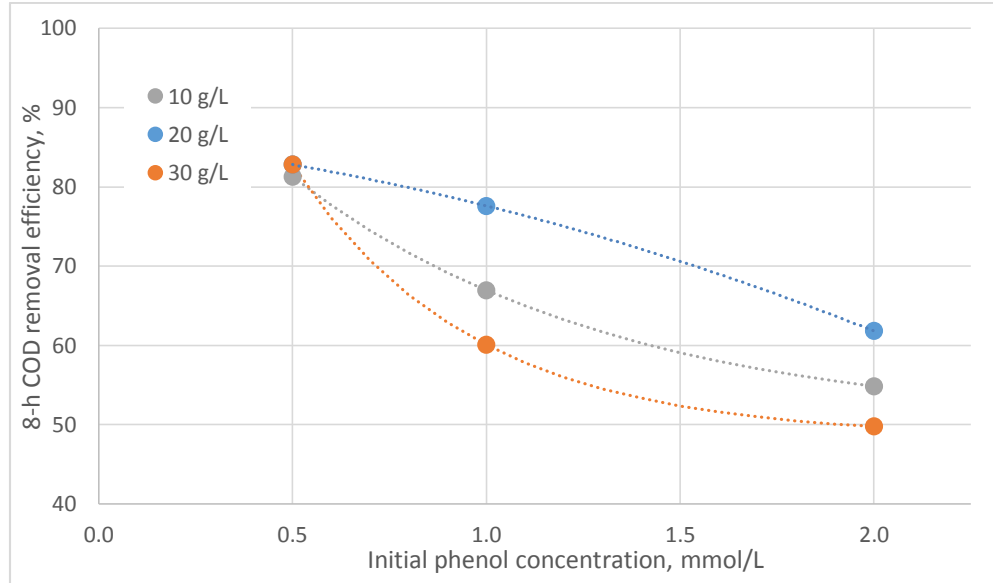
Figure 4.28. 8-h COD removal efficiency variation with initial phenol concentration for different single-layer-357 μm-silica gel beads concentrations
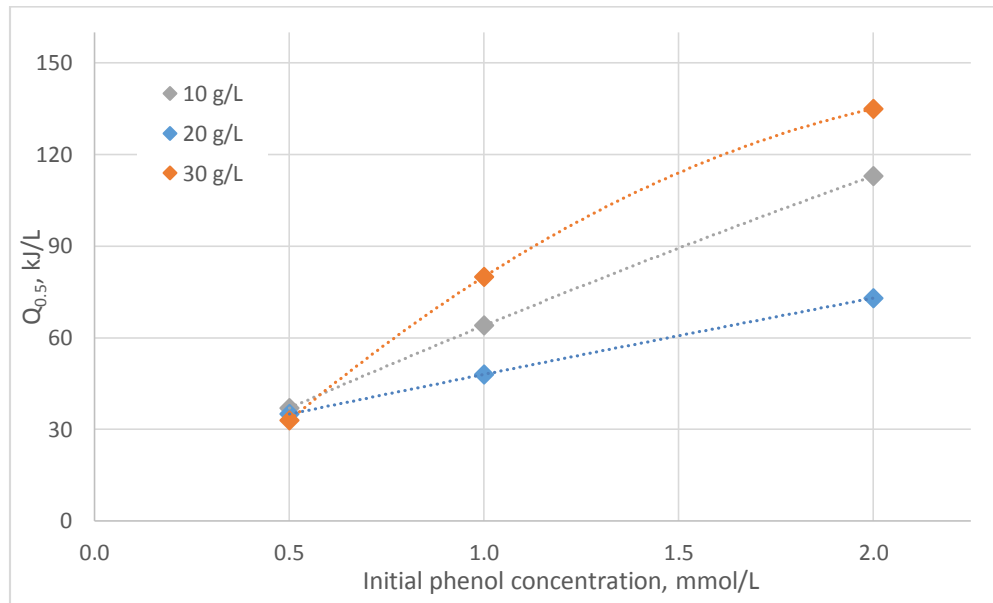
Figure 4.29. $Q_{0.5}$ variation with initial phenol concentration for different single-layer-357 μm-silica gel beads surface area concentrations

92

Both COD removal efficiency and $Q_{0.5}$ show the tendency to plateau at silica gel mass loads other than the optimal as the initial phenol concentration increases. In the case of low silica concentration, this trend is indicative of system exhaustion, or the hindering of the photo-oxidation capabilities of the system owing to saturation and reduced photonic activation of the catalyst surface produced by an excessive substrate concentration relative to the available photo-generated active sites. In the case of too-high silica concentrations, the light blocking effect of particles overload is also responsible for the decreased catalyst activation rate.

Similar observations have been reported in studies on the photocatalytic oxidation of phenol in oxygenated solutions with TiO_2 powder in suspension. It was found that high initial phenol concentrations affected negatively the pseudo-first order reaction rate constant, producing an inhibitory effect on the apparent rate constant, or that phenol mineralization decreased with increasing initial phenol concentration (Augugliaro et al., 1988; Wei and Wan, 1991; Alnaizy and Akgerman, 2000, Singh et al., 2007). This phenomenon is attributed to the photonic nature of the photocatalytic reactions, which means that, at high enough substrate concentrations, photocatalyst deactivation occurs due to the simultaneous saturation of the TiO_2 surface and reduction of the photonic efficiency (Saquib and Muneer, 2003; Chong et al., 2010). Some authors have proposed that such decrement in the reaction rate at high substrate concentration is due to the presence of back reactions (Minero, 1999, Minero and Vione), scenario that considers the possibility of a substrate radical being able to inject an electron into the conduction band of the semiconductor surface (Villareal et al., 2004). Figures 4.30 and 4.31 show signs of the above mentioned catalyst deactivation at high phenol concentrations.
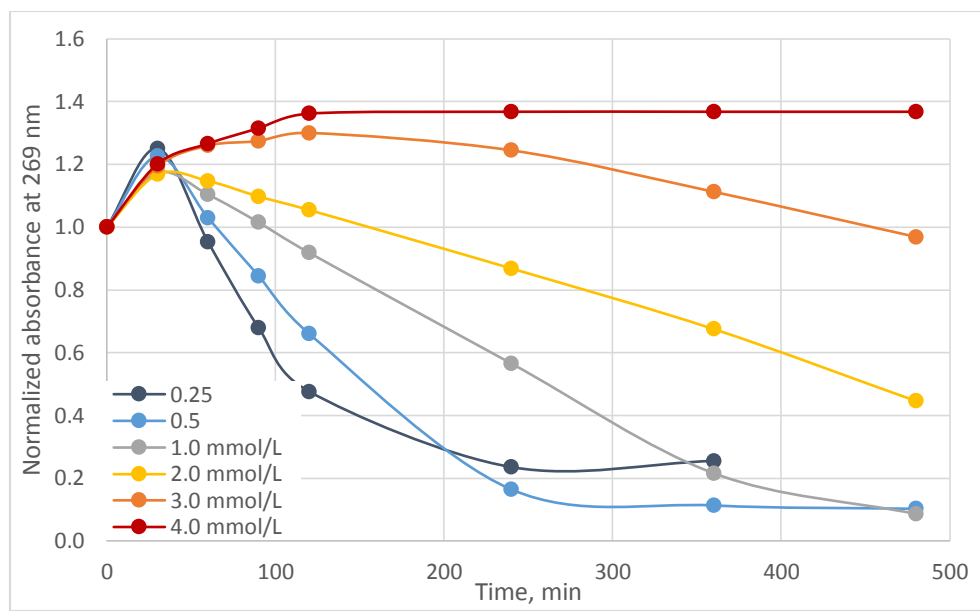
Figure 4.30. Absorption profile at 269 nm during photocatalytic treatment of a mixture with 20 g L^{-1} of single-layer 357 μm-silica gel beads for different initial phenol concentrations
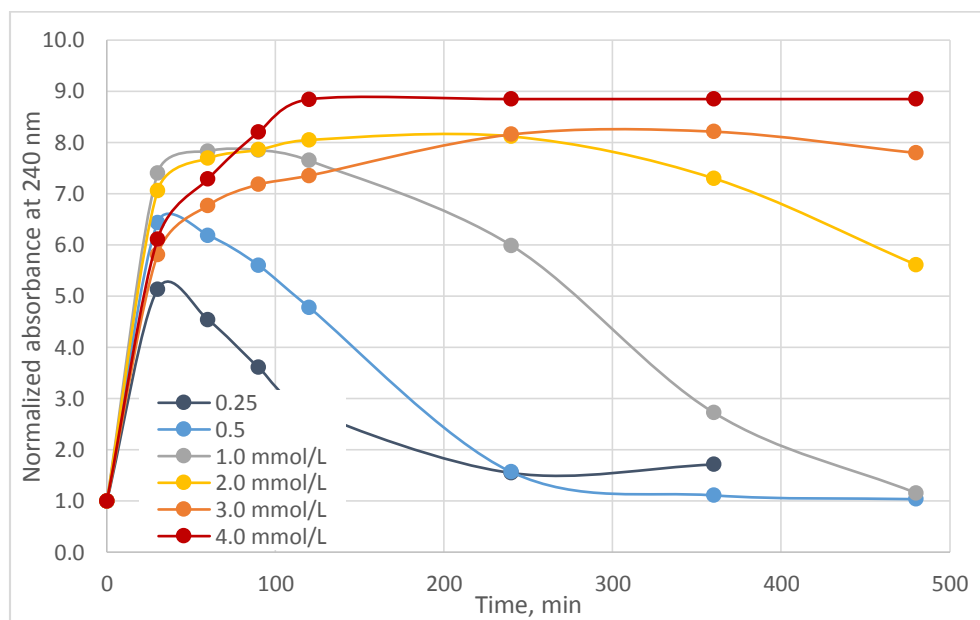
Figure 4.31. Absorption profile at 240 nm during photocatalytic treatment of a mixture with 20 g L^{-1} of single-layer 357 μm-silica gel beads for different initial phenol concentrations

The disappearance of phenol at 269 nm, and destruction of the phenolic ring recorded at 240 nm, is presented in Figures 4.30 and 4.31, respectively. Here, at low phenol concentrations, complete mineralization is observed to occur at a high rate, but as the concentration increases, phenol elimination slows down, and at an initial phenol concentration of 4.0 mmol L^{-1}, it completely stops after about 120 min of treatment. This behavior, indicative of system saturation leading to catalyst deactivation, means that phenol is not being converted to intermediates, and that the intermediates that have been already formed remain unaltered in solution, in other words, that mineralization is no longer underway, as shown in Figure 4.32.
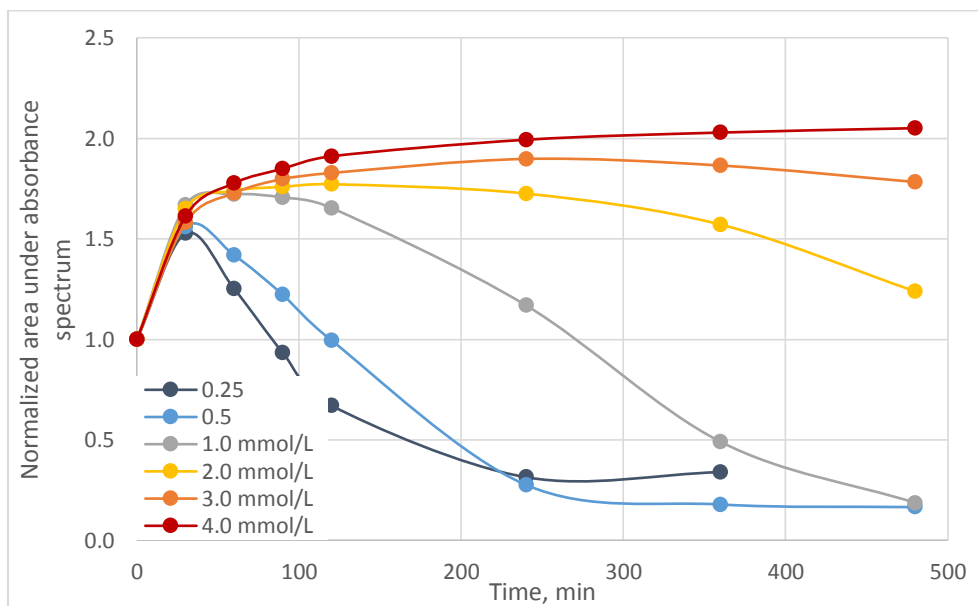
Figure 4.32. Area under absorption spectrum during photocatalytic treatment of a mixture with 20 g L^{-1} of single-layer 357 μm-silica gel beads for different initial phenol concentrations

95

4.2.4. Effect of initial pH.

The pH of the solution is an important variable in the evaluation of aqueous phase mediated photocatalytic reactions. It has been determined that pH has a dominant effect on the process because many properties, such as the surface state of the semiconductor, the flat-band potential, the dissociation of organic contaminant, show a strong dependence on pH (Dyk and Heyns, 1998; Kormann et al., 1991; Munter, 2001).

The effect of pH on the photocatalytic degradation efficiency of phenol-derived COD in the synthetic mixture was studied through several typical experiment by varying the initial pH of the solution from 3 to 9.5, using either NaOH or HCl for pH adjustment, as explained in Section 3.4. For all experiments, a mixture of 20 g/L of 357-μm silica gel beads with a single TiO$_2$ layer and 1.0 mmol L^{-1} of phenol in deionized water was used. The natural, unbuffered pH of the mixture was 5.5. Results are presented in Figure 4.33.
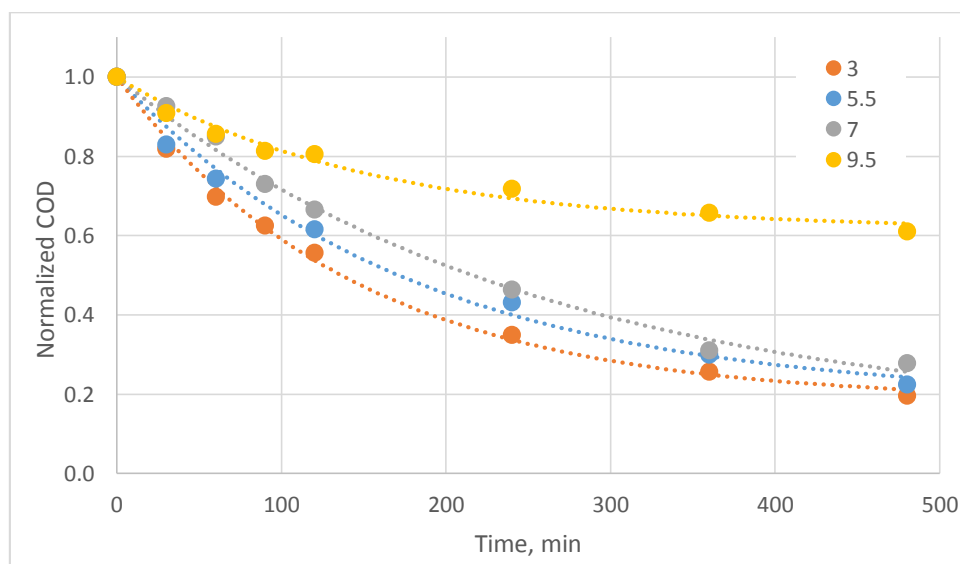
Figure 4.33. COD photocatalytic degradation profile in a mixture of 20 g L^{-1} single-layer 357 μm-silica gel beads and 1.0 mmol L^{-1} phenol for different initial pHs.

The COD photocatalytic removal efficiency decreased considerably with increasing pH, showing at pH 9.5 a 50% reduction from a maximum of 80% at pH 3. $Q_{0.5}$ is also affected by the solution pH, and at alkaline pH, the system does not even achieve 50% COD removal at the end of the 8-h experiment. Under acidic conditions, the photocatalytic removal of COD is enhanced, and higher degradation rate is obtained at pH 3. Figures 4.34 and 4.35 show the variation of the process efficiency with pH.

A number of authors have reported similar observations. Low pHs seem to affect positively the process performance, with pH 3.5 being the optimum for the photocatalytic decomposition of phenol (Okamoto et al., 1985, Serpone et al., 1996, Leyva et al., 1998; Laoufi et al., 2008). Other substrates such as 2,4-dichlorophenol and landfill leachate have been optimally degraded at pH 3.0 (Yung-Hsu and Ting-Shan, 1995; Munter, 2001).
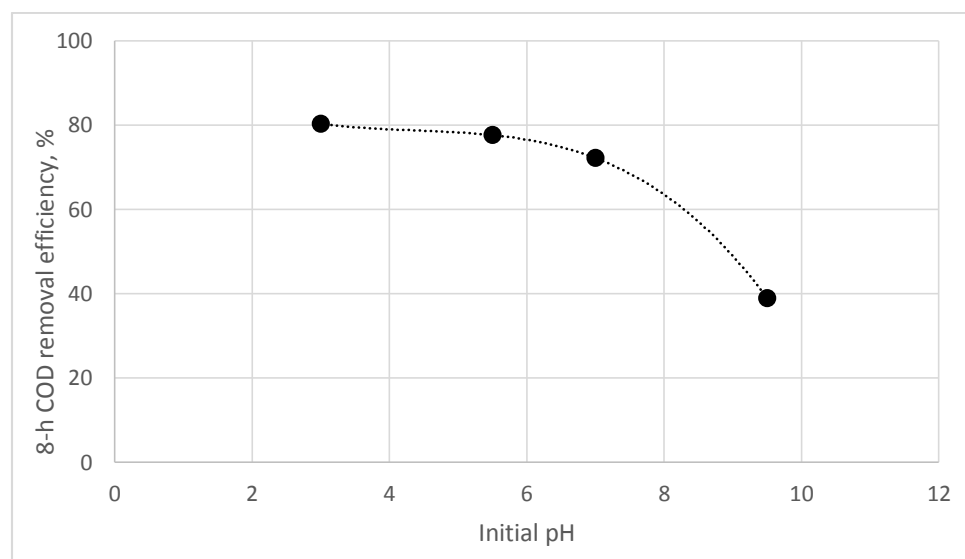
Figure 4.34. 8-h COD removal efficiency variation with initial pH

The influence of this parameter on the semiconductor-mediated photo-degradation of organics have been explained through the effect of the solution pH on the isoelectric

point or the surface charge of TiO_2 (Chong et al., 2009; Ochuma et al., 2007; Chin et al., 2006; Toor et al., 2006).
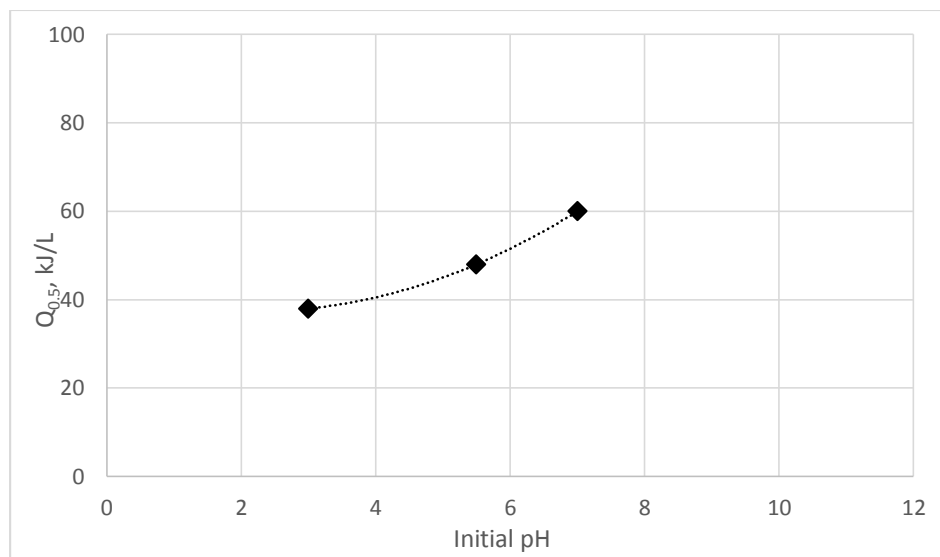
Figure 4.35. $Q_{0.5}$ variation with initial pH

At the point of zero charge (PZC), which lies between 4.5 and 7, the surface charge of TiO_2 is zero or neutral (Chong, 2010), and the interaction between the photocatalyst particles and substrate is minimal due to the absence of electrostatic forces. At pH below the PZC, the surface charge of the catalyst becomes positively charged and exerts a polar attraction towards the charged anionic organic compounds, which results in intensified adsorption onto the photon activated TiO_2 surface for subsequent photocatalytic reactions (Xu and Langford, 2000; Chong et al., 2010). At pHs above the PZC, the catalyst surface becomes negatively charged, repulsing the anionic compounds in water. However, acidic conditions with pH values less than 2 do not favor the photocatalytic oxidation of phenol (Wei and Wan, 1991).

From the evolution of the solution absorbance at 269 nm presented in Figure 4.36, previous observations are corroborated. At pH 3, the disappearance of the phenol peak occurs at the fastest pace, while it is very slow at pH 9.5. This rate is almost identical for neutral pH 5.5, and 7.
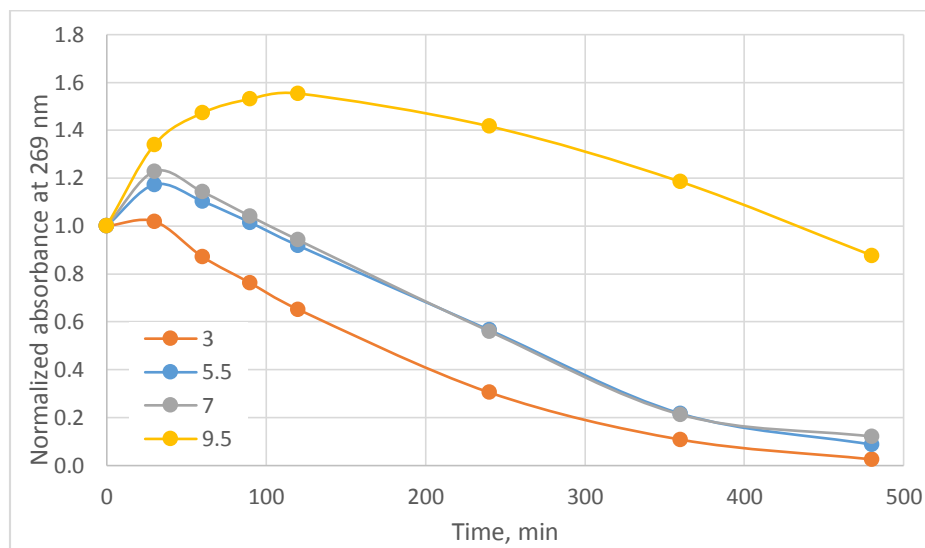
Figure 4.36. Absorption profile at 269 nm of a mixture of 20 g L^{-1} of single-layer 357 µm-silica gel beads and 1.0 mmol L^{-1} phenol for different initial pHs
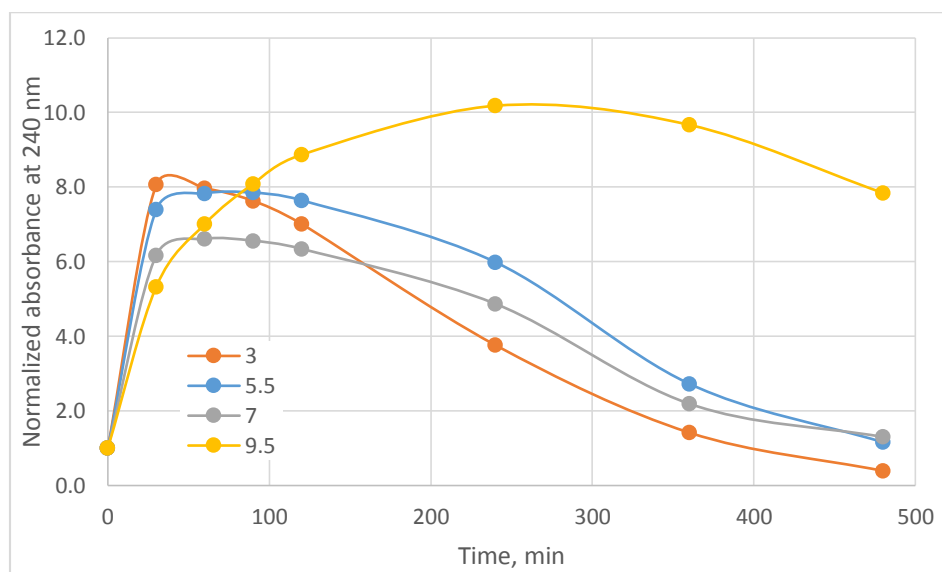
Figure 4.37. Absorption profile at 240 nm of a mixture of 20 g L^{-1} of single-layer 357 µm-silica gel beads and 1.0 mmol L^{-1} phenol for different initial pHs
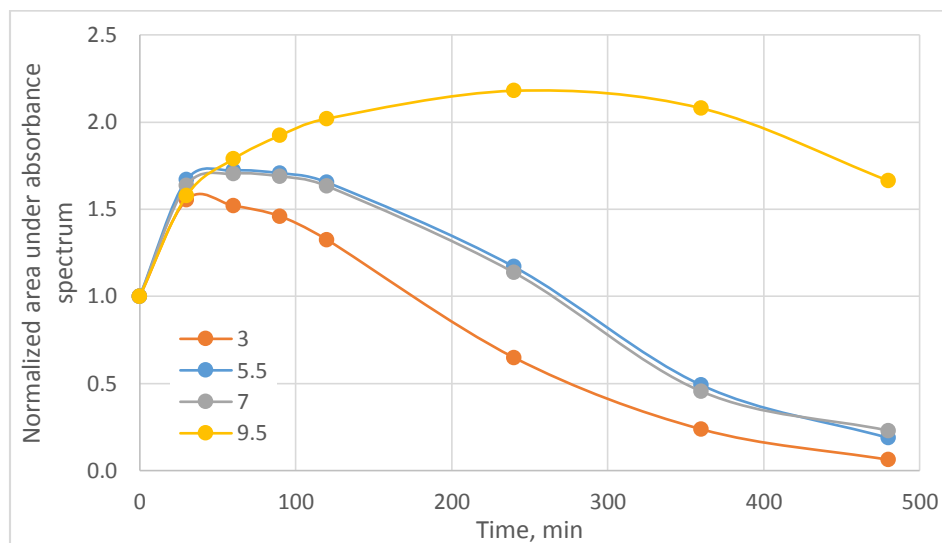
Figure 4.38. Area under absorption spectrum of a mixture of 20 g L^{-1} of single-layer 357 μm-silica gel beads and 1.0 mmol L^{-1} phenol for different initial pHs

The absorption profile at 240 nm presented in Figure 4.37, shows that intermediate compounds form and degrade very rapidly at pH 3, with mineralization progressing at a high rate under acidic conditions, as indicated by Figure 4.38. This trend is compatible with the previously explained effect of low pH on the interaction between catalyst surface and substrate molecules, and indicates the prevalence of surface bound kinetics, where the organic adsorbate (phenol) is oxidized either directly by trapped holes or indirectly by surface-adjacent radicals. At alkaline pHs, the photomineralization mechanism is inhibited, with the elimination of phenol and transformation of intermediates proceeding at a very low rate. At pH 9.5, disappearance of intermediates begins after 300 min of irradiation, as opposed to 30 min for pH 3.

4.2.5. Effect of Salinity.

The effect of solution salinity on the photocatalytic degradation of phenol was studied through controlled change in initial conductivity by means of NaCl addition. The control 1.0 mmol L^{-1} aqueous phenol solution, with a conductivity of 8.0 µS cm^{-1}, was altered by adding 2 and 20 mmol L^{-1} of NaCl, bringing the conductivity up to 5.5 and 38.6 mS cm^{-1}, respectively. Typical experiments were run using mixtures of these solutions and 20 g L^{-1} of 357 µm silica gel beads with a single TiO_2 layer. Results are shown in Figure 4.39.
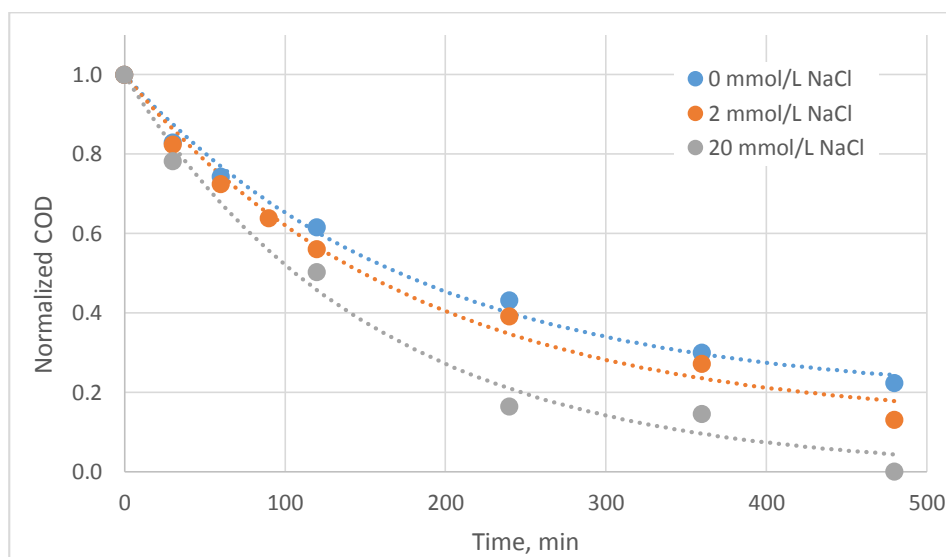
Figure 4.39. COD photocatalytic degradation profile in a mixture of 20 g/L single-layer 357 µm-silica gel beads and 1.0 mmol L^{-1} phenol for different initial NaCl concentrations

Under the experimental conditions, the medium salinity due to dissolved NaCl had a noticeable effect on the COD removal efficiency, as indicated by Figure 4.40 and 4.41. COD elimination rate increased with increasing NaCl concentration, and at 20 mmol L^{-1} of NaCl, COD was completely removed from solution after 8 h of UV-C irradiation. In

general, an increment in reaction rate constants accompanied by a decrease in the absorption ones have been observed. Also, during the photocatalytic oxidation of phenol with powdered TiO_2, the concentration of intermediates formed increased with salinity (Azevedo et al., 2009).
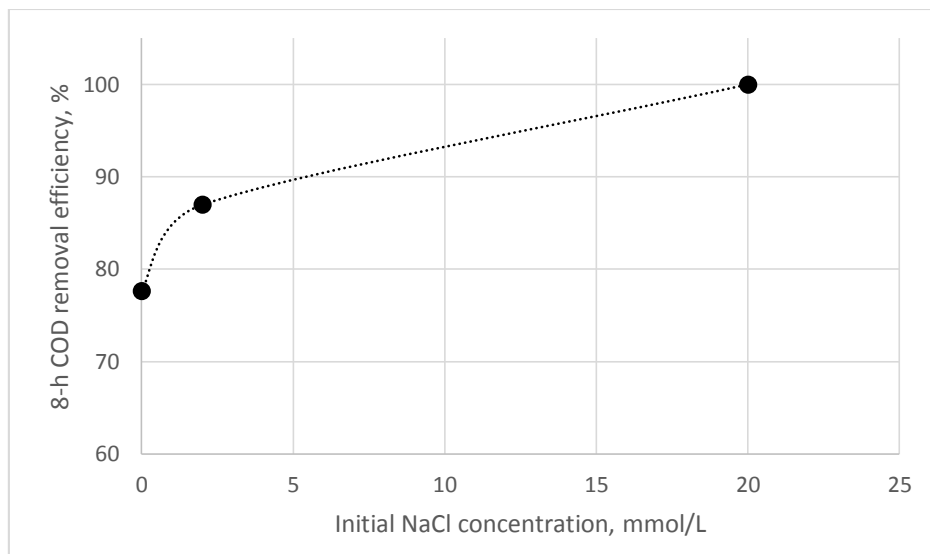
Figure 4.40. 8-h COD removal efficiency variation with NaCl concentration
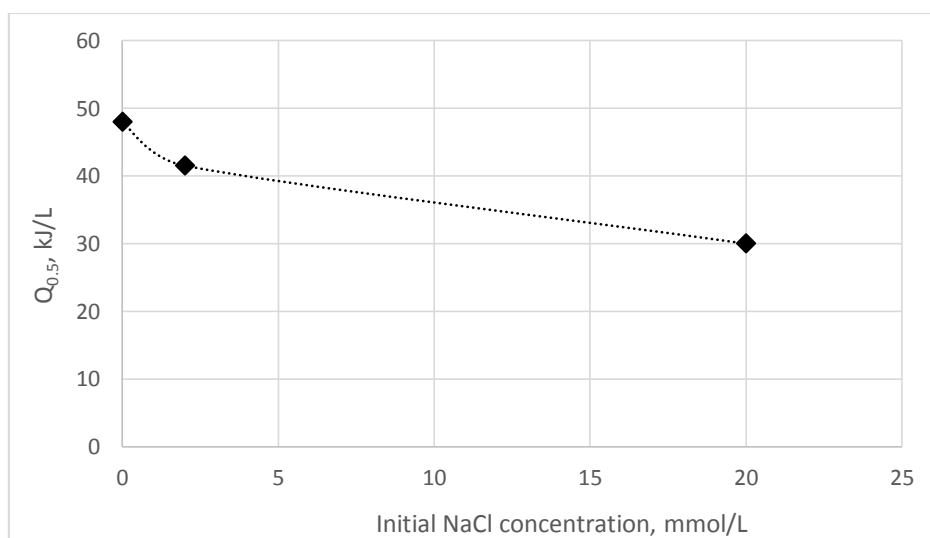
Figure 4.41. $Q_{0.5}$ variation with NaCl concentration

4.2.6. Effect of Dissolved Oxygen.

The importance of dissolved oxygen in the TiO_2-mediated photocatalytic mineralization of organics have been attributed to its role as electron scavenger for conduction band photo-generated electrons. Although the organic substrate itself can be reduced by conduction band electrons (Hisanaga et al., 1990), the usual scavenger of electrons is molecular adsorbed oxygen (Pelizzetti et al., 1992; Gerisher and Heller, 1992; Minero et al., 1996; Szczepankiewicz et al., 2000; Xiao-e et al., 2000; Berger et al., 2005), as per Equation 2.20, which prevents the recombination reactions and leads the vacancies to exert their oxidizing actions directly on the organic material or by intermediate generation of $OH^\bullet$ radicals (Equations 2.18 and 2.19). Dissolved oxygen may also be involved in the formation of other radical oxidative species and the stabilization of radical intermediates (Equations 2.21 through 2.25), mineralization and direct photocatalytic reactions (Chong et al., 2010).

The influence of dissolved oxygen on the photocatalytic elimination of phenol/COD was investigated by comparing the results obtained from photocatalytic experiments with and without added oxygen. During the course of a typical experiment, pressurized pure oxygen was fed through a valve at the top of the photo-reactor, thus maintaining the mixture in permanent contact with the gas at approximately $1x10^3$ kPa (1 atm), as explained in Section 3.1. As it has been found by others (Bedford et al., 1994; Wyness et al., 1994; Klausner and Goswami, 1995), there is no need to bubble the gas through the reaction mixture since the performance does not depend on aeration. The absorption of oxygen by the surface of the solution is sufficient for photocatalytic

oxidation. This means that the absorption of oxygen by the liquid phase is not the rate limiting process (Munter, 2001).

During the alternative experiment, no oxygen was supplied and the reactor was kept sealed at the top, impeding the entrance of atmospheric air. Results are presented in Figure 4.42.
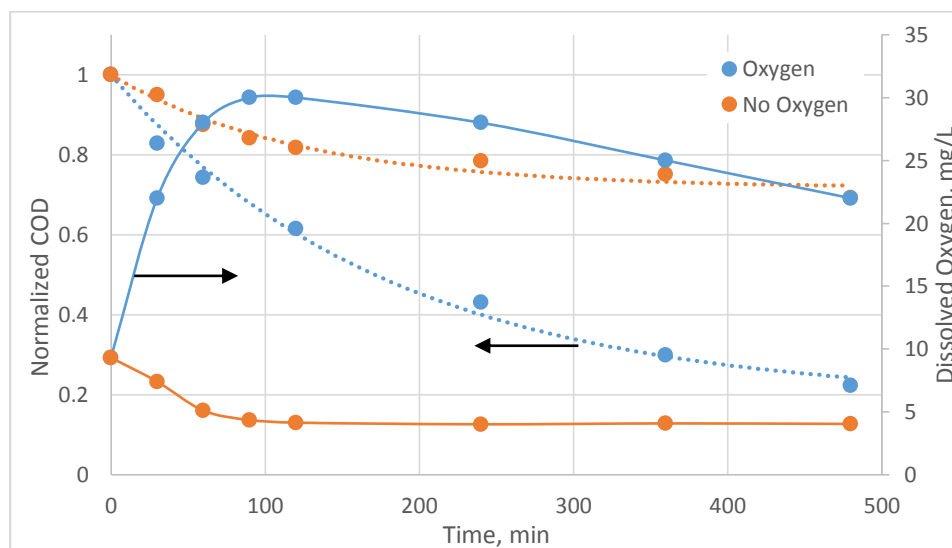
Figure 4.42. COD photocatalytic degradation and dissolved oxygen concentration profiles in a mixture of 20 g L^{-1} single-layer 357 μm-silica gel beads and 1.0 mmol L^{-1} phenol with and without added oxygen

During the non-oxygenated experiment, dissolved oxygen concentration decreases with irradiation time, reaching a minimum of 4 mg L^{-1} after 90 min. The beginning of this phase of maximum oxygen deficit coincides with a drastic reduction in the COD elimination rate. Under oxygenated conditions, the oxygen concentration in solution reaches saturation during the first 90 min of the experiment, meaning that the gas is effectively absorbed by the liquid phase through its surface. Oxygen concentration decreases with irradiation time as the operating temperature increases (Figure 4.43). After

8-h of irradiation, 78% COD removal is achieved if oxygen is added, while only 30% of COD is eliminated if not.
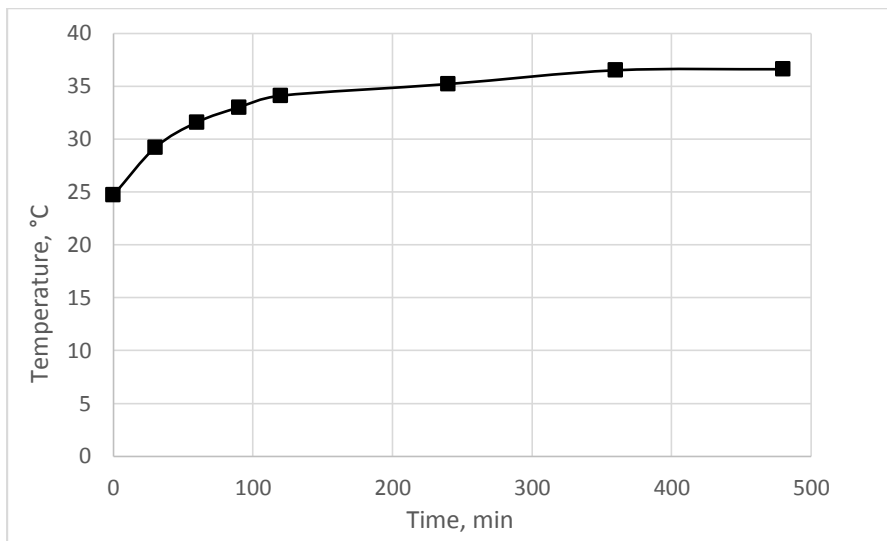
Figure 4.43. Temperature profile during a typical photocatalytic experiment

Figures 4.44 through 4.46 show the evolution of phenol mineralization with and without added oxygen. In the latter case, not only the disappearance of the phenol absorption peak at 269 nm slows down considerably, but also the maximum concentration of intermediates formed during irradiation time is roughly half of that achieved when oxygen is supplied to the system.

These results may imply that the rate-limiting reaction step is the formation of active oxygen species through reactions involving the solvent as per Equations 2.18 through 2.25 (Turchi and Ollis, 1990). They also demonstrate the synergism between photocatalytic oxidation and reduction processes on UV-illuminated TiO_2.
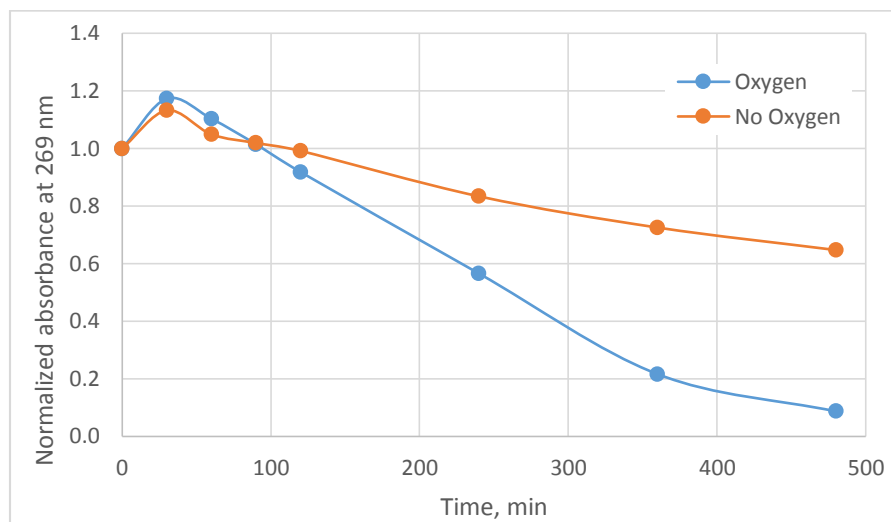
Figure 4.44. Absorption profile at 269 nm of a mixture of 20 g L^{-1} of single-layer 357 μm-silica gel beads and 1.0 mmol L^{-1} phenol with and without added oxygen
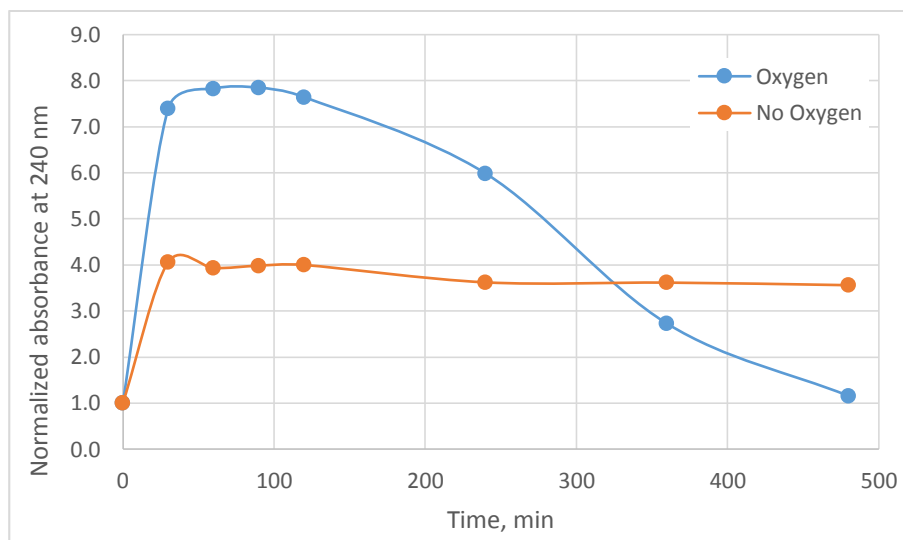
Figure 4.45. Absorption profile at 240 nm of a mixture of 20 g L^{-1} of single-layer 357 μm-silica gel beads and 1.0 mmol L^{-1} phenol with and without added oxygen
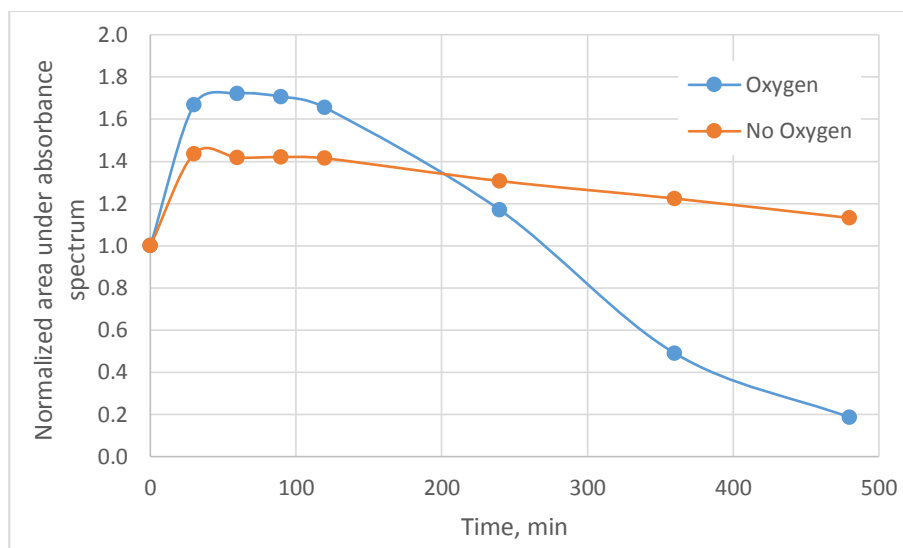
Figure 4.46. Area under absorption spectrum of a mixture of 20 g L^{-1} of single-layer 357 μm-silica gel beads and 1.0 mmol L^{-1} phenol with and without added oxygen

It has been suggested that efficient photocatalytic systems for decontaminating water can only be realized if both the oxidation and reduction half-reactions occur rapidly. Therefore, it is essential to consider and possibly optimize reduction when designing photocatalytic system for oxidation applications and vice versa for reduction applications (Prairie, et al., 1993). This means, among other considerations, pressurizing the reactor with air or oxygen (Pelizzetti and Serpone, 1988).

4.2.7. Effect of number of TiO$_2$ Layers.

The silica gel beads used as catalyst support (Figure 4.47) are of high-purity grade (Davisil Grade 636) with a very large surface area, approximately 480 m^2 g^{-1}, and a pore size of 60 Å. TiO$_2$ was deposited on these beads through the sol-gel technique describe in Section 3.3, which involves direct synthesis of the catalyst on their surface. Energy-dispersive X-ray spectroscopic observations of the cross-section of silica gel beads with

107

fixed TiO$_2$ have shown that the catalyst deposited only on the surface of the beads. This means that the precursor sol does not penetrate the silica micropores since ethanol molecules already occupy these (Kobayakawa et al., 1998).

Due to the nature of the precursor deposition and catalyst synthesis processes, quality and uniformity of the TiO$_2$ layer depend on many factors, such as grade of reagents, age of sol precursor, mass of silica gel per batch, frequency and velocity of silica beads/sol precursor stirring, air flow rate during calcination, among others. Although it has been found that, once the photocatalyst adheres to the support, a very thin layer of a few hundred angstroms is sufficient to absorb all the available light (Bideau et al., 1995), repeated depositions could be necessary to ensure full coverage of the silica gel particle.
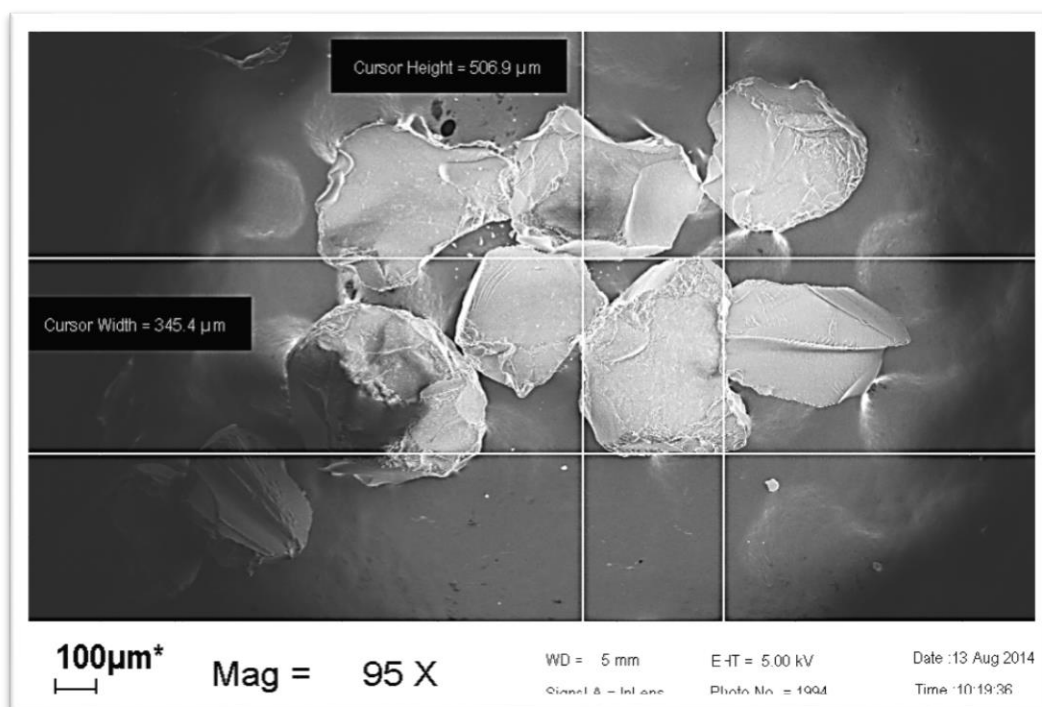
Figure 4.47. SEM image of uncoated silica gel beads with average diameter of 357 μm

Scanning electron microscopy of the coated silica beads (Figures 4.48 through 4.50) shows that a single coat of photocatalyst deposits as an irregular film with visible creases (Figures 4.48.a and b). In some areas, this first coating may have fractured and fallen off, leaving behind pieces of catalyst that remained attached to the surface.

Additional coatings lead to the formation of a thicker but cracked catalyst layer (Figures 4.49.a, b and c). Figure 4.50 shows a SEM image of TiO_2 particles agglomeration taken on silica beads after three coatings. The observed morphology resembles that of anatase as reported by the literature (de Lasa et al., 2005).
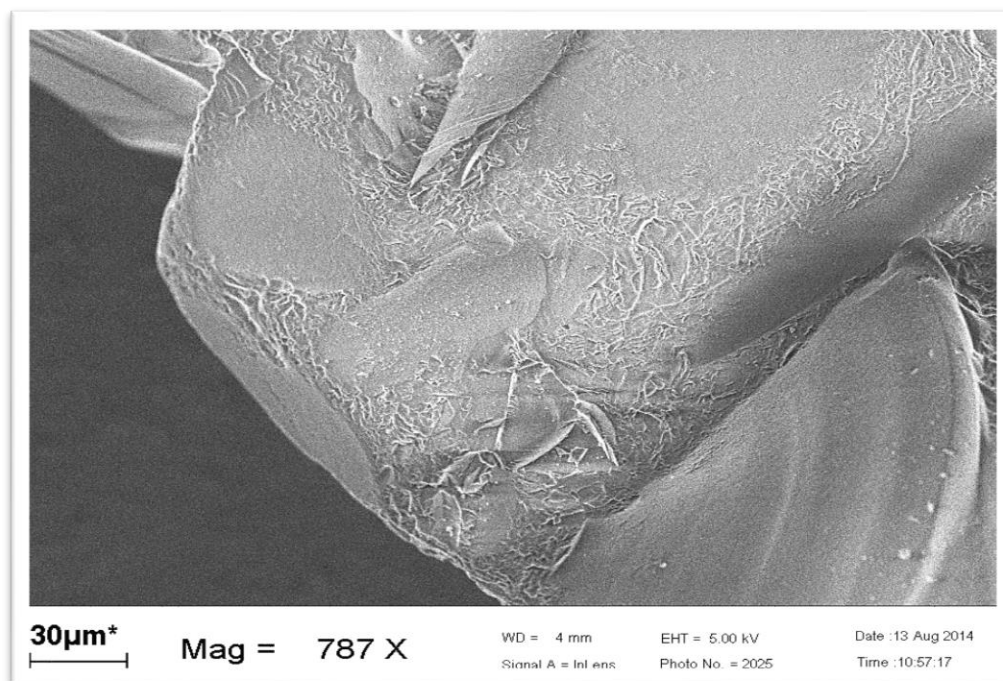
Figure 4.48.a. SEM image of silica gel beads after one TiO_2 coating
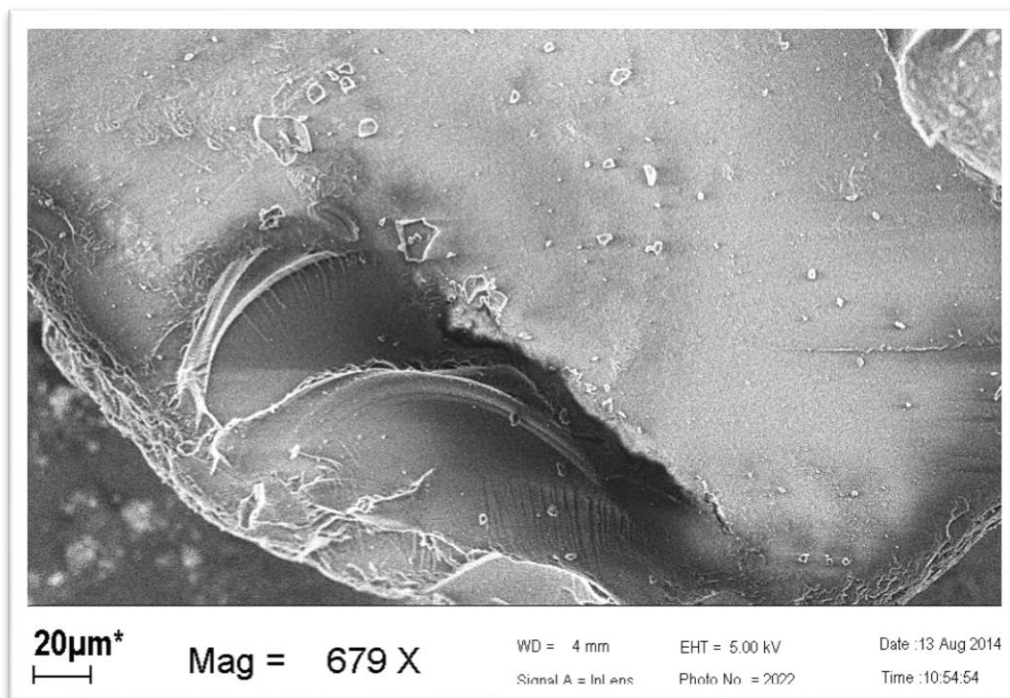
Figure 4.48.b. SEM image of silica gel beads after one TiO$_2$ coating
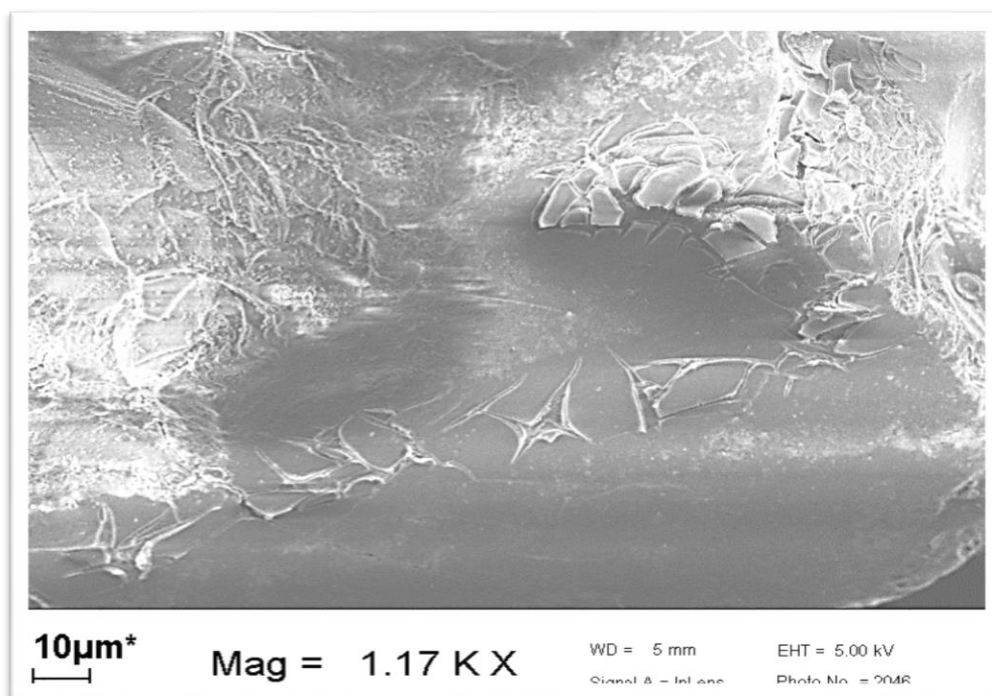
Figure 4.49.a. SEM image of silica gel beads after three TiO$_2$ coatings
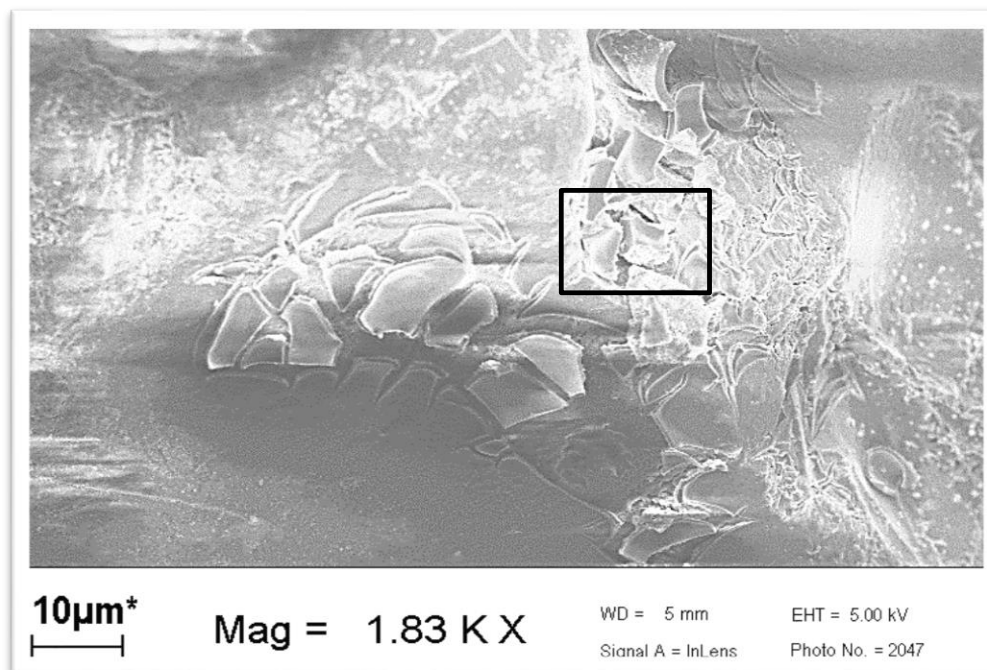
Figure 4.49.b. SEM image of silica gel beads after three TiO$_2$ coatings
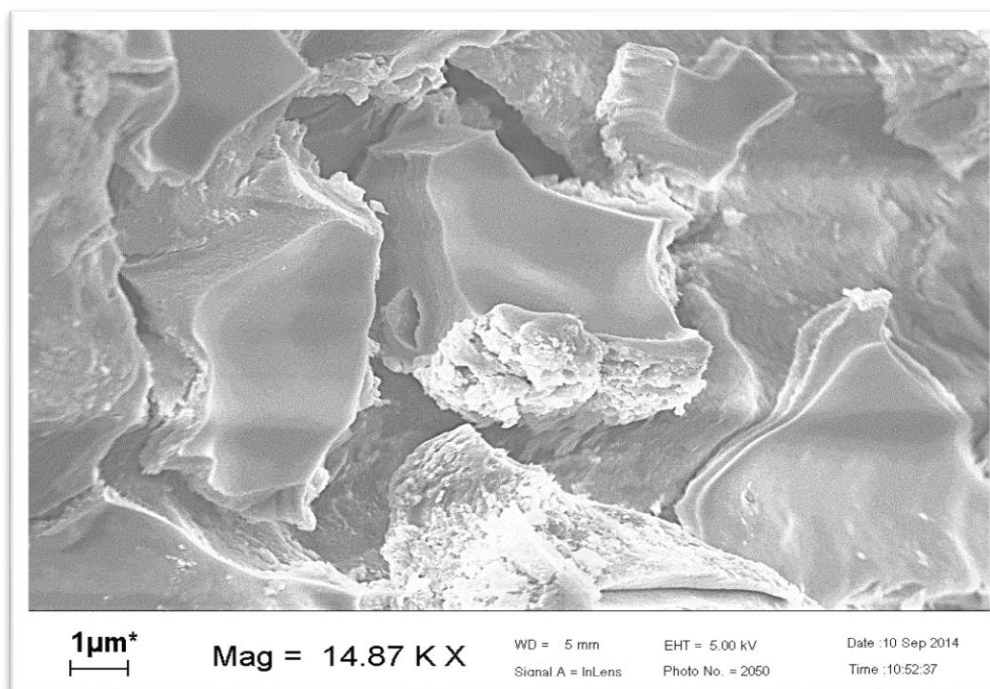
Figure 4.49.c. SEM image of silica gel beads after three TiO$_2$ coatings (detail)
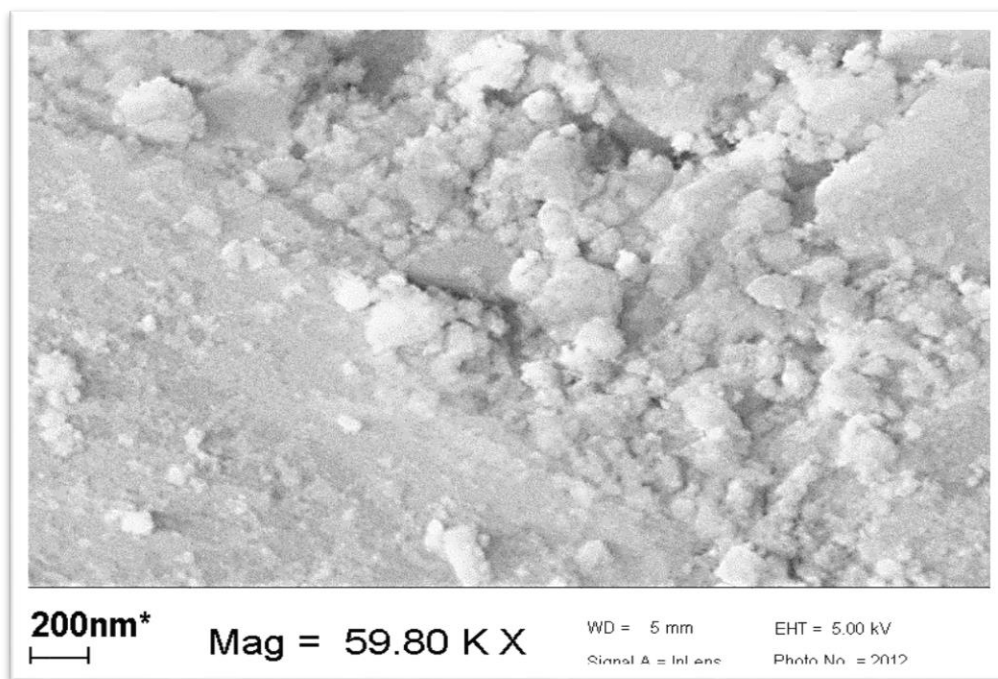
Figure 4.50. SEM image of TiO$_2$ primary particles (anatase) agglomeration

Reports on grain average diameter of anatase synthetized by the sol-gel method, measured through scanning electron micrographs, show a particle size ranging from 80 to 200 nm (Rodriguez and Matousek, 2004; de Lasa et al., 2005), which coincides with that of the small and isolated grains observed in Figure 4.50. The also common mineral form of TiO$_2$, rutile, forms larger particles in the range of 300 to 1060 nm (de Lasa et al., 2005).

Up to three consecutive coats of TiO$_2$ were applied onto the silica gel beads, as described in Section 3.3, and their weight increase after each application is reported in Table 4.2. In average, each coating deposited 6.5% of the silica mass as TiO$_2$.

Table 4.2. Percent weight increase of 357 μm-silica gel beads with number of TiO_2 layers

	Silica gel Mass (g)			% Weight Increase	Cumulative % Increase
Uncoated	60.6366				
1 Coat	64.7888	34.478		6.85	6.85
2 Coats		36.6025	19.5084	6.16	13.43
3 Coats			20.7739	6.49	20.79

The COD removal efficiency achieved when using silica gel beads of 357 μm in average diameter with one, two and three TiO_2 coats was measured by means of typical photocatalytic experiments run with a mixture of an aqueous phenol solution of 1.0 mmol L^{-1} and 20 g L^{-1} of coated silica beads. The results obtained with each type of silica particles is presented on Figure 4.51.
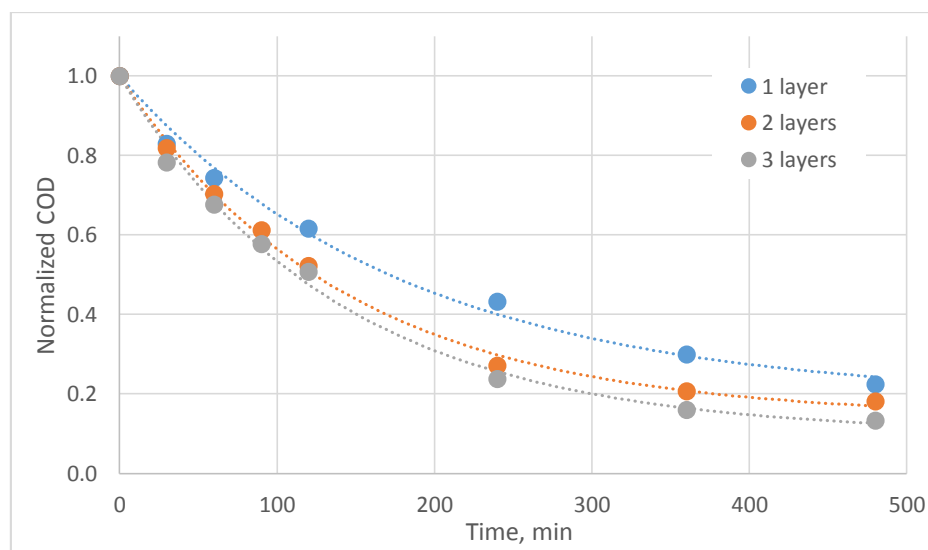
Figure 4.51. COD photocatalytic degradation profile in a mixture of 1.0 mmol L^{-1} phenol and 20 g L^{-1} of 357 μm-silica gel beads with different number of TiO_2 layers

As expected, the system efficiency increased with the number of photocatalyst layers, indicating that the added TiO_2 mass improved catalyst availability for photon absorption and substrate oxidation. As shown in Figure 4.52, COD removal efficiency after 8 hours of irradiation increased by 10% after two additional layers of TiO_2 were applied onto the catalyst support. Similarly, $Q_{0.5}$ decreased from 48 to 31 kJ L^{-1}, as shown in Figure 4.53.
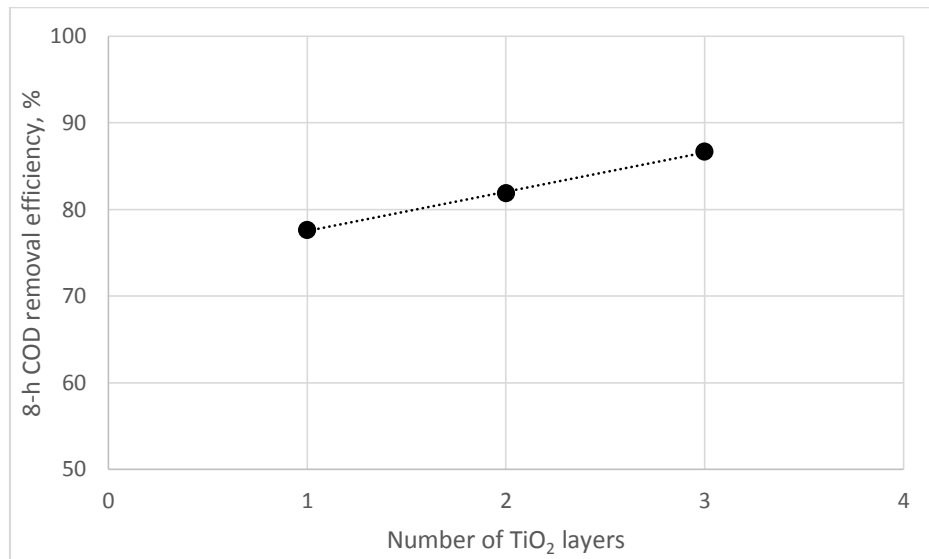
Figure 4.52. 8-h COD removal efficiency variation with number of TiO_2 layers
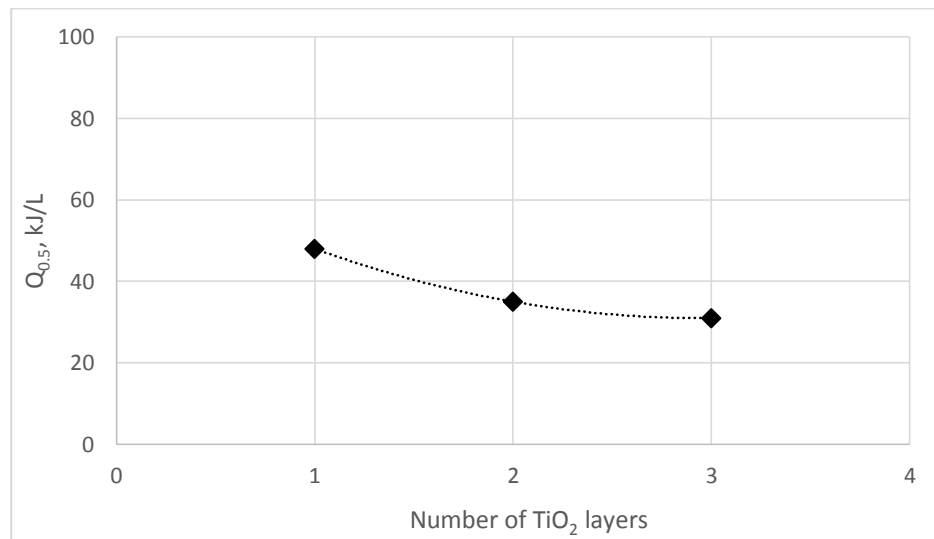
Figure 4.53. $Q_{0.5}$ variation with number of TiO_2 layers
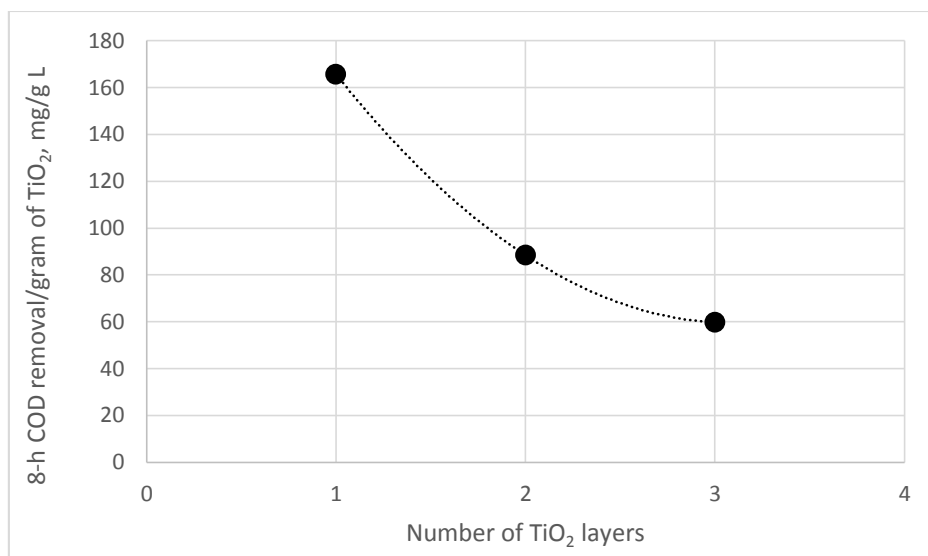
Figure 4.54. Variation of 8-h COD removal per gram of TiO_2 with number of TiO_2 layers

In general, the deposition of additional photocatalyst through the experimental technique herein utilized improves COD removal by enhancing silica coverage and therefore, increasing the TiO_2 surface area exposed to irradiation. However, in a mg L^{-1}- of COD-removed per gram-of-deposited-catalyst basis, the opposite is true, as shown by Figure 4.54. Such results confirm that the catalyst deposits as a layer on the silica surface, and that is not the thickness of this layer but its extension that influence the photocatalytic degradation rate of the organic substrates.

4.3. COD Removal Efficiency by Process Type and Photo-Reactor Maximum Efficiency

The ability of the studied photocatalytic system to remove phenol-derived COD under different conditions other than those so far described was measured by means of control experiments. By changing the operational settings of the photo-reactor, the COD oxidation efficiency in an aqueous solution with 1.0 mmol L^{-1} initial phenol concentration was evaluated for the following processes:

i) Adsorption only, by running an experiment "in the dark" with a mixture of the phenol solution and 20 mg L^{-1} of 357 μm-uncoated silica gel beads.

ii) Photolysis only, by irradiating the phenol solution with UV-C light in the absence of silica beads and a catalyst.

iii) Photolysis + adsorption, through a typical experiment using a mixture of the phenol solution and 20 g L^{-1} of 357 μm-uncoated silica.

iv) Photocatalysis with anatase powder, by running the system as a slurry type reactor, where the mixture consisted of a suspension of the phenol solution and 1.25 g L^{-1} of TiO_2 nano-powder (This amount of TiO_2 is equivalent to the mass of catalyst deposited on 20 g L^{-1} of silica gel beads after a single sol-gel coating).

The results of this set of control experiments is presented in Figure 4.55. For comparison purposes, results of the photocatalytic experiments preformed using a mixture of the phenol solution and silica beds with one and three TiO_2 layers has also been included.
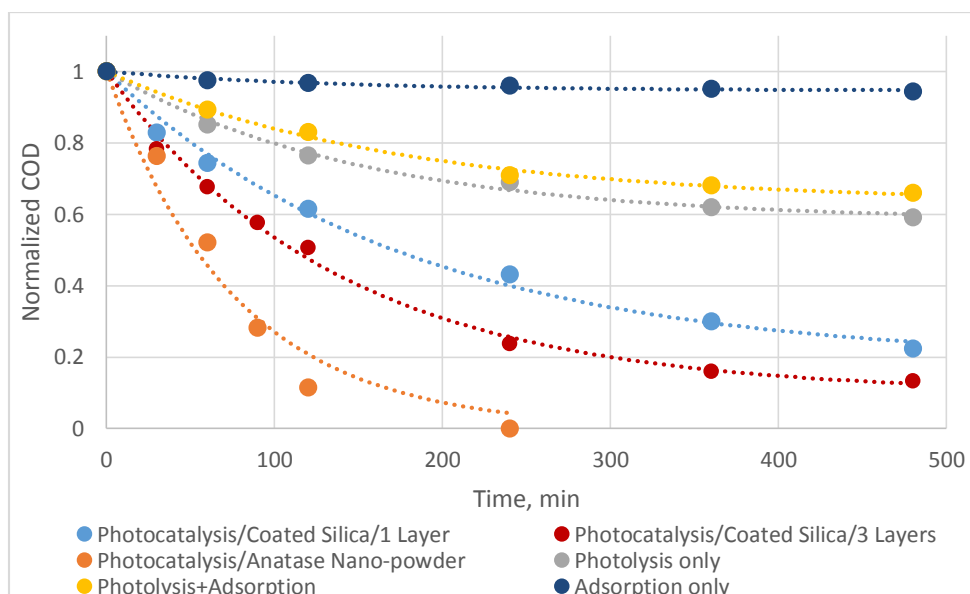
Figure 4.55. COD elimination profile in a 1.0 mmol L^{-1} phenol solution for different processes

Adsorption of phenol on the silica gel particles is low, and COD removal after 8 hours of contact is negligible. On the other hand, photocatalysis with anatase nano-powder is a highly efficient process, removing 100% of the COD after only 4 hours of irradiation. Photolysis only was slightly more efficient than photolysis in the presence of uncoated silica, evidencing the light-blocking effect of the silica beads. Photocatalysis with TiO_2-coated silica gel was 100% more efficient than photolysis only, being able to remove more than twice the initial COD after 8 hours of treatment.

Absorption profiles of the phenol solution acquired during the course of the experiments, presented in Figures 4.56 through 4.58, show the differences in the mineralization progress for each process type. The rate of phenol mineralization is the fastest for anatase nano-powder photocatalysis. This rate is lower for coated-silica photocatalysis, and it tends to zero in the case of adsorption. Although UV-C photolysis is capable of oxidizing phenol by itself, the pace at which the phenol peak at 269 nm disappears and intermediates are eliminated, is noticeably slower than that for both modes of photocatalysis.

As discussed in Section 4.2.3, the initial substrate concentration in the target solution has a significant effect on the photocatalytic COD removal efficiency. Figures 4.59 and 4.60 show that this variable not only affects the fixed-catalyst photo-mineralization process, but that it has a marked influence on the organics photo-oxidation mechanism. By measuring the COD removal in a solution with different initial phenol concentrations, the effect of substrate load on process efficiency was evaluated in the case of photolysis only and anatase nano-powder photocatalysis, and compared to that of its TiO_2-coated-silica gel counterpart.
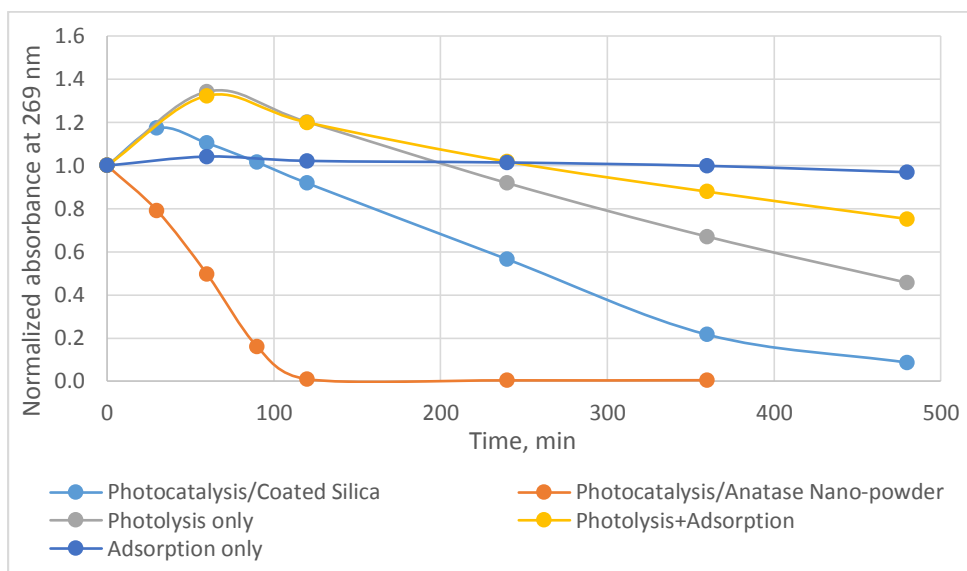
Figure 4.56. Absorption profile at 269 nm of a 1.0 mmol L^{-1} phenol solution for different processes
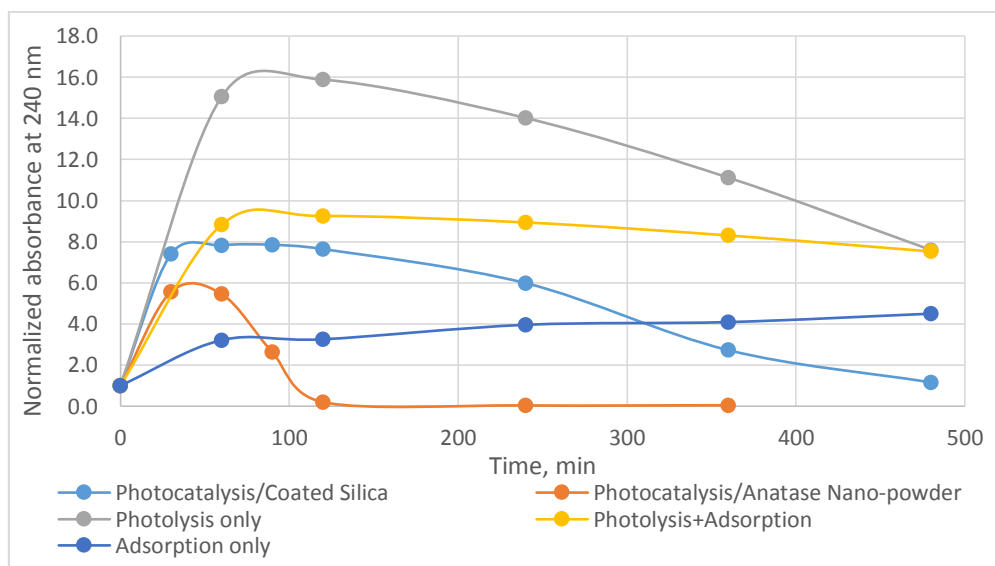
Figure 4.57. Absorption profile at 240 nm of a 1.0 mmol L^{-1} phenol solution for different processes
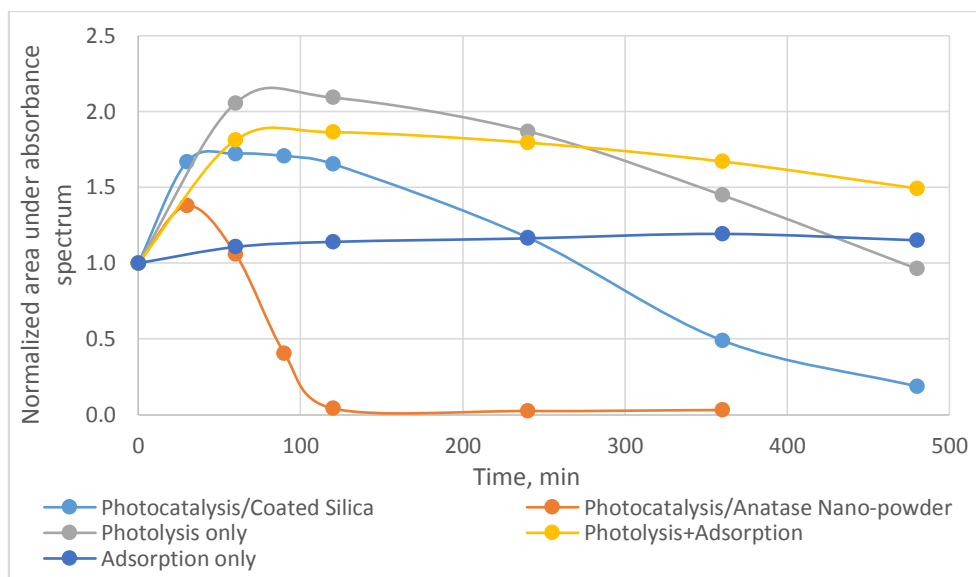
Figure 4.58. Area under absorption spectrum of a 1.0 mmol L^{-1} phenol solution for different processes

The maximum photo-reactor efficiency is achieved under slurry-type conditions when using TiO$_2$ nano-powder as catalyst. Such a process removes the totality of the COD in solution with initial phenol concentration of up to 2.0 mmol L^{-1}. Beyond this point, the 8-h removal efficiency decreases with increasing substrate load. After 8 hours of treatment, at the low and high end phenol concentrations, 0.25 and 4 mmol L^{-1}, respectively, photocatalysis over suspended anatase powder is as efficient as the photocatalysis over tripled-coated silica. Also, at very low substrate concentrations, photolysis and photocatalysis over single-coated silica reach the same level of COD removal.

Energy consumption for COD removal increases with substrate load for all the compared photo-oxidation processes across the full range of experimental initial phenol concentrations, with nano-powder photocatalysis being the most efficient. Figure 4.60 shows that for both types of photocatalysis, the Q$_{0.5}$ increases with the phenol concentration in the irradiated suspension, and under the experimental operational conditions, these processes are capable of removing at least

119

50% of the initial COD. However, photolysis can only achieve the half-concentration point at very low phenol initial loads (less than 0.25 mmol L^{-1}).
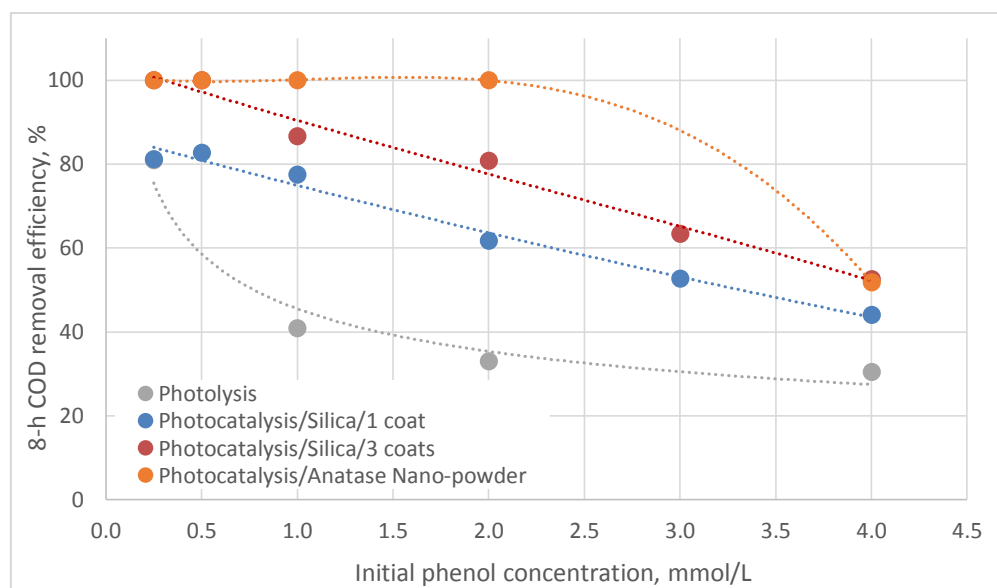
Figure 4.59. 8-h COD removal efficiency variation with initial phenol concentration for different photo-oxidation processes
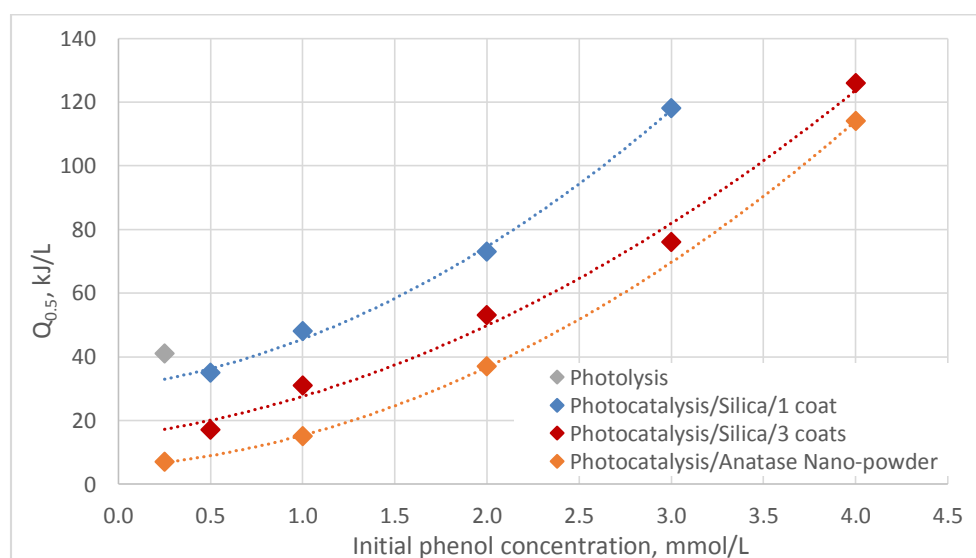
Figure 4.60. $Q_{0.5}$ variation with initial phenol concentration for different photo-oxidation processes

The photolytic degradation of phenol has been found to be considerably more efficient under UV-C ($\lambda < 254$ nm) than under UV-A ($\lambda > 350$ nm) light (Matthews and McEvoy, 1992; Chun et al., 2000; Puma and Yue, 2002), owing to the shorter penetration capability of the higher energy photons yielding more electron-hole pairs available for the substrate molecules. But when a photocatalyst is added to a system where the emission spectrum of the light source coincides with that of the target compound, as is the case in the studied photo-reactor, both the catalyst and the organic molecules will compete for the photons, with one of the two mechanisms predominating in the process (Bayarri et al, 2007). Therefore, comparing photolysis and photocatalysis under similar experimental conditions gives an idea of the magnitude of the contribution of the former to substrate removal. By the results shown in Figure 4.59, concomitant photolytic and photocatalytic reactions play a part in COD degradation at very low phenol concentrations, but as the latter increases, the fraction of photons absorbed by the TiO$_2$ surface also increases, and then mineralization proceeds mainly through photocatalytic mechanisms.

In general, the presence of TiO$_2$ as catalyst, either as a fixed layer on fluidized silica gel beads or as powder suspended in the mixture, enhances the process efficiency significantly over that of UV-C photolysis by increasing photon uptake (Bayarri et al., 2007). However, at high phenol concentrations, substrate oxidation by photocatalysis becomes ineffective and energy consuming.

4.4. Photo-Reactor Modeling

Developing a comprehensive kinetic model for the photocatalytic oxidation of organic substrates poses a particular challenge for kineticists since experimental data has shown a

dependence of the Langmuir adsorption constant on the intensity of the photon flux (Emeline et al., 2000). Such a fact is a contradiction of the Langmuir-Hinshelwood model premise that assumes equilibrated adsorption/desorption of reactants during irradiation. Besides, the adsorption constants of contaminants on the TiO_2 surface obtained from adsorption equilibrium experiments in the dark do not correspond with those obtained from kinetic experiments (Chen and Ray, 1999).

The L-H model does not represent the mechanism of heterogeneous photocatalysis since it ignores a number of steps such as: the generation of charge-carriers by absorption of photons, free electrons in the conduction band and free holes in the valence band, reduction of oxygen by the photogenerated electrons, trapping of photogenerated holes in surface states, recombination of charge carriers, oxidation of organic matter by free holes or surface holes, and presence of back reactions (Valencia et al., 2011). However, despite this discordance, many studies are still basing their kinetic analysis of organics photocatalysis on the calculation of the L-H adsorption/desorption constant.

In the case of multi-organic matrices treatment, a more realistic approach to process modeling can be done by studying the photo-mineralization of global lump-sum parameters such as TOC or COD under controlled operational conditions, as suggested in Section 2.6 through Equation 3.33. This has been done in a number of studies for photo-reactors operated as slurry-type systems (Minero et al., 1996; Bayarri et al, 2007).

The photocatalytic system developed in this research uses TiO_2-coated silica beads fluidized in the bulk liquid. The COD decay profile obtained with this system may indicate catalyst saturation occurs during irradiation for it reaches a plateau or minimum COD. Such behavior was not observed when using anatase nano-powder (Section 4.3). The system also lacks a temperature

control mechanism, thus temperature increases with irradiation time, as shown in Figure 4.43, which has an accelerating effect on reaction rates during phenol mineralization (Section 4.2.2, Comninellis and Pulgarin, 1993). These conditions of non-ideality make the fitting of the experimental data to conventional kinetic models or the development of new ones very challenging, placing it beyond the scope of this research.

However, for practical purposes, the system performance can be predicted for any given initial phenol concentration through a simple model based on correlation of parameters derived from statistical analysis of the experimental data. As mentioned before, in the case of photocatalytic degradation over fixed TiO_2, the concentration of COD in the mixture decays exponentially with irradiation time (or energy consumption), and even at low phenol concentrations, substrate concentration plateaus before reaching complete elimination. Thus, experimental data points can be fitted through non-linear regression (GraphPad Prism 6 ®) to a one phase decay model of the form:

$$Y = (Y_0 - Plateau)e^{-kX} + Plateau \tag{4.2}$$

Which can be rewritten for the case of COD decay vs. time as:

$$C_t = (C_0 - C_L)e^{-kt} + C_L \tag{4.3}$$

where C_t represents the COD (in mg/L) remaining at time t (in min); C_0 and C_L are the initial and minimum COD, respectively, and k is the photocatalytic pseudo-constant in min^{-1}.

Statistical fitting was done on data from typical photocatalytic experiments using a mixture containing 20 g L^{-1} of 357 μm silica gel beads with a single coat of TiO_2 in aqueous phenol solution

of different initial concentrations, unbuffered pH, and no NaCl added. Figure 4.61 show the experimental data points and best fit curves for different initial phenol concentrations.
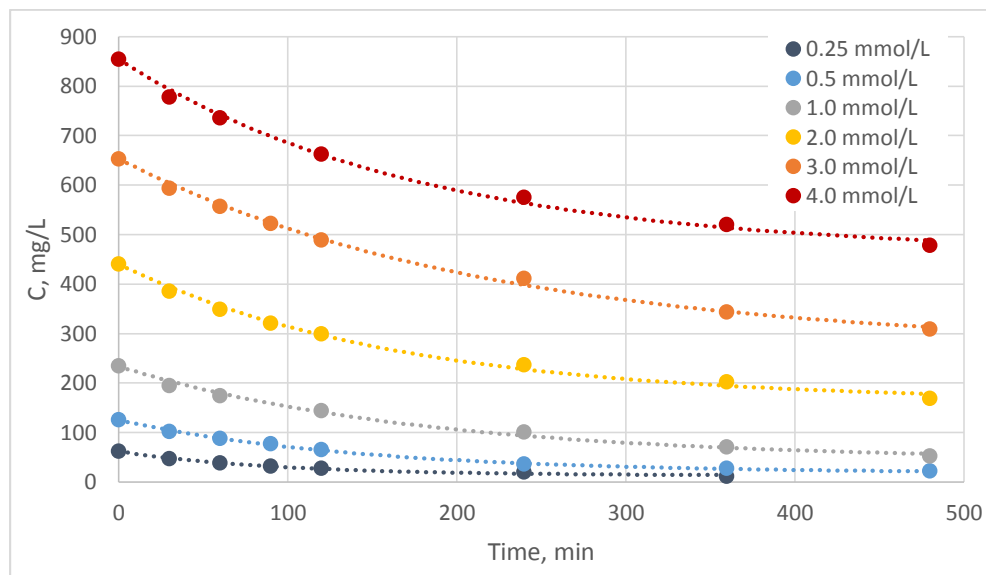
Figure 4.61. COD vs time experimental points and exponential decay fit curves for photocatalytic experiments using a mixture of 20 g L^{-1} 357 μm-silica gel beads coated once and different initial phenol concentrations

The values of k and C_L obtained from fitting the data to Equation 4.3 are different for each initial concentration, as expected; however, with further data manipulation, these parameters can be expressed as a function of C_0. Statistical analysis shows that the pseudo constant k also varies exponentially with respect to the initial COD, C_0; thus the exponential decay model in Equation 4.2 can be rewritten as:

$$k = (k_0 - k_L)e^{k'C_0} + k_L \tag{4.4}$$

where k_0, k_L and k' are correlation constants for this particular system. Results of the non-linear regression fit of k as a function of C_0 through Equation 4.4 are presented in Figure 4.62.
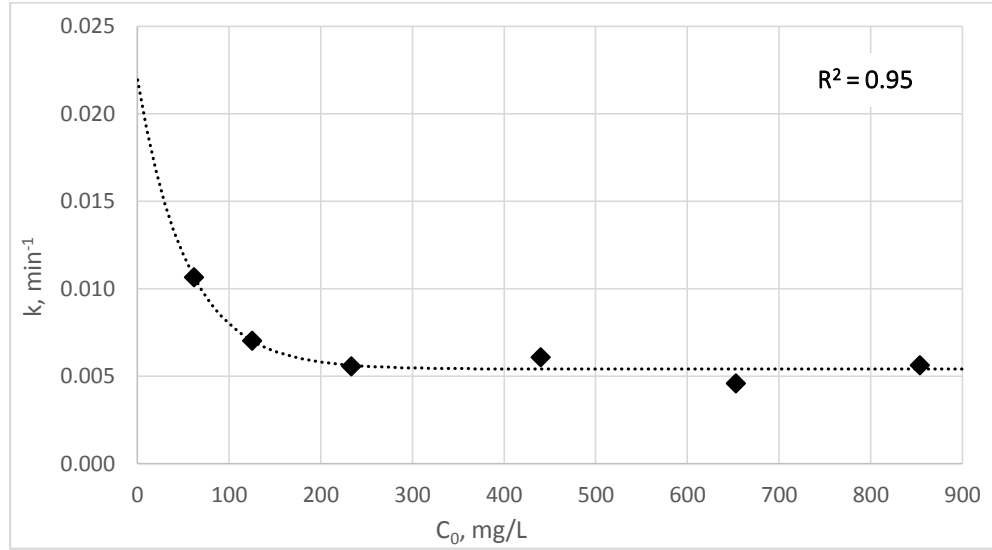
Figure 4.62. k vs C_0 exponential fit for photocatalytic experiments using a mixture of 20 g L^{-1} 357 μm-silica gel beads coated once and different initial phenol concentrations

Similarly, the minimum COD, C_L, can be written as a power function of C_0, as follows:

$$C_L = k_\omega C_0^{k^*} \tag{4.5}$$

where k_ω and k^* are also constant for the system under study. The regression results are shown in Figure 4.63.

In Section 4.2.7 it was shown that COD removal efficiency increases with the number of TiO$_2$ coatings. Therefore, a similar procedure for modeling the system when using silica gel beads coated with three layers of TiO$_2$ was applied, and results are presented in Figures 4.64 through 4.66. All other experimental conditions were kept unchanged.

125
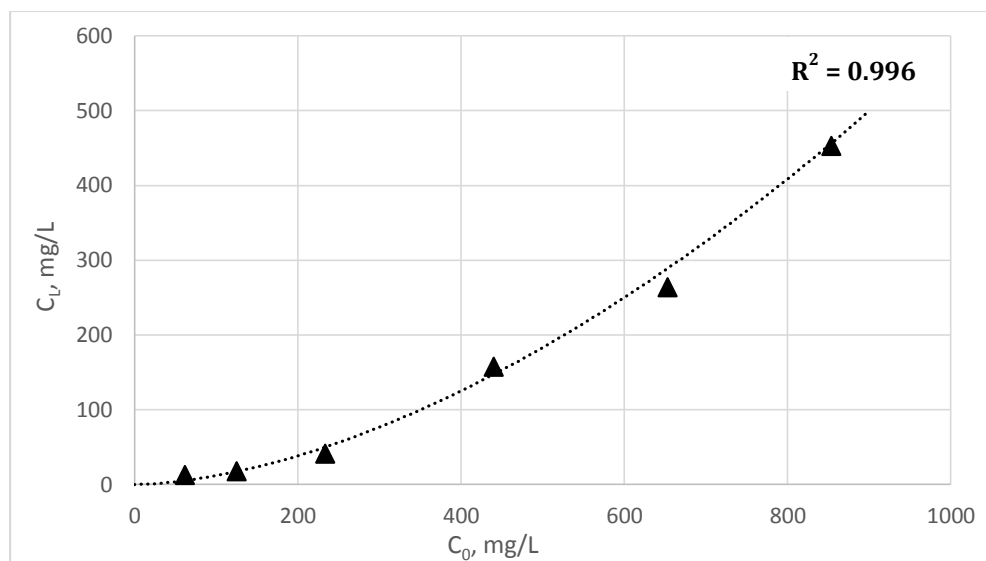
Figure 4.63. C_L vs C_0 power fit for photocatalytic experiments using a mixture of 20 g L⁻¹ 357 µm-silica gel beads coated one and different initial phenol concentrations
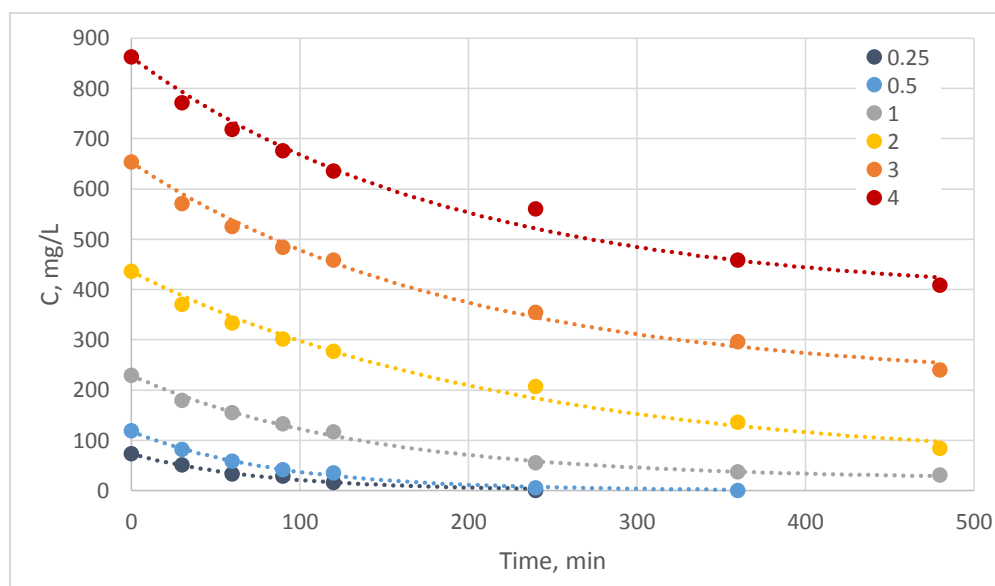
Figure 4.64. COD vs time experimental points and exponential decay fit curves for photocatalytic experiments using a mixture of 20 g L⁻¹ 357 µm-silica gel beads with three coats and different initial phenol concentrations
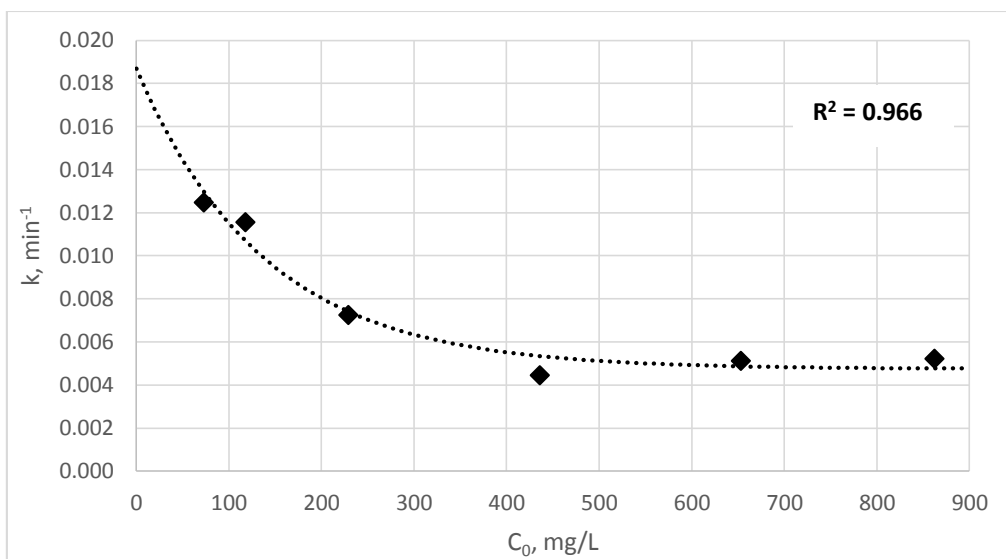
Figure 4.65. k vs C_0 exponential fit for photocatalytic experiments using a mixture of 20 g L^{-1} 357 μm-silica gel beads with three coats and different initial phenol concentrations
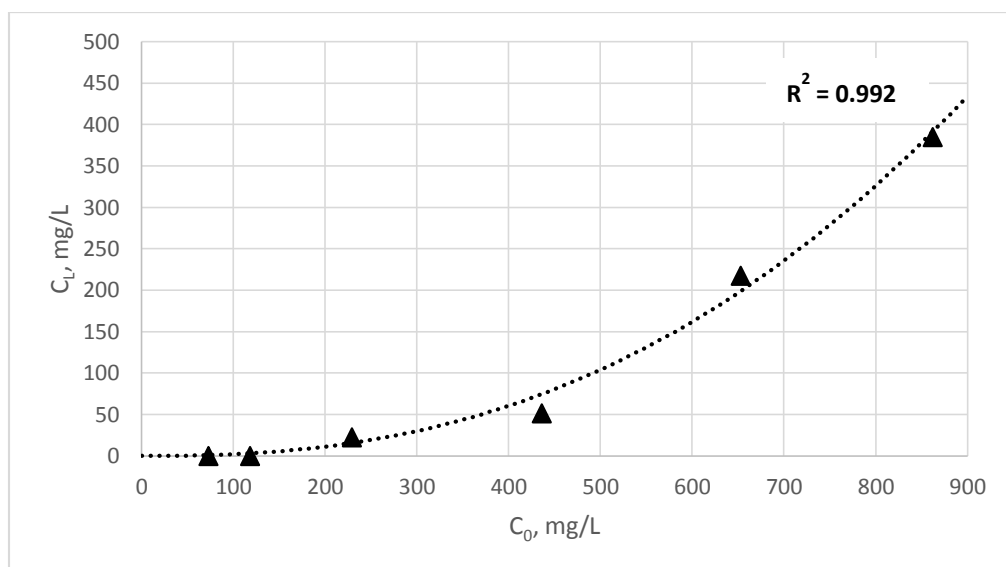
Figure 4.66. C_L vs C_0 power fit for photocatalytic experiments using a mixture of 20 g L^{-1} 357 μm-silica gel beads with three coats and different initial phenol concentrations

Table 4.3 summarizes the statistical analysis results for the two different set of experiments. These constants allow for calculation of k and C_L through Equations 4.4 and 4.5. Then with

Equation 4.3, remaining COD at any time during irradiation can be predicted for any given initial concentration between 50 and 900 mg L^{-1} of phenol-derived COD.

Table 4.3. Statistical model correlation constants for the photo-reactor system using silica gel beads with one and three TiO$_2$ coatings

	One TiO$_2$ coat	Three TiO$_2$ coats
k_0 , min^{-1}	2.19E-02	1.87E-02
k_L, min-1	5.41E-03	4.74E-03
k', L mg^{-1}	1.86E-02	7.22E-03
k_ω	4.50E-03	2.80E-05
k^*	1.708	2.432

Figures 4.67 and 4.68 show the performance curves generated using the proposed statistical model.
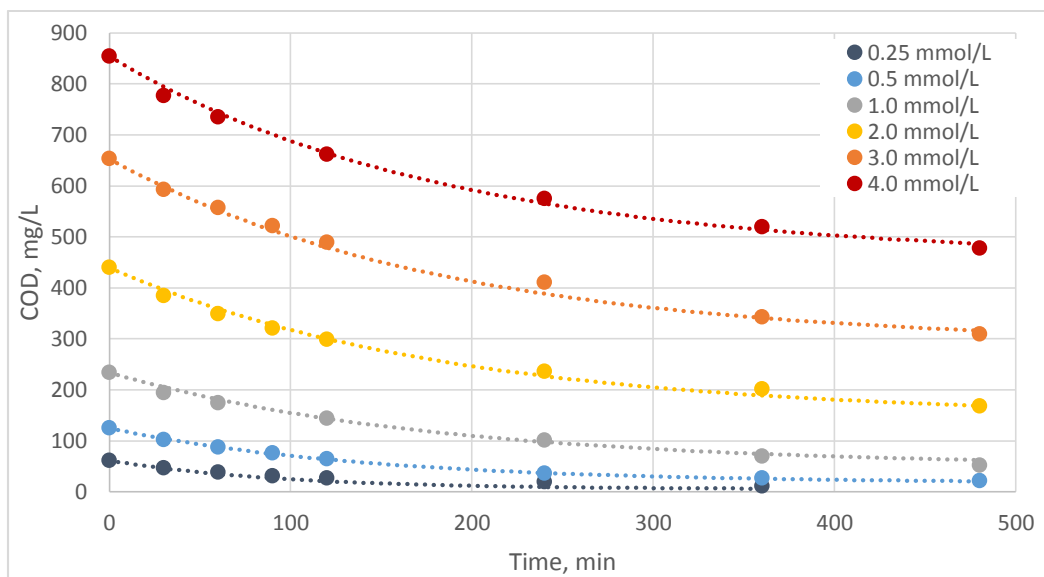
Figure 4.67. COD vs time experimental points and statistical model curves for photocatalytic experiments using a mixture of 20 g L^{-1} 357 μm-silica gel beads coated once and different initial phenol concentrations
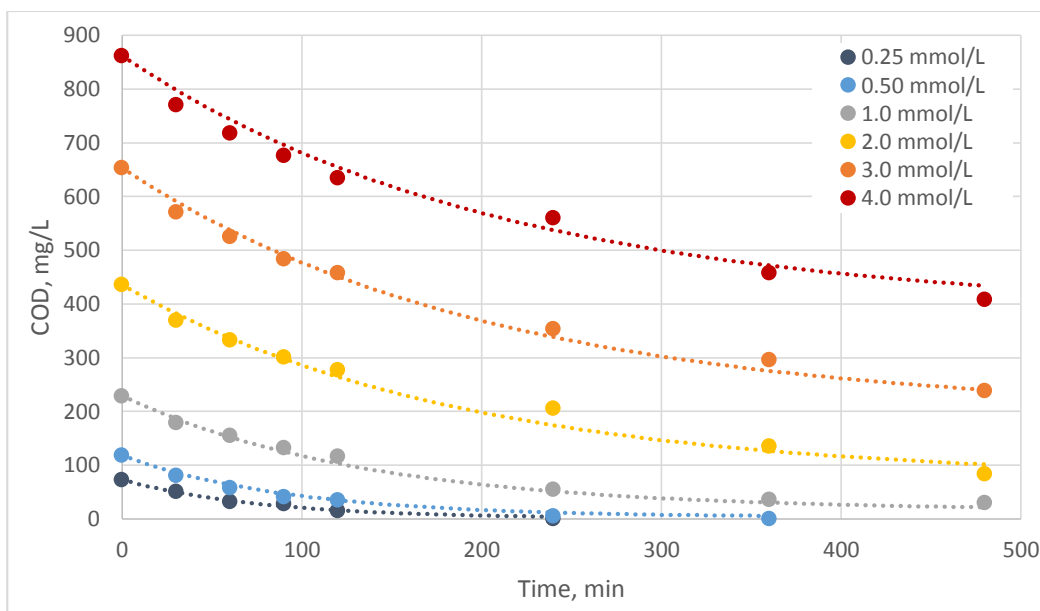
Figure 4.68. COD vs time experimental points and statistical model fit curves for photocatalytic experiments using a mixture of 20 g L^{-1} 357 μm-silica gel beads with three coats and different initial phenol concentrations

The coefficient of determination or R^2 values of the experimental data fit to the exponential decay and statistical model for both types of coated silica gel beads are presented in Table 4.4.

Table 4.4. Coefficients of determination of experimental data fit to exponential decay and statistical model

Initial phenol concentration (mmol L^{-1})	R^2 (Exponential decay fit)		R^2 (Statistical model fit)	
	Number of TiO$_2$ coats			
	One	Three	One	Three
0.25	0.9892	0.9916	0.9898	0.9870
0.5	0.9985	0.9964	0.9985	0.9963
1.0	0.9921	0.9953	0.9930	0.9954
2.0	0.9940	0.9873	0.9952	0.9840
3.0	0.9968	0.9902	0.9939	0.9944
4.0	0.9950	0.9847	0.9963	0.9878

Coefficient of determinations or the goodness of fit of the experimental data to the predicted degradation profile curves generated with the proposed statistical model (Table 4.4) are all higher than 0.98. It is safe to say then that this procedure allows for process output estimation with acceptable accuracy.

The values shown in Table 4.3 apply only to this specific type of process where the photocatalytic reactor geometry, light intensity, type of photocatalyst and contaminant and operational conditions are the ones used during the experimental phase of this research, all of which have been described in previous sections of this document. Nonetheless, given the complexity of the photocatalytic oxidation process and the inherent difficulty in generating the necessary data for developing a detailed kinetic model, a practical predictive tool like the model herein presented can be generated for different reactor configurations using fluidized TiO_2-coated support and any organic substrates through similar statistical analysis of experimental data.

5

Summary, Conclusions and Recommendations

TiO$_2$ heterogeneous photocatalysis is an effective process for oxidizing a variety of organic and inorganic contaminants, but so far the use of this technology has been restricted mostly to slurry-type systems, in which the photocatalyst nano-powder is directly mixed with the liquid waste. Such an approach, although ideal from the photo-reaction kinetics standpoint due to the maximization of the catalyst surface area to photon flux ratio, is inherently costly and energy intensive because of the need for catalyst powder removal from the effluent. Alternative methods consisting of immobilization of the photocatalyst have also been developed (Table 1.1), offering the advantage of continuous operation without catalyst separation but sacrificing quantum efficiency owing to light scattering and lower catalyst surface availability.

The present research investigates the feasibility of degrading phenol through photocatalysis on TiO$_2$ that has been synthetized in the laboratory and deposited on silica gel beads through a sol-gel method, then fluidizing a bed of the coated silica in a tubular bench-scale batch reactor with recirculation (Figures 3.4.a and b) equipped with a concentrically positioned UV-light bulb as source of high-energy photons.

Experimental results showed that the photo-reactor tubular configuration makes the removal of COD highly sensitive to changes in the amount and size of the fluidized coated silica gel beads. 20 g of silica per liter of mixture was found to be the optimum reactor mass load for all

the beads sizes available (224, 357 and 461 μm), with process efficiency decreasing for lower and higher silica concentrations.

The size of the catalyst-support particles also has a significant effect on the COD elimination rate under the experimental conditions. Maximum COD removal and minimum $Q_{0.5}$ was obtained with 20 g L^{-1} of 224-μm beads (equivalent surface area of 0.8 m^2 L^{-1}). In general, for any mass of fluidized silica gel, the process efficiency decreased with increasing silica gel particle size. For the same mass concentration of silica gel, the smaller the particle the higher the COD photo-oxidation rate, meaning that the surface area of photocatalyst increases with decreasing particle diameter. However, this effect was found to be not only related to the extension of the catalyst surface area but also to the presence of the silica bead in the mixture. For a constant surface area concentration, process efficiency decreased with increasing silica particle diameter, indicating that the size of the bead affects photon efficiency. A larger support particle circulating in the immediate vicinity of the light source increases apparent mixture turbidity, preventing irradiation from reaching particles in the background.

The presence of intermediate compounds formed during phenol photo-mineralization was indirectly determined through UV-Vis spectrophotometry. Absorption spectra captured at 240 and 269 nm, and the magnitude of the area under this spectra was used to infer the rate at which phenol disappeared and intermediates were produced. Solution absorbance readings at high phenol concentrations gave evidence of intermediates and acids formation and elimination reactions occurring simultaneously in the mixture during the course of irradiation. The presence of these compounds is believed to slow down the photocatalytic oxidation process by increasing the time and energy necessary for COD elimination due to the direct competition over limited unselective

reactive sites on the semiconductor surface and to the reduction in photon efficiency caused by the increased absorbance of the mixture.

The decrease in process efficiency with substrate concentration is an expected outcome in this type of photo-reactors, given the light-absorbing nature of the substrate and its reaction by-products, as mentioned before. COD removal rate was highest at 0.25 mmol L^{-1} of phenol, and decreased with increasing phenol concentration. But besides this predictable finding, by looking at the behavior of COD degradation for different initial phenol and silica gel concentrations, it could also be observed that there exists an optimal load of silica particles at which removal is highest and that such a load is independent of substrate concentration. This behavior confirms that the optimum catalyst-support load in the mixture is a design parameter determined by the photo-reactor configuration and type of organic substrate.

The observed tendency of both COD removal efficiency and $Q_{0.5}$ to plateau at silica gel mass loads other than the optimal as the initial phenol concentration increases can be interpreted, in the case of too low silica gel concentrations, as a sign of saturation of the photo-oxidation capabilities of the system due to an excess of substrate relative to the available catalyst surface. In the case of too-high silica concentrations, the light blocking effect of particles overload is the main factor responsible for the decreased removal efficiency.

The initial pH of the mixture was also found to affect the photo-reactor performance. Under acidic conditions, the photocatalytic removal of COD was enhanced, reaching the highest degradation rate at pH 3, which is considered the optimum for this type of process. In the pH range investigated, efficiency decreased with increasing pH, and at 9.5 it is 35 % less efficient than at pH 3. Such effect is attribute to inhibition of the photo-mineralization mechanism in alkaline medium.

The effect of the solution salinity on the photocatalytic degradation of phenol was studied through controlled change in initial conductivity by means of NaCl addition. Under the experimental conditions, the medium salinity had a noticeable effect on the COD removal efficiency, which increased with increasing NaCl concentration, and at 20 mmol/L of NaCl, COD was completely removed from solution after 8 h of UV-C irradiation.

The influence of dissolved oxygen on the photocatalytic elimination of phenol/COD was investigated by comparing the results obtained from photocatalytic experiments with and without added oxygen. Dissolved oxygen was found to be indispensable for the activation and progress of photo-mineralization reactions, since the formation of active oxygen species in aqueous medium is a rate-limiting reaction step. It was also confirmed that there is no need to bubble the gas through the reaction mixture since the performance does not depend on aeration. The absorption of oxygen by the surface of the solution is sufficient for photocatalytic oxidation to occur.

The 357-μm silica gel beads used as TiO_2 support were coated up to three times through the selected sol-gel method. The presence of the deposited catalyst was confirmed by scanning electron microscopic observation of the silica surface. On beads coated only once, the photocatalyst appeared as an irregular film with visible fractures while additional coatings lead to the formation of a thicker but cracked catalyst layer. Catalyst surface morphology and grain size indicated the formation of anatase as the dominant form of synthetized TiO_2. The results from photocatalytic experiments performed with silica beads coated once and three times showed that COD removal efficiency increased with the number of photocatalyst layers, signaling improved catalyst availability for photon absorption and substrate oxidation owing to the added TiO_2 mass. Further analysis of these results also confirmed that the catalyst deposits as a layer on the silica

surface, and that is not the thickness of this layer but its extension that influence the photocatalytic degradation rate of the organic substrate.

The maximum photo-reactor efficiency was found by running the reactor in slurry mode using anatase nano-powder in a concentration of 1.25 g L^{-1}. When comparing results from photocatalysis over TiO_2 nano-powder, silica gel beads with one and three coatings and photolysis, the nano-powder type process was more efficient than the others for the entire range of phenol concentrations, but as efficient as photocatalysis over silica beads with three coatings at end low and high phenol concentrations, 0.25 and 4.0 mmol L^{-1}, respectively. Absorption spectra from these experiments showed that both photolytic and photocatalytic reactions occur during COD degradation at very low phenol concentrations, but as the latter increases, the fraction of photons absorbed by the TiO_2 surface also increases, and then mineralization proceeds mainly through photocatalytic mechanisms.

Finally, through statistical analysis of the experimental data it was determined that the photocatalytic degradation of phenol-derived COD in the tubular bench-scale reactor follows exponential decay behavior, with the COD concentration reaching a plateau at some point during irradiation. The degradation pattern was the same for silica gel beads with one and three TiO_2 coatings. Thus, experimental data points were fitted through non-linear regression to a one phase decay model using GraphPad Prism 6 ®. Mathematical expressions relating the parameters from the decay-model fit equations to initial substrate concentrations were also found, which allowed for generating a statistical model specific for the experimental system that accurately predicts the COD in the effluent at any time during irradiation knowing the initial COD of the mixture.

Regarding the role and effect of the evaluated intrinsic parameters on the photocatalytic degradation of phenol, the following conclusion can be drawn:

The sol-gel technique used for catalyst deposition onto silica gel particles produces anatase as the main TiO_2 form. The particle surface coverage by the catalyst increases with the number of coating procedures, with each coating increasing the weight of the silica gel particles by 6.5% in average.

The adherence of the deposited catalyst onto the silica bead surface is mediocre. COD removal efficiency achieved with particles coated three consecutive times decreases by 15 % after 72 hours of use, due to the catalyst layer washing off the silica surface.

Experiments performed with silica gel beads coated three times produced an 8-h COD removal 10% higher and a $Q_{0.5}$ 17 kJ L^{-1} lower than those with beads coated only once. Therefore, it is necessary to subject silica particles to at least three consecutive sol-gel coating procedures for added catalyst stability and treatment efficiency.

For the experimental reactor configuration, 20 g of silica gel per liter of mixture is the optimum concentration for achieving maximum COD removal. This was true for all particle sizes evaluated. However, for the same silica mass load, process efficiency increases with decreasing silica gel particle size.

All of the extrinsic parameters investigated have a measurable and significant effect on the photocatalysis of phenol under the experimental conditions. Based on the experimental results, the following conclusions can be made:

Process removal efficiency decreases with increasing substrate concentration, regardless of the size and load of the silica gel particles used for catalyst support.

The initial pH affects the photocatalytic reaction mechanism. Highest removal efficiency was achieved at initial pH 3, and it decreases with increasing pH.

In the presence of NaCl, it was found that photocatalytic COD removal increases with increasing salinity.

The role of dissolved oxygen in the treated solution is that of an electron-hole scavenger. Continuous oxygen supply during the course of the experiment is indispensable for photocatalysis to proceed. Oxygen saturation of the mixture in the experimental photo-reactor can be effectively achieved by keeping the liquid in contact with pure oxygen at 1 atm.

Photocatalytic degradation of phenol-derived COD on TiO_2-coated silica gel beads in the tubular reactor fits an exponential decay model, regardless of the experimental conditions of the system.

The statistical model presented allows for estimation of the reactor efficiency for any initial COD of the mixture with high accuracy (minimum R^2 of 0.9840). It is reasonable to expect that a similar model based on statistical analysis of performance data can be generated for any tubular reactor using fluidized catalyst-coated silica gel for photocatalytic mineralization of dissolved pollutants.

In general, the proposed photocatalytic system can be considered a viable alternative to slurry-type reactors for complete mineralization of phenol. When comparing the use of silica gel beads coated three times with that of anatase nano-powder in the experimental system, both exhibit

a similar 8-h COD removal efficiency at initial phenol concentrations less than 0.25 mmol L^{-1}, and a maximum difference of 20 % efficiency at 2.0 mmol L^{-1}, while the latter results in a $Q_{0.5}$ 20 kJ L^{-1} lower for the entire range of phenol concentrations.

The main limitations of the proposed technology are related to the stability of the deposited catalyst layer and the efficiency of photon penetration through the bulk liquid. Dealing with the first one requires continuing research on different TiO_2 deposition or synthesis techniques, and even exploring the use of other types of semiconductor catalysts for improved adherence and decreased energy consumption.

Photonic efficiency can be improved by modifying the system design. In a tubular reactor with a concentric UV source, the annular space thickness or depth of the bulk liquid must be the minimal as to allow for support fluidization and full light penetration. The wavelength of the emitted light can also be increased in order to prevent photons from being absorbed by the target substrate and to lower energy expenditure. Therefore, further research should look into reducing the annular space between the bulb casing and the internal walls of the reactor and also into studying the effect of replacing UV-C for UV-B and UV-A light.

References

Abdullah, M.; Low, G.K.C.; Matthews, R.W. (1990). "Effects of common inorganic anions on rates of photocatalytic oxidation of organic carbon over illuminated titanium dioxide". *Journal of Physical Chemistry*, 94: 6820-6825.

Abhang, R.M.; Kumar, D.; and Taralkar, S.V. (2011) "Design of photocatalytic reactor for degradation of phenol in wastewater". International Jounral of Chemical Engineering and Applications, 2(5):337-341.

Abe, R.; Sayama, K.; Domen, K.; and Arakawa, H. (2001). "A new type of water splitting system composed of two different TiO_2 photocatalysts (anatase, rutile) and a IO_3^-/I^- shuttle redox mediator". Chemical Physics Letters, 344(3):339-344.

Abrahams, J.; Davidson, R.S.; and Morrison, C.L. (1985). "Optimization of the photocatalytic properties of titanium dioxide". Journal of Photochemistry, 29:353-361.

Agrios, A. and Pichat, P. (2006). "Recombination rate of photogenerated charges vs. surface area: Opposing effects of TiO_2 sintering temperature on photocatalytic removal of phenol, anisole and pyridine in water". Journal of Photochemistry and Photobiology A: Chemistry, 180:130-135.

Akpan, U. G.; and Hameed, B. H. (2009). "Parameters affecting the photocatalytic degradation of dyes using TiO_2-based photocatalysts: A review." Journal of Hazardous Materials, 170:520.

Aladjem, A. (1973) "Anodic oxidation of titanium and its alloys". Journal of Materials Science, 8(5):688-704.

Albert, M.; Gao, Y-M.; Toft, D.; Dwight, K., and Wold, A. (1992). "Photoassisted gold deposition of titanium dioxide". Materials Research Bulletin, 27(8): 961-966.

Albery, W.J.; and Barlett, P.N. (1984). "The transport and kinetics of photogenerated carriers in colloidal semiconductor electrode particles". Journal of the Electrochemical Society, 131(2):315-325.

Alfano, O.; Bahnemann, D.; Cassano, A.; Dillert, R.; and Goslich, R. (2000). "Photocatalysis in water environments using artificial and solar light." Catalysis Today, 58: 199-230.

Alnaizy, R. and Akgerman, A. (2000). "Advanced oxidation of phenolic compounds". Advances in Environmental Reseach, 4:233-244.

Al-Rasheed, R.; and Cardin, D.J. (2003) "Photocatalytic degradation of humic acid in saline waters: Part 2. Effects of various photocatalytic materials". Applied Catalysis A, 246:39-48.

Al-Sayyed, G.; D'Oliveira, J.-C.; and Pichat, P. (1991). "Semiconductor-sensitized photodegradation of 4-chlorophenol in water". Journal of Photochemistry and Photobiology A: Chemistry, 58:99-114.

Ammar, I.A.; and Kamal, I. (1971a) "Kinetics of anodic oxide-film growth on titanium-I. Acid media". Electrochimica Acta, 16:1555-1568.

Ammar, I.A.; and Kamal, I. (1971b) "Kinetics of anodic oxide-film growth on titanium-I. Neutral and alkaline media". Electrochimica Acta, 16:1539-1553.

An, T.; Zhang, W.; Xiao, X.; Sheng, G.; Fu, J. and Zhu, X. (2004). "Photoelectrocatalytic degradation of quinoline with a novel three-dimensional electrode-packed bed photocatalytic reactor," Journal of Photochemistry and Photobiology A: Chemistry, 161:233–242.

Angelidis, T.N.; Koutlemani, M.; and Poulios, I. (1998). "Kinetic study of the photocatalytic recovery of Pt from aqueous solution by TiO_2, in a closed-loop reactor". Applied Catalysis B: Environmental, 16:347-357.

Aprile, C.; Corma, A.; and Garcia, H. (2008). "Enhancement of the photocatalytic activity of TiO_2 through spatial structuring and particle size control: from subnanometric to submillimetric length scale." Physical Chemistry Chemical Physics, 10:769-783.

Araña, J.; Dona, J.; Portillo, D.; Fernandez, C.; Perez, J.; Gonzalez, O.; Navio, J. and Macias, M. (2010). "Photocatalytic degradation of phenolic compounds with new TiO_2 catalyst". Applied Catalysis B: Environmental, 100(1-2):346-354.

Argonne National Laboratory (2009). "Produced Water Volumes and Management Practices in the United States," Environmental Science Division, Argonne National Laboratory, downloaded at http://www.osti.gov/bridge

Arsov, Lj.D.; Kormann, C.; and Plieth, W. (1991) "Electrochemical synthesis and in situ Raman spectroscopy of thin films of titanium dioxide". Journal of Raman Spectroscopy, 22(10):573-575.

Asahi, R.; Morikawa, T.; Ohwaki, T.; Aoki, K.; and Taga, Y. (2001). "Visible-light photocatalysis in nitrogen-doped titanium dioxides". Science, 293:269-271.

Augugliaro, V.; Palmisano, L.; Sclafani, A.; Minero, C. and Pelizzetti, E. (1988). "Photocatalytic degradation of phenol in aqueous titanium dioxide dispersions". Toxicology and Environmental Chemistry, 16:89-90.

Ayieko, C.; Musembi, R.; Waita, S.; Aduda, B. and Jain, P. (2012). "Structural and optical characterization of nitrogen-doped TiO2 thin films deposited by spray pyrolysis on fluorine doped tin oxide (FTO) coated glass slides." International Journal of Energy Engineering, 2(3):67-72.

Azevedo, E.B.; Torres, A.R.; Aquino-Neto, F.R.; and Dezotti, M. (2009) "TiO_2-photocatalyzed degradation of phenol in saline media in an annular reactor: Hydrodynamics, Lumped kinetics, intermediates and acute toxicity". Brazilian Journal of Chemical Engineering, 26:75-87.

Bahnemann D. W.; Kormann C.; and Hoffmann M. R. (1987). "Preparation and Characterization of Quantum-Size Zinc Oxide – A Detailed Spectroscopic Study". Journal of Physical Chemistry, 91:3789-3798.

Bahnemann, D.W.; Hilgendorff, M.; and Memming, R. (1997). "Charge carrier dynamics at TiO2 particles: Reactivity of free and trapped holes". Journal of Physical Chemistry B, 101(21): 4265–4275.

Balasubramanian, G,; Dionysiou, D.D.; Suidan, M.T.; Baudin, I.; and Laine, J.M. (2004). "Evaluating the activities of immobilized TiO2 powder films for the photocatalytic degradation of organic contaminants in water". Applied Catalysis B: Environmental, 47:73-84.

Bard, A.J., and Faulkner, L.R. (2000). Electrochemical Methods: Fundamental and Applications, Wiley. USA.

Bard, A.J.; Memming, R.; and Miller, B. (1991). "Terminology in semiconductor electrochemistry and photoelectrochemical energy conversion". Pure and Applied Chemistry, 63(4):569-596.

Basca, R.R.; and Kiwi, K. (1998). "Effect of rutile phase on the photocatalytic properties of nanocrystalline titania during the degradation of p-coumaric acid". Applied Catalysis B: Environmental, 16(1):19-29.

Bayarri, B.; Abellan, M.; Gimenez, J.; Esplugas, S. (2007). "Study of the wavelength effect in the photolysis and heterogeneous photocatalysis". Catalysis Today, 129:231-239.

Bedford, J.; Klausner, J.; Goswami, D.; Schanze, K. (1994). "Performance of nonconcentrating solar photocatalytic oxidation reactors, part 2: Shallow pond configuration". Journal of Solar Energy Engineering, 116:8-13.

Berger, T.; Sterrer, M.; Diwald, O.; Knozinger, E.; Panayotov, D.; Thompson, T.L.; and Yates, J.T. (2005). "Light-induced charge separation in anatase TiO_2 particles". Journal of Physical Chemistry B, 109(13):6061-6068.

Berry, R. J.; and Mueller, M. R. (1994). "Photocatalytic decomposition of crude oil slicks using TiO_2 on a floating substrate." Microchemical Journal, 50:28.

Bessa, E.; Sant'Anna, G.L.; and Dezotti, M. (2001) "Photocatalytic/H_2O_2 treatment of oil field produced waters". Applied Catalysis B: Environmental, 29:125-134.

Beydoun, D.; Tse, H.; Amal, R.; Low, G.; and McEvoy S. (2002). "Effect of copper(II) on the photocatalytic degradation of sucrose". Journal of Molecular Catalysis A: Chemical, 177(2):265-272.

Bhatkhande, D.; Pangarkar, V.G.; and Beenackers, A.A.C.M. (2002). "Photocatalytic degradation for environmental applications-a review". Journal of Chemical Technology and Biotechnology, 77:102-116.

Bideau, M.; Claudel, B.; Dubien, C.; and Kazouan, H. (1995). "On the immobilization of titanium dioxide in the photocatalytic oxidation of spent waters". Journal of Photochemistry and Photobiology A: Chemistry, 91:137-144.

Brown, E., Travers, J. and Resnikoff, M. (2009). "White Paper, Proposed NPDES Permit for Oil and Gas Exploration, Development, & Production Facilities Located Within Territorial Seas of Louisiana (LAG260000)," Prepared for the Louisiana Environmental Action Network (LEAN), Radioactive Waste Management Associates, New York, NY.

Byrne, J.A.; Davidson, A.; Dunlop, P.S.M.; and Eggins, B.R. (2002). "Water treatment using nano-crystalline TiO_2 electrodes". Journal of Photochemistry and Photobiology A: Chemistry, 148: 365-374.

Byrne, J.A.; Eggins, B.R.; Brown, N.M.D.; McKinley, B.; and Rouse, M. (1998). "Immobilization of TiO_2 powder for the treatment of polluted water". Applied Catalysis B: Environmental, 17: 25-36.

Cai, R.; Hashimoto, K.; Itoh, K.; Kubota, Y. and Fujishima, A. (1991) Photokilling of malignant cells with ultrafine TiO2 powder. Bulletin of the Chemical Society of Japan: 64, 1268–1273.

Cao, F.; Oskam, G.; Meyer, G.; and Searson, P.C. (1996) "Electron transport in porous nanocrystalline TiO$_2$ photoelectrochemical cells". Journal of Physical Chemistry, 100(42):17021-17027.

Carraway, E. R.; Hoffman, A. J.; and Hoffmann, M. R. (1994). "Photocatalytic oxidation of organic acids on quantum-sized semiconductor colloids". *Environmental Science and Technology, 28:* 786–793.

Carroll, D.L.; Liang, Y.; and Bonnell, D.A. (1994). "Investigation of the growth and structure of aluminum overlayers on TiO$_2$(100) by scanning tunneling microscopy". Journal of Vacuum Science and Technology A, 13:2298-2303.

Charlton, G.; Howes, P.B.; Nicklin, C.L.; Steadman, P.; Taylor, J.S.G.; Muryn, C.A.; Harte, S.P.; Mercer, J.; McGrath, R.; Norman, D.; Turner, T.S.; and Thornton, G. (1997). "Relaxation of TiO$_2$ (110)-(1x1) using surface X-Ray diffraction". Physical Review Letters, 78:495-498.

Chen, D.; and Ray, A.K. (1999). "Photocatalytic effects of phenol and its derivatives over UV irradiated TiO$_2$". Applied Catalysis B: Environmental, 23:143-157.

Chen, G. (2004) "Electrochemical technologies in wastewater treatment." Separation and Purification Techonology, 38:11-41.

Chen, H.Y.; Zahraa, O.; and Bouchy, M. (1997). "Inhibition of the adsorption and photocatalytic degradation of an organic contaminant in an aqueous suspension of TiO$_2$ by inorganic ions". Journal of Photochemistry and Photobiology A: Chemistry, 108(3):37-44.

Chen, J.; Ollis, D.F.; Rulkens, W.H.; and Bruning, H. (1999a). "Photocatalyzed oxidation of alcohols and organochlorides in the presence of native TiO2 and metalized TiO2 suspensions. Part (I): photocatalytic activity and pH influence". Water Research, 33(3):661-668.

Chen, J.; Ollis, D.F.; Rulkens, W.H.; and Bruning, H. (1999b). "Photocatalyzed oxidation of alcohols and organochlorides in the presence of native TiO2 and metalized TiO2 suspensions. Part (II): photocatalytic mechanisms". Water Research, 33(3):669-676.

Chen, X.; Chen, G.; and Yue, P.L. (2000). "Electrocoagulation and electroflotation of restaurant wastewater." Journal of Environmental Engineering (ASCE), 126(9):858-863.

Chen, X.; and Mao, S.S. (2007) "Titaniun dioxide nanomaterials: Synthesis, properties, modifications, and applications", Chemical Reviews, 107(7):2891-2959.

Chhabra, V.; Pillai, V.; Mishra, B.K.; Morrone, A.; and Shah, D.O. (1995). "Synthesis, characterization, and properties of microemulsion-mediated nanophase TiO$_2$ particles". Langmuir, 11:3307-3311.

Chin, S.; Chiang, K. and Fane, A. (2006). "The stability of polymeric membranes in TiO$_2$ photocatalysis process". Journal of Membrane Science, 275:202-211.

Choi, W.; Termin, A.; Hoffman, M.R. (1994). "The role of metal ion dopants in quantum-sized TiO$_2$: correlation between photoreactivity and charge carrier recombination dynamics". Journal of Physical Chemistry, 98:13669-13679.

Chong, M.N.; Jin, B.; Chow, C.W.K.; Saint, C. (2010). "Recent developments in photocatalytic water treatment technology: A review". Water Research, 44:2997-3027.

Chong, M.N.; Jin, B.; Zhu, H.Y.; Chow, C.W.K.; and Saint, C. (2009). "Application of H-titanate nanofibers for degradation of Congo red in an annular slurry photoreactor". Chemical Engineering Journal, 150:49-54.

Chun, H.; Yizhong, W. and Hongxiao, T. (2000). "Destruction of phenol aqueous solution by photocatalysis or direct photolysis". Chemosphere, 41(8):1205-1209.

Colombo, D.P.Jr.; and Bowman, R.M. (1995). "Femtosecond diffuse reflectance spectroscopy of TiO_2 powders". Journal of Physical Chemistry, 99(30):11752-11756.

Colombo, D.P.Jr.; and Bowman, R.M. (1996). "Does interfacial charge transfer compete with charge carrier recombination? A femtosecond diffuse reflectance investigation of TiO2 nanoparticles". Journal of Physical Chemistry, 100(47):18445-18449.

Colorado School of Mines. (2009) "Thecnical Assesment of Produced Water Treatment Technologies", RPSEA Project 07122-12.

Comninellis, Ch. and Pulgarin, C. (1993). "Electrochemical oxidation of phenol for wastewater treatment using SnO_2 anodes". Journal of Applied Electrochemistry, 23:108-112.

Crittenden, J.C.; Liu, J.; Hand, D.W.; and Perram, D.L. (1997). "Photocatalytic oxidation of chlorinated hydrocarbons in water". Water Research, 31(3): 429-438.

D'Auria, M.; Emanuele, L.; Racioppi, R.; and Velluzzi, V. (2009), "Photochemical degradation of crude oil: Comparison between direct irradiation, photocatalysis, and photocatalysis on zeolite." Journal of Hazardous Materials, 164:32.

De Lasa, H.; Serrano, B.; and Salaices, M. (2005). "Photocatalytic reaction engineering". Springer, USA.

Ding, Z.; Zhu, H.Y.; Lu, G.Q.; and Greenfield, P.F. (1999). "Photocatalytic properties of titania pillared clays by different drying methods". Journal of Colloid and Interface Science, 209 (1): 193-199.

Diwald, O.; Thompson, T.L.; Goralski, E.G.; Walck, S.D.; and Yates, J. (2004). "The effect of nitrogen ion implantation on the photoactivity of TiO_2 rutile single crystals". The Journal of Physical Chemistry B, 108:52-57.

D'Oliveira, J.C.; Al-Sayyed, G.; and Pichat, P. (1990) "Photodegradation of 2-chlorophenol and 3-chlorophenol in TiO_2 aqueous suspensions". Environmental Science & Technology, 24:990-996.

Domenech, X. (1993) In: Ollis, D.F.; Al-Ekabi, H. (edS) "Photocatalytic purification and treatment of water and air". Elsevier, 337.

Duonghong, D.; Borgarello, E.; and Gratzel, M. (1981). "Dynamics of light-induced water cleavage in colloidal systems". Journal of the American Chemical Society, 103(16):4685-4690.

Dyk, A.C.; and Heyns, A.M. (1998). "Dispersion stability and photo-activity of rutile (TiO_2) powders". Journal of Colloid and Interface Science, 206(2):381-391.

Emeline, A.; Ryabchuk, V. and Serpone, N. (2000). "Factors affecting the efficiency of a photocatalyzed process in aqueous metal-oxide dispersions: Prospect of distinguishing between two kinetic models". Journal of Photochemistry and Photobiology A: Chemistry, 133(1-2):89-97.

Enriquez, R. and Pichat, P. (2006). "Different net effect of TiO_2 sintering temperature on the photocatalytic removal rates of 4-chlorobenzoic acid and dichloroacetic acid in water. Journal of Environmental Science and Health A: Toxic/Hazardous Substances and Environmental Engineering, 41:955-966.

Eyring, H. (1970). Physical Chemistry. Academic Press Inc. USA.

Fernandez, A.; Lassaletta, G.; Jimenez, V.M.; Justo, A.; Gonzalez-Elipe, A.R.; Jerrmann, J.M.; Tahiri, H.; and Ait-Ichou, Y. (1995). "Preparation and characterization of TiO2 photocatalysts supported on various rigid supports (glass, quartz and stainless steel). Comparative studies of photocatalytic activity in water purification". Applied Catalysis B: Environmental, 7:49-63.

Fernandez-Nieves, A.; and de las Nieves, F.J. (1999). "The role of ζ potential in the colloidal stability of different TiO2/electrolyte solution interfaces". Colloids and Surfaces A: Physicochemical and Engineering Aspects, 148(3):231-243.

Fisher, C.H.; Lilie, J.; Weller, H.; Katsikas, L.; and Henglein, A. (1989). "Photochemistry of colloidal semiconductors 29. Fractionation of CdS sols on small particles by exclusion chromatography". Berichte der Bunsengesellschaft fur physikalische Chemie, 93:61-64.

Fonseca, C.; Traverse, A.; Tadjeddine, A.; Cunha Belo, M. (1995) "A characterization of titanium anodic oxides by X-ray absorption spectroscopy and grazing X-ray diffraction", Journal of Electroanalytical Chemistry, 388:115-122.

Fotiadis, C.; Xekoukoulotakis, N.P.; and Mantzavinos, D. (2007) "Photocatalytic treatment of wastewater from cottonseed processing: Effect of operating conditions, aerobic biodegradability and ecotoxicity". Catalysis Today, 124(3):247-253.

Fox, M.A.; and Dulay, M.T. (1993). "Heterogeneous photocatalysis". Chemical Reviews, 93:341-357.
Fox, M.A.; and Tien T.-P. (1988). "Photoelectrochemical detector for high-pressure liquid chromatography". Analytical Chemistry, 60(20):2278–2282.

Franco, G.; Gehring, J.; Peter, L.M.; Ponomarev, E.A.; and Uhlendorf, I. (1999). "Frequency-resolved optical detection of photoinjected electrons in dye-sensitized nanocrystalline photovoltaic cells". Journal of Physical Chemistry B, 103(4):692-698.

Frank, S. N.; and Bard, A. J. (1977). Heterogeneous photocatalytic oxidation of cyanide ion in aqueous solutions at TiO2 powder. Journal of the American Chemical Society, 99: 303–304.

Fujishima, A. and Honda, K. (1972). "Electrochemical photolysis of water at a semiconductor electrode". Nature, 238: 37-38.

Fujishima, A.; Hashimoto, K.; Watanabe, T. (1999). "TiO_2 Photocatalysis Fundamentals and Applications", BKC Inc.

Fujishima, A.; Rao, T.N.; and Tryk, D.A. (2000). "Titanium dioxide photocatalysis". Journal of Photochemistry and Photobiology C: Photochemistry Reviews, 1: 1-21.

Gamboa, J.A.; and Pasquevich, D.M. (1992). "Effect of chlorine atmosphere on the anatase-rutile transformation". Journal of the American Ceramic Society, 75(11):2934-2938.

Gaya, U. I.; and Abdullah, A. H. (2008). "Heterogeneous photocatalytic degradation of organic contaminants over titanium dioxide: A review of fundamentals, progress and problems." Journal of Photochemistry and Photobiology C, 9:1.

Gerischer, H. (1993). "Photoelectrochemical catalysis of the oxidation of organic molecules by oxygen on small semiconductor particles with TiO_2 as an example". Electrochimica Acta, 38(1):3-9.

Gerischer, H.; and Heller, A. (1992). "Photocatalytic oxidation of organic molecules at TiO_2 particles by sunlight in aerated water". Journal of the Electrochemical Society, 139:113-118.

Gonzalez-Elipe, A.R.; Munuera, G.; and Soria, J. (1979). "Photo-adsorption and photo-desorption of oxygen on highly hydroxylated TiO_2 surfaces. Part 2.- Study of radical intermediates by electron paramagnetic resonance". Journal of the Chemical Society, Faraday Transactions 1: Physical Chemistry in Condensed Phases, 75:748-761.

Gopal, M.; Moberly Chan, W.J.; and De Jonghe, L.C. (1997) "Room temperature synthesis of crystalline metal oxides", Journal of Material Science, 32(22):6001-6008.

Gratzel, M. (1981). "Artificial photosynthesis: Water cleavage into hydrogen and oxygen by visible light". Accounts of Chemical Research, 14:376-384.

Gratzel, M. (1988). Heterogeneous Photochemical Electron Transfer. CRC Press, USA.

Gimes, S. and Ngwang, H. (2000). "Methodology for studying oxidation of organic species in solution". Journal of AOAC International, 83(3):584-587.

Haarstrick, A.; Kut, O.M.; and Heinzle, E. (1996). "TiO_2-assisted degradation of environmentally relevant organic compounds in wastewater using a novel fluidized bed photoreactor", Environmental Science & Technology, 30:817-824.

Hagfeldt, A., and Gratzel, M. (2000). "Molecular photovoltaics". Accounts of Chemical Research, 33(5):269-277.

Hagfeldt, A.; Bjorksten, U.; and Lindquist, S-E. (1992). "Photoelectrochemical studies of colloidal TiO_2-films: the charge separation process studied by means of action spectra in the UV region". Solar Energy Materials and Solar Cells, 27(4):293-304.

Hagfeldt, A; and Grätzel, M. (1995). "Light-induced redox reactions in nanocrystalline systems". Chemical Reviews, 95:49–68.

Hanel, A.; Moren, P.; Zaleska, A.; and Hupka, J. (2010) "Photocatalytic activity of TiO_2 immobilized on glass beads". Physicochemical Problems of Mineral Processing, 45:49-56.

Hashimoto, K., Irie, H., and Fujishima, A. (2005). "TiO_2 photocatalysis: A historical overview and future prospects". Japanese Journal of Applied Physics, 44, 8269.

Heller, A. (1995). "Chemistry and applications of photocatalytic oxidation of thin organic films," Accounts of Chemical Research, 28(12): 503–508.

Henderson, M.A.; Epling, W.S.; Peden, C.H.F.; and Perkins, C.L. (2003). "Insights into photoexcited electron scavenging processes on TiO_2 obtained from studies of the reaction of O_2 with OH groups adsorbed at electronic defects on TiO_2 (110)". Journal of Physical Chemistry B, 107(2):534-545.

Heneghan, C.S.; Hutchings, G.J., and Taylor, S.H. (2004). "Destruction of volatile organic compounds by heterogeneous catalytic oxidation". Catalysis, 17.

Herrmann, J.-M. (1999). "Heterogeneous photocatalysis: fundamentals and applications to the removal of various types of aqueous pollutants". Catalysis Today, 53:115-129.
Herrmann, J.-M. (2001). "Active agents in heterogeneous photocatalysis: atomic species vs. OH$^{\cdot}$ radicals: Related quantum yields". Helvetica Chimica Acta, 84(9):2731-2750.

Herrmann, J.-M. (2005). "Heterogeneous photocatalysis: State of the art and present applications". Topics in Catalysis, 34: 49-65.

Hirakawa, T.; and Nosaka, Y. (2002). "Properties of $O_2^{\cdot-}$ and OH$^{\cdot}$ formed in TiO_2 aqueous suspensions by photocatalytic reaction and the influence of H_2O_2 and some ions". Langmuir, 18(8):3247-3254.

Hisanaga, T.; Harada, K. and Tanaka, K. (1990). "Photocatalytic degradation of organochloric compounds in suspended TiO_2". Journal of Photochemistry and Photobiology A: Chemistry, 54:113-118.

Hodes, G.; Howell, D.J.; and Peter, L.M. (1992). "Nanocrystalline photoelectrochemical cells. A new concept in photovoltaic cells". Journal of the Electrochemical Society, 139(11):3136-3140.

Hoffmann, M.R.; Martin, S.T.; and Choi, W. (1995). "Environmental applications of semiconductor photocatalysis". Chemical Reviews, 95: 69-96.

Howe, R.F. (1998). "Recent developments in photocatalysis". Developments in Chemical Engineering and Mineral Processing, 6:55-84.

Huang, X.; Meng, Y.; Liang, P.; and Qian, Y. (2007) "Operational conditions of a membrane filtration reactor coupled with photocatalytic oxidation". Separation and Purification Technology, 55:165-172.

Hufschmidt, D.; Liu, L.; Selzer, V.; and Bahnemann, D. (2004). "Photocatalytic water treatment: fundamentl knowledge required for its practical application". Water Science & Technology, 49(4):135-140.

Ilisz, I.; Laszlo, Z.; and Dombi, A. (1999). "Investigation of the photodecomposition of phenol in near-UV-irradiated aqueous TiO_2 suspensions. I: Effect of charge-trapping species on the degradation kinetics". Applied Catalysis A: General, 180:25-33.

Inet, Y.; and Ertek, D. (1993). "Photocatalytic deposition of bismuth(III) ions onto TiO2 powder". Journal of the Chemical Society, Faraday Transactions, 89(1): 129-133.

Ishibashi, K.; Fujishima, A.; Watanabe, T.; and Hashimoto, K. (2000). "Quantum yields of active oxidative species formed on TiO2 photocatalyst". Journal of Photochemistry and Photobiology A" Chemistry, 134:139-142.

Jacquot, F.; Guiliano, M.; Doumenq, P.; Munoz, D.; and Mille, G. (1996). "In vitro photooxidation of crude oil maltenic fractions: evolution of fossil biomarkers and polycyclic aromatic hydrocarbons." Chemosphere,33:671.

Jeong, Y. (1993) "The Structural Chemistry of Anodic Alumina", University of Manchester Institute of Science and Technology, United Kingdom.

Jung, S.C.; Kim, S.J.; Imaishi, N.; and Cho, Y.I. (2005) "Effect of TiO_2 thin film thickness and specific surface area by low-pressure metal-organic chemical vapor deposition on photocatalytic activities". Applied Catalysis B: Environmental, 55(4):253-257.

Kaesche, H. (2003). Corrosion of Metals: Physicochemical Principles and Current Problems. Springer, USA.

Kempster, A., Recent Developments in Chemical Vapor Deposition, 1 July 2008, http://www.btinternet.com/~catechnology/surfaceweb/swebjournalspage_files/kempster.htm

Khan, S.U.M.; Al-Shahry, M; and Ingler, W.B. (2002). "Efficient photochemical water splitting by a chemically modified n-TiO_2". Science, 297:2243-2245.

Kim, D.H.; and Anderson, M.A. (1994). "Photoelectrocatalytic degradation of formic acid using a porous titanium dioxide thin-film electrode". Environmental Science & Technology, 28:479-483.

Kim. Y.-C.; Lee, K.-H.; Sasaki, S.; Hashimoto, K.; Ikebukuro, K.; and Karube, I. (2000). "Photocatalytic sensor for chemical oxygen demand determination based on oxygen electrode". Analytical Chemistry, 72(14):3379-3382.

Kiwi, J. (1981). "Electron injection studies on semiconductor surfaces active in water splitting processes". Chemical Physics Letters, 83(3):594-599.

Klausner, J. and Goswami, D. (1995). "Solar detoxification of wastewater using nonconcentrating reactors". American Institute of Chemical Engineers, Symposium: Heat Transfer. 89:445-451.

Kobayakawa, K.; Nakazawa, Y.; Ikeda, M.; Sato, Y.; and Fujishima, A. (1990). "Influence of the density of surface hydroxyl group on TiO_2 photocatalytic activities". Berichte der Bunsengesellschaft fur Physikalische Chemie, 94(12):1439-1443.

Kobayakawa, K.; Sato, C.; Sato, Y.; and Fujishima, A. (1998) "Continous-flow photoreactor packed with titanium dioxide immobilized on large silica gel beads to decompose oxalic acid in excess water". Hournal of Photochemistry & Photobiology A: Chemistry, 118:65-69.

Kobya, M.; Can, O.T.; and Bayramoglu, M. (2003). "Treatment of textile wastewaters by electrocoagulation using iron and aluminum electrodes." Journal of Hazardous Materials, 100:163-178.

Kormann, C.; Bahnemann, D.W.; and Hoffmann, M.R. (1991). "Photolysis of chloroform and other organic molecules in aqueous titanium dioxide suspensions". Environmental Science & Technology, 25(3):494-500.

Kositzi, M.; Poulios, I.; Malato, S.; Caceres, J. and Campos, A. (2004) "Solar photocatalytic treatment of synthetic municipal wastewater". Water Research, 38:1147-1154.

Lam, S.W.; Chiang, K.; Lim, T.M.; Amal, R.; and Low, G.K.-C. (2005). Effect of charge trapping species of cupric ions on the photocatalytic oxidation of resorcinol". Applied Catalysis B: Environmental, 55:123-132.

Laoufi, N.A.; Tassalit, D.; and Bentahar, F. (2008) "The degradation of phenol in water solution by TiO_2 photocatalysis in a helical reactor". Global NEST Journal, 10(3):404-418.

Leyva, E.; Moctezuma, E.; Ruiz, M. and Torres, L. (1998). "Photodegradation of phenol and 4-chlorophenol by $BaO-Li_2O-TiO_2$ catalysts. Catalysis Today, 40:367-376.

Li, G.; Ana, T.; Chena, J.; Sheng, G.; Fua, J.; Chena, F.; Zhang, S.; and Zhaob, H. (2006). "Photoelectrocatalytic decontamination of oilfield produced wastewater containing refractory organic pollutants in the presence of high concentration of chloride ions," Journal of Hazardous Materials, B138:392–400.

Lindgren, T., (2004). "In Search of the Holy Grail of Photoelectrochemistry – A Study of Thin Film Electrodes for Solar Hydrogen Generation". Acta Universitatis Upsaliensis, Sweden.

Lindsay, R.; Wander, A.; Ernst, A.; Montanari, B.; Thornton, G.; and Harrison N.M. (2005). "Revisiting the surface structure of TiO_2 (110): A quantitative low-energy electron diffraction study". Physical Review Letters, 94:246102.1-246102.4.

Linsebigler, A.L.; Guangquan, L.; and Yates, T.J. (1995). "Photocatalysis on TiO_2 surfaces: Principles, mechanisms and selected results". Chemical Reviews, 95: 735-758.

Litter, M.I. (1999). "Heterogeneous photocatalysis: Transition metal ions in photocatalytic systems". Applied Catalysis B: Environmental, 23: 89-114.

Lu, M.C.; Chen, J.N.; and Lin, H.D. (1999). "The influence of metal ions on the photocatalytic oxidation of 2-chlorophenol in aqueous titanium dioxide suspensions". Journal of Environmental Science and Health B: Pesticides, Food Contaminants and Agricultural Wastes, 34:17-32.

Malato, S.; Blanco, J.; Vidal, A.; and Richter, C. (2002). "Photocatalysis with solar energy at a pilot-plant scale: an overview". Applied Catalysis B: Environmental, 37(1): 1-15.

Mali, S.; Shinde, P.; Betty, C.; Bhosale, P.; Lee, W. and Patil, P. (2011). "Nanocoral Architecture of TiO_2 by hydrothermal process: Synthesis and characterization", Applied Surface Science, 257:9737-9746.

Mao, Y.; Schoeneich, C.; and Asmus, K.D. (1991). "Identification of organic acids and other intermediates in oxidative degradation of chlorinated ethanes on titania surfaces en route to mineralization: a combined photocatalytic and radiation chemical study". Journal of Physical Chemistry, 95(24):10080-10089.

Matthews, R.W. (1984). "Hydroxylation reactions induced by near-ultraviolet photolysis of aqueous titanium dioxide suspensions". Journal of the Chemical Society, Faraday Transactions 1: Physical Chemistry in Condensed Phases, 80: 457-471.

Matthews, R.W. (1990). "Purification of water with near-UV illuminated suspensions of titanium dioxide". Water Research, 24(5):653-660.

Matthews, R.W. (1991). "Photooxidative degradation of colored organics in water using supported catalysts: TiO_2 on sand". Water Research, 25: 1169-1176.

Matthews, R. and McEvoy, S. (1992). "A comparison of 254 nm and 350 nm excitation of TiO_2 in simple photocatalytic reactors". Journal of Photochemistry and Photobiology A: Chemistry, 66(3):355-366.

Mattsson, R.W.; and Rolander, U. (1985) "Structure and Morphology of Anodic Oxide Films on Titanium GIPR-264", Chalmers University if Technology, Sweden.

Mills, A. and Le Hunte, S. (1997). "An overview of semiconductor photocatalysis". Journal of Photochemistry and Photobiology A: Chemistry, 108: 1-35.

Mills, A.; and Sawunyama, P. (1994). "Photocatalytic degradation of 4-chlorophenol mediated by TiO_2. A comparative study of the activity of laboratory made and commercial TiO_2 samples". Journal of Photochemistry and Photobiology A: Chemistry, (84):305-309.

Mills, A.; Morris, S.; and Davies, R. (1993). " Photomineralisation of 4-chlorophenol sensitized by titanium dioxide: a study of the intermediates". Journal of Photochemistry and Photobiology A: Chemistry, 70(2):183-191.

Minero, C. (1999). "Kinetic analysis of photoinduced reactions of photoinduced reactions at the water semiconductor interface". Catalysis Today, 54:205-216.

Minero, C.; Pelizetti, E.; Malato, S.; Blanco, J. (1996). "Large solar plant photocatalytic water decontamination: effect of operational parameters". Solar Energy, 56:421-428.

Minero, C. and Vione, D. (2006). "A quantitative evaluation of the photocatalytic performance of TiO2 slurries". Applied Catalysis B: Environmental, 67:257-269.

Morrison, S.R. (1980). Electrochemistry at Semiconductor and Oxidized Metal Electrodes. Springer, USA.

Munter, R. (2001). "Advanced oxidation processes: Current status and prospects". Proceedings of the Estonian Academy of Science. Chemistry, 50(2):59-80.

Murakami Corporation, Hydrophilic Clear Mirror, 21 June 2008, www.murakami-kaimeido.co.jp/english/mirror/mirror_e_tech_hcm.html.

Murakami, T.N.; Kijitori, Y.; Kawashima, N.; and Miyasaka, T. (2004) "Low temperature preparation of mesoporous TiO_2 films for efficient dye-sensitized photoelectrode by chemical vapor deposition combined with UV light irradiation". Journal of Photochemistry and Photobiology A: Chemistry, 164:187-191.

Nazeeruddin, M. K.; Kay, A.; Rodicio, I.; Humphry-Baker, R.; Müller, E.; Liska, P.; Vlachopoulos, N.; Grätzel, M. (1993). "Conversion of light to electricity by cis-X2bis (2,2'-bipyridyl-4,4'-dicarboxylate)ruthenium(II) charge-transfer sensitizers (X = Cl-, Br-, I-, CN-, and SCN-) on nanocrystalline titanium dioxide electrodes" Journal of the American Chemical Society, 115:6382.

Nazeeruddin, M. K.; Pechy, P.; and Grätzel, M. (1997). "Efficient panchromatic sensitization of nanocrystalline TiO2 films by a black dye based on a trithiocyanato-ruthenium complex". Chemical Communications, 18(18): 1705–1706.

Nazeeruddin, M. K.; Pechy, P.; Gratzel, M. (1997). "Efficient panchromatic sensitization of nanocrystalline TiO_2 films by a black dye based on a trithiocyanato-ruthenium complex". Chemical Communications, 18(18): 1705–1706.

Niederberger, M. (2007) "Nonaqueous sol-gel routes to metal oxides nanoparticles". Accounts of Chemical Research, 40(9):793-800.

Nogueira, R.F.P.; and Jardim, W.F. (1996). "TiO$_2$-fixed-bed reactors for water decontamination using solar light". Solar Energy, 56(5): 471-477.

Ochuma, I.; Fishwick, R.; Wood, J. and Winterbottom, J. (2007). "Optimization of degradation conditions of 1,8-diazabicyclo[5.4.0]unde-7-ene in water and reaction kinetics analysis using a concurrent downflow contactor photocatalytic reactor". Applied Catalysis B: Environmental, 73:259-268.

Ohtani, B. (2008). "Preparing articles on photocatalysis: beyond the illusions, misconceptions, and speculation". Chemistry Letters, 37(3):216-229.

Okamoto, K.; Yamamoto, Y.; Tanaka, H.; Tanaka, M.; and Itaya, A. (1985). "Heterogeneous photocatalytic decomposition of phenol over TiO$_2$ powder". Bulletin of the Chemical Society of Japan, 58(7):2015-2022.

Ollis, D.F. (1985). "Contaminant degradation in water". Environmental Science & Technology, 19(6):480-484.

Ollis, D.F. (2005). "Kinetic disguises in heterogeneous photocatalysis". Topics in Catalysis, 35:217-223. Ollis, D.F.; Pelizzetti, E.; and Serpone, N. (1991) "Photocatalyzed destruction of water contaminants." Environmental Science and Technology, 35: 971-976.

Oosawa, Y.; and Gratzel, M. (1984) "Enhancement of photocatalytic oxygen evolution in aqueous TiO2 suspensions by removal of surface-OH groups". Journal of the Chemical Society, Chemical Communications, 1984(24):1629-1630.

Oosawa, Y.; and Gratzel, M. (1988) "Effect of surface hydroxyl density on photocatalytic oxygen generation in aqueous TiO$_2$ suspensions". Journal of the Chemical Society, Faraday Transactions 1, 84(1):197-205.

Oppelt, E.T. (1998). Handbook on Advanced Photochemical Oxidation Processes, Environmental Protection Agency, USA.

OSPAR (2006). "OSPAR Recommendation 2006/4 Amending OSPAR Recommendation 2001/1 For The Management Of Produced Water From Offshore Installations," OSPAR Convention For The Protection Of The Marine Environment Of The North-East Atlantic, Meeting of the OSPAR Commission (OSPAR), Stockholm: 26-30 June.

Pareek, V.; Chong, S.; Tade, M.; and Adesina, A.A. (2008) "Light intensity distribution in heterogeneous photocatalytic reactors". Asia-Pacific Journal of Chemical Engineering, 3:171-201.

Parent, Y.; Blake, D.; Magrini-Bair, K.; Lyons, C.; Turchi, C.; Watt, A.; Wolfrum, E.; and Prairie, M. (1996). "Solar photocatalytic processes for the purification of water: State of development and barriers to commercialization". Solar Energy, 56(5): 429-437.

Parra, S.; Olivero, J.; and Pulgarin, C. (2002). "Relationships between physicochemical properties and photoreactivity of four biorecalcitrant phenylurea herbicides in aqueous TiO2 suspension." Applied Catalysis B: Environmental, 36:75-85.

Peiro, A.; Ayllon, J.; Peral, J. and Domenech, X. (2001). "TiO$_2$-photocatalyzed degradation of phenol and ortho-substituted phenolic compounds". Application Catalysis B, 30:359-373.

Pelizzeti, E.; Carlin, V.; Minero, C.; Gratzel, M. (1992). "Enhancement of the rate of photocatalytic degradation on TiO2 of 2-chlorophenol, 2,7-dichlorodibenzodioxin, and atrazine by inorganic oxidizing species". Cheminform, 23(21):336-336.

Pelizzetti, E. and Serpone, N. (1988). In Photocatalysis and Environment, Kluwer Academic Publishers, Boston, 469-497.

Pichat, P. (2007). "A brief overview of photocatalytic mechanisms and pathways in water". Water Science and Technology, 55:167-173.

Piera, E.; Tejedor-Tejedor, M. I.; Zorn, M. E.; and Anderson, M. A. (2003). "Relationship concerning the nature and concentration of Fe(III) species on the surface of TiO_2 particles and photocatalytic activity of the catalyst". *Applied Catalysis B:Environmental, 46*: 671–685.

Pilkington Group Limited (2008), How self-cleaning glass works, http://www.pilkingtonselfcleaningglass.co.uk/howitworks.

Poirier, G.E.; Hance, B.K.; and White, J.M. (1993). "Tunneling probe manipulation of individual rhodium nanoparticles supported on titania". The Journal of Physical Chemistry, 97(24):6500-6503.

Pozzo, R.L.; Baltanas, M.A.; Cassano, A.E. (1997). "Supported titanium dioxide as photocatalyst in water decontamination: state of the art". Catalysis Today, 39: 219-231.

Prairie, M.; Evans, L.; Stange, B.; Martinez, S. (1993). "An investigation of TiO_2 photocatalysis for the treatment of water contaminated with metals and organic chemicals" Environmental Science and Technology, 27:1776-1782.

Puma, G. and Yue, P. (2002). "Effect of the radiation wavelength on the rate of photocatalytic oxidation of organic pollutants". Industrial & Engineering Chemistry Research, 41(23):5594-5600.

Purifics ES Incorporated, Photo-Cat, 15 June 2008, http://www.purifics.com/technology/photo-cat.html.

Rice, G.W. (1987). "Laser-driven pyrolysis: Synthesis of TiO_2 from titanium isopropoxide". Journal of the American Ceramic Society, 70(5):117-120.

Richard, C. and Boule, P. (1994). "Photocatalytic oxidation of phenolic derivatives: influence of OH^* and h^+ on the distribution of products". New Journal of Chemistry, 18:547-552.

Riegel, G.; and Bolton, J.R. (1995). "Photocatalytic efficiency variability in TiO_2 particles". Journal of Physical Chemistry, 99(12):4215-4224.

Rincón, G.J.; La Motta, E.J.; and Mickler, B. (2013). "Kinetics of electrocoagulation of hexane extractable materials (HEM) in artificial bilge water treatment". Journal of Ship Production and Design, 29(2):57-65.

Rodriguez, L. and Matousek, J. (2004). "Properties of sol-gel TiO2 layers on glass substrate". Ceramics, 48(2):66-71.

Sakthivel, S.; Shankar, M.V.; Palanichamy, M.; Arabindoo, B.; and Murugesan, V. (2002) "Photocatalytic decomposition of leather dye. Comparative study of TiO2 supported on alumina and glass beads". Journal of Photochemistry & Photobiology A: Chemistry, 148:153-159.

Saquib, M. and Muneer, M. (2003). "TiO$_2$-mediated photocatalytic degradation of a triphenylmethane dye (gentian violet), in aqueous suspensions". Dyes and Pigments, 56:37-49.

Satterfield, C.N. (1970). Mass transfer in heterogeneous catalysis. MIT Press, 177-179.

Schubert, U. (2005) "Chemical modification of titanium alkoxides for sol-gel processing", Journal of Materials Chemistry, 15:3701-3715.

Serpone, N. (1997). "Relative photonic efficiencies and quantum yields in heterogeneous photocatalysis". Journal of Photochemistry and Photobiology A: Chemistry, 104:1-12.

Serpone, N.; Terzian, R.; Minero, C.; and Pelizzetti, E. (1993) "Heterogeneous photocatalyzed oxidation". American Chemical Society, USA.

Serpone, N. and Pelizzetti, E. (1989). Photocatalysis: Fundamentals and Applications. Wiley, USA.

Serpone, N.; Sauve, G.; Koch, R.; Tahiri, H.; Pichat, P.; Piccinini, P.; Pelizzetti, E.; and Hidaka, H. (1996) "Standardization protocol of process efficiencies and activation parameters in heterogeneous photocatalysis: relative photonic efficiencies zeta(r)". Journal of Photochemistry and Photobiology A: Chemistry, 94:191–203.

Serpone. N. (1995). "Brief introductory remarks on heterogeneous photocatalysis". Solar Energy Materials and Solar Cells, 38:369-379.

Shinde, P.S.; and Bhosale, C.H. (2008) "Properties of chemical vapour deposited nanocrystalline TiO$_2$ thin films and their use in dye-sensitized solar cells". Journal of Analytical and Applied Pyrolysis, 82:83-88.

Shinde, P.; Sadale, S.; Patil, P.; Bhosale, P.; Bruger, A.; Neumann-Spallart, M. and Bhosale, C. (2008). "Properties of spray deposited titanium dioxide thin films and their application in photoelectrocatalysis." Solar Energy Materials and Solar Cells, 92:283-290.

Singh, H.K.; Saquib, M.; HAque, M.M.; and Muneer, M. (2007) "Heterogeneous photocatalysed degradation of 4-chlorophenoxyacetic acid in aqueous suspensions", Journal of Hazardous Materials, 142:374-380.

Singleton, J. (2001). Band Theory and Electronic Properties of Solids. Oxford University Press, USA.

Soedergren, S.; Hagfeldt, A.; Olsson, J.; and Lindquist, S-E. (1994). "Theoretical models for the action spectrum and the current-voltage characteristics of microporous semiconductor films in photoelectrochemical cells". Journal of Physical Chemistry, 98(21):5552-5556.

Sul, Y.T.; Johansson, C.B.; Jeong, Y.; and Albrektsson, T. (2001). "The electrochemical oxide growth behavious on titanium in acid and alkaline electrolytes". Medical Engineering & Physics, 23(5), 329-346.

Sullivan, W.F.; Cole, S.S. (1959) "Thermal chemistry of colloidal titanium dioxide". Journal of the American Ceramic Society, 42(3):127-133.

Sun, D.; Wong, M.; Sun, L.; Li, Y.; Miyatake, N.; Sue, H-J. (2007). "Purification and stabilization of colloidal ZnO nanoparticles in methanol". Journal of Sol-Gel Science and Technology, 43:237-243.

Sun, Y.; and Pignatello, J. (1995). "Evidence for a surface dual hole-radical mechanism in the titanium dioxide photocatalytic oxidation of 2,4-D.". Environmental Science & Technology, 29(8):2065-2072.

Surender, G.D.; Fotou, G.P.; and Pratsinis, S.E. (1998). "Titania-based aqueous phase photocatalytic remediation processes: Strategies for enhancement of quantum efficiency". Trends in Chemical Engineering, 4:145-159.

Svetlichnyi, V.; Chaikovskaya, O.; Bazyl, O.; Kuznetsova, R.; Sokolova, I.; Kopylova, T. and Mechalkin, Yu. (2001). "Photolysis of phenol and para-chlorophenol by UV laser excitation". High Energy Chemistry, 35(4):258-264.

Swamy, V.; Muscat, J.; Gale, J.D.; and Harrison, N.M. (2002) "Simulation of low index rutile surfaces with a transferable variable-charge Ti-O interatomic potential and comparison with ab initio results". Surface Science, 504:115-124.

Szczepankiewicz, S.H.; Colussi, A.J.; and Hoffmann, M.R. (2000). "Infrared spectra of photoinduced species on hydroxylated titania surfaces". Journal of Physical Chemistry B, 104(42):9842-9850.

Szczepankiewicz, S.H.; Moss, J.A.; and Hoffmann, M.R. (2002). "Slow surface charge trapping kinetics on irradiated TiO_2". Journal of Physical Chemistry B, 106(11):2922-2927.

Tabrizi, R. (1989) "Surface Treatments of Titanium and its Alloy", University of Manchester Institute of Science and Technology, U.K.

Tada, H.; Kiyonaga, T.; and Naya, S.-I. (2009). "Rational design and applications of highly efficient reaction systems photocatalyzed by noble metal nanoparticle-loaded titanium(iv) dioxide." Chemical Society Reviews, 38:1849.

Taga, Y. (2009). "Titanium oxide based visible light photocatalysts: Materials design and applications." Thin Solid Films, 517:3167.

Tahiri, H.; Ichou, Y.A.; and Herrmann, J.-M. (1998). "Photocatalytic degradation of chlorobenzoic isomers in aqueous suspensions of neat and modified titania". Journal of Photochemistry and Photobiology A: Chemistry, 114(3):219-226.

Tang, C.; and Chen, V. (2004) "The photocatalytic degradation of reactive black 5 using TiO_2/UV in an annular photoreactor". Water Research, 38:2775-2781.

Tao, Y.; Cheng, Z.L.; Ting, K.E. and Yin, X.J. (2013). "Photocatalytic degradation of phenol using a nanocatalyst: The mechanism and kinetics". Journal of Catalysis, 2013:ID 364275

Thompson, T.L.; and Yates, J.T. (2006). "Surface science studies of the photoactivation of TiO2. New photochemical processes". Chemical Reviews, 106(10:4428-4453.

Toor, A.; Verna, A.; Jotshi, C.; Bajpai, P. and Singh, V. (2006). "Photocatalytic degradation of direct yellow 12 die using UV/TiO_2 in a shallow pond slurry reactor". Dyes and Pigments, 68:53-60.

TOTO Limited, Principle of Hydrotech Technology, 20 June 2008, http://www.toto.co.jp/products/hydro/genri_en.htm.

Trillas, M.; Pujol, M.; and Domenech, X. (1992). "Phenol photodegradation over titanium dioxide". Journal of Chemical Technology and Biotechnology, 55:85-90.

Turchi, C.S.; and Ollis, D.F. (1988) "Photocatalytic reactor design: An example of mass transfer limitations with an immobilized catalyst". Journal of Physical Chemistry, 92: 6852-6853.

Turchi, C.S.; and Ollis, D.F. (1990). "Photocatalytic degradation of organic water contaminants: Mechanisms involving hydroxyl radical attack". Journal of Catalysis, 122:178-192.

Ueda, J.; Takeshita, K.; Matsumoto, S.; Yazaki, K.; Kawaguchi, M.; and Ozawa, T. (2003). "Singlet oxygen-mediated hydroxyl radical production in the presence of phenols: whether DMPO-OH formation really indicates production of OH?" Photochemistry and Photobiology, 77(2):165-170.

Valencia, S.; Catano, F.; Rios, L.; Restrepo, G.; and Marin, J. (2011) "A new kinetic model for heterogeneous photocatalysis with titanium oxide: Case of non-specific adsorption considering back reaction". Applied Catalysis B: Environmental, 104:300-304.

Vik, E.A. (2007). "Produced Water Management on the Norwegian Continental Shelf-Environmental Technology Challenges Experienced." Exploration and Production – Oil And Gas Review–Issue II. http://www.touchoilandgas.com/download.cfm?step=2&type=art&type_id=7807

Villarreal, T.L.; Gómez, R.; González, M.; and Salvador, P. (2004). "A kinetic model for distinguishing between direct and indirect interfacial hole transfer in the heterogeneous photooxidation of dissolved organics on TiO_2 nanoparticle suspensions". Journal of Physical Chemistry B, 108(52):20278–20290.

Vinodgopal, K.; and Kamat, P.V. (1995). "Electrochemically assisted photocatalyst using nanocrystalline semiconductor thin films". Solar Energy Materials and Solar Cells, 38:401-410.

Ward, M.D.; White, J.R.; and Bard, A.J. (1983). "Electrochemical investigation of the energetic of particulate titanium dioxide photocatalysts. The methyl viologen-acetate system". Journal of the American Chemical Society, 105:27-31.

Wei, T. and Wan, C. (1991). "Heterogeneous photocatalytic oxidation of phenol with titanium dioxide powders". Industrial &.Engineering Chemistry Research, 30:1293-1300.

Wyness, P.; Klausner, J.; Goswami, D.; Schanze, K. (1994). "Performance of nonconcentrating solar photocatalytic oxidation reactors, part 1: Flat plate configuration". Journal of Solar Energy Engineering, 116:2-7.

Xiao-e, L.; Green, A.N.M.; Haque, S.A.; Mills, A.; and Durtant, J.R. (2004). "Light-driven oxygen scavenging by titania/polymer nanocomposite films". Journal of Photochemistry and Photobiology A: Chemistry, 162:253-259.

Xu, Y. and Langford, C. (2000). "Variation of Langmuir adsorption constant determined for TiO_2-photocatalyzed degradation of acetophenone under different light intensity". Journal of Photochemistry and Photobiology A: Chemistry, 133:67-71.

Xu, N.; Shi, Z.; Fan, Y.; Dong, J.; Shi, J.; and Hu, M.Z.-C. (1999). "Effects of particle size of TiO_2 on photocatalityc degradation of methylene blue in aqueous suspensions". Industrial & Engineering Chemistry Research, 38(2):373-379.

Yahalom, J.; and Zahavi, J. (1970) "Electrolytic breakdown crystallization of anodic oxide films on A1, Ta and Ti". Electrochimica Acta, 15(9):1429-1435.

Yang, J.; Huang, Y.X.; and Ferreira J.M.F. (1997). "Inhibitory effect of alumina additive on the titania phase transformation of a sol-gel derived powder". Journal of Materials Science Letters, 16(23):1933-1935.

Ying, J.Y.; and Sun, T. (1997) "Research needs assessment on nanostructured catalysts". Journal of Electroceramics, 1:219-238.

Yoldas, B.E. (1982) "Effect of variations in polymerized oxides on sintering and crystalline transformations", Journal of the American Ceramic Society, 65(8):387-393.

Yoldas, B.E. (1984) "Modification of polymer-gel structures". Journal of Non-Crystalline Solids, 63:145-154.

Young, L. (1961) "Anodic oxide films". Academic Press, London.

Yue, X.; Zhang, R.; Wang, W.; Wang, L.; and Yang, Y. (2008). "Effect of TiO_2 doping technique on decomposition of crude oil absorbed into expanded graphite". Materials Letters, 62:1919-1922.

Yum, J.H.; Kim, S.S.; Kim, D.Y.; and Sung, Y.E. (2005) "Electrophoretically deposited TiO2 photo-electrodes for use in flexible dye-sensitized solar cells". Journal of Photochemistry and Photobiology A: Chemistry, 173:1-6.

Yung-Hsu, H. and Ting-Shan, C. (1995). Proceedings of the 27th Middle Atlantic Industrial Waste Conference, Baltimore, MD. 469.

Zhang, Y.; Crittenden, J.C.; and Hand, D.W. (1994). "Fixed-bed photocatalyst for solar decontamination of water". Environmental Science & Technology, 28: 435-442.

Zhang, Y.; Crittenden, J.C.; and Hand, D.W. (1996). "Destruction of organic compounds in water using supported photocatalysis". Journal of Solar Energy Engineering, 118: 123-129.

Zhao, H.; Jiang, D.; Zhang, S.; Catterall, K.; and John, R. (2004). "Development of a direct photoelectrochemical method for determination of chemical oxygen demand". Analytical Chemistry, 76:155-160.

Zou, L; Li, Y; and Hung, Y. (2007). "Wet Air Oxidtion for Water Treatment", Chapter 13. Handbook of Environmental Engineering, 5:588.

Appendix

A. Results of Photocatalytic Experiments by Date

This section presents the raw experimental results. Each insert contains a description of the type of experiment, size of silica gel particle, quartz sleeve diameter, initial phenol concentration, volume of solution in the reactor, pump's controller setting, catalyst coating characteristics, and experiment's objective.

		Photolysis (UV only)+oxigeno								
		1" sleeve		Photolysis experiment. UV + O2 only.						
	ID :	6/19/2014								
	C$_{phenol}$=	1 mmol/L								
	Vol =	800 ml	Speed = 8							
	Silica =	none								
		Time (min)	**COD (mg/L)**	**pH**	**DO (mg/L)**	**T**	**λ @ 269**	**λ @ 254**	**λ @ 240**	**Integral**
9:00	0	0	242	6.1	9.41	21.9	1.430	0.512	0.102	107.36
10:00	1	60	206	3.9	35	32	1.920	1.673	1.536	220.75
11:00	2	120	185	3.7	35	32	1.719	1.587	1.620	224.60
1:00	4	240	167	3.6	35	35	1.314	1.279	1.430	200.73
3:00	6	360	150	3.5	35	35	0.959	0.982	1.134	155.49
5:00	8	480	143	3.5	35	35	0.609	0.653	0.775	103.35

		UV + TiO2									
		50 mesh (300 μm)			Photocatalytic experiment using 30 g. per liter (24 g.) of silica gel size larger than 300 μm. Compare to 5, 10 and 20 g/L of same size silica.						
		1" sleeve (new)									
ID :		7/1/2014									
C$_{phenol}$=		1 mmol/L									
Vol =		800 ml		Speed =	8						
Silica =		24 g (30 g/L)		1 coat	new						
		Time (min)	**COD (mg/L)**	**pH**	**DO (mg/L)**	**T**	**λ @ 269**	**λ @ 254**	**λ @ 240**	**Integral**	
8:00		-60	235	5.3	8.25	21	1.459	0.517	0.078	105.51	
9:00		0	248	5.1	35	23	1.411	0.567	0.170	109.04	
9:30		30	221	4.3	35	28	1.560	1.118	0.973	172.23	
10:00		60	196	4.1	35	28	1.468	1.098	1.041	179.04	
10:30		90	181	4.0	35	32	1.356	1.043	1.038	177.23	
11:00		120	169	3.9	35	34	1.251	1.006	1.035	173.72	
1:00		240	144	3.7	35	35	0.770	0.721	0.809	124.34	
3:00		360	117	3.7	35	35	0.377	0.400	0.470	66.22	
5:00		480	99	3.8	35	35	0.156	0.177	0.208	27.72	

		UV + TiO2									
		50 mesh (300 μm)			Photocatalytic experiment using 5 g. per liter (4 g.) of silica gel size larger than 300 μm. Compare to 10, 20 and 30 g/L of same size silica.						
		1" sleeve (new)									
ID :		7/2/2014									
C$_{phenol}$=		1 mmol/L									
Vol =		800 ml		Speed =	8						
Silica =		4 g (5 g/L)		1 coat	new						
		Time (min)	**COD (mg/L)**	**pH**	**DO (mg/L)**	**T**	**λ @ 269**	**λ @ 254**	**λ @ 240**	**Integral**	
8:00		-60	229	5.6	8.25	21	1.427	0.501	0.075	105.12	
9:00		0	237	5.1	35	22	1.368	0.508	0.097	103.38	
9:30		30	199	4.0	35	28	1.812	1.473	1.240	194.69	
10:00		60	179	3.8	35	32	1.748	1.465	1.347	206.07	
10:30		90	171	3.7	35	35	1.648	1.400	1.358	206.75	
11:00		120	159	3.6	35	35	1.526	1.327	1.335	203.22	
1:00		240	129	3.5	35	36	1.192	1.125	1.237	183.81	
3:00		360	119	3.5	35		0.846	0.865	0.994	139.18	
5:00		480	109	3.5	35	36.1	0.390	0.454	0.550	70.18	

	UV + TiO2								
	50 mesh (300 µm)	**Repeat of Jun-28**. Photocatalytic experiment using 10 g. per liter (8 g.) of silica gel size larger than 300 µm. Compare to 5, 20 and 30 g/L of same size silica.							
	1" sleeve (new)								
ID :	7/10/2014								
C_{phenol}=	1 mmol/L								
Vol =	800 ml	Speed =	8						
Silica =	8 g (10g/L)	1 coat	new						
	Time (min)	**COD (mg/L)**	**pH**	**DO (mg/L)**	**T**	**λ @ 269**	**λ @ 254**	**λ @ 240**	**Integral**
8:00	-60	233	5.8	8.71	22.1	1.442	0.492	0.071	107.18
9:00	0	236	5.3	20		1.413	0.542	0.134	108.22
9:30	30	195	4.2	35	28	1.727	1.330	1.154	188.84
10:00	60	183	4.0	35	28	1.644	1.312	1.234	197.00
10:30	90	169	3.8	35	28	1.537	1.258	1.237	196.58
11:00	120	161	3.8	35	32	1.434	1.216	1.238	194.34
1:00	240	122	3.6	35	32	1.016	0.967	1.076	161.04
3:00	360	97	3.5	35	34	0.551	0.588	0.684	94.82
5:00	480	78	3.6	20	36	0.120	0.138	0.167	22.98

	UV + TiO2								
	75 mesh (200 µm)	Photocatalytic experiment using 20 g. per liter (16 g.) of silica gel size larger than 200 µm. Compare to 20 g/L of size 300, 425 silica.							
	1" sleeve (new)								
ID :	7/11/2014								
C_{phenol}=	1 mmol/L								
Vol =	800 ml	Speed =	8						
Silica =	16 g (20g/L)	1 coat	new						
	Time (min)	**COD (mg/L)**	**pH**	**DO (mg/L)**	**T**	**λ @ 269**	**λ @ 254**	**λ @ 240**	**Integral**
8:00	-60	229	5.5	8.71	22.1	1.430	0.507	0.084	107.24
9:00	0	233	5.0	20	24	1.414	0.583	0.191	112.52
9:30	30	188	4.2	>20	28	1.482	1.074	0.957	171.55
10:00	60	160	4.1	35	28	1.290	0.956	0.930	168.39
10:30	90	144	3.9	35	28	1.157	0.896	0.910	163.26
11:00	120	131	3.9	35	32	1.047	0.852	0.889	154.61
1:00	240	90.4	3.7	35	32	0.573	0.549	0.620	94.14
3:00	360	59.6	3.8	35	34	0.235	0.269	0.312	38.34
5:00	480	56.2	4.2	20	36	0.146	0.182	0.208	22.17

	UV + TiO2 40 mesh (425 μm) 1" sleeve (new)		Photocatalytic experiment using 20 g. per liter (16 g.) of silica gel size larger than 425 μm. Compare to 20 g/L of size 200, 300 silica.								
ID :	7/12/2014										
C$_{phenol}$=	1 mmol/L										
Vol =	800 ml	Speed =	8								
Silica =	16 g (20g/L)	1 coat	new								
	Time (min)	**COD (mg/L)**	**pH**	**DO (mg/L)**	**T**	**λ @ 269**	**λ @ 254**	**λ @ 240**	**Integral**		
8:00	-60	233	5.5	8.71	22.1	1.446	0.525	0.092	107.55		
9:00	0	232	5.6	20	24	1.399	0.548	0.144	109.31		
9:30	30	192	4.4	>20	28	1.682	1.301	1.131	187.21		
10:00	60	177	4.1	35	28	1.586	1.253	1.184	193.69		
10:30	90	161	4.0	35	28	1.459	1.172	1.158	190.89		
11:00	120	149	4.0	35	32	1.344	1.108	1.132	186.37		
1:00	240	112	3.8	35	32	0.934	0.854	0.944	147.94		
3:00	360	88.7	3.7	35	34	0.544	0.557	0.645	92.87		
5:00	480	75.9	3.8	20	36	0.216	0.247	0.291	37.74		

	UV + TiO2 50 mesh (300 μm) 1" sleeve (new)		**Repeat of Jun-30**. Photocatalytic experiment using 20 g. per liter (16 g.) of silica gel size larger than 300 μm. Compare to 5, 10 and 30 g/L of same size silica.								
ID :	7/14/2014										
C$_{phenol}$=	1 mmol/L										
Vol =	800 ml	Speed =	8								
Silica =	16 g (20 g/L)	1 coat	new								
	Time (min)	**COD (mg/L)**	**pH**	**DO (mg/L)**	**T**	**λ @ 269**	**λ @ 254**	**λ @ 240**	**Integral**		
8:00	-60	230	5.5	8.25	22.9	1.434	0.494	0.084	110.18		
9:00	0	228	5.3	>20	24.7	1.397	0.536	0.146	110.43		
9:30	30	195	4.3	>20	29.2	1.639	1.230	1.080	184.24		
10:00	60	172	4.2	>20	31.6	1.542	1.196	1.143	190.16		
10:30	90	159	4.0	>20	32.9	1.418	1.140	1.146	188.44		
11:00	120	145	3.9	>20	34.1	1.283	1.073	1.116	182.71		
1:00	240	106	3.7	>20	35.2	0.790	0.772	0.874	129.13		
3:00	360	73	3.7	>20	36.5	0.302	0.334	0.398	54.16		
5:00	480	57.9	3.9	>20	36.6	0.121	0.144	0.169	20.62		

	UV + TiO2									
	40 mesh (425 μm)		Photocatalytic experiment using 10 g. per liter (16 g.) of silica gel size larger than 425 μm. Compare to 10 of size 200 and 300 silica.							
	1" sleeve (new)									
ID :	7/15/2014									
C_{phenol}=	1 mmol/L									
Vol =	800 ml	Speed =	8							
Silica =	8 g (10 g/L)	1 coat	new							
	Time (min)	COD (mg/L)	pH	DO (mg/L)	T	λ @ 269	λ @ 254	λ @ 240	Integral	
8:00	-60	235	5.2	8.25	22.9	1.456	0.515	0.089	108.86	
9:00	0	234	5.1	>20	24.7	1.413	0.546	0.136	109.39	
9:30	30	202	4.3	>20	29.2	1.791	1.414	1.192	192.13	
10:00	60	184	4.1	>20	31.6	1.708	1.364	1.256	200.46	
10:30	90	170	3.9	>20	32.9	1.618	1.318	1.273	201.90	
11:00	120	161	3.8	>20	34.1	1.522	1.258	1.258	199.40	
1:00	240	146	3.7	>20	35.2	1.190	1.068	1.161	182.06	
3:00	360	125	3.6	>20	36.5	0.911	0.881	1.001	148.18	
5:00	480	107	3.6	>20	36.6	0.589	0.622	0.729	100.67	

	UV + TiO2									
	75 mesh (200 μm)		Photocatalytic experiment using 10 g. per liter (8 g.) of silica gel size larger than 200 μm. Compare to 10 of size 300 and 425 silica.							
	1" sleeve (new)									
ID :	7/16/2014									
C_{phenol}=	1 mmol/L									
Vol =	800 ml	Speed =	8							
Silica =	8 g (10 g/L)	1 coat	new							
	Time (min)	COD (mg/L)	pH	DO (mg/L)	T	λ @ 269	λ @ 254	λ @ 240	Integral	
8:00	-60		5.5	8.25	22.9	1.469	0.520	0.090	109.77	
9:00	0	238	5.0	>20	24.7	1.429	0.552	0.140	110.52	
9:30	30	198	4.2	>20	29.2	1.646	1.223	1.061	182.65	
10:00	60	177	4.0	>20	31.6	1.506	1.132	1.067	184.41	
10:30	90	166	3.9	>20	32.9	1.401	1.080	1.063	182.80	
11:00	120	149	3.8	>20	34.1	1.262	0.993	1.013	175.93	
1:00	240	111	3.6	>20	35.2	0.841	0.738	0.803	132.13	
3:00	360	82.5	3.6	>20	36.5	0.407	0.387	0.438	68.01	
5:00	480	60.3	3.8	>20	36.6	0.147	0.157	0.183	24.51	

	UV + TiO2		Photocatalytic experiment using 20 g. per liter (16 g.) of silica gel size larger than 300 µm and phenol concentration of 0.5 mmol. Compare to higher phenol concentrations.						
	50 mesh (300 µm)								
	1" sleeve (new)								
ID :	7/17/2014								
C_{phenol}=	0.5 mmol/L								
Vol =	800 ml	Speed =	8						
Silica =	16 g (20 g/L)	1 coat	new						
	Time (min)	**COD (mg/L)**	**pH**	**DO (mg/L)**	**T**	**λ @ 269**	**λ @ 254**	**λ @ 240**	**Integral**
8:00	-60	122	5.5	8.25	22.9	0.751	0.262	0.046	76.25
9:00	0	125	5.2	>20	24.7	0.748	0.309	0.108	78.69
9:30	30	102	4.5	>20	29.2	0.917	0.757	0.695	122.77
10:00	60	87.8	4.2	>20	31.6	0.770	0.659	0.668	111.67
10:30	90	76.5	4.0	>20	32.9	0.632	0.569	0.605	96.16
11:00	120	64.9	3.9	>20	34.1	0.494	0.472	0.516	78.31
1:00	240	35.9	4.0	>20	35.2	0.123	0.142	0.169	21.71
3:00	360	27.3	4.3	>20	36.5	0.085	0.104	0.120	14.07
5:00	480	21.5	4.4	>20	36.6	0.077	0.096	0.112	13.03

	UV + TiO2		Photocatalytic experiment using 20 g. per liter (16 g.) of silica gel size larger than 300 µm and phenol concentration of 2.0 mmol. Compare to various phenol concentrations.						
	50 mesh (300 µm)								
	1" sleeve (new)								
ID :	7/21/2014								
C_{phenol}=	2.0 mmol/L								
Vol =	800 ml	Speed =	8						
Silica =	16 g (20 g/L)	1 coat	new						
	Time (min)	**COD (mg/L)**	**pH**	**DO (mg/L)**	**T**	**λ @ 269**	**λ @ 254**	**λ @ 240**	**Integral**
8:00	-60	453	5.5	8.25	22.9	2.472	1.000	0.176	148.20
9:00	0	440	5.5	>20	24.7	2.421	1.020	0.232	147.29
9:30	30	385	4.4	>20	29.2	2.828	2.009	1.636	242.95
10:00	60	349	4.2	>20	31.6	2.777	2.017	1.783	256.14
10:30	90	321	3.9	>20	32.9	2.657	1.961	1.822	259.12
11:00	120	299	3.9	>20	34.1	2.553	1.942	1.867	261.08
1:00	240	236	3.6	>20	35.2	2.102	1.776	1.883	254.20
3:00	360	202	3.5	>20	36.5	1.635	1.524	1.693	231.46
5:00	480	168	3.5	>20	36.6	1.080	1.129	1.302	182.51

	UV + TiO2 50 mesh (300 µm) 1" sleeve (new)		Photocatalytic experiment using 20 g. per liter (16 g.) of silica gel size larger than 300 µm and phenol concentration of 3.0 mmol. Compare to various phenol concentrations.							
ID :	7/22/2014									
C$_{phenol}$=	3.0 mmol/L									
Vol =	800 ml	Speed =	8							
Silica =	16 g (20 g/L)	1 coat	new							
	Time (min)	**COD (mg/L)**	**pH**	**DO (mg/L)**	**T**	**λ @ 269**	**λ @ 254**	**λ @ 240**	**Integral**	
8:00	-60	683	5.4	8.25	22.9	2.690	1.508	0.284	170.75	
9:00	0	653	5.3	>20	24.7	2.702	1.524	0.344	173.39	
9:30	30	593	4.4	>20	29.2	3.225	2.700	1.998	274.19	
10:00	60	557	4.1	>20	31.6	3.404	2.833	2.328	299.76	
10:30	90	518	3.9	>20	32.9	3.443	2.828	2.470	311.87	
11:00	120	489	3.8	>20	34.1	3.513	2.795	2.529	317.02	
1:00	240	411	3.6	>20	35.2	3.363	2.749	2.805	329.17	
3:00	360	343	3.5	>20	36.5	3.006	2.604	2.824	323.48	
5:00	480	309	3.4	>20	36.6	2.618	2.416	2.681	309.25	

	UV + TiO2 50 mesh (300 µm) 1" sleeve (new)		Photocatalytic experiment using 10 g. per liter (8 g.) of silica gel size larger than 300 µm and phenol concentration of 0.5 mmol. Compare to higher phenol concentrations.							
ID :	7/23/2014									
C$_{phenol}$=	0.5 mmol/L									
Vol =	800 ml	Speed =	8							
Silica =	8 g (10 g/L)	1 coat	new							
	Time (min)	**COD (mg/L)**	**pH**	**DO (mg/L)**	**T**	**λ @ 269**	**λ @ 254**	**λ @ 240**	**Integral**	
8:00	-60	125	5.5	8.25	22.9	0.746	0.263	0.045	76.00	
9:00	0	130	5.4	>20	24.7	0.757	0.311	0.108	80.27	
9:30	30	107	4.2	>20	29.2	0.946	0.787	0.719	127.65	
10:00	60	91.7	4.0	>20	31.6	0.823	0.719	0.720	119.14	
10:30	90	82.2	3.9	>20	32.9	0.685	0.626	0.662	104.05	
11:00	120	68.8	3.8	>20	34.1	0.530	0.516	0.563	84.13	
1:00	240	40.9	3.9	>20	35.2	0.102	0.115	0.136	18.64	
3:00	360	31.9	4.1	>20	36.5	0.071	0.085	0.097	12.14	
5:00	480	24.3	4.3	>20	36.6	0.069	0.084	0.097	11.64	

	UV + TiO2								
	50 mesh (300 µm)		Photocatalytic experiment using 10 g. per liter (8 g.) of silica gel size larger than 300 µm and phenol concentration of 2.0 mmol. Compare to different phenol concentrations.						
	1" sleeve (new)								
ID :	7/24/2014								
C_{phenol}=	2.0 mmol/L								
Vol =	800 ml	Speed =	8						
Silica =	8 g (10 g/L)	1 coat	new						
	Time (min)	**COD (mg/L)**	**pH**	**DO (mg/L)**	**T**	**λ @ 269**	**λ @ 254**	**λ @ 240**	**Integral**
8:00	-60	460	5.3	8.25	22.9	2.484	1.020	0.179	149.14
9:00	0	456	5.1	>20	24.7	2.432	1.057	0.239	148.05
9:30	30	398	4.0	>20	29.2	2.929	2.171	1.718	249.40
10:00	60	369	3.9	>20	31.6	2.978	2.284	1.970	270.43
10:30	90	330	3.8	>20	32.9	2.949	2.261	2.056	277.69
11:00	120	301	3.7	>20	34.1	2.879	2.235	2.110	281.12
1:00	240	269	3.5	>20	35.2	2.520	2.136	2.258	285.65
3:00	360	244	3.5	>20	36.5	2.184	1.993	2.203	275.75
5:00	480	206	3.4	>20	36.6	1.831	1.795	2.038	257.72

	UV + TiO2								
	50 mesh (300 µm)		Photocatalytic experiment using 30 g. per liter (24 g.) of silica gel size larger than 300 µm and phenol concentration of 0.5 mmol. Compare to higher phenol concentrations.						
	1" sleeve (new)								
ID :	7/25/2014								
C_{phenol}=	0.5 mmol/L								
Vol =	800 ml	Speed =	8						
Silica =	24 g (30 g/L)	1 coat	new						
	Time (min)	**COD (mg/L)**	**pH**	**DO (mg/L)**	**T**	**λ @ 269**	**λ @ 254**	**λ @ 240**	**Integral**
8:00	-60	118	5.4	8.25	22.9	0.745	0.263	0.043	75.52
9:00	0	118	5.3	>20	24.7	0.763	0.323	0.126	81.15
9:30	30	97	4.4	>20	29.2	0.861	0.676	0.632	116.46
10:00	60	80.6	4.1	>20	31.6	0.733	0.616	0.631	105.95
10:30	90	69.6	4.0	>20	32.9	0.595	0.539	0.579	90.24
11:00	120	57.9	3.9	>20	34.1	0.447	0.431	0.476	70.40
1:00	240	36.6	3.9	>20	35.2	0.154	0.180	0.211	25.28
3:00	360	29.4	4.2	>20	36.5	0.132	0.163	0.189	20.90
5:00	480	20.3	4.3	>20	36.6	0.142	0.178	0.208	22.80

	UV + TiO2			Photocatalytic experiment using 30 g. per liter (24 g.) of silica gel size larger than 300 μm and phenol concentration of 2.0 mmol. Compare to different phenol concentrations.						
	50 mesh (300 μm)									
	1" sleeve (new)									
ID :	7/26/2014									
C_{phenol}=	2.0 mmol/L									
Vol =	800 ml	Speed =	8							
Silica =	24 g (30 g/L)	1 coat	new							
	Time (min)	**COD (mg/L)**	**pH**	**DO (mg/L)**	**T**	**λ @ 269**	**λ @ 254**	**λ @ 240**	**Integral**	
8:00	-60	453	5.4	8.25	22.9	2.474	1.015	0.176	148.54	
9:00	0	446	5.5	>20	24.7	2.420	1.041	0.275	152.90	
9:30	30	392	4.5	>20	29.2	2.914	2.109	1.710	248.03	
10:00	60	366	4.2	>20	31.6	2.925	2.160	1.942	269.89	
10:30	90	344	4.0	>20	32.9	2.888	2.127	2.005	276.57	
11:00	120	321	3.9	>20	34.1	2.824	2.121	2.057	279.64	
1:00	240	273	3.7	>20	35.2	2.538	2.063	2.168	281.52	
3:00	360	253	3.6	>20	36.5	2.213	1.911	2.113	271.70	
5:00	480	224	3.5	>20	36.6	1.887	1.746	1.992	257.40	

	UV + TiO2			Photocatalytic experiment using 1 g. (1.25 g/l) of anatase and phenol concentration of 1.0 mmol. Compare to experimentes using coated silica.						
	Anatase powder									
	1" sleeve (new)									
ID :	7/29/2014									
C_{phenol}=	1.0 mmol									
Vol =	800 ml	Speed =	8							
Anatase=	1 g	Powder	new							
	Time (min)	**COD (mg/L)**	**pH**	**DO (mg/L)**	**T**	**λ @ 269**	**λ @ 254**	**λ @ 240**	**Integral**	
8:00	-60	234	5.3	8.25	22.9	1.468	0.513	0.090	111.31	
9:00	0	232	4.6	>20	24.7	1.414	0.521	0.106	108.50	
9:30	30	177	3.8	>20	29.2	1.118	0.624	0.589	149.56	
10:00	60	121	3.6	>20	31.6	0.701	0.505	0.578	115.01	
10:30	90	65.3	3.7	>20	32.9	0.227	0.220	0.278	44.04	
11:00	120	26.6	4.1	>20	34.1	0.014	0.016	0.021	4.55	
1:00	240	0	4.5	>20	35.2	0.006	0.005	0.004	2.67	
3:00	360	0	4.4	>20	36.5	0.007	0.005	0.005	3.44	
5:00	480	0		>20	36.6					

	UV + Silica+O2									
	50 mesh (300 μm)									
	1" sleeve (new)		**Repeat of Jul-30.** Photolysis experiment. UV+uncoated silica+ O2 only.							
ID :	7/31/2014									
C$_{phenol}$=	1 mmol/L									
Vol =	800 ml	Speed =	8		Conduct	8.00	μS/cm			
Silica =	16 g	uncoated								
	Time (min)	**COD (mg/L)**	**pH**	**DO (mg/L)**	**T**	**λ @ 269**	**λ @ 254**	**λ @ 240**	**Integral**	
8:00	-60	241	5.4	8.25		1.474	0.527	0.096	111.57	
9:00	0	241	6.2	>20		1.430	0.557	0.144	112.26	
10:00	60	215	4.6	>20		1.893	1.495	1.271	203.38	
11:00	120	200	4.2	>20		1.716	1.375	1.332	209.21	
1:00	240	171	4.0	>20		1.456	1.218	1.287	201.46	
3:00	360	164	3.8	>20		1.257	1.088	1.196	187.55	
5:00	480	159	3.8	>20		1.076	0.961	1.084	167.64	

	UV + TiO2										
	50 mesh (300 μm)										
	1" sleeve (new)		Photocatalytic experiment using 20 g. per liter (16 g.) of silica gel size larger than 300 μm. Added 2 mmol of NaCl.								
ID :	8/1/2014										
C$_{phenol}$=	1 mmol/L										
Vol =	800 ml	Speed =	8		NaCl =	2 mmol/L	1.688 mg/L				
Silica =	16 g (20 g/L)	1 coat	new		Cond. =	5.51	mS/cm				
	Time (min)	**COD (mg/L)**	**pH**	**C (mS/cm)**	**DO (mg/L)**	**T**	**λ @ 269**	**λ @ 254**	**λ @ 240**	**Integral**	**Phenol**
8:00	-60	238	5.6	5.51	8.25	22.9	1.459	0.514	0.088	110.92	109
9:00	0	221	4.6	5.74	>20	24.7	1.379	0.510	0.103	107.98	
9:30	30	182	4.1	5.95	>20	29.2	1.278	0.897	0.814	157.31	
10:00	60	160	4.0	6.16	>20	31.6	1.103	0.804	0.814	156.60	
10:30	90	141	3.9	6.21	>20	32.9	0.966	0.729	0.782	151.61	
11:00	120	124	3.8	6.37	>20	34.1	0.830	0.652	0.732	137.79	18
1:00	240	86.4	3.7	6.13	>20	35.2	0.386	0.365	0.464	76.80	10
3:00	360	60.1	3.8	6.46	>20	36.5	0.082	0.092	0.130	20.92	8
5:00	480	28.8	4.0	6.33	>20	36.6	0.025	0.028	0.034	5.78	7

		UV + TiO2									
		50 mesh (300 μm)		Photocatalytic experiment using 20 g. per liter (16 g.) of silica gel size larger than 300 μm. Added 20 mmol of NaCl.							
		1" sleeve (new)									
ID :	8/4/2014										
C_{phenol}=	1 mmol/L										
Vol =	800 ml	Speed =	8			NaCl =	20 mmol/l	16.88 mg/L			
Silica =	16 g (20 g/	1 coat	new			Cond. =		38.6 mS/cm			
	Time (min)	**COD (mg/L)**	**pH**	**C (mS/cm)**	**DO (mg/L)**	**T**	**λ @ 269**	**λ @ 254**	**λ @ 240**	**Integral**	
8:00	-60	200.8	5.5	38.60	8.25	22.9	1.467	0.522	0.093	111.22	
9:00	0	172	4.5	34.40	>20	24.7					
9:10	10	127.2									
9:20	20	140.8									
9:30	30	134.4	4.2	37.10	>20	29.2	1.280	0.889	0.751	150.60	
10:00	60	27.2	4.1	47.40	>20	31.6	1.156	0.826	0.804	155.54	
10:30					>20	32.9					
11:00	120	86.4	4.0	93.50	>20	34.1	0.883	0.650	0.724	145.60	
1:00	240	28.24	3.8		>20	35.2	0.534	0.472	0.601	108.42	
3:00	360	25.12	3.8		>20	36.5	0.285	0.292	0.395	71.24	
5:00	480	0	4.0		>20	36.6	0.135	0.150	0.224	41.40	

		UV + TiO2								
		50 mesh (300 μm)		Photocatalytic experiment using 20 g. per liter (16 g.) of silica gel size larger than 300 μm. 0.25 mmol/L of phenol.						
		1" sleeve (new)								
ID :	8/5/2014									
C_{phenol}=	0.25 mmol/L									
Vol =	800 ml	Speed =	8							
Silica =	16 g (20 g/L)	1 coat	new							
	Time (min)	**COD (mg/L)**	**pH**	**DO (mg/L)**	**T**	**λ @ 269**	**λ @ 254**	**λ @ 240**	**Integral**	
8:00	-60	56.4	5.5	8.25	22.9	0.382	0.133	0.022	40.89	
9:00	0	61.7	5.5	>20	24.7	0.403	0.184	0.084	44.86	
9:15	15	50.3	5.0	>20	26	0.544	0.462	0.395	69.31	
9:30	30	46.4	4.8	>20	29.2	0.504	0.454	0.431	68.50	
10:00	60	38.2	4.6	>20	31.6	0.384	0.364	0.381	56.14	
10:30	90	31.5	4.5	>20	32.9	0.274	0.278	0.303	41.87	
11:00	120	27.4	4.4	>20	34.1	0.192	0.208	0.232	30.08	
1:00	240	19.5	4.7	>20	35.2	0.095	0.115	0.130	14.10	
3:00	360	11.6	4.8	>20	36.5	0.103	0.127	0.144	15.25	
5:00	480		4.0	>20	36.6					

		UV + TiO2									
		50 mesh (300 µm)		Photocatalytic experiment using 20 g. per liter (16 g.) of silica gel size larger than 300 µm. 4.0 mmol/L of phenol.								
		1" sleeve (new)									
ID :		8/5/2014									
C_{phenol}=		4.0 mmol/L									
Vol =		800 ml		Speed =	8						
Silica =		16 g (20 g/L)		1 coat	new						
		Time (min)	**COD (mg/L)**	**pH**	**DO (mg/L)**	**T**	**λ @ 269**	**λ @ 254**	**λ @ 240**	**Integral**	
8:00		-60	899	4.4	8.25	22.9	2.732	1.976	0.360	188.15	
9:00		0	854	5.6	>20	24.7	2.740	1.977	0.419	188.32	
9:30		30	777	4.5	>20	29.2	3.291	3.509	2.559	303.88	
10:00		60	735	4.2	>20	31.6	3.469	3.727	3.052	334.79	
10:30		90			>20	32.9					
11:00		120	662	3.9	>20	34.1	3.731	3.727	3.704	360.01	
1:00		240	575	3.7	>20	35.2	3.747	3.727	3.706	375.50	
3:00		360	520	3.6	>20	36.5	3.747	3.727	3.706	382.22	
5:00		480	478	3.5	>20	36.6	3.747	3.727	3.706	386.31	

		UV + TiO2									
		50 mesh (300 µm)		Photocatalytic experiment using 20 g. per liter (16 g.) of silica gel size larger than 300 µm. pH adjusted to 3 (2.9)								
		1" sleeve (new)									
ID :		8/7/2014									
C_{phenol}=		1 mmol/L									
Vol =		800 ml		Speed =	8		pH		3		
Silica =		16 g (20 g/L)		1 coat	new						
		Time (min)	**COD (mg/L)**	**pH**	**DO (mg/L)**	**T**	**λ @ 269**	**λ @ 254**	**λ @ 240**	**Integral**	
8:00		-60	250	2.9	8.25	22.9	1.462	0.515	0.088	110.78	
9:00		0	232	3.5	>20	24.7	1.405	0.526	0.113	109.15	
9:30		30	190	3.4	>20	29.2	1.432	1.043	0.911	169.59	
10:00		60	162	3.3	>20	31.6	1.225	0.934	0.900	166.00	
10:30		90	145	3.3	>20	32.9	1.071	0.845	0.862	159.35	
11:00		120	129	3.2	>20	34.1	0.916	0.749	0.792	144.63	
1:00		240	81	3.2	>20	35.2	0.428	0.388	0.425	70.74	
3:00		360	59.6	3.2	>20	36.5	0.151	0.143	0.160	25.88	
5:00		480	45.6	3.3	>20	36.6	0.035	0.037	0.044	6.73	

	UV + TiO2									
	50 mesh (300 μm)			Photocatalytic experiment using 20 g. per liter (16 g.) of silica gel size larger than 300 μm. pH adjusted to 9.5						
	1" sleeve (new)									
ID :	8/8/2014									
C$_{phenol}$=	1 mmol/L									
Vol =	800 ml	Speed =	8		pH	9.5				
Silica =	16 g (20 g/L)	1 coat	new							
	Time (min)	**COD (mg/L)**	**pH**	**DO (mg/L)**	**T**	**λ @ 269**	**λ @ 254**	**λ @ 240**	**Integral**	
8:30	-60	231	9.5	8.25	22.9	1.411	0.596	1.580	170.76	
9:30	0	231	7.1	>20	24.7	1.471	0.596	0.195	116.73	
10:00	30	210	6.5	>20	29.2	1.972	1.480	1.039	184.09	
10:30	60	198	6.3	>20	31.6	2.166	1.829	1.366	208.70	
11:00	90	188	6.1	>20	32.9	2.252	2.004	1.577	224.48	
11:30	120	186	6.2	>20	34.1	2.286	2.094	1.729	235.80	
1:30	240	166	5.3	>20	35.2	2.084	2.030	1.985	254.49	
3:30	360	162	4.9	>20	36.5	1.743	1.754	1.885	242.76	
5:30	480	141	4.6	>20	36.6	1.290	1.371	1.529	194.16	

	UV + TiO2									
	50 mesh (300 μm)			Photocatalytic experiment using 20 g. per liter (16 g.) of silica gel size larger than 300 μm. pH adjusted to 7.0 with NaOH 1N. Formation of an orange-colored compound in the first 30 min.						
	1" sleeve (new)									
ID :	8/14/2014									
C$_{phenol}$=	1 mmol/L									
Vol =	800 ml	Speed =	8		pH =	7				
Silica =	16 g (20 g/L)	1 coat	new							
	Time (min)	**COD (mg/L)**	**pH**	**pH (filt.)**	**DO (mg/L)**	**T**	**λ @ 269**	**λ @ 254**	**λ @ 240**	**Integral**
8:00	-60	239	7.0		8.25	22.9	1.483	0.519	0.091	113.56
9:00	0	233	6.2	5.6	>20	24.7	1.462	0.593	0.184	115.14
9:30	30	216	5.0	5.0	>20	29.2	1.796	1.362	1.136	188.51
10:00	60	198	4.6		>20	31.6	1.671	1.298	1.216	196.23
10:30	90	170	4.3		>20	32.9	1.522	1.223	1.207	194.43
11:00	120	165	4.2		>20	34.1	1.377	1.137	1.167	188.02
1:00	240	108	3.9		>20	35.2	0.819	0.802	0.896	130.80
3:00	360	72.4	3.9		>20	36.5	0.310	0.345	0.403	52.31
5:00	480	64.9	4.3		>20	36.6	0.176	0.209	0.239	26.35

	UV + TiO2									
	50 mesh (300 µm)			Photocatalytic experiment using 20 g. per liter (16 g.) of silica gel size larger than 300 µm. pH adjusted to 8.0 with NaOH 1N. Formation of an orange-colored compound in the first 30 min.						
	1" sleeve (new)									
ID :	8/14/2014									
C$_{phenol}$=	1 mmol/L									
Vol =	800 ml	Speed =	8	pH =	8	**Down to 7.1 after 10 hours**				
Silica =	16 g (20 g/L)	1 coat	new							
	Time (min)	**COD (mg/L)**	**pH**	**DO (mg/L)**	**T**	**λ @ 269**	**λ @ 254**	**λ @ 240**	**Integral**	
8:00	-60	242	8.0	8.25	22.9	1.453	0.531	0.196	114.63	
9:00	0	237	6.3	>20	24.7	1.415	0.556	0.153	111.83	
9:30	30	205	5.3	>20	29.2	1.830	1.414	1.118	186.70	
10:00	60	191	4.8	>20	31.6	1.720	1.375	1.257	198.73	
10:30	90	169	4.5	>20	32.9	1.562	1.268	1.246	197.88	
11:00	120	153	4.3	>20	34.1	1.431	1.199	1.222	193.20	
1:00	240	106	4.0	>20	35.2	0.790	0.779	0.872	126.65	
3:00	360	68.8	4.0	>20	36.5	0.270	0.302	0.357	47.59	
5:00	480	61.2	4.4	>20	36.6	0.137	0.161	0.184	22.10	

	Photolysis (UV only)+oxygen									
	1" sleeve			Photolysis experiment. UV + O2 only.						
ID :	8/19/2014									
C$_{phenol}$=	0.25 mmol/L									
Vol =	800 ml	Speed =	8							
Silica =	none									
	Time (min)	**COD (mg/L)**	**pH**	**DO (mg/L)**	**T**	**λ @ 269**	**λ @ 254**	**λ @ 240**	**Integral**	
8:00	0	54.9	5.5	9.41	21.9	0.377	0.128	0.018	40.18	
9:00	60	40.2	4.3	35	32	0.484	0.468	0.443	68.21	
10:00	120	38.2	4.1	35	32	0.227	0.243	0.263	36.43	
12:00	240	11.2	4.2	35	35	0.030	0.032	0.033	5.79	
2:00	360	9.89	4.5	35	35	0.012	0.012	0.011	2.99	
4:00	480			35	35					

		UV + O2									
		1" sleeve (new)			Photolysis + O2						
	ID :	8/20/2014									
	C_{phenol}=	2.0 mmol/L									
	Vol =	800 ml		Speed =	8						
	Silica =	none									
		Time (min)	**COD (mg/L)**	**pH**	**DO (mg/L)**	**T**	**λ @ 269**	**λ @ 254**	**λ @ 240**	**Integral**	
8:00		0	454	5.6	8.25	22.9	2.483	1.019	0.177	151.22	
9:00		60	393	3.9	>20	24.7	3.210	2.841	2.402	296.32	
10:00		120	365	3.7	>20	31.6	3.290	2.949	2.770	323.18	
12:00		240	331	3.4	>20	34.1	3.292	3.069	3.388	348.68	
2:00		360	322	3.3	>20	35.2	3.062	2.988	3.647	349.91	
4:00		480	304	3.3	>20	36.5	2.840	2.844	3.534	342.83	

		UV + O2									
		1" sleeve (new)			Photolysis + O2						
	ID :	8/21/2014									
	C_{phenol}=	4.0 mmol/L									
	Vol =	800 ml		Speed =	8						
	Silica =	none									
		Time (min)	**COD (mg/L)**	**pH**	**DO (mg/L)**	**T**	**λ @ 269**	**λ @ 254**	**λ @ 240**	**Integral**	
8:00		0	932	5.6	8.25	22.9	2.768	1.960	0.355	191.35	
9:00		60	830	4.0	>20	24.7	3.567	3.726	3.705	354.35	
10:00		120	773	3.6	>20	31.6	3.746	3.726	3.705	381.56	
12:00		240	724	3.4	>20	34.1	3.746	3.726	3.705	414.12	
2:00		360	688	3.2	>20	35.2	3.746	3.726	3.705	431.93	
4:00		480	648	3.2	>20	36.5	3.746	3.726	3.705	442.41	

		UV + TiO2									
		Anatase powder		Photocatalytic experiment using 1 g. (1.25 g/l) of anatase and phenol concentration of 0.25 mmol. Compare to experimentes using coated silica.							
		1" sleeve (new)									
ID :		8/23/2014									
C_{phenol}=		0.25 mmol									
Vol =		800 ml		Speed =	8						
Anatase=		1 g		Powder	new						
		Time (min)	COD (mg/L)	pH	DO (mg/L)	T	λ @ 269	λ @ 254	λ @ 240	Integral	
8:00		-60	48	5.6	8.25	22.9	0.380	0.130	0.021	40.79	
9:00		0	43.6	4.8	>20	24.7	0.374	0.143	0.037	40.67	
9:30		30	20	4.2	>20	29.2	0.093	0.077	0.092	17.74	
10:00		60	4.36	4.5	>20	31.6	0.009	0.007	0.006	2.01	
10:30		90	3.45	4.7	>20	32.9	0.006	0.005	0.003	1.67	
11:00		120			>20	34.1					
1:00		240	0		>20	35.2					
3:00		360	0		>20	36.5					
5:00		480	0		>20	36.6					

		UV + TiO2									
		Anatase powder		Photocatalytic experiment using 1 g. (1.25 g/l) of anatase and phenol concentration of 2.0 mmol. Compare to experimentes using coated silica.							
		1" sleeve (new)									
ID :		8/25/2014									
C_{phenol}=		2.0 mmol									
Vol =		800 ml		Speed =	8						
Anatase=		1 g		Powder	new						
		Time (min)	COD (mg/L)	pH	DO (mg/L)	T	λ @ 269	λ @ 254	λ @ 240	Integral	
8:00		-60	466	5.3	8.25	22.9	2.479	0.995	0.177	151.04	
9:00		0	459	4.8	>20	24.7	2.394	0.980	0.185	144.41	
9:30		30	398	3.8	>20	29.2	2.426	1.205	0.853	202.37	
10:00		60	349	3.6	>20	31.6	2.231	1.191	0.987	207.69	
10:30		90	317	3.5	>20	32.9	2.028	1.138	1.021	205.23	
11:00		120	278	3.5	>20	34.1	1.790	1.046	0.981	196.68	
1:00		240	134	3.6	>20	35.2	0.620	0.440	0.470	99.99	
3:00		360	22.2	4.5	>20	36.5	0.007	0.007	0.007	1.99	
5:00		480	0	4.8	>20	36.6	0.005	0.004	0.003	1.84	

	UV + TiO2								
	Anatase powder								
	1" sleeve (new)		Photocatalytic experiment using 1 g. (1.25 g/l) of anatase and phenol concentration of 4.0 mmol. Compare to experimentes using coated silica.						
ID :	8/26/2014								
C_{phenol}=	4.0 mmol								
Vol =	800 ml	**Speed =**	8						
Anatase=	1 g	Powder	new						
	Time (min)	**COD (mg/L)**	**pH**	**DO (mg/L)**	**T**	**λ @ 269**	**λ @ 254**	**λ @ 240**	**Integral**
8:00	-60	936	5.3	8.25	22.9	2.747	1.982	0.362	189.72
9:00	0	893	5.2	>20	24.7	2.707	1.927	0.363	183.16
9:30	30	801	3.8	>20	29.2	3.165	2.500	1.474	265.21
10:00	60	774	3.6	>20	31.6	3.323	2.677	1.880	291.93
10:30	90	721	3.5	>20	32.9	3.444	2.789	2.159	309.16
11:00	120	684	3.4	>20	34.1	3.576	2.900	2.364	321.11
1:00	240	588	3.4	>20	35.2	3.741	3.060	2.888	343.77
3:00	360	433	3.2	>20	36.5	3.594	2.872	2.938	340.15
5:00	480	433	3.2	>20	36.6	3.038	2.483	2.628	313.15

	UV + TiO2								
	50 mesh (300 μm)								
	1" sleeve (new)		Photocatalytic experiment using 20 g. per liter (16 g.) of silica gel size larger than 300 μm coated twice.						
ID :	8/27/2014								
C_{phenol}=	1 mmol/L								
Vol =	800 ml	**Speed =**	8						
Silica =	16 g (20 g/L)	2 coat	new						
	Time (min)	**COD (mg/L)**	**pH**	**DO (mg/L)**	**T**	**λ @ 269**	**λ @ 254**	**λ @ 240**	**Integral**
8:00	-60	240	5.3	8.25	22.9	1.464	0.524	0.094	111.14
9:00	0	232	5.0	>20	24.7	1.492	0.630	0.227	121.93
9:30	30	190	4.3	>20	29.2	1.509	1.031	0.891	171.12
10:00	60	163	4.0	>20	31.6	1.318	0.959	0.902	168.10
10:30	90	142	3.9	>20	32.9	1.140	0.881	0.869	159.76
11:00	120	121	3.9	>20	34.1	0.963	0.787	0.798	140.20
1:00	240	63	3.8	>20	35.2	0.360	0.365	0.398	54.37
3:00	360	48	4.1	>20	36.5	0.184	0.214	0.234	25.97
5:00	480	42	4.3	>20	36.6	0.152	0.180	0.196	21.72

	UV + TiO2 50 mesh (300 μm) 1" sleeve (new)		Photocatalytic experiment using 20 g. per liter (16 g.) of silica gel size larger than 300 μm coated three times.							

ID :	8/27/2014									
C$_{phenol}$=	1 mmol/L									
Vol =	800 ml	Speed =	8							
Silica =	16 g (20 g/L)	3 coats	new							
	Time (min)	**COD (mg/L)**	**pH**	**DO (mg/L)**	**T**	**λ @ 269**	**λ @ 254**	**λ @ 240**	**Integral**	
8:00	-60	236	5.0	8.25	22.9	1.473	0.526	0.090	110.47	
9:00	0	229	4.9	>20	24.7	1.377	0.529	0.122	108.86	
9:30	30	179	4.1	>20	29.2	1.403	0.939	0.797	162.49	
10:00	60	155	3.9	>20	31.6	1.296	0.941	0.887	167.29	
10:30	90	132	3.7	>20	32.9	1.119	0.878	0.873	159.21	
11:00	120	116	3.7	>20	34.1	0.978	0.818	0.840	143.29	
1:00	240	54.4	3.8	>20	35.2	0.328	0.345	0.378	49.48	
3:00	360	36.5	4.2	>20	36.5	0.194	0.224	0.241	27.06	
5:00	480	30.5	4.4	>20	36.6	0.188	0.219	0.237	26.12	

	UV + TiO2 50 mesh (300 μm) 1" sleeve (new)		Photocatalytic experiment using 20 g. per liter (16 g.) of silica gel size larger than 300 μm. No oxygen.							

ID :	9/2/2014									
C$_{phenol}$=	1 mmol/L									
Vol =	800 ml	Speed =	8							
Silica =	16 g (20 g/L)	1 coat	new							
	Time (min)	**COD (mg/L)**	**pH**	**DO (mg/L)**	**T**	**λ @ 269**	**λ @ 254**	**λ @ 240**	**Integral**	
8:00	-60	247	5.5	8.00	22.9	1.501	0.537	0.094	109.91	
9:00	0	241	6.0	11.32	24.7	1.457	0.598	0.196	115.29	
9:30	30	229	5.1	7.41	29.2	1.650	1.033	0.796	165.58	
10:00	60	211	4.9	5.11	34.2	1.529	0.938	0.771	163.50	
10:30	90	203	4.8	4.36	34.9	1.485	0.917	0.781	163.78	
11:00	120	214	4.8	5.15	35.1	1.445	0.903	0.784	163.09	
1:00	240	189	4.7	4.02	36.9	1.215	0.786	0.710	150.67	
3:00	360	181	4.6	4.09	36.9	1.057	0.742	0.709	141.11	
5:00	480	167	4.6	4.05	37.2	0.943	0.705	0.698	130.49	

	UV + TiO2										
	50 mesh (300 μm)		Photocatalytic experiment using 20 g. per liter (16 g.) of silica gel size larger than 300 μm coated once								
	1" sleeve (new)										
ID :	9/6/2014										
C$_{phenol}$=	1 mmol/L										
Vol =	800 ml	Speed =	8								
Silica =	16 g (20 g/L)	1 coat	new								
	Time (min)	COD (mg/L)	pH	DO (mg/L)	T	λ @ 269	λ @ 254	λ @ 240	Integral	Phenol(mg/L)	
8:00	-60	239	5.5	8.25	22.9	1.473	0.526	0.090	110.47	105.000	
9:00	0	239	5.7	>20	24.7	1.434	0.564	0.156	112.30	103.000	
9:30	30	194	4.6	>20	29.2	1.597	1.131	0.974	176.10		
10:00	60	175	4.3	>20	31.6	1.474	1.094	1.027	179.78	45.000	
10:30	90										
11:00	120	142	4.0	0	34.1	1.191	0.960	0.989	169.88	26.000	
1:00	240	95.7	3.8	0	35.2	0.588	0.563	0.623	93.94	8.000	
3:00	360	67.2	4.3	0	36.5	0.164	0.179	0.208	26.71	0.000	
5:00	480	47	4.4	0	36.6	0.093	0.111	0.126	14.73	0.000	

	UV + TiO2								
	50 mesh (300 μm)		Photocatalytic experiment using 20 g. per liter (16 g.) of silica gel size larger than 300 μm coated three times						
	1" sleeve (new)								
ID :	10/13/2014								
C$_{phenol}$=	0.25 mmol/L								
Vol =	800 ml	Speed =	8						
Silica =	16 g (20 g/L)	3 coats	new						
	Time (min)	COD (mg/L)	pH	DO (mg/L)	T	λ @ 269	λ @ 254	λ @ 240	Integral
8:00	-60	63.2	6.6	8.25	22.9	0.394	0.133	0.017	41.99
9:00	0	73	5.3	>20	24.7	0.428	0.198	0.095	48.92
9:30	30	50.7	4.4	>20	29.2	0.294	0.248	0.251	42.27
10:00	60	32.1	4.2	>20	31.6	0.192	0.192	0.207	28.31
10:30	90	28.3	4.3	>20		0.160	0.182	0.197	23.15
11:00	120	15.4	4.3	>20	34.1	0.126	0.147	0.158	17.96
1:00	240	0	4.4	>20	35.2	0.141	0.167	0.182	20.08
3:00	360	0	4.5	>20	36.5	0.119	0.143	0.155	17.03
5:00	480	0		>20	36.6				

		UV + TiO2								
		50 mesh (300 μm)		Photocatalytic experiment using 20 g. per liter (16 g.) of silica gel size larger than 300 μm coated three times						
		1" sleeve (new)								
ID :		10/14/2014								
C$_{phenol}$=		0.50 mmol/L								
Vol =		800 ml		Speed =	8					
Silica =		16 g (20 g/L)		3 coats	new					
		Time (min)	**COD (mg/L)**	**pH**	**DO (mg/L)**	**T**	**λ @ 269**	**λ @ 254**	**λ @ 240**	**Integral**
8:00		-60	118	5.5	8.25	22.9	0.748	0.256	0.038	76.33
9:00		0	118	5.1	>20	24.7	0.766	0.332	0.131	80.45
9:30		30	80.9	4.4	>20	29.2	0.661	0.502	0.478	90.79
10:00		60	57.6	4.2	>20	31.6	0.481	0.413	0.424	69.59
10:30		90	41.3	4.2	>20		0.338	0.333	0.357	49.79
11:00		120	34.7	4.2	>20	34.1	0.233	0.256	0.280	34.10
1:00		240	5	4.5	>20	35.2	0.164	0.197	0.214	22.72
3:00		360	0	4.7	>20	36.5	0.173	0.210	0.230	24.00
5:00		480	0	4.8	>20	36.6	0.188	0.229	0.252	26.28

		UV + TiO2								
		50 mesh (300 μm)		Photocatalytic experiment using 20 g. per liter (16 g.) of silica gel size larger than 300 μm coated three times						
		1" sleeve (new)								
ID :		10/15/2014								
C$_{phenol}$=		2.00 mmol/L								
Vol =		800 ml		Speed =	8					
Silica =		16 g (20 g/L)		3 coats	new					
		Time (min)	**COD (mg/L)**	**pH**	**DO (mg/L)**	**T**	**λ @ 269**	**λ @ 254**	**λ @ 240**	**Integral**
8:00		-60	458	5.5	8.25	22.9	2.491	1.015	0.173	151.18
9:00		0	436	5.1	>20	24.7	2.461	1.066	0.264	154.09
9:30		30	370	4.2	>20	29.2	2.685	1.787	1.412	227.89
10:00		60	333	4.0	>20	31.6	2.559	1.756	1.516	235.48
10:30		90	301	3.8	>20		2.411	1.696	1.544	236.15
11:00		120	277	3.8	>20	34.1	2.271	1.651	1.557	235.02
1:00		240	206	3.5	>20	35.2	1.648	1.369	1.419	212.82
3:00		360	135	3.5	>20	36.5	0.897	0.840	0.915	141.59
5:00		480	83.7	3.7	>20	36.6	0.329	0.343	0.382	51.19

	UV + TiO2 50 mesh (300 μm) 1" sleeve (new)	Photocatalytic experiment using 20 g. per liter (16 g.) of silica gel size larger than 300 μm coated three times							
ID :	10/16/2014								
C$_{phenol}$=	3.00 mmol/L								
Vol =	800 ml	Speed =	8						
Silica =	16 g (20 g/L)	3 coats	new						
	Time (min)	**COD (mg/L)**	**pH**	**DO (mg/L)**	**T**	**λ @ 269**	**λ @ 254**	**λ @ 240**	**Integral**
8:00	-60	697	5.2	8.25	22.9	2.699	1.519	0.259	175.80
9:00	0	653	5.2	>20	24.7	2.738	1.572	0.389	181.14
9:30	30	571	4.2	>20	29.2	3.206	2.643	1.976	271.89
10:00	60	525	4.0	>20	31.6	3.341	2.676	2.187	288.53
10:30	90	484	3.8	>20		3.394	2.673	2.316	298.93
11:00	120	458	3.7	>20	34.1	3.377	2.618	2.339	300.92
1:00	240	364	3.5	>20	35.2	3.014	2.397	2.362	297.87
3:00	360	296	3.4	>20	36.5	2.522	2.144	2.245	282.38
5:00	480	239	3.4	>20	36.6	1.919	1.767	1.912	250.28

	UV + TiO2 50 mesh (300 μm) 1" sleeve (new)	Photocatalytic experiment using 20 g. per liter (16 g.) of silica gel size larger than 300 μm coated three times							
ID :	10/17/2014								
C$_{phenol}$=	4.00 mmol/L								
Vol =	800 ml	Speed =	8						
Silica =	16 g (20 g/L)	3 coats	new						
	Time (min)	**COD (mg/L)**	**pH**	**DO (mg/L)**	**T**	**λ @ 269**	**λ @ 254**	**λ @ 240**	**Integral**
8:00	-60	915	5.4	8.25	22.9	2.770	1.951	0.351	191.60
9:00	0	862	5.1	>20	24.7	2.774	1.983	0.442	193.02
9:30	30	771	4.4	>20	29.2	3.259	3.265	2.359	295.45
10:00	60	718	4.1	>20	31.6	3.446	3.460	2.747	320.99
10:30	90	676	4.0	>20		3.581	3.621	2.987	336.48
11:00	120	635	3.8	>20	34.1	3.675	3.665	3.103	343.78
1:00	240	560	3.5	>20	35.2	3.739	3.490	3.424	357.69
3:00	360	458	3.5	>20	36.5	3.662	3.221	3.483	357.09
5:00	480	408	3.4	>20	36.6	3.358	2.960	3.268	344.40

Vita

Guillermo Rincon obtained his BS degree in chemical engineering from University of Zulia, Venezuela in 2000. His undergraduate senior project dealing with fresh water treatment for high pressure vapor generation in heavy oil recovery brought him into the environmental field, in which he continued working after becoming part of Petróleos de Venezuela SA, the largest oil corporation in Venezuela. Here, as part of the infrastructure engineering team for an on-shore crude oil production division, he not only participated in the oil and gas transport network maintenance and expansion, but also supervised operations and optimization of process equipment units in a produced water treatment plant and was directly involved in chemical treatment assessment and selection.

In 2009 he was admitted to the graduate school at the University of New Orleans, completing his masters in environmental engineering in 2011. During this time, he conducted research on removal of oil and grease from bilge water using an electro-coagulation/flotation process under the supervision of Dr. Enrique La Motta. Latter, as a doctoral candidate, Guillermo performed extensive experimental work on semiconductor photo-catalytic oxidation of recalcitrant compounds on titanium oxide. He obtained his PhD in engineering and applied science from UNO in 2015.